Advanced storage concepts for solar and low energy buildings

IEA Task 32 final report

Furbo, Simon; Schultz, Jørgen Munthe; Andersen, Elsa

Publication date:
2008

Document Version
Publisher's PDF, also known as Version of record

BYG·DTU

Jørgen M. Schultz
Elsa Andersen
Simon Furbo

Advanced storage concepts for solar and low energy buildings, IEA-SHC Task 32

Slutrapport

DANMARKS
TEKNISKE
UNIVERSITET

Sagsrapport
BYG·DTU SR-08-01
2008
ISSN 1601 - 8605

Advanced storage concepts for solar and low energy buidings, IEA-SHC Task 32. Slutrapport

Jørgen M. Schultz, Elsa Andersen og Simon Furbo

Indholdsfortegnelse

Bilagsfortegnelse

1. Indledning

Denne rapport beskriver aktiviteterne, som er gennemført i forbindelse med EFP-06 projektet ”Advanced storage concepts for solar and low energy buildings, IEA – SHC Task32”, j.nr.: 33032-0005. Projektet har dækket den danske deltagelse i det internationale Task 32 projekt. Den danske deltagelse har været fokuseret om subtask C: Storage concepts based on phase change materials og subtask D: Storage concepts based on advanced water tanks and special devices.

I kapitel 2 omtales kort de gennemførte aktiviteter vedrørende smeltevarmelagre og i kapitel 3 aktiviterne vedrørende avancerede vandlagre. Aktiviterne er detaljeret beskrevet i rapporter, papers og artikler, som fremgår af rapportens 10 bilag.

2. Smeltevarmelagre med stabil underafkøling

2.1 Teoretiske undersøgelser

Smeltevarmelagre har været undersøgt gennem mange år som en mulighed for at øge lagringskapaciteten pr. volumenenhed set i forhold til traditionelle vandlagre gennem udnyttelse af energien knyttet til faseskiftet mellem fast og flydende form. Nogle faseskiftematerialer har en tendens til at underafkøle, hvilket generelt set er et problem, fordi man da ikke under afladning af lageret får frigivet den energi, der er knyttet til faseændringen.

Imidlertid kan evnen til at underafkøle udnyttes positivt i forbindelse med sæsonlagring, hvis det kombineres med en metode til kontrolleret aktivering af faseskiftet i et underafkølet faseskiftemateriale. Den positive effekt optræder når et fuldt smeltet lager underafkøler f.eks. på grund af varmetab til omgivelserne. På et tidspunkt vil lagerets temperatur have nået omgivelsernes temperatur, hvorved lageret bliver varmetabsfrit. I denne tilstand kan lageret forblive indtil der opstår et behov for varme og der foretages en aktivering af faseskiftet, hvorved lagerets temperatur næsten øjeblikkeligt stiger til materialets smeltepunkt under frigørelse af energien knyttet til smeltevarmen. Et særligt interessant materiale i denne sammenhæng er natriumacetat trihydrat, der underafkøler stabilt og har en smeltevarme på ca. 265 kJ/kg. Smeltetemperaturen er på 58 °C, hvilket er en temperatur anvendelig for både rumvarme og varmt brugsvand.

Figur 1 illustrerer underafkølingsprincippet og viser lagringskapaciteten pr. liter natriumacetat (sodium acetate) sammenlignet med vand.

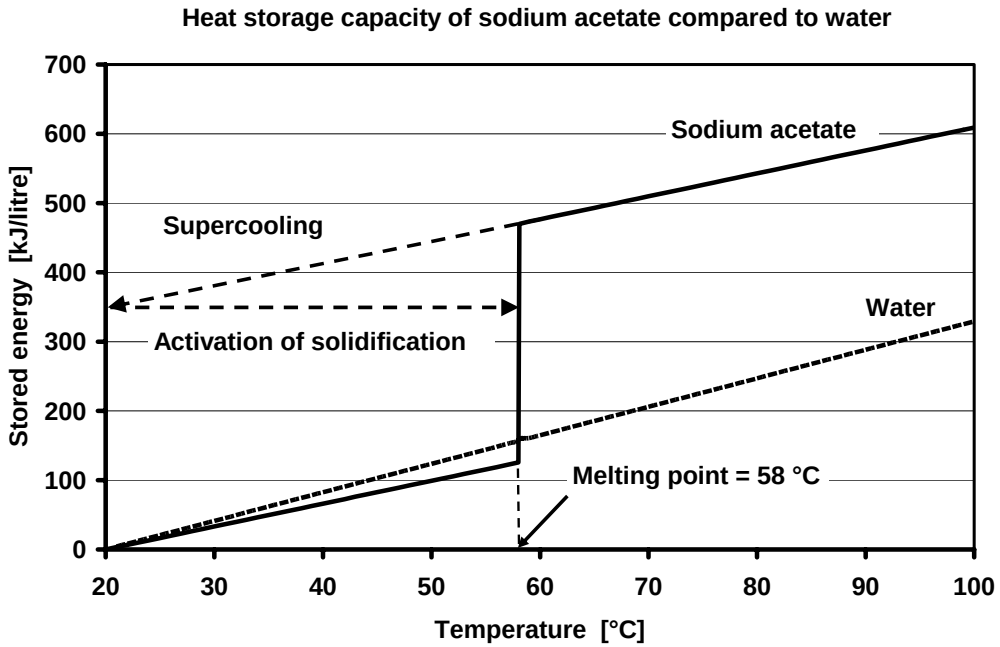

Figur 1. Illustration af underafkøling (supercooling) og lagringskapacitet i natriumacetat trihydrat sammenlignet med vand.

Anvendelse af natriumacetat med aktiv udnyttelse af underafkøling til reduktion af varmetabet fra sæsonvarmelagre kræver en opdeling af det samlede lager i mindre adskilte sektioner, således, at det er muligt at aktivere faseskiftet i et begrænset underafkølet volumen svarende til behovet, mens resten af lageret kan forblive underafkølet.

Tidligere undersøgelser har vist [1], at det vil være muligt for et solvarmeanlæg at opnå 100 % dækning af både varmt brugsvand og rumvarme i et lavenergihus placeret i Danmark, isoleret til ”passivhus” niveau, med et sæsonsmeltevarmelager, der udnytter underafkøling. Imidlertid er et smeltevarmelager væsentlig dyrere end et vandlager, hvorfor en minimering af det totale nødvendige lagervolumen er nødvendig. Der er en lang række af forhold der har betydning for det nødvendige lagervolumen for opnåelse af 100 % dækning, blandt andet:

- Solfangerareal og hældning
- Størrelsen af lagerets delvolumener
- Varmeoverføringen mellem solfangervæske og lager
- Varmeoverføring mellem afladningskreds og lager
- Lagerets isoleringsgrad
- Lagerets integration i bygningen (mulighed for at udnytte varmetabet)

Ovenstående forhold er undersøgt teoretisk via opbygning af en model i TRNSYS 15 af solvarmeanlægget vist i figur 2.

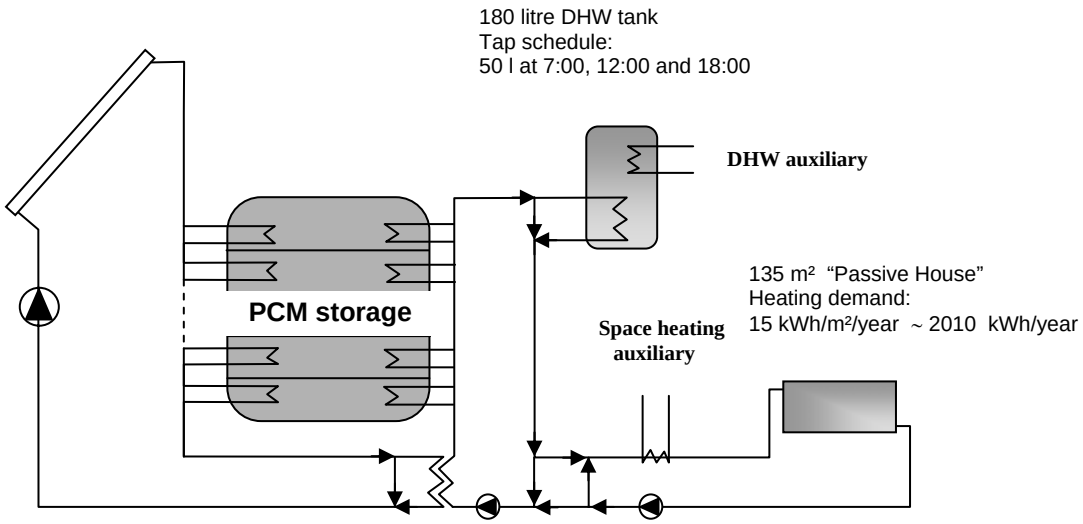

Figur 2. Solvarmeanlæg anvendt ved simuleringer i TRNSYS.

Solvarmeanlægget indeholder 2 lagerbeholdere, dels selve sæsonsmeltevarmelageret (PCM storage) og dels et 180 liter varmtvandsbeholder (DHW tank). Sidstnævnte er nødvendig for at kunne levere den nødvendige effekt ved tapning af varmt vand. Varmtvandsbeholderen kan opvarmes enten via varmeveksling med solfangerkredsen eller via smeltevarmelageret. Rumvarmeanlægget er et lavtemperaturanlæg, f.eks. gulvvarme, der ligeledes kan forsynes direkte via varmeveksling med solfangerkredsen eller via smeltevarmelageret. Solfangeren er en sydvendt højeffektiv plan solfanger med en starteffektivitet på 0,82 samt 1. og 2. ordens varmetabskoefficienter på hhv. 2,44 W/m^2K og 0,005 W/m^2K^2 . Indfaldsvinkelkorrektionsfaktoren er 3,6 (tangens udtryk). Den optimale hældning er fundet til 75°. Den næsten lodrette solfanger udnytter bedre det sparsomme solindfald i vinter og overgangsperioderne samtidig med at overtemperaturproblemet i sommermånederne reduceres.

Solfangerareal

Solfangerarealets indflydelse på det nødvendige smeltevarmelagervolumen for opnåelse af 100 % dækning er fundet ved simuleringer med ovenstående model. Ved simuleringerne er størrelsen af delvolumener i lageret fastholdt på 100 liter uanset lagerets samlede volumen. Resultatet af parameterundersøgelsen er vist i figur 3.

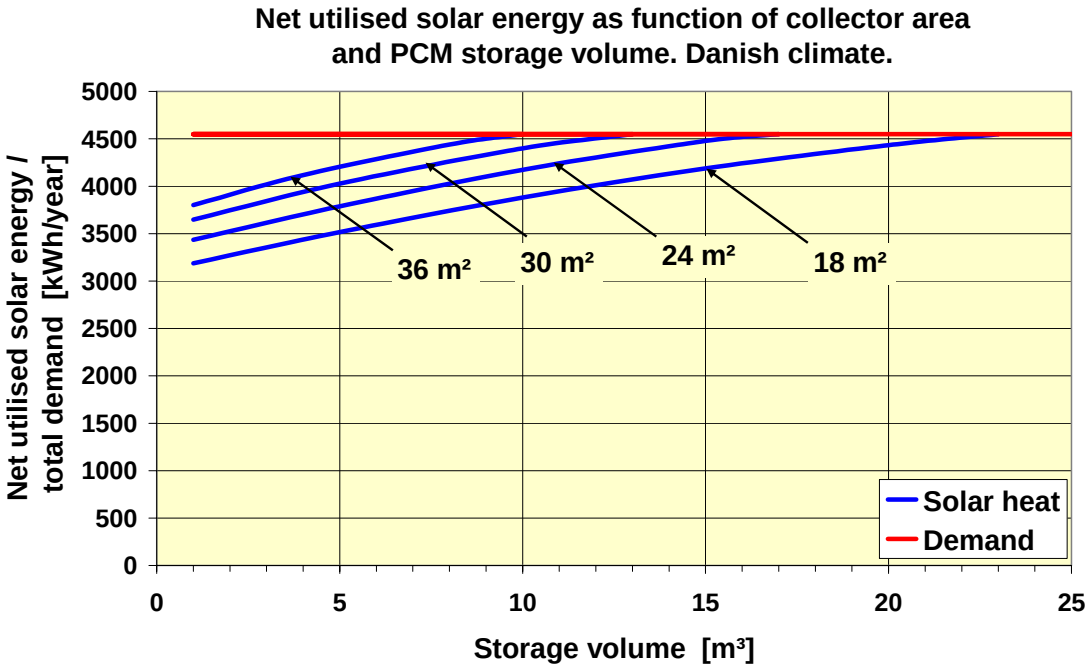

Figur 3. Nettoydelsen som funktion af solfangerareal og det totale volumen af smeltevarmelageret. Den røde vandrette linje viser det samlede årlige energibehov til varmt brugsvand og rumopvarmning. Delvolumenstørrelsen er 100 liter uanset lagerets samlede volumen. Varmeoverføringen er 500 W/K mellem smeltevarmelageret og hhv. solfangerkreds og afladningskreds. Lagerets effektive varmetabskoefficient er 0,6 W/m^{2}K.

Figur 3 viser, at der ved et solfangerareal på 18 m^2 kræves et smeltevarmelagervolumen på ca. 22 m^3 for at opnå 100 % dækning (den blå kurve møder den røde). Øges solfanger arealet til 36 m^2 reduceres det nødvendige smeltevarmelagervolumen til knap 10 m^3.

Figur 4 viser fordelen ved et sæsonsmeltevarmelager med aktiv udnyttelse af under-afkøling sammenlignet med et vandlager for hvilket, det, med det givne solfangerareal, ikke vil være muligt at opnå 100 % dækning med vandlager.

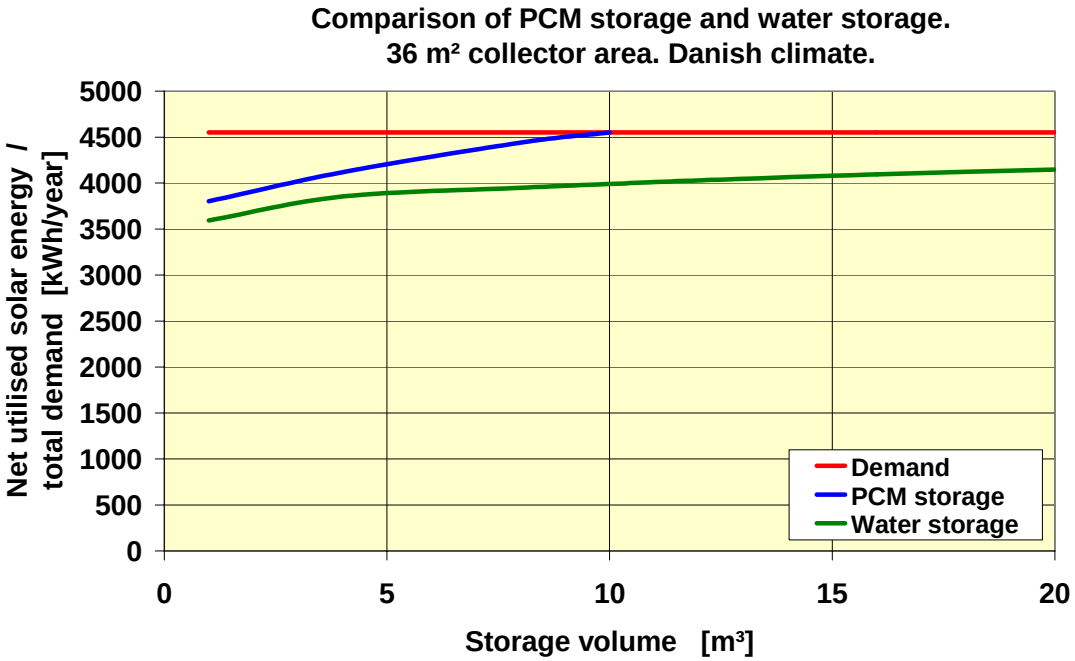

Figur 4. Nettoydelsen som funktion af det totale volumen af smeltevarmelager/ vandlager. Den røde vandrette linje viser det samlede årlige energibehov til varmt brugsvand og rumopvarmning. Delvolumenstørrelsen er 100 liter uanset lagerets samlede volumen. Varmeoverføringen er 500 W/K mellem smeltevarmelageret og hhv. solfangerkreds og afladningskreds. Lagerets effektive varmetabskoefficient er 0,6 W/m^{2}K.

Størrelsen af delvolumen

I ovenstående parameteranalyse var delvolumenernes størrelse fastsat til 100 liter, hvilket for et 10 m^3 lager betyder, at der skal etableres 100 adskilte delvolumener med hver deres individuelle styring. Det vil derfor være ønskeligt, at kunne reducere antallet af delvolumener. Figur 5 viser sammenhængen mellem delvolumenstørrelse og det nødvendige smeltevarmelagervolumen for opnåelse af 100 % dækning.

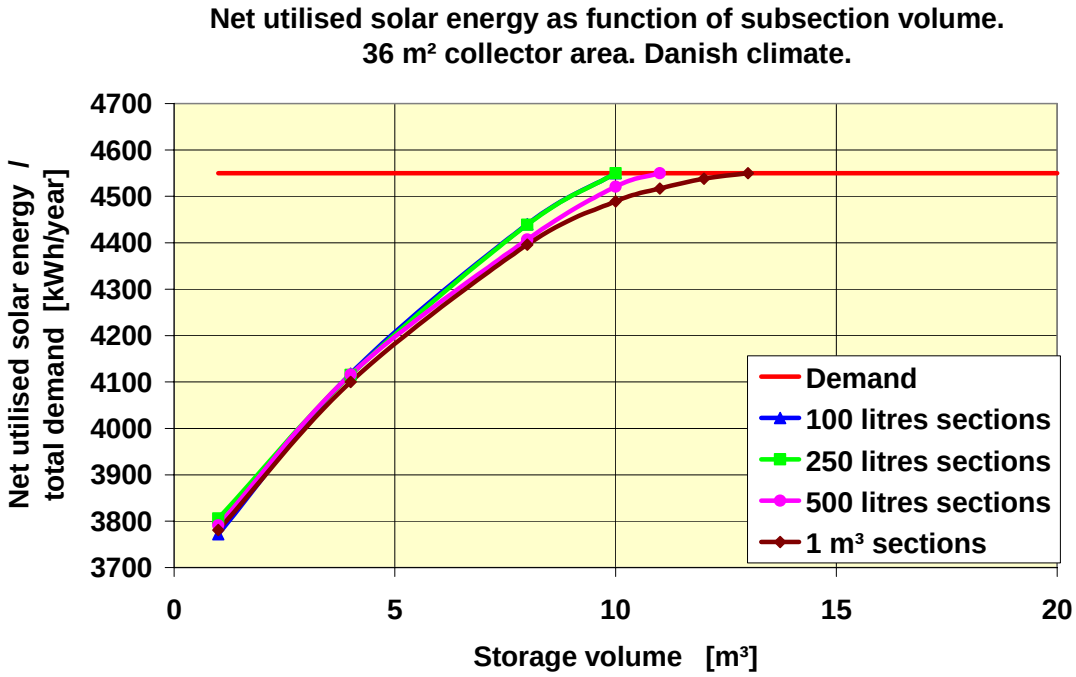

Figur 5. Nettoydelsen som funktion af delvolumenstørrelsen. Den røde vandrette linje viser det samlede årlige energibehov til varmt brugsvand og rumopvarmning. Solfangerarealet er 36 m^2. Varmeoverføringen er 500 W/K mellem smeltevarmelageret og hhv. solfangerkreds og afladningskreds. Lagerets effektive varmetabskoefficient er 0,6 W/m^2K.

Figur 5 viser, at det er muligt at øge delvolumenstørrelsen til 250 liter uden, at det går ud over nettoydelsen for solvarmeanlægget og uden at øge det nødvendige totale volumen af smeltevarmelageret. Øges delvolumenstørrelsen til 500 l øges det nødvendige totale volumen til ca. 11 m^3 og ved 1000 liter i delvolumenerne kræves et totalt volumen på ca. 13 m^3. Til gengæld reduceres det samlede antal delvolumener fra 40, ved 10 m^3 og 250 liter, til 13 ved 13 m^3 og 1000 liter i delvolumenet. En endelig optimering må bero på en økonomisk analyse.

Varmeoverføring

Varmeoverføringen mellem smeltevarmelageret og hhv. solfangerkredsen og afladningskredsen har i de tidligere parameterundersøgelser været fastholdt på 500 W/K. En parameterundersøgelse har vist, at en forøgelse af varmeoverføringsevnen ud over de 500 W/K ikke medfører en forøget nettoydelse og dermed mulighed for at reducere smeltevarmelagerets volumen yderligere. Derimod vil en nedsat varmeoverføringsevne i afladningskredsen betyde, at det ikke er muligt at opnå 100 % dækning, sandsynligvis fordi varmtvandsbeholderen ikke kan nå at blive opladet mellem tapningerne.

Lagerets isoleringsniveau

Fordelen ved smeltevarmelageret med udnyttelse af underafkøling er et væsentlig reduceret varmetab sammenlignet med et vandlager. Figur 6 viser sammenhængen mellem lagerets isoleringsniveau og det nødvendige totale smeltevarmelagervolumen.

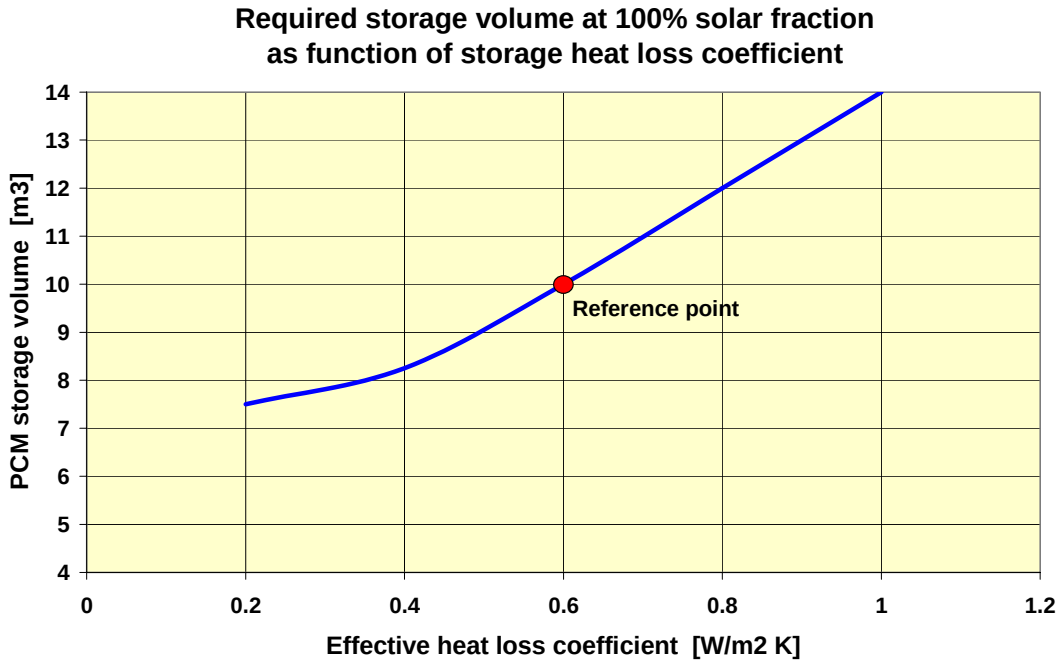

Figur 6. Det nødvendige smeltevarmelagervolumen som funktion af den effektive varmetabskoefficient for lageret. Solfangerarealet er 36 m^2. Varmeoverføringen er 500 W/K mellem smeltevarmelageret og hhv. solfangerkreds og afladningskreds. Delvolumenstørrelsen er 250 liter.

Figur 6 viser at det nødvendige smeltevarmelagervolumen for opnåelse af 100 % dækning er stærkt afhængig af lagerets isoleringsniveau. Ved at reducere den effektive varmetabskoefficient fra 0,6 til 0,4 W/m^2K reduceres det nødvendige lagervolumen fra 10 m^3 til ca. 8 m^3.

Udnyttelse af lagerets varmetab

I de foregående analyser er lagerets varmetab regnet som rent spild, men ved en passende placering af lageret i bygningen vil det være muligt at udnytte varmetabet fra lageret til dækning af en del af rumopvarmningsbehovet. Betydningen af dette er undersøgt ved at modregne lagerets varmetab i den hidtil afsatte effekt fra varmeanlægget når der er et opvarmningsbehov. Resultatet af denne undersøgelse er vist i figur 7, hvoraf det fremgår, at det teoretisk set vil være muligt at reducere det nødvendige lagervolumen fra 10 m^3 til ca. 6,5 m^3 ved en varmetabskoefficient for lageret på 0,6 W/m^2K. Sænkes varmetabskoefficienten til 0,4 W/m^2K reduceres det nødvendige lagervolumen til 6 m^3.

Placeringen af varmelageret i huset kræver imidlertid også en løsning, der kan lede varmen fra lagerets varmetab væk i perioder uden opvarmningsbehov.

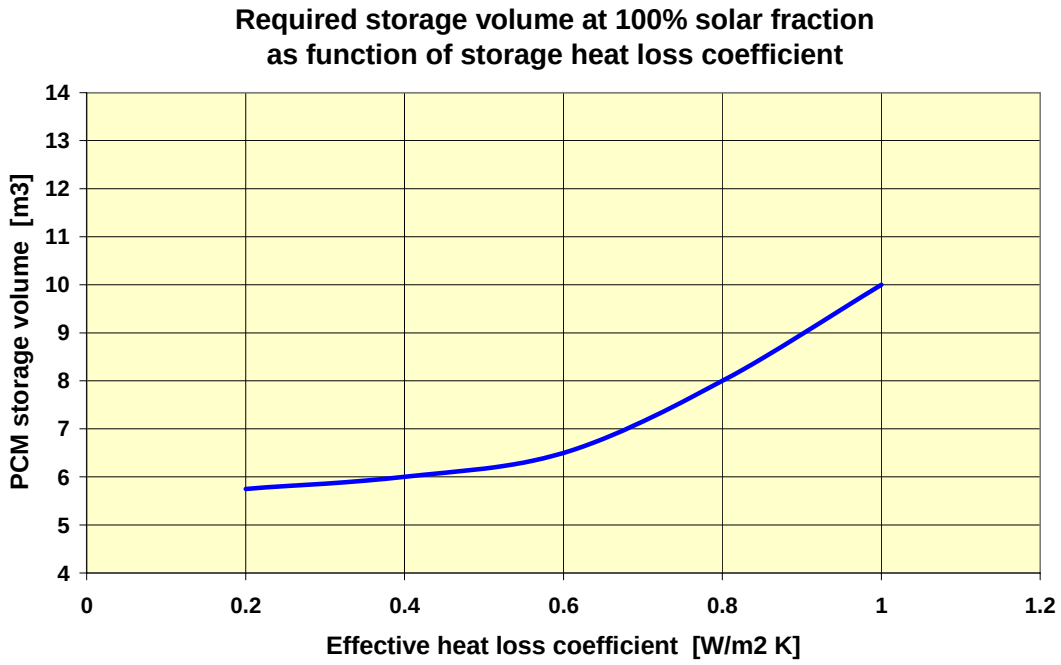

Figur 7. Det nødvendige smeltevarmelagervolumen som funktion af den effektive varmetabskoefficient for lageret i tilfældet, hvor lagerets varmetab kan udnyttes til reduktion af opvarmningsbehovet. Solfangerarealet er 36 m^2. Varmeoverføringen er 500 W/K mellem smeltevarmelageret og hhv. solfangerkreds og afladningskreds. Delvolumenstørrelsen er 250 liter.

2.2 Eksperimentelle undersøgelser

Baggrund

De eksperimentelle undersøgelser bygger videre på resultater og erfaringer fra [1], hvor der blev opbygget et prototypelager, der havde til formål dels at vise underafkølings-princippet i praksis og dels til bestemmelse af varmeoverføringsevnen til og fra salthydratet i dets forskellige faser ved henholdsvis opvarmning og afkøling. Prototype-lageret var opbygget som vist skematisk i figur 8, hvor opvarmningen skete ved cirkulation af varmt vand i et 10 mm højt hulrum under salthydratet og afkølingen skete ved cirkulation af koldt vand i et 10 mm højt hulrum over salthydratet. Designet var valgt ud fra ønsket om at skabe en naturlig intern konvektion i lageret under både op- og afladning. Saltet var placeret i en lav lukket bakke (højde $\times$ bredde $\times$ længde: 0,03 $\times$ 0,47 $\times$ 0,97 m), hvilket giver et stort varmeoverføringsareal set i relation til lagervolumenet.

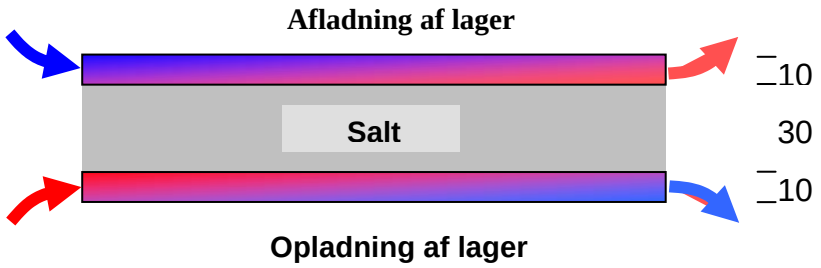

Figur 8. Skematisk tegning (lodret snit) af forsøgssmeltevarmelageret.

Resultatet af de udførte forsøg var en varmeoverføring ved opvarmning af saltet på 171 – 221 W/m^{2}K mens der under afkøling kun blev fundet en varmeoverføring på 22 - 46 W/m^{2}K.

Varmeoverføringen ved opvarmning er sandsynligvis mere end tilstrækkelig med udgangspunkt i resultatet fra de teoretiske undersøgelser, der viste at en varmeoverføring på 500 W/K er tilstrækkelig. Det betyder, at det varmeoverførende areal blot skal være over 2,5 m^2 svarende til f.eks. et cirkulært lager med en diameter på 1,8 m eller et kvadratisk lager med en kantlængde på 1,35 m, hvilket er mindre end anvendt i simuleringerne for et optimalt designet lager med størst muligt forhold mellem volumen og overfladeareal.

Derimod er varmeoverføringen ved afkøling af lageret vist i figur 1 langt fra tilstrækkelig, hvilket skyldes flere forhold:

- Det lykkedes ikke at opnå underafkøling i salthydratet, hvilket betød, at den påregnede naturlige konvektion i saltet ved afkøling oppe fra aldrig optrådte.
- Salthydratet fylder mindre i størknet tilstand end i flydende tilstand, hvorfor der sandsynligvis opstår et hulrum mellem det størknede salt og den varmeoverførende flade over saltet, hvilket vil nedsætte varmeoverføringen betragteligt. Hulrumsdannelsen forstærkes af, at lageret ved fyldning, blev fyldt med ca. 80 °C varmt smeltet salt, der i sig selv vil fylde mindre ved afkøling ned til smeltepunktet på 58 °C

Den manglende underafkøling skyldtes et dårligt design af smeltevarmelageret, idet det viste sig, at der befandt sig salt i lagerets påfyldningsstudse, der aldrig blev smeltet og derfor straks igangsatte størkningsprocessen ved afkøling af lageret til under smeltepunktet.

Håndtering af salthydrat

Et væsentligt problem i forbindelse med de hidtidige forsøg var forbundet med smeltning af store mængder salthydrat og ikke mindst påfyldning af lagerprototypen med det varme smeltede salthydrat. Dette forhold blev løst ved indkøb af en smeltebeholder i rustfrit stål med en udvendig kappe (figur 9). I kappen blev der cirkuleret vand ved ca. 80 °C til smeltning af salthydratet i smeltebeholderen. Det havde ved små indledende tests vist sig fordelagtigt med omrøring i salthydratet, hvilket i dette tilfælde er etableret ved hjælp af en slangepumpe, der cirkulerer smeltet salt fra beholderens bund til beholderens top.

For at undgå størkning i slangepumpen og de tilhørende rørforbindelser blev disse forsynet med elektriske varmekabler. Slangepumpen og de tilhørende rørforbindelser gør det endvidere muligt på simpel måde at tappe varmt smeltet salt direkte fra smeltebeholderen til et prototypelager (figur 10).

Figur 9. Venstre: Smeltebeholder med monteret varmelegeme til opvarmning af kappen.
Højre: Smeltebeholder isoleret og monteret med slangepumpe (gul) til cirkulation af smeltet salthydrat.

Figur 10. Tapning af flydende salt fra smeltetank til lagerenhed.

Prøvesmeltevarmelager 1

Baseret på erfaringerne fra foregående projekts prototypedesign blev en ide til et nyt og prisbilligt lagerdesign baseret på anvendelse af laminerede plastfoliesække afprøvet. Plastfolielaminatet er opbygget af 4 lag: PETP 12 μm/ Aluminium 9 μm/ PETP 12 μm/ LLDPE 80 μm. Folien kan modstå temperaturer op til ca. 100 °C Fordelen ved at anvende plastfoliesække er flere:

- Plastfoliesækkene medfører en meget lille varmekapacitet i selve "beholdermaterialet", hvilket har betydning for lagerets effektivitet specielt når et underafkølet salthydrat aktiveres med hensyn til krystallisering, hvor lageret opvarmes fra omkring stuetemperatur til salthydratets smeltepunkt på 58 °C. Energien til opvarmningen tages fra salthydratets smeltevarme, og hvis beholdermaterialet har en høj varmekapacitet, kan det i yderste konsekvens betyde, at lageret aldrig når op på de 58 °C, hvorved muligheden for opvarmning af varmt brugsvand går tabt. Risikoen er selvfølgelig størst jo mindre forholdet er mellem lagerets volumen og lagerets overfladeareal.
- Plastfoliesækkene er fleksible, hvorved de kan ændre form i takt med salthydratets volumenændringer – især ved faseskift. Dette kombineret med et design som vist i figur 11, vil sikre at der altid vil være en god termisk kontakt mellem salthydratet og de omkringliggende vandfyldte lag (rød/blå lag), der hhv. anvendes til opvarmning og afkøling af salthydratlageret.

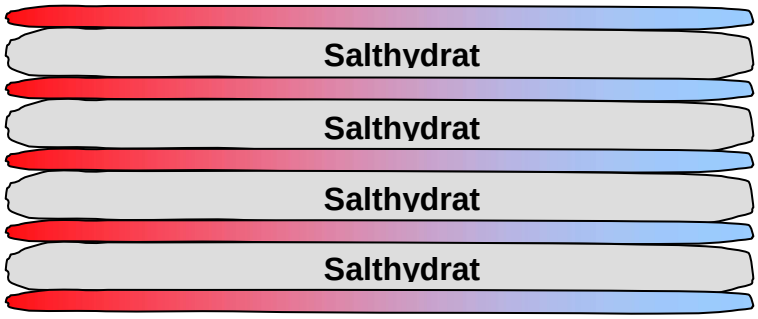

Figur 11. Ide til smeltevarmelager opbygget af fleksible plastfoliesække, hvor hver 2. lag indeholder salthydrat og hvert 2. lag gennemstrømmes af vand til hhv. op- og afladning af den enkelte sektion

Figur 12 viser et diagram over det påtænkte prototypelager, der indeholder 3 lag med salthydrat, hvor hvert lag individuelt kan køles/opvarmes fra oven eller fra neden ved cirkulation af vand gennem plastfoliesække identiske til de salthydratfyldte. Hvilket af de vandfyldte lag der er aktivt kontrolleres ved hjælp af trevejs- og magnetventiler.

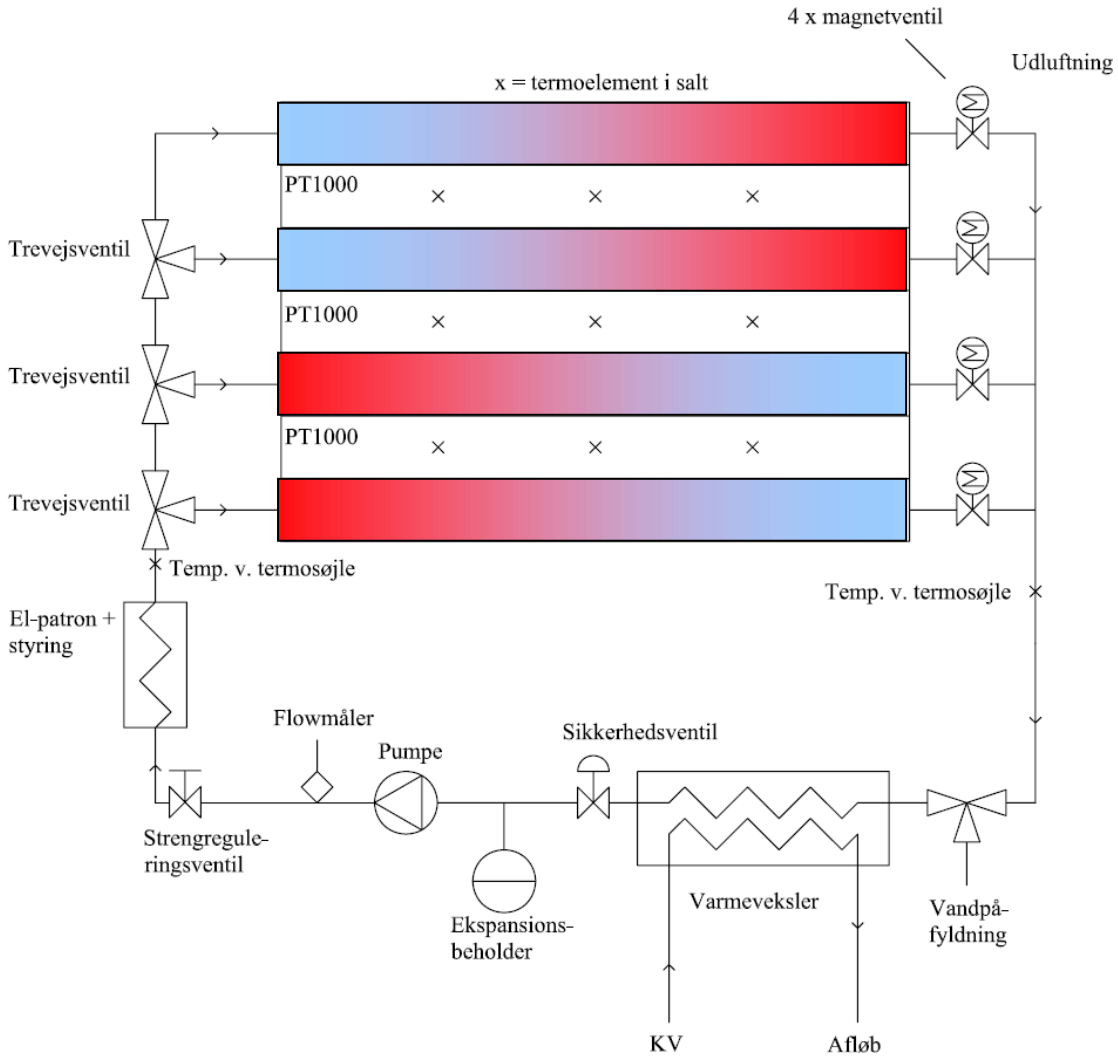

Figur 12. Diagram over planlagt prototypelager.

Princippet med fleksible vandfyldte lag mellem salthydratlagene medfører, at hvert vandfyldt lag der ikke benyttes må afspærres på både tilløbs- og afløbssiden, så vandtrykket i laget bibeholdes. Hvis ikke dette sikres, vil det fleksible lag klappe sammen på grund af vægten af de salthydrat- og vandlag, der ligger oven på. Et andet forhold, der skal tages hensyn til, er at sækkene meget let glider på hinanden, hvorfor hele lageret skal placeres i en stiv ramme, der kan fastholde sækkene horisontalt. Endelig skal rørforbindelserne være fleksible, så de kan følge med de vertikale bevægelser forårsaget af varierende volumen af salthydratlagene.

Forud for opbygning af prototypelageret beskrevet ovenstående blev en vandfyldt plastfoliesæk belastet med en vægt på 720 kg, uden at der opstod utætheder i svejsninger og omkring rørtilslutninger. Sækken blev herefter placeret på en blød mineraluldsmåtte og fyldt med ca. 15 liter natriumacetat trihydrat ved en temperatur på ca. 70 °C og efterladt ved rumtemperatur med det formål at lade salthydratet underafkøle.

Det viste sig desværre, at salthydratet ikke underafkølede. Tidligere små laboratorieforsøg havde vist, at underafkølingen er meget følsom overfor salthydratets vandindhold, der skal være over 41 – 42 % for at sikre en stabil underafkøling. Det aktuelle vandindhold viste sig kun at være ca. 38 % på grund af fordampning under opvarmningen og håndteringen af saltet, hvorfor ekstra vand blev tilsat. Den efterfølgende smeltning af salthydratet skete ved at placere plastfoliesækken ved ca. 72 °C i en varmluftovn i ca. et døgn liggende på den bløde mineraluldsplade. Under opvarmningen opstod der en lækage i en af sækkens svejsesømme, hvorved det delvist smeltede salt flød ud.

Årsagen til utætheden er ikke fuldt klarlagt, men en mulig forklaring er, at smelteprocessen starter i et lille område nær sækkens overflade. Ved smeltningen udvider salthydratet sig, og da det smeltende salt stadig er omgivet af størknet salt, der ikke giver efter, kan det tænkes, at der lokalt opstår et så stort tryk, at sækkens svejsesømme ikke kan modstå belastningen.

Efter dette og tidligere forsøg, der alle resulterede i lækager, måtte det konstateres, at løsningen med plastfoliesækkene desværre ikke kunne realiseres med den type sække, det havde været muligt at fremskaffe inden for projektets rammer.

Prøvesmeltevarmelager 2

Plastfoliesækkenes skrøbelighed krævede et nyt design af et prototypelager, der er i stand til at modstå de kræfter, der opstår i lageret ved faseskift. Derudover skal lageret stadig optimeres med hensyn til varmeovergangen ved afladning af lageret, jf. afsnit 2.2.1. Der er derfor opbygget et forsøgssmeltevarmelager i rustfrit stål med en klar akrylplade som låg, så man under forsøgene visuelt kan se, hvad der sker med hensyn til underafkøling og eventuel krystaldannelse. Forsøgssmeltevarmelageret måler indvendigt $1{,}14 \times 0{,}47 \times 0{,}05$ m^3, og det har to indbyggede kobbervarmevekslerspiraler, der hver har en længde på ca. 13,7 m og et overfladeareal på ca. 0,43 m^2 (ydre diameter = 10 mm). Nettovolumenet af lageret er 24,6 liter. De to varmevekslerspiraler er placeret henholdsvis liggende på lagerets bund og ca. 40 mm over bunden, dvs. i toppen af lageret. Herved bliver det muligt at aflade lageret fra toppen og oplade lageret fra bunden, hvorved den interne konvektion i lageret giver de mest gunstige betingelser for varmeoverføringen. Figur 13 viser en skitse af forsøgsvarmelagerets opbygning og figur 14 viser et foto af smeltevarmelageret med smeltet salt, hvor topisoleringen er fjernet.

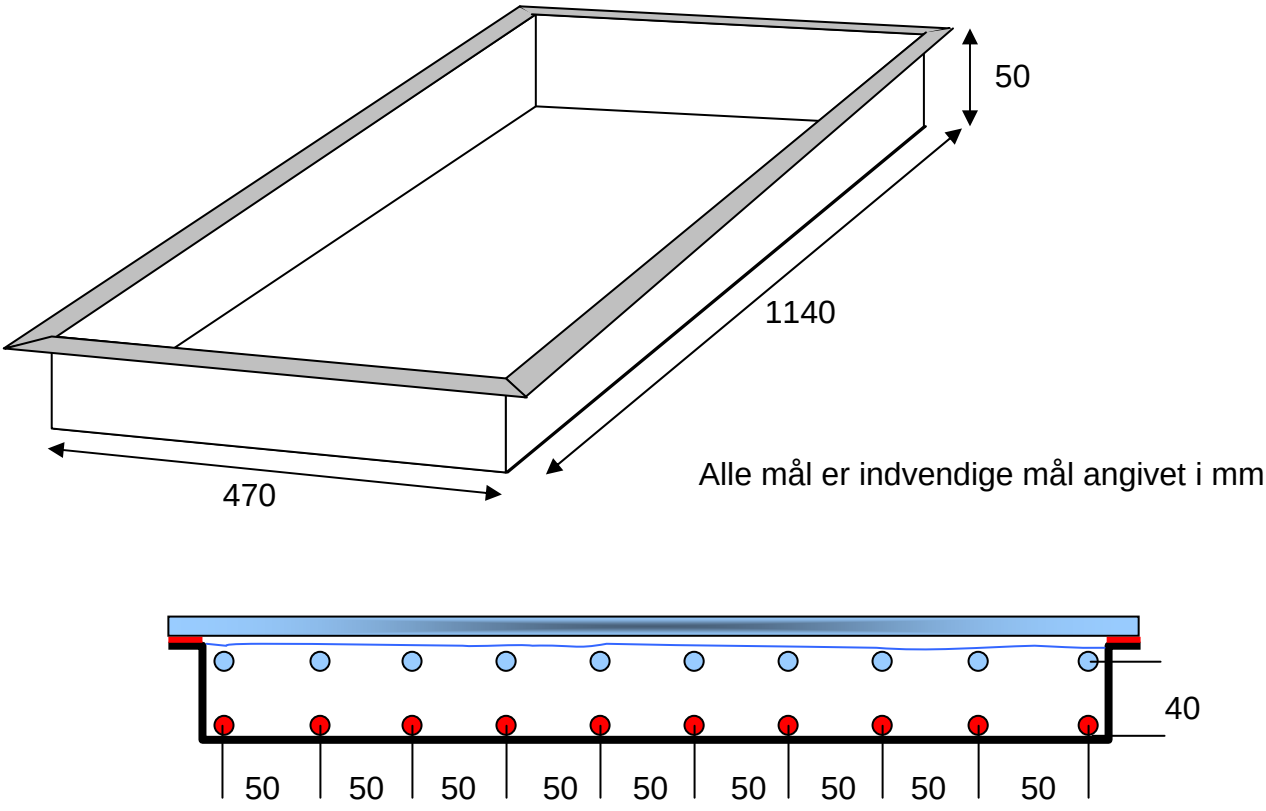

Figur 13. Skitse af forsøgssmeltevarmelagret. Nederst er vist et lodret snit, der viser placeringen af de to varmevekslere (rød og blå).

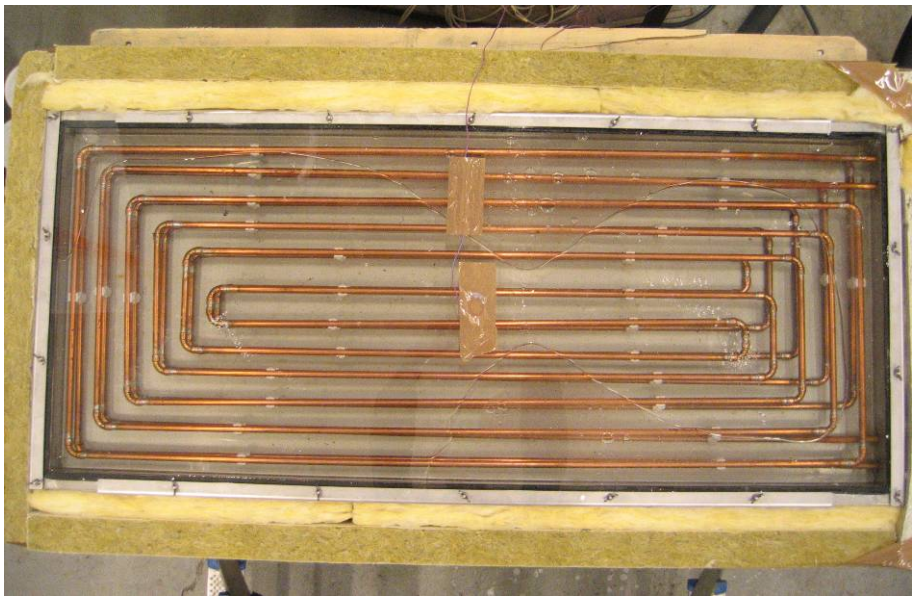

Figur 14. Foto af forsøgssmeltevarmelageret med smeltet salt.

Der er udført forsøg med opvarmning af størknet salt via varmevekslerspiralen i bunden af lageret og forsøg med afkøling af smeltet varmt salt via varmevekslerspiralen i lagerets top. Forsøgenes primære formål er at bestemme varmeoverføringsevnen mellem varmeveksleren og salthydratet i dets forskellige faser. Sekundært har forsøgene haft til formål at eftervise funktionen af underafkøling i praksis.

Figur 15 viser temperaturforløb og varmeoverføring ved opvarmning af størknet salt fra stuetemperatur til ca. 65 °C.

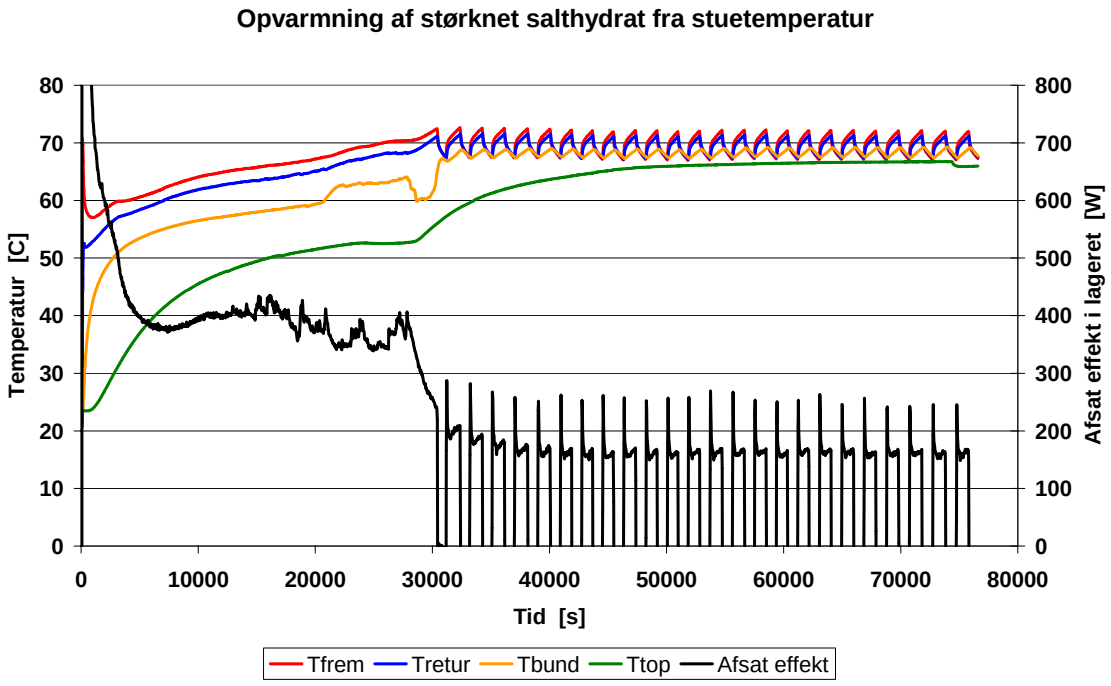

Figur 15. Opvarmning af størknet salthydrat fra stuetemperatur til ca. 65 °C. Rød og blå kurve er henholdsvis fremløbstemperatur og returtemperatur fra varmeveksleren. Orange kurve viser overfladetemperaturen midt på lagerets underside, dvs. udvendigt på den rustfrie stålbund. Den grønne kurve viser temperaturen midt på lagerets udvendige låg-overflade.

Figur 15 viser, at der hurtigt sker en opvarmning af lagerets nederste lag omkring varmeveksleren (orange kurve). Efter ca. 20.000 sekunder observeres et pudsigt hop på kurven, der indikerer, at hele laget omkring varmeveksleren er smeltet og den afsatte effekt derefter i højere grad anvendes til at øge temperaturen frem for til smeltning af saltet. Under hele denne proces er varmeoverføringen fra varmeveksleren næsten konstant på ca. 400 W.

Efter ca. 30.000 sekunder falder temperaturen ved lagerets bund brat, mens temperaturen ved lagerets top (grøn kurve) stiger markant. Årsagen hertil kan være, at det sidste lag salt i toppen af lageret netop er smeltet, hvorved den naturlige konvektion i lageret bevirker en kraftig opvarmning af lagerets top. Efter 30.000 sekunder begynder varmelegemets termostat at begrænse effektafgivelsen.

Varmeoverføringen for varmevekslerspiralen er altså fundet til ca. 400 W, hvilket svarer til ca. 62 W/K baseret på middeltemperaturen af frem og retur og temperaturen i bunden af lageret, hvor varmeveksleren er placeret. Varmeoverføringskoefficienten beregnet for varmevekslerspiralens overfladeareal på 0,43 m^2 bliver dermed ca. 145 W/m^2K. Volumenstrømmen gennem varmevekslerspiralen var under forsøget 2,64 liter/minut.

De teoretiske undersøgelser viste, at størrelsen af delvolumenerne i et sæsonvarmelager mindst skal være på 250 liter, hvilket er 10 gange større end det testede prøvelager. Dermed kan det konkluderes, at hvis varmevekslerspiralen opskaleres tilsvarende vil varmeoverføringskoefficient ved opvarmning blive større end 500 W/K og dermed være fuldt ud tilstrækkelig.

Figur 16 viser temperaturforløb og varmeoverføring ved afkøling af smeltet salt fra ca. 62 °C og ned til ca. 12 °C.

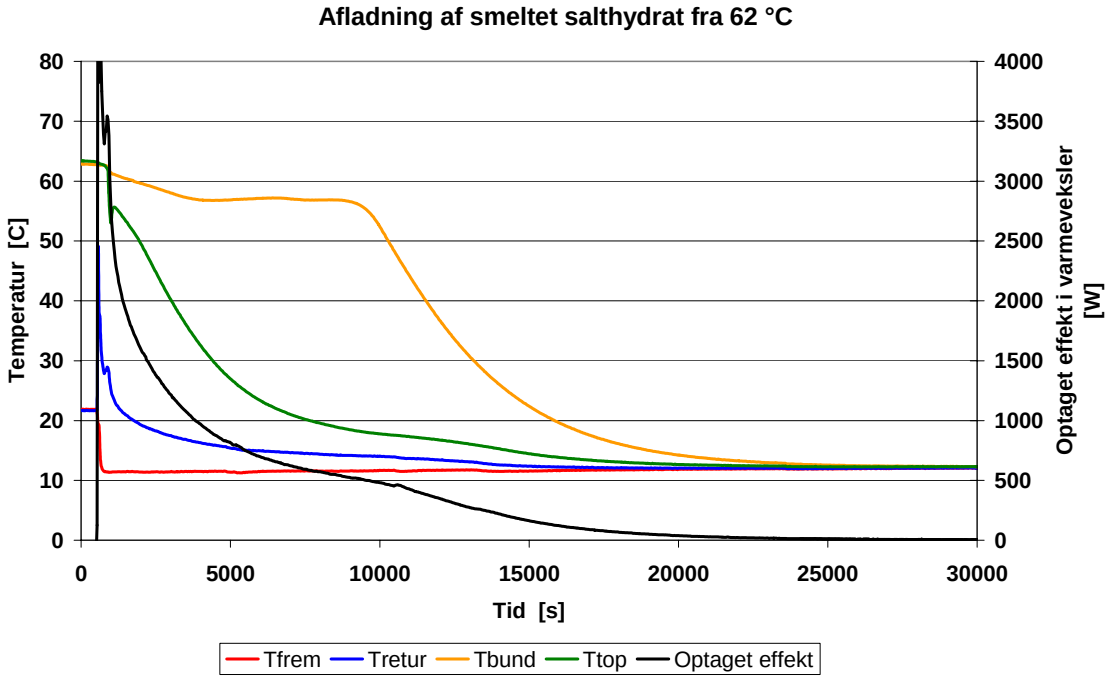

Figur 16. Afladning af smeltet salthydrat fra ca. 65 °C ned til ca. 12 °C.
Rød og blå kurve er henholdsvis fremløbstemperatur og returtemperatur fra varmeveksleren. Orange kurve viser overfladetemperaturen midt på lagerets underside, dvs. udvendigt på den rustfrie stålbund. Den grønne kurve viser temperaturen midt på lagerets udvendige låg-overflade.

Afladning af prøvelaget er foretaget ved at tilslutte fremløbet på varmeveksleren til koldtvandshanen i laboratoriet. I dette tilfælde er volumenstrømmen gennem varmeveksleren ca. 2,9 liter/minut.

Straks det kolde vand nåede indløbet til varmeveksleren begyndte saltet at krystallisere omkring varmeveksleren – først lige ved indløbet, hvor det var koldest, og derefter bredte krystaldannelsen sig langsomt rundt om varmevekslerens rør. Ved krystaldannelsen

udløses smeltevarmen for den del af saltet der er krystalliseret, hvilket også kan ses af temperaturkurverne i figur 16 for lagerets top (grøn kurve) og returtemperaturen fra varmeveksleren (blå kurve), hvor der kan konstateres et svagt ophold i temperaturfaldet i området 1000 - 1500 sekunder efter start. Det skal bemærkes at målingen af temperaturen ved lagerets top ikke repræsenterer saltets temperatur særlig godt, da målingen er foretaget oven på en 5 mm tyk akrylplade, der udgør lagerets "låg".

Temperaturen ved lagerets bund (orange kurve) viser tydeligt den karakteristiske temperaturkurve for et faseændringsmateriale. Først falder temperaturen ned til smeltepunktet (ca. 58 °C), hvorefter temperaturen er konstant indtil alt salthydratet er størknet, hvorefter temperaturen atter falder.

Effektoptagelsen i varmeveksleren (sort kurve) falder jævnt hen gennem afladningsprocessen, hvilket skyldes et jævnt voksende lag isolerende krystalliseret salt omkring varmevekslerrørene. I det øjeblik, at alt salthydratet i lageret er størknet, kan der opserveres et knæk på effektkurven, der viser, at der ikke mere frigives smeltevarme i lageret, og temperaturforskellen mellem varmeveksleren og lageret falder.

Varmeoverføringen mellem varmeveksleren og salthydratet er beregnet for perioden indtil alt saltet er størknet, dvs. ca. indtil 9000 sekunder efter start, hvor der er regnet med at lagertemperaturen svarer til temperaturen målt på lagerets underside. Varmeoverføringen er således fundet til ca. 22 W/K, hvilket svarer til en varmeoverføringskoefficient på 52 W/m^2K. Den lave varmeoverføringskoefficient sammenlignet med opvarmningssituationen skyldes selvfølgelig den øjeblikkelige krystaldannelse omkring varmeveksleren. På basis af resultatet vurderes det, at varmeoverføringsevnen for et fuldskala varmelager vil være tilstrækkelig høj.

Der er ikke umiddelbart nogen forklaring på, hvorfor krystaldannelsen med det samme optrådte omkring varmevekslerspiralen, idet vandindholdet i salthydratet er over de 41 – 42 %, der tidligere har vist sig at være nødvendigt. Figur 17 viser et billede af lageret efter forsøgets afslutning, hvoraf det tydeligt fremgår, at krystaldannelsen er sket omkring varmeveksleren og, at der er overskydende vand mellem varmevekslerens rør.

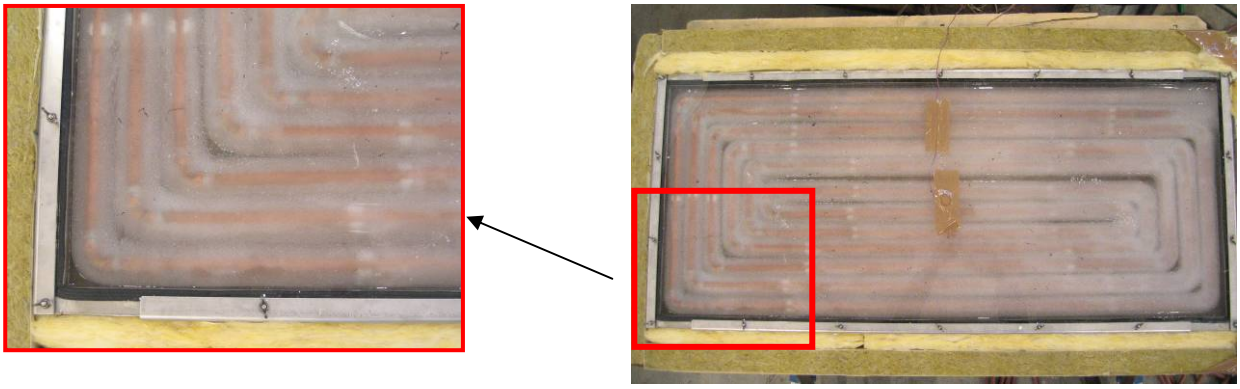

Figur 17. Foto af forsøgsmeltevarmelager efter afladningsforsøg. Krystaldannelsen er tydeligt lokaliseret omkring varmevekslerspiralen med overskydende vand rundt omkring.

Aktivering af faseskift i underafkølet salthydrat

Der er blevet udført en række små laboratorieforsøg med det formål at undersøge forskellige muligheder for en kontrolleret og automatiseret måde at udløse krystaldannelsen i et underafkølet salthydrat. Undersøgelserne har omfattet ultralyd, magnetisk påvirkning samt lokal kraftig opvarmning, men den mest lovende løsning er aktivering med et stempel, der er styret af en magnet.

Funktionen af stemplet er, at når stemplet skydes ind i et flydende salt, og derefter trækkes ud igen, vil der på stemplet befinde sig salthydrat, der omdannes til krystaller ved afkøling og udtørring. Når der derefter er behov for aktivering af det underafkølede salthydrat i lagret skydes stemplet ind i det underafkølet salt, hvorved krystallerne på stemplet igangsætter krystaldannelsen i lageret. Figur 18 viser et foto af opstillingen til aktiveringsforsøget.

Figur 18. Opstilling til afprøvning af magnetdrevet stempel til aktivering af krystaldannelsen i et underafkølet salthydrat.

Alternativt kan stemplet forbindes med en lille metalskive placeret inde i lageret, der ved en mekanisk påvirkning kan starte krystaldannelsen.

3. Avancerede vandlagre

I laboratoriet er der opbygget en prøvestand, hvor holdbarheden af forskelligt udformede nyudviklede stratifikationsindløbsrør bestående af stof kan undersøges.

Baggrund:

Temperaturlagdeling (stratificering) i varmtvandstanke spiller en vigtig rolle for effektiviteten af det energisystem som tanken er en del af. Et energisystem med en velstratificeret tank har en meget højere effektivitet end et energisystem med en tank uden stratificering. Temperaturlagdeling kan opbygges med forskellige metoder. En yderst simpel og effektiv metode er anvendelse af stratifikationsindløbsrør, f.eks. stratifications-indløbsrør fremstillet af stof. Stratifikationsindløbsrør af stof er ikke et kommercielt produkt

endnu. Nærværende skrivelse omhandler de undersøgelser der er gennemført som led i modning af produktet til kommercielt brug.

De første eksperimenter med stofindløbsrør blev gennemført med rør bestående af et stoflag. Ulempen ved denne konstruktion var et relativt stort varmetab fra stofrøret der førte til opvarmning af den nederste del af tanken.

De efterfølgende eksperimenter blev gennemført med rør bestående af to stoflag. Det uønskede varmetab blev reduceret drastisk. Eksperimenterne viste at der kan opbygges en god temperaturlagdeling med to lags stofindløbsrør både under opvarmnings- og afkølingsforsøg samt ved forsøg hvor toppen af tanken er varmet op til en temperatur der er højere end indløbstemperaturen mens bunden af tanken er koldere end indløbstemperaturen. Syv forskellige stoftyper blev afprøvet:

- Style 314, Texturized Nylon 6.6 Stretch Fabric, Double Knit
- Style 361, Spun Nylon 6.6 DuPont Type 200 Woven Fabric (ISO 105/F03)
- Style 703, Texturized Polyester, Woven
- Style 769, 100% Spun Dacron Type 54 Knit (Disperse Dyeable)
- Style 864, Spun Orlon Type 75 Acrylic Plain Weave
- Style 867, Acrilian 16 Acrylic Knit
- Style 981, Creslan Acrylic Type 61

Figur 20 - figur 22 viser temperaturerne målt i forskellige niveauer i en forsøgstank for hver 5. minut igennem et opvarmningsforløb med 50 minutters varighed for tre forskellige stratifikationsindløbsrør: Indløbsrør bestående af et stoflag, indløbsrør bestående af to stoflag samt et plastikrør med huller hvori der er monteret en flap der kan åbne og lukke fra det tyske firme Solvis GmbH & Co KG. Figurerne viser også temperaturer som de ville have været efter 20 og 50 minutter hvis der ikke forekom omrøring, dvs. at stratifications-indløbsrørene virkede perfekt. Indløbet til stratifikationsrøret er igennem bunden af tanken (de stiplede linier). Udløbet er også placeret i bunden af tanken. Indløbstemperaturen er omkring 40°C og den pumpedrevne volumenstrøm er 2 l/min.

Skematiske illustrationer af plastrøret med huller med flapper (flapperne fungerer som kontraventiler hvor vand kan forlade røret men ikke løbe ind i røret) og indløbsrøret bestående af to stoflag er vist i figur 19.

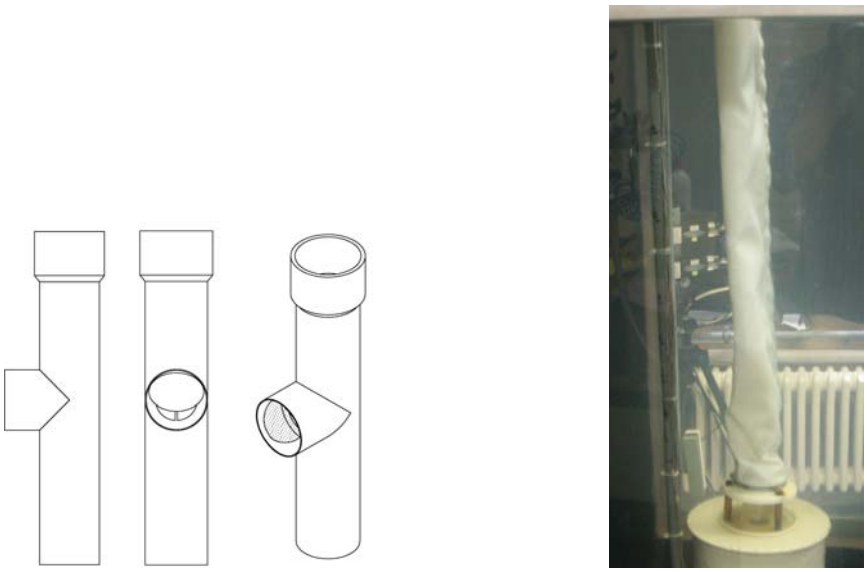

Figur 19. Venstre: Sektioner af plastrør med huller med flapper. Højre: Storindløbsrør.

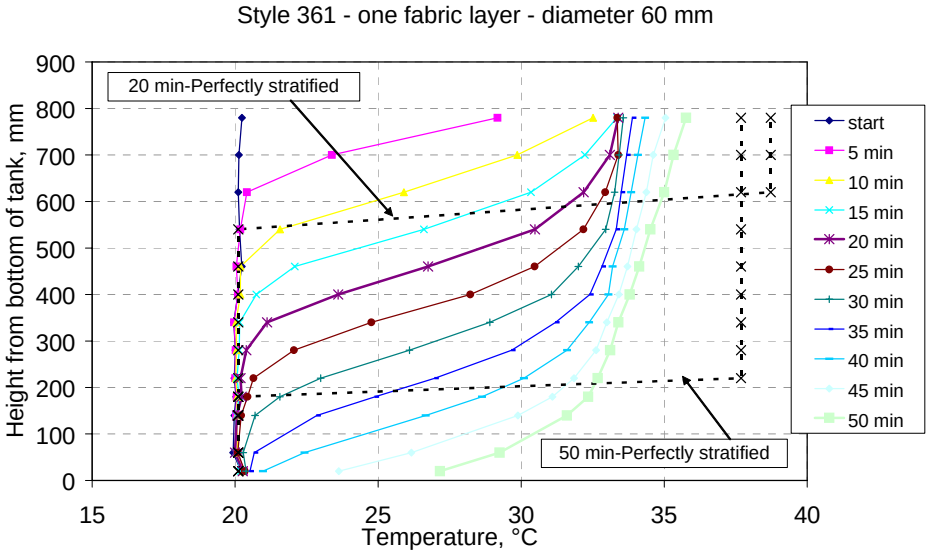

Figur 20. Temperaturprofiler i tanken til forskellige tidspunkter under opvarmningsforløbet med et stofindløbsrør bestående af et stoflag.

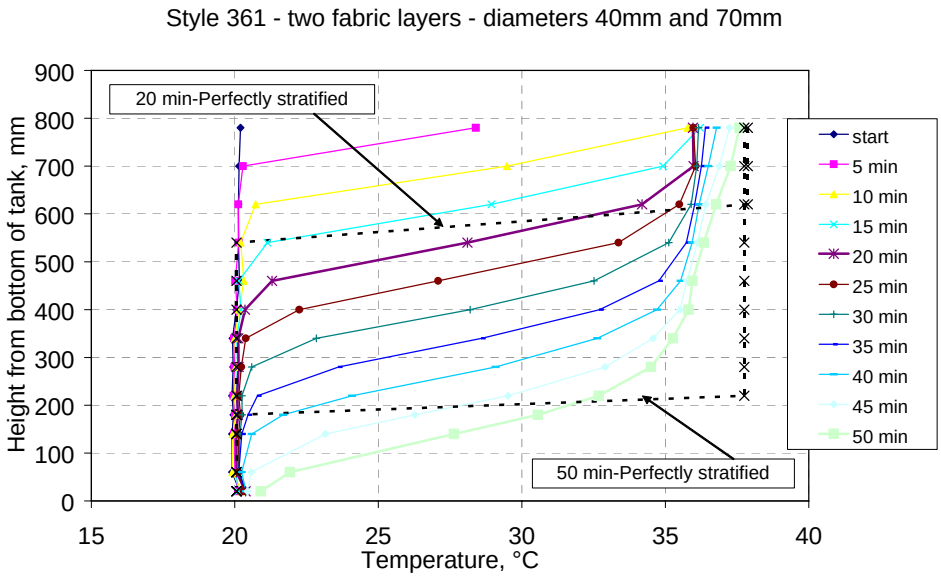

Figur 21. Temperaturprofiler i tanken til forskellige tidspunkter under opvarmningsforløbet med et stofindløbsrør bestående af to stoflag.

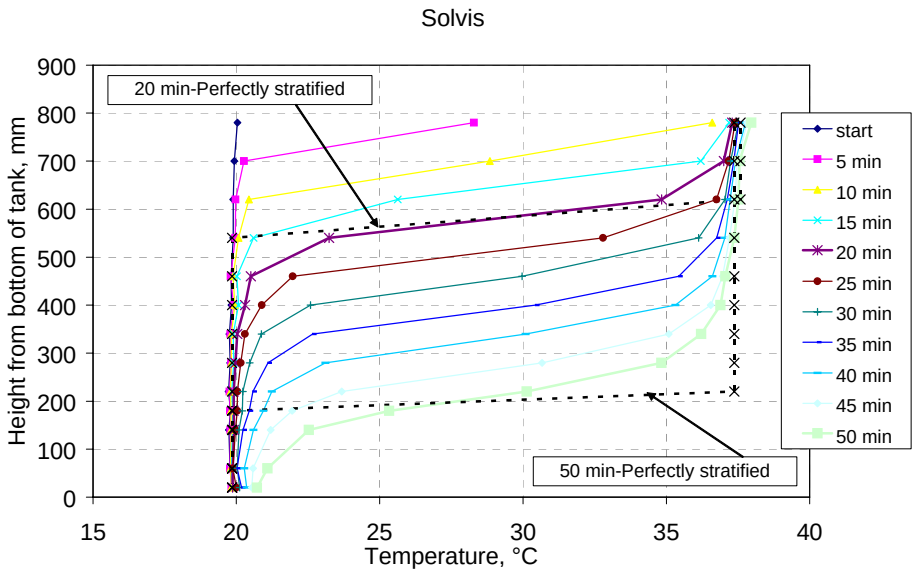

Figur 22. Temperaturprofiler i tanken til forskellige tidspunkter under opvarmningsforløbet med plastrøret med huller med flapper.

Undersøgelserne er detaljeret beskrevet i [2].

Flere eksperimenter blev udført med forskellige volumenstrømme. Ved undersøgelserne blev plastrøret med huller med flapper samt to forskellige stratifikationindløbsrør bestående af to stoflag anvendt:

- Style 864, Spun Orlon Type 75 Acrylic Plain Weave (ikke-strækbar)
- Style 700-12, Filament polyester, Poly-Lycra (strækbar)

Der blev anvendt volumenstrømmene på 6, 8 og 10 l/min under opvarmningsforsøg hvor en tank blev opvarmet igennem et stratifikationsindløbsrør fra 20°C til 32- 40°C (faldende fremløbstemperatur for stigende volumenstrøm).

Indløbet til stratifikationsrøret er igennem bunden af tanken. Udløbet er også placeret i bunden af tanken. Undersøgelserne viser at stofrøret funger virkelig godt ved høje volumenstrømme. Især det afprøvede stofrør bestående af fleksibelt stof klarede sig godt med høje volumenstrømme.

Figur 23 – figur 25 viser den dimensionsløse temperaturer målt i forskellige niveauer i en forsøgstank efter udskiftning af 30, 60 og 90 liter for de tre forskellige stratifikations-indløbsrør.

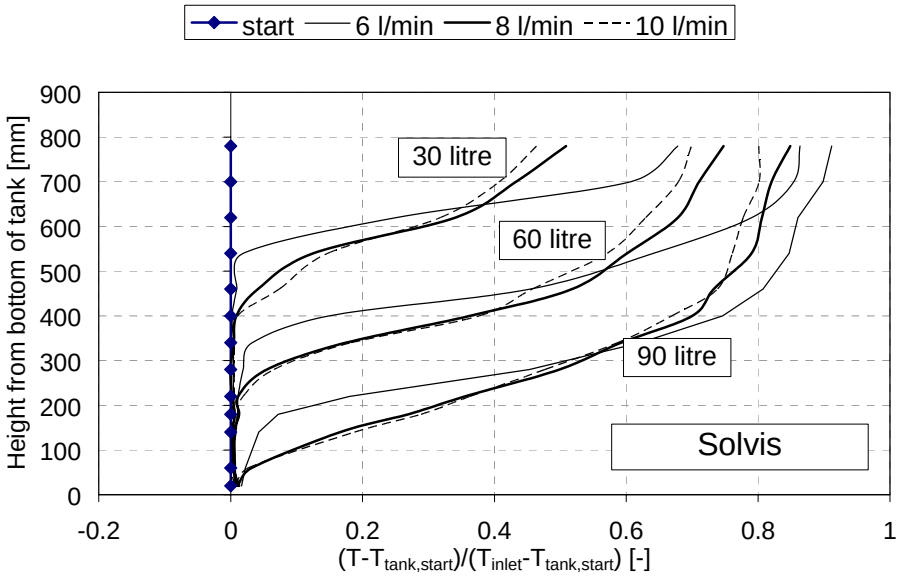

Figur 23. Temperaturprofiler i tanken til forskellige tidspunkter under opvarmningsforløbet med plastrøret med huller med flapper. Den pumpedrevne volumenstrøm er 6 l/min, 8 l/min and 10 l/min.

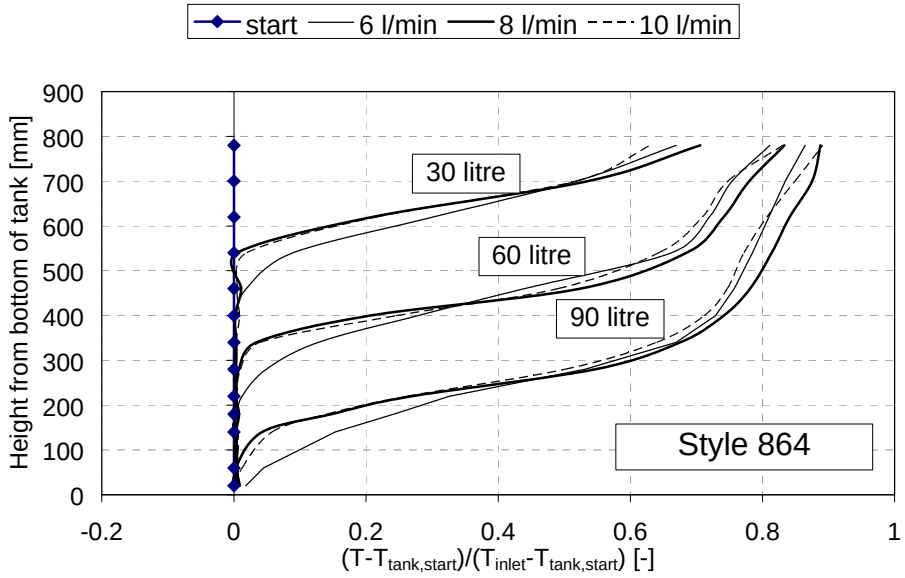

Figur 24. Temperaturprofiler i tanken til forskellige tidspunkter under opvarmningsforløbet med et stofindløbsrør bestående af to stoflag (Style 864). Den pumpedrevne volumenstrøm er 6 l/min, 8 l/min and 10 l/min.

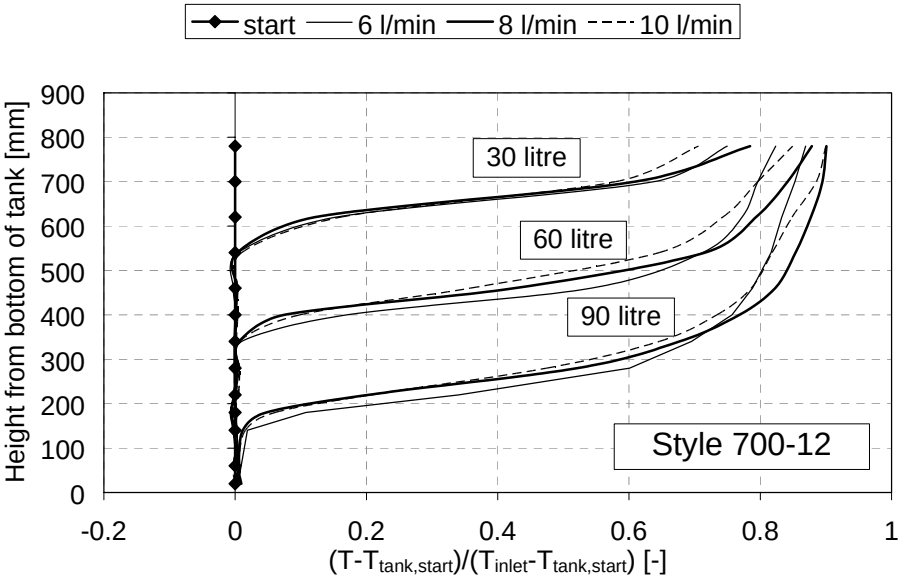

Figur 25. Temperaturprofiler i tanken til forskellige tidspunkter under opvarmningsforløbet med et stofindløbsrør bestående af to stoflag (Style 700-12). Den pumpedrevne volumenstrøm er 6 l/min, 8 l/min and 10 l/min.

Undersøgelserne er detaljeret beskrevet i [3] og [4].

På baggrund af de meget lovende resultater blev stofstratifikationsindløbsrøret patenteret i august 2006.

Langtidsholdbarhedstests:
Undersøgelserne blev påbegyndt i 2007. Formålet med forsøgene er at undersøge om stofrørenes evne til at opbygge temperaturlagdeling i vandtanke reduceres igennem tiden, evt. som følge af kalk eller som følge af belægninger på stoffets overflade.

Stratifikationsindløbsrør fremstillet af syv forskellige stoftyper samt plastrøret med huller med flapper er eksperimentelt undersøgt i to forskellige tanke med tankvolumen på 400 liter: En tank er en brugsvandstank hvor frisk koldt brugsvand føres ind i bunden af tanken under tapning (frisk vand indeholder mere eller mindre kalk afhængig af hvor i landet vandet kommer fra). Den anden tank er en rumvarmetank hvor vandet ikke udskiftes, blot cirkuleres. De to anlæg benævnes henholdsvis ”Running water” og ”Still water”. Alle stofrørene består af to lag stof med en indre diameter på 40 mm og en ydre diameter på 70 mm. Plastrøret har en indre diameter på 60 mm og der er 300 mm mellem udløbåbningerne.

De eksperimentelt undersøgte stoftyper er

- Style 864, Spun Orlon Type 75 Acrylic Plain Weave width 45” Weight 135 gm/m^2
- Style 769, 100% Dacron Type 51 Knit (Disperse Dyeable) Width 30” Weight 231 gm/m^2
- Style 700-12, Poly-Lycra Width 63” Weigth 4.3oz
- Style 700-3, Poly Taffetta Width 60” Weight 1.8oz
- Style 361, Spun Nylon 6.6 DuPont Type 200 Woven Fabric Width 42”/43” Weight 124 gm/m^2 (ISO 105/F03)
- Style 981, Creslan Acrylic Type 61 Width 45” Weight 135 gm/m^2
- Style 867, Spun Acrilian 16 Acrylic Knit Width 44”/45” Weight 143 gm/m^2

Figur 26Figur 26. Billeder af tanke og stratifikationsindløbsrør under installationen på DTU BYG.viser billeder af de to forskellige tanke og stratifikationsrørene under installationen.

Stratifikationsindløbsrørene er monteret i en cirkel omkring tankens centerlinie. Stofrørene bestående af to lag stof er monteret koncentrisk på studse tilvirket af plastik. I toppen er stofrørene ligeledes monteret koncentrisk på plastikstudse. I toppen er der monteret et lag stof således at vand kan forlade det inderste rør i vertikal retning. Plastrøret med huller med flapper består af fire sektioner og det er åbent i toppen således at vand kan forlade plastrøret i vertikal retning.

Figur 26. Billeder af tanke og stratifikationsindløbsrør under installationen på DTU BYG.

Resultater:

De eksperimentelle undersøgelser er udført som opvarmningsforsøg hvor en kold tank er opvarmet via et stratifikationsindløbsrør ad gangen. Volumenstrømmen under opvarmning er 6 l/min og fremløbstemperaturen er 50ºC.

Figur 27 - figur 34 viser som eksempel temperaturlagdelingen ved opvarmningsforsøg i rumvarmetanken kaldet "Still water". Y-aksen viser tankhøjden regnet fra bunden af tanken og x-aksen viser den dimensionsløse temperatur. Graferne fra de forskellige opvarmningsforløb kan dermed direkte sammenlignes.

Figurerne viser at alle stratifikationsindløbsrørene er gode til at opbygge temperature-lagdeling i tanken, specielt er plastrøret og stoftypen 867 gode til det. Det ses ved at der opnås de højeste temperaturer i toppen af tanken.

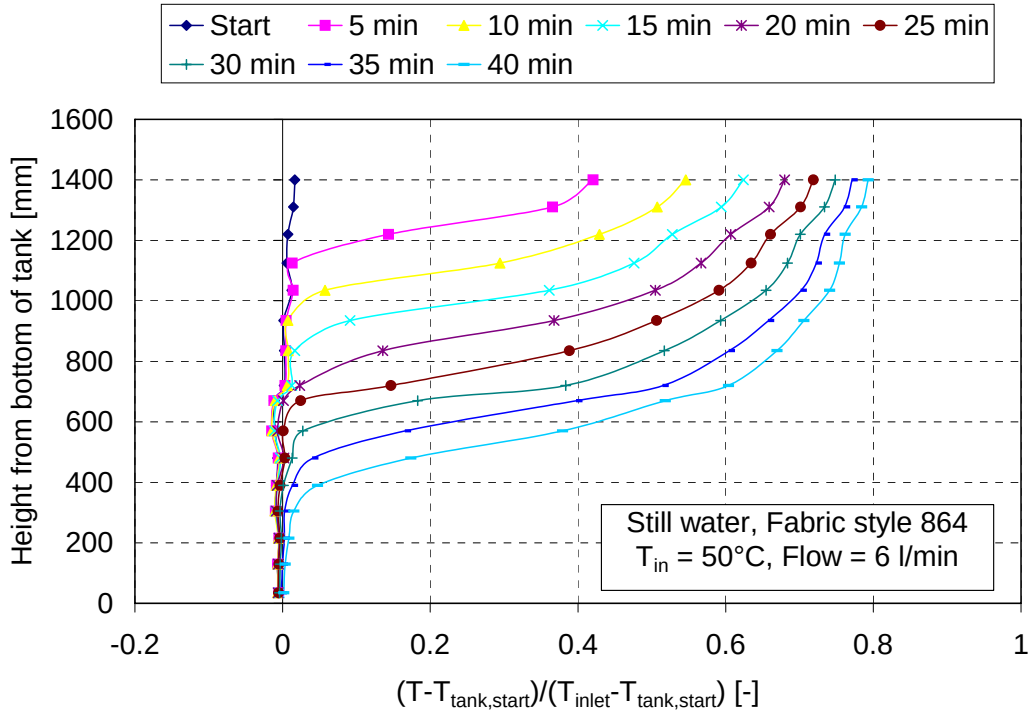

Figur 27. Temperaturprofiler i rumvarmetanken til forskellige tidspunkter under opvarmningen med et stofindløbsrør bestående af to stoflag (Style 864). Den pumpedrevne volumenstrøm er 6 l/min.

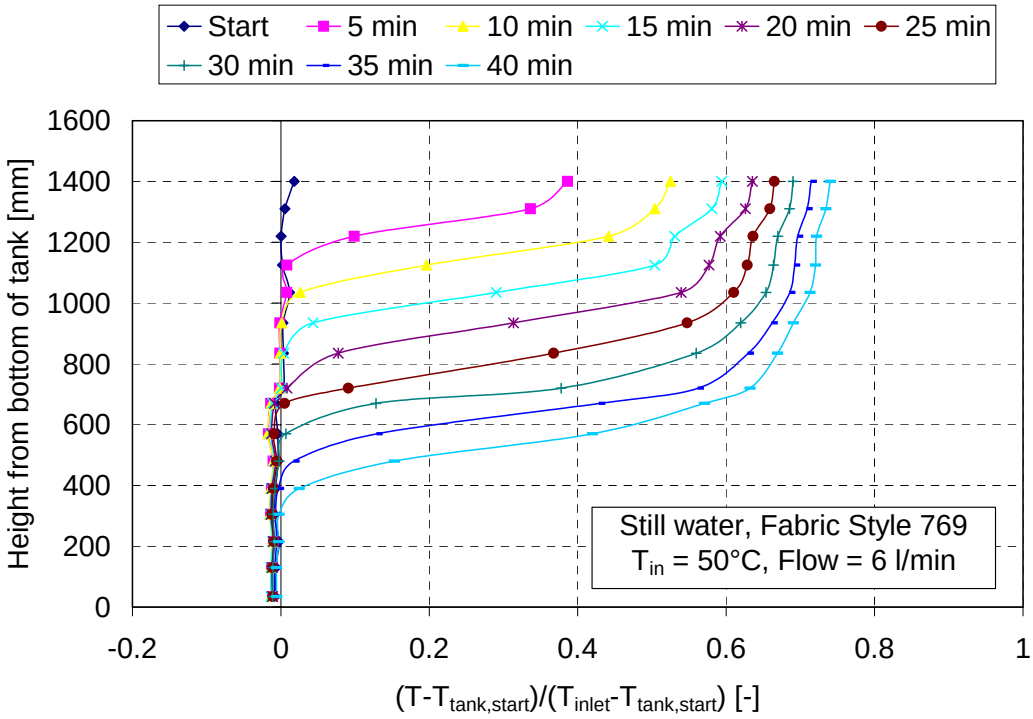

Figur 28. Temperaturprofiler i rumvarmetanken til forskellige tidspunkter under opvarmningen med et stofindløbsrør bestående af to stoflag (Style 769). Den pumpedrevne volumenstrøm er 6 l/min.

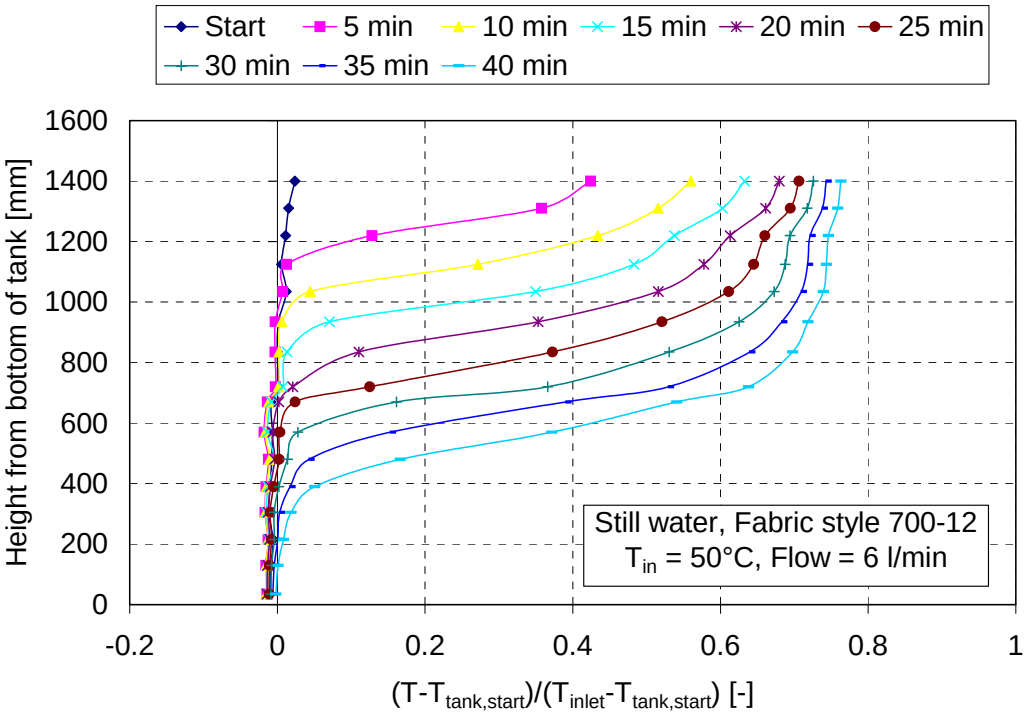

Figur 29. Temperaturprofiler i rumvarmetanken til forskellige tidspunkter under opvarmningen med et stofindløbsrør bestående af to stoflag (Style 700-12). Den pumpedrevne volumenstrøm er 6 l/min.

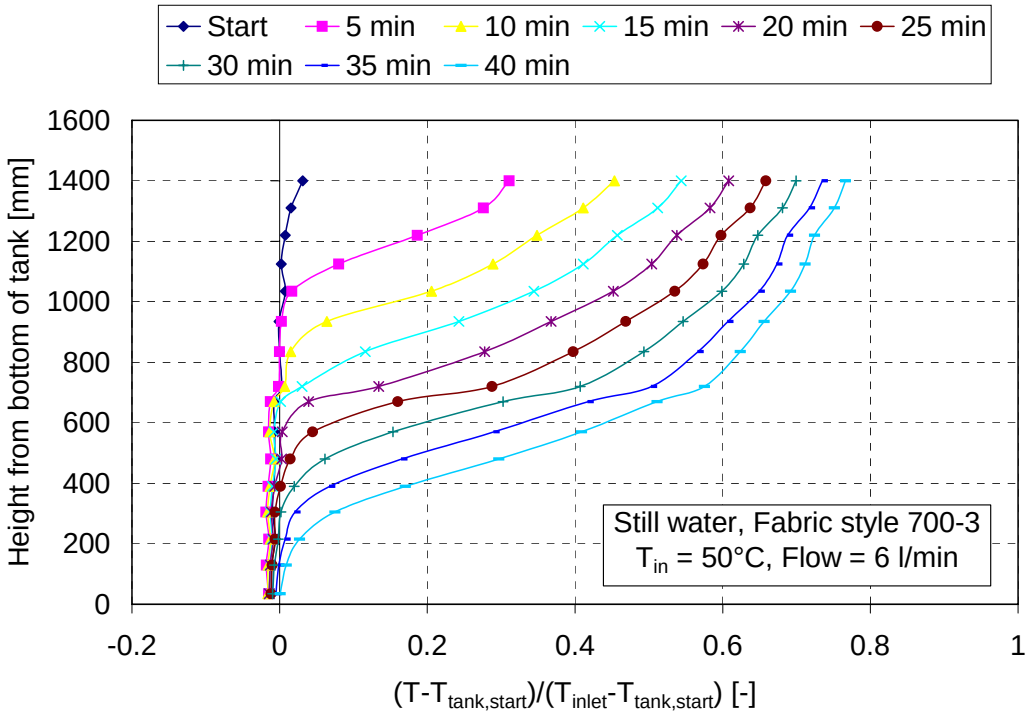

Figur 30. Temperaturprofiler i rumvarmetanken til forskellige tidspunkter under opvarmningen med et stofindløbsrør bestående af to stoflag (Style 700-3). Den pumpedrevne volumenstrøm er 6 l/min.

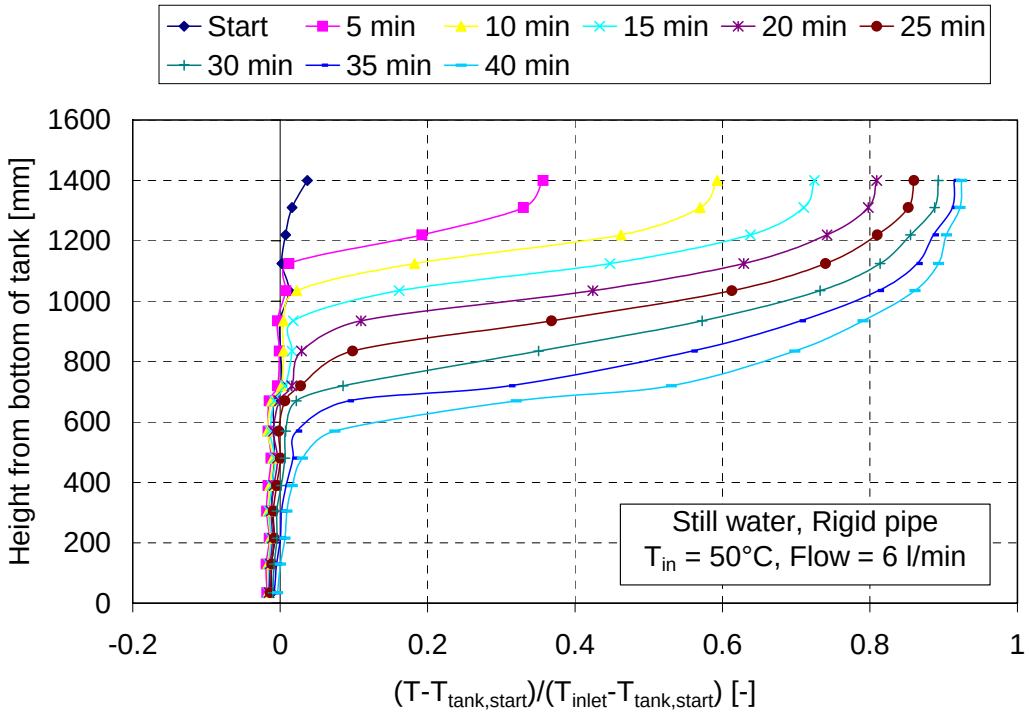

Figur 31. Temperaturprofiler i rumvarmetanken til forskellige tidspunkter under opvarmningen med Plastrøret med huller med flapper. Den pumpedrevne volumenstrøm er 6 l/min.

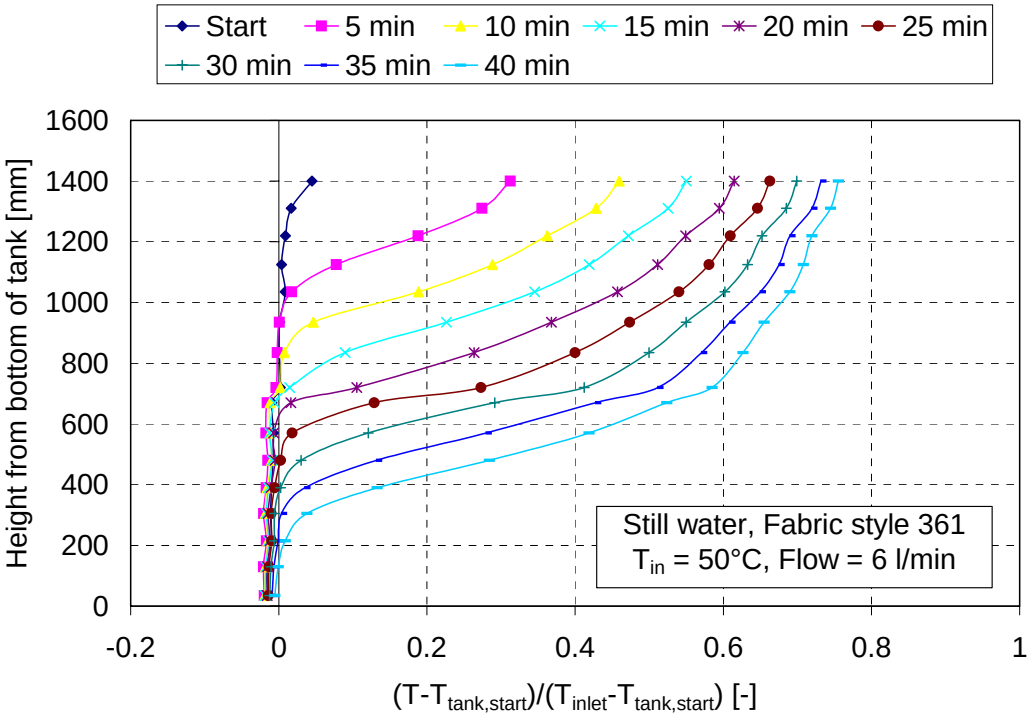

Figur 32. Temperaturprofiler i rumvarmetanken til forskellige tidspunkter under opvarmningen med et stofindløbsrør bestående af to stoflag (Style 361). Den pumpedrevne volumenstrøm er 6 l/min.

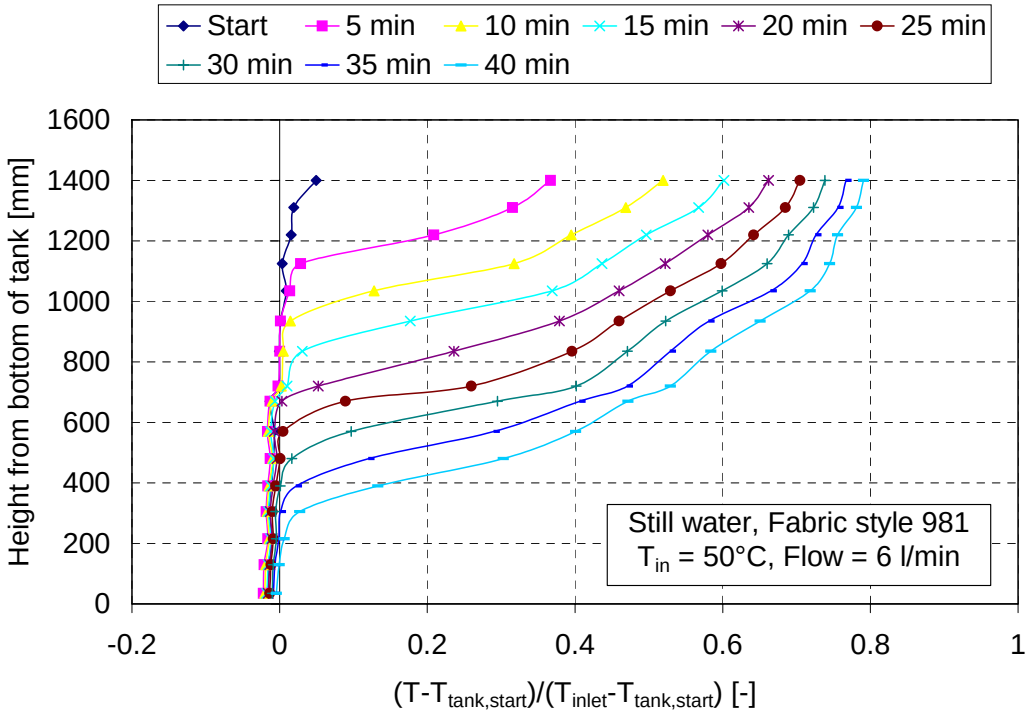

Figur 33. Temperaturprofiler i rumvarmetanken til forskellige tidspunkter under opvarmningen med et stofindløbsrør bestående af to stoflag (Style 981). Den pumpedrevne volumenstrøm er 6 l/min.

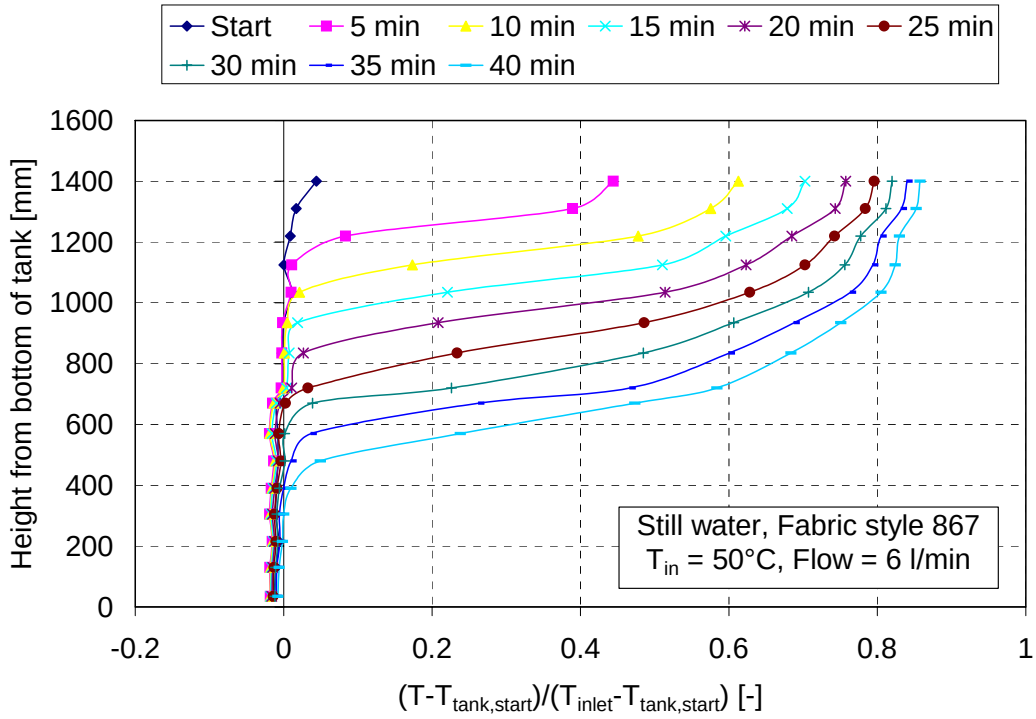

Figur 34. Temperaturprofiler i rumvarmetanken til forskellige tidspunkter under opvarmningen med et stofindløbsrør bestående af to stoflag (Style 867). Den pumpedrevne volumenstrøm er 6 l/min.

Erfaringer:

En af de vigtigste erfaringer der er gjort er at stofrørene er følsomme overfor forkert montering. Stofrørene skal således monteres med en indbyrdes afstand mellem det inderste og yderste stofrør i hele rørets udstrækning (f.eks. ved at fastholde røret i koncentriske cirkler i både bund og top). Desuden skal stofrøret monteres helt lodret, og stofrøret skal strække sig hele vejen fra tankens bund til tankens top.

Der er indtil videre ikke konstateret nogen ændringer i form af nedadgående ydelse. De foreløbige resultater tyder altså på en god holdbarheden af stofindløbsrørene.

På basis af holdbarhedsforsøgene er komplette solvarmeanlæg med indbyggede stofstratifikationsindløbsrør i varmelagrene opbygget og afprøvet.
Desuden er der gennemført et stort antal beregninger af ydelsen af solvarmeanlæg med og uden stratifikationsindløbsrør. På basis heraf er de ydelsesmæssige fordele ved stratifikationsindløbsrør bestemt. Ydelsen af solvarmeanlæg med varmelagre med stratifikationsindløbsrør kan forøges med op til 15% sammenlignet med traditionelle solvarmeanlæg.

4. Afslutning

De undersøgte koncepter: Sæsonvarmelagring baseret på et stabilt underafkølende salthydrat og avancerede vandlagre med indbyggede stofindløbsrør er særdeles lovende. Derfor vil der blive ansøgt om midler til at færdigudvikle sæsonsmeltevarmelagre og avancerede vandlagre med indbyggede stofindløbsrør vil blive forsøgt markedsmodnet i samarbejde med beholderfabrikanter.

5. Referencer

[1] Furbo, S.; Andersen, E.; Schultz, J.M. „Advanced storage concepts for solar thermal systems in low energy buildings". BYG•DTU SR-06-01, 2006.

[2] Andersen, E., Furbo, S., Jianhua, F., 2007. Investigations of fabric stratifiers for solar tanks, Solar Energy, Vol. 81, No. 10, pp. 1219-1226.

[3] Andersen, E., Furbo, S., 2006. Fabric inlet stratifiers for solar tanks with different volume flow rates, in proceedings of EuroSun 2006 Congress, Glasgow, Scotland.

[4] Andersen, E., Furbo, S., Hampel, M., Heidemann, W., Müller-Steinhagen, H., 2007. Investigations on stratification devices for hot water heat stores, International Journal of Energy Research.

Bilag 1

Simulation and optimization report – Theoretical investigations of solar combisystems.

IEA SH&C Task 32 Subtask D. November 2007.

Elsa Andersen

Simulation and optimization Report – Theoretical investigations of Solar Combisystems

A report of IEA Solar Heating and Cooling programme - Task 32
Advanced storage concepts for solar and low energy buildings
Report of Subtask D

Date: November 2007

Author:
Elsa Andersen

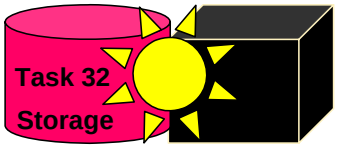

Content

1 General description of the Solar Combisystems

Main features

The solar combisystems are meant to supply single family houses with domestic hot water and space heating. Schematics of the solar combisystems are shown in Figure 1. The investigation is theoretical and the systems are modelled in TRNSYS.

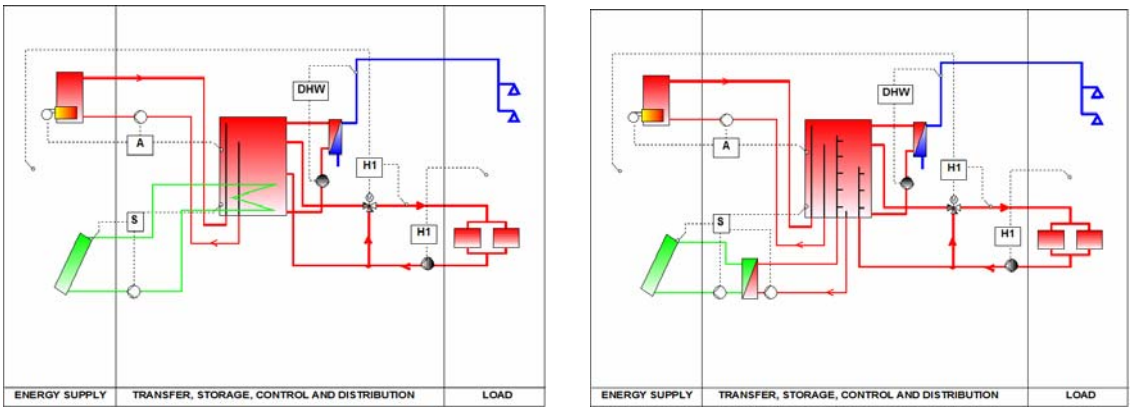

Figure 1. Schematics of the solar combisystems used in the investigations.

The first solar combisystem, shown to the left in Figure 1, is based on a space heating storage with an external heat exchanger mounted in a side arm for domestic hot water preparation. Solar energy is transferred to the storage through an emerged heat exchanger spiral situated in the lower part of the storage (relative inlet/outlet height 0.3/0.01) and direct flow outlet to and return inlet from the space heating loop (relative return inlet height 0.3).
The second solar combisystem, shown to the right in Figure 1, is also based on a space heating storage with an external heat exchanger mounted in a side arm for domestic hot water preparation. Energy from the solar collector is transferred to the storage via an external heat exchanger and a perfectly working stratification inlet pipe and the return inlet from the space heating loop is lead through a perfectly working inlet stratification pipe.

2 Modelling of the Solar Combisystems

2.1 TRNSYS model

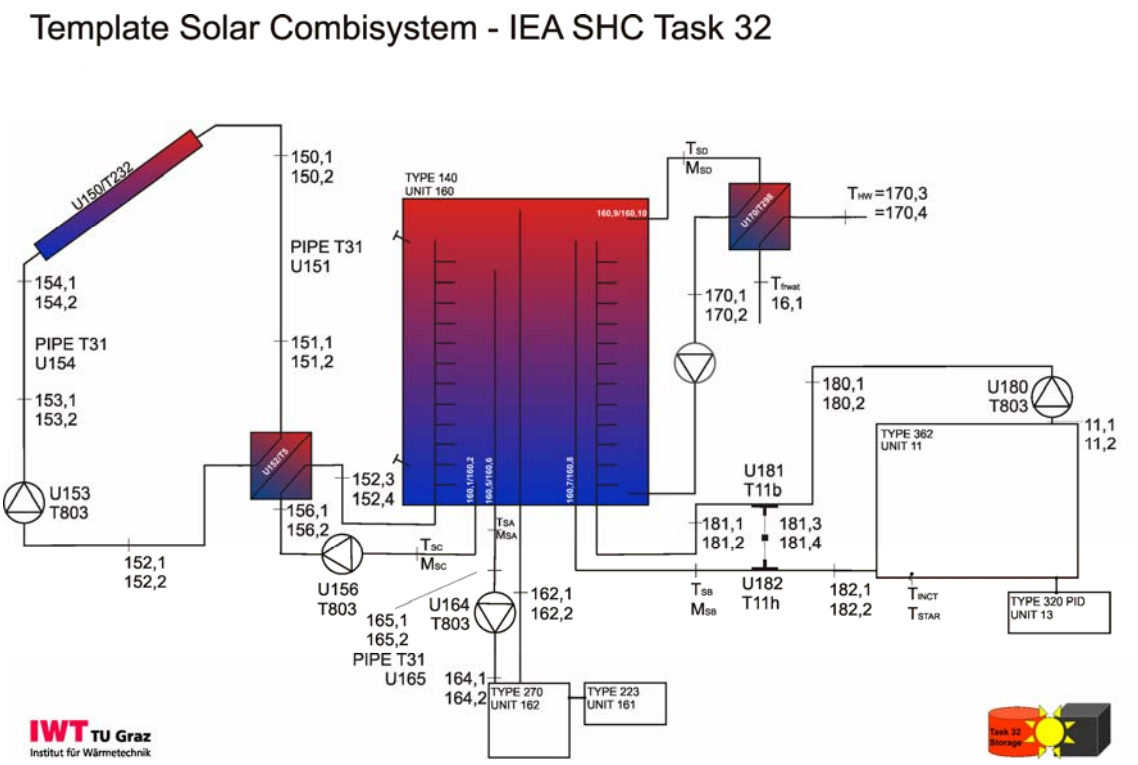

Figure 2. Modelling of Solar Combisystem in TRNSYS

2.2 Definition of the components included in the system and standard input data

2.2.1 General Setting in the TRNEDIT template

General Settings (to be chosen by TRNEDIT):

Main	
simulation timestep	1/20 h
tolerance integration / convergence	0.003 / 0.003
length of simulation	13 months
climate	Zürich/Stockholm/Madrid/Barcelona
building	SFH15/SFH30/SFH60/SFH100
Auxiliary	
Nominal Power of Auxiliary	90000 kJ/h
Set temperature Auxiliary into store	62 °C
Auxiliary temperature rise	10 K
Collector	
type	flat plate selective (ref)
aperture area	5 – 40 m^2
tilt angle	45°
azimuth (0° = south, 90° = west, 270° east)	0°
primary loop specific mass flow rate (Low flow – High flow)	15 kg/(h·m^2) – 72 kg/(h·m^2)
upper / lower dead band (switch on / off, Low flow – High flow)	7 K/4 K – 7 K/1 K
relative height of low temperature sensor in store (Low flow – High flow)	0.05 / 0.1
cut-off temperature of collector	90 °C
boiling temperature of collector fluid	110 °C
Store	
storage volume	1.00 m^3
insulation thickness (λ=0.042 W/mK)	0.16 m
correction factor for heat loss	1.4

All other parameters are detailed specified in the reference template (Heimrath and Haller, 2007). No space cooling demand of the house during summer in hot climates is considered, only space heating demand is considered.

3 Parameter variations

3.1 Presentation of results

The parameters varied are the location, the climate, the insulation degree of the single family house and the size of the heating system and the solar collector area. The results are shown as Fsav,therm (Letz, 2002) as function of the solar collector area. Also the extra Fsav,therm as

function of the solar collector area is shown. The extra Fsav,therm is the difference in Fsav,therm between the to solar combisystems (strsol_strSH – hxsol_fixSH).

Parameter:	Collector size [m^2] (fixed store size 1.0 m^3 and weather data from Zürich)	5 – 40 m^2

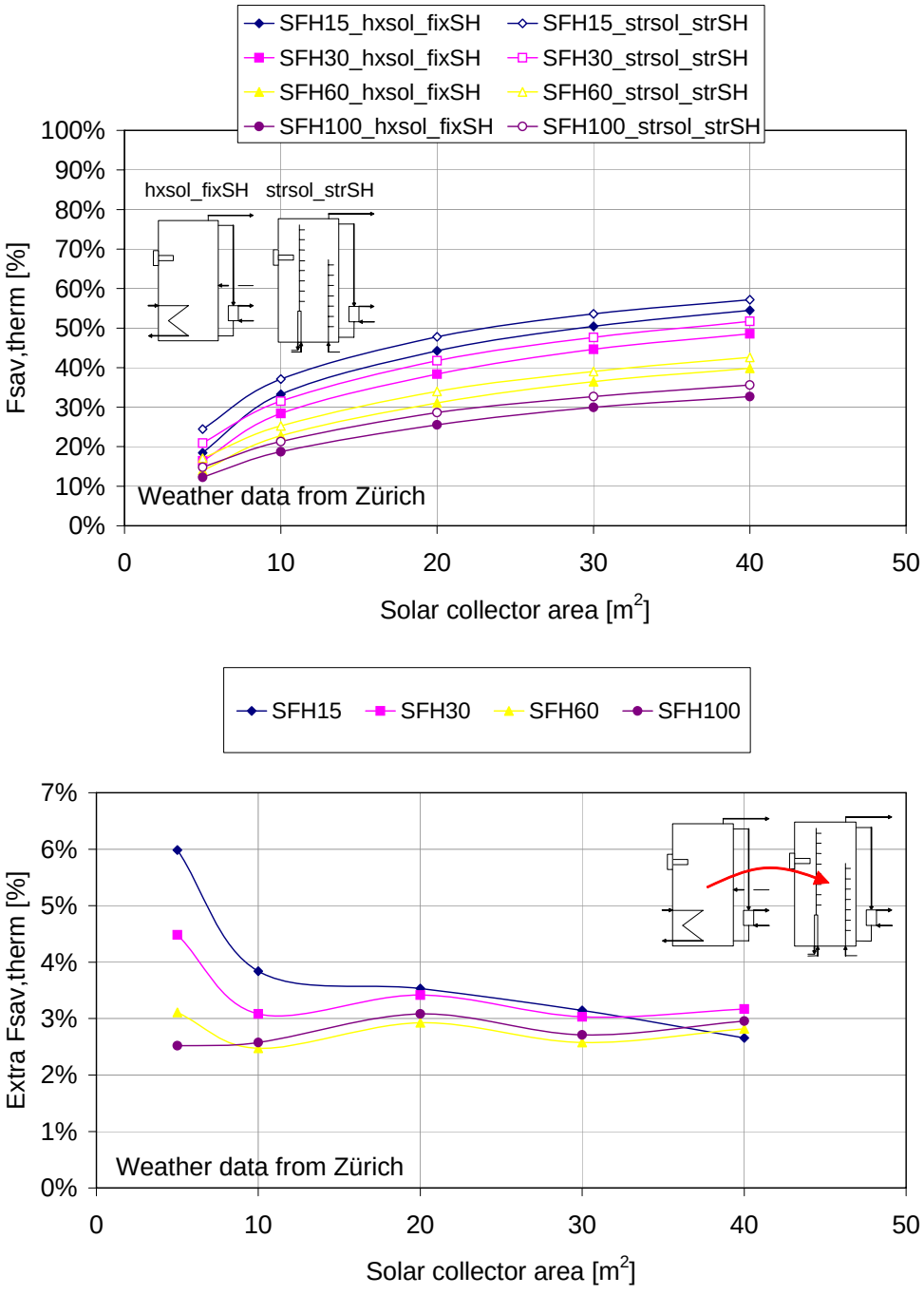

Figure 3. Variation of fractional energy savings with collector size with fixed store volume of 1.0 m^3 and weather data from Zürich.

Parameter:	Collector size [m^2] (fixed store size 1.0 m^3 and weather data from Stockholm)	5 – 40 m^2

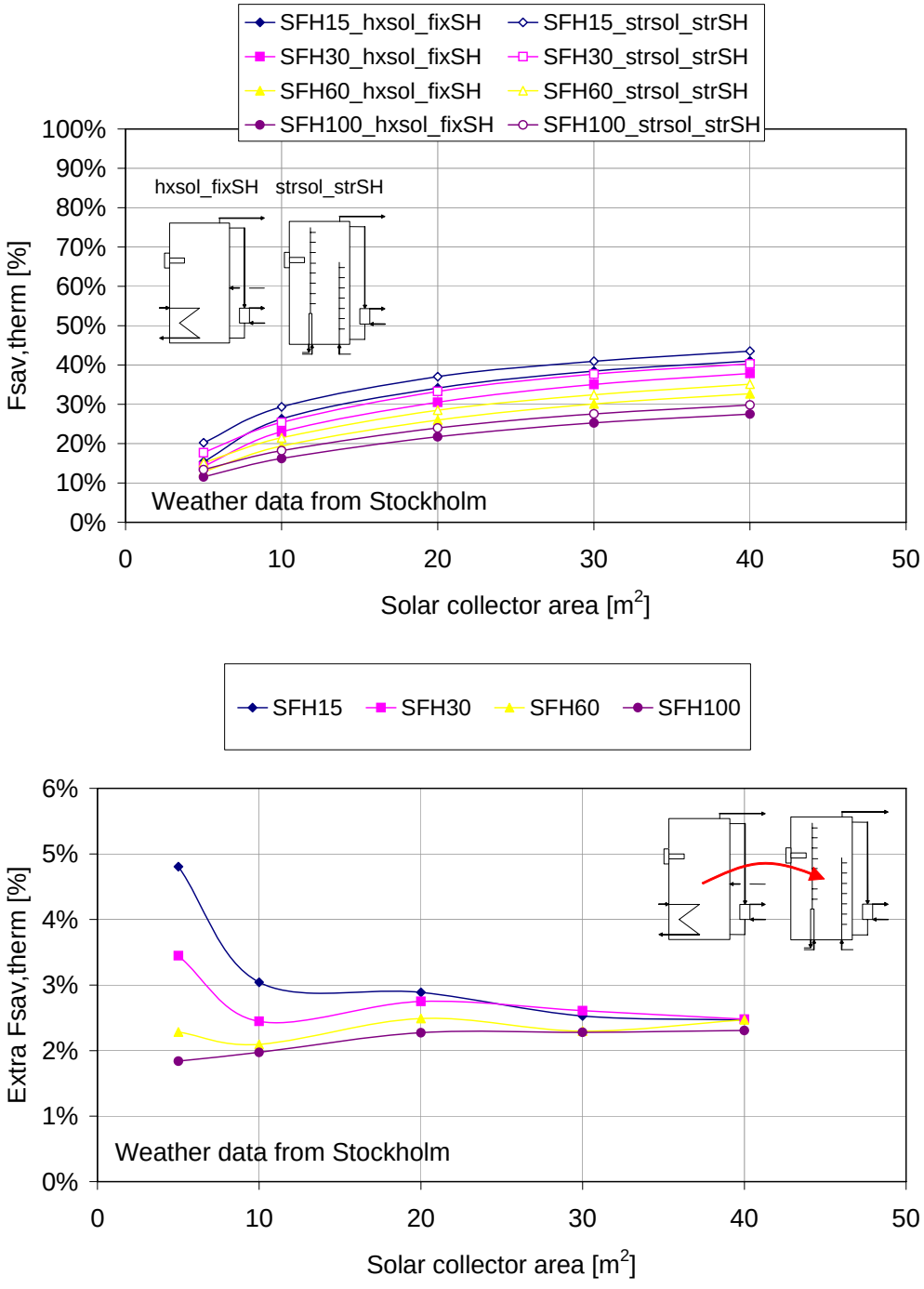

Figure 4. Variation of fractional energy savings with collector size with fixed store volume of 1.0 m^3 and weather data from Stockholm.

Parameter:	Collector size [m^2] (fixed store size 1.0 m^3 and weather data from Madrid)	5 – 40 m^2

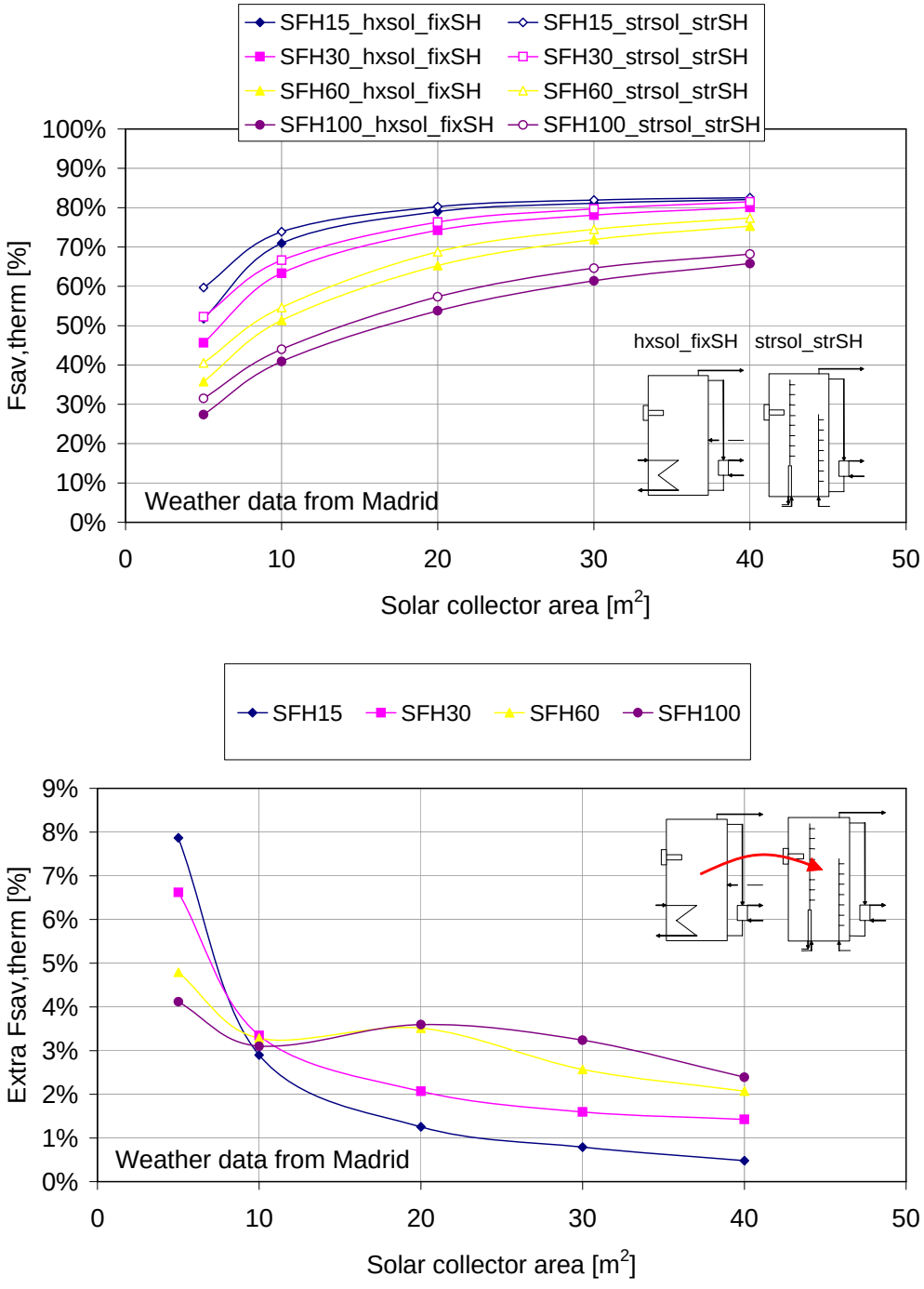

Figure 5. Variation of fractional energy savings with collector size with fixed store volume of 1.0 m^3 and weather data from Madrid.

Parameter:	Collector size [m^2] (fixed store size 1.0 m^3 and weather data from Barcelona)	5 – 40 m^2

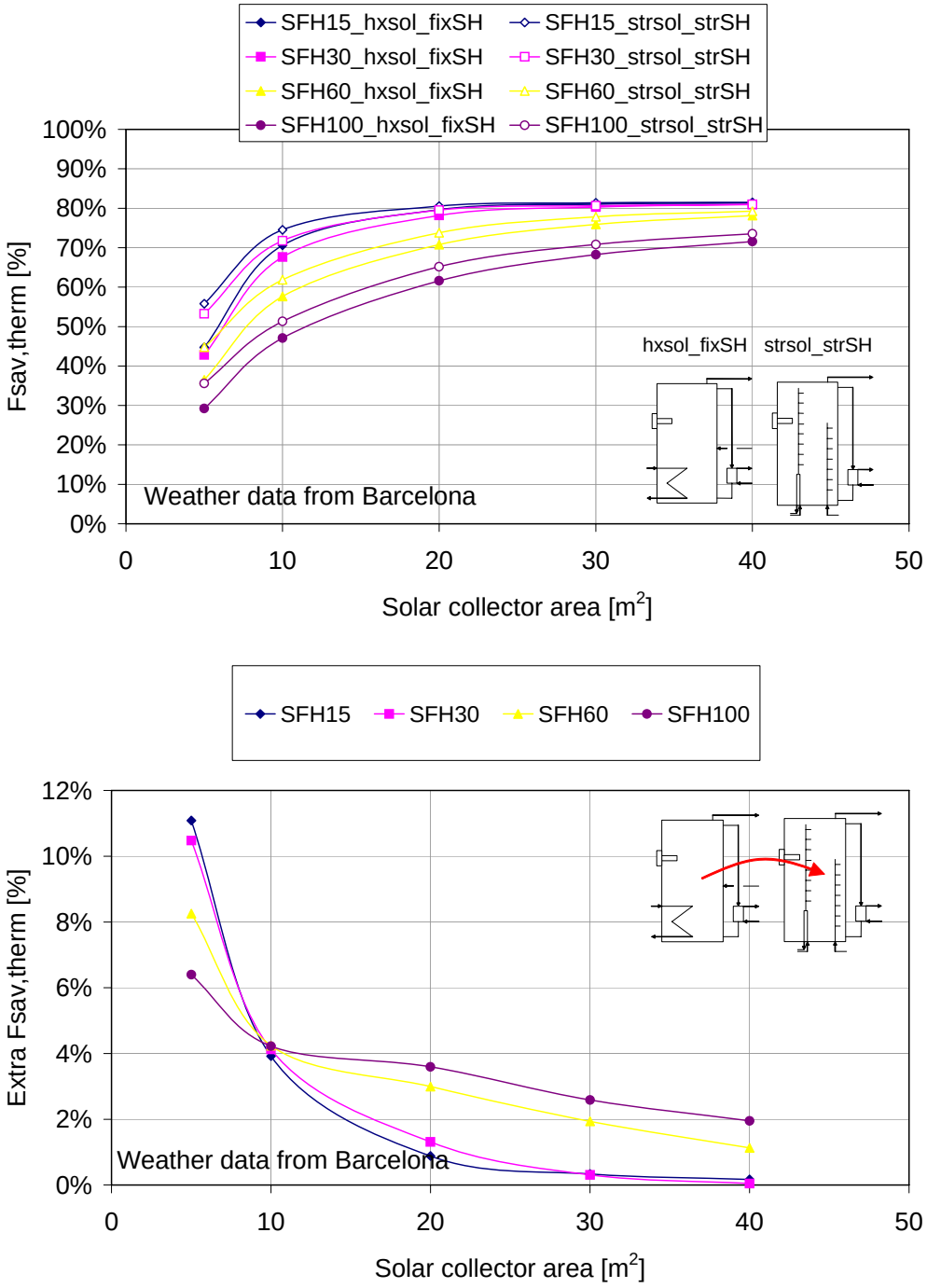

Figure 6. Variation of fractional energy savings with collector size with fixed store volume of 1.0 m^3 and weather data from Barcelona.

Description of Results

The fractional energy savings increase with increasing solar collector area and the extra fractional energy saving, by using perfectly working stratifiers, decreases with increasing solar collector area. For fractional energy savings of about 80%, the extra fractional energy

saving, by using perfectly working stratifiers, is less than 2%. The largest extra fractional energy savings, by using perfectly working stratifiers, is achieved with the smallest systems with the lowest fractional energy savings.

4 Analysis using FSC

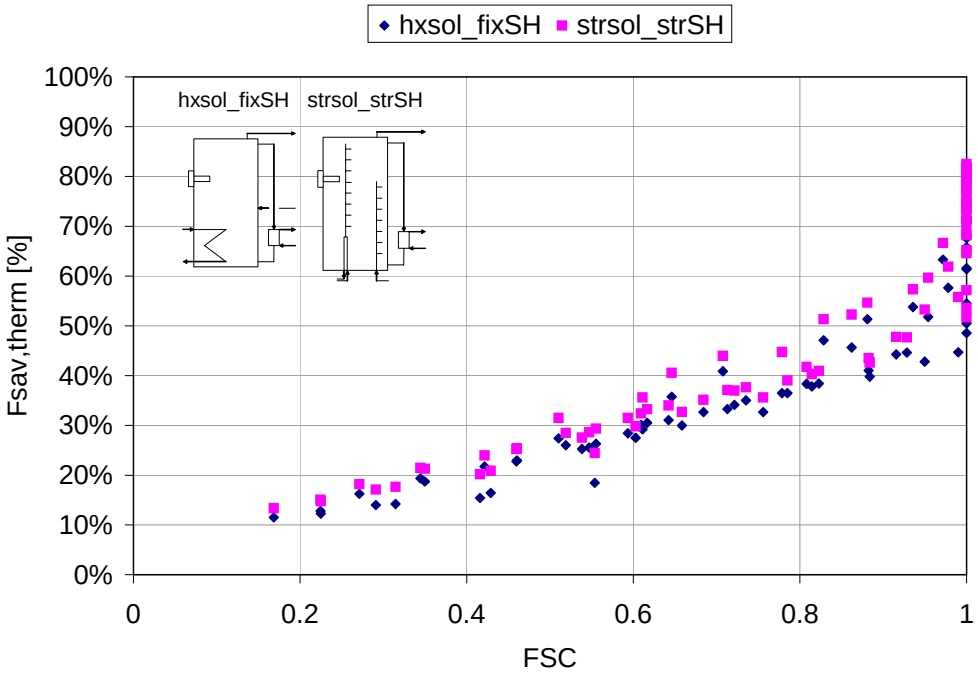

Figure 7. Variation of fractional energy savings with the fractional solar consumption for 4 climates (Zürich, Stockholm, Madrid and Barcelona) and 4 loads (15, 30, 60 and 100 kWh/m²a single family building). The storage volume is 1000 litres and the solar collector area is varied from 5 m^2 – 40 m^2.

5 References

Heimrath R., Haller, M., 2007, Project Report A2 of Subtask A, the Reference Heating System, the Template Solar System, A Report of the IEA-SHC Task32

Letz T., 2002, FSC Method, internal paper Task 26

6 Appendix 1: Description of Components specific to this System

These are components are not part of the TRNSYS standard library.

6.1 Type 340 : Multiport Storage Model

Version 1.99F, March 2006

Parameters : 126
Inputs : 30
Outputs : 86+number of nodes

Please refer to TRNSYS Description of Type 340 – by Harald Drück, Institut für Thermodynamik und Wärmetechnik (ITW), University Stuttgart, Germany

Availibility : ITW

Bilag 2

Type 185. Phase change material storage with supercooling.

January 2008.

Jørgen M. Schultz

TYPE 185
Phase Change Material storage with supercooling

Jørgen M. Schultz
Department of Civil Engineering, Technical University of Denmark
Building 118, Brovej, DK-2800 Kgs. Lyngby
Tel: +45 4525 1902, Fax: +45 45883282, E-mail: js@byg.dtu.dk

General description of the principle

The supercooling characteristic of some Phase Change Materials (PCM's) can be used in seasonal PCM-storages to lower the heat loss from the storage, i.e. the storage can cool down below the melting point without solidifying and the heat of fusion energy is not released. If the supercooled storage temperature reaches the temperature of the surroundings no further heat loss will take place and the storage becomes heat loss free. When a need for energy occurs the solidification of the supercooled PCM can be activated and heat of fusion is released leading to an almost immediate rise in temperature to the melting point. Some of the heat of fusion energy is used to heat up the PCM but still a large amount of energy is available. The principle is shown in figure 8.1.1 for Sodium Acetate Tri-hydrate that has a melting point of 58°C and a heat of fusion energy of 265 kJ/kg.

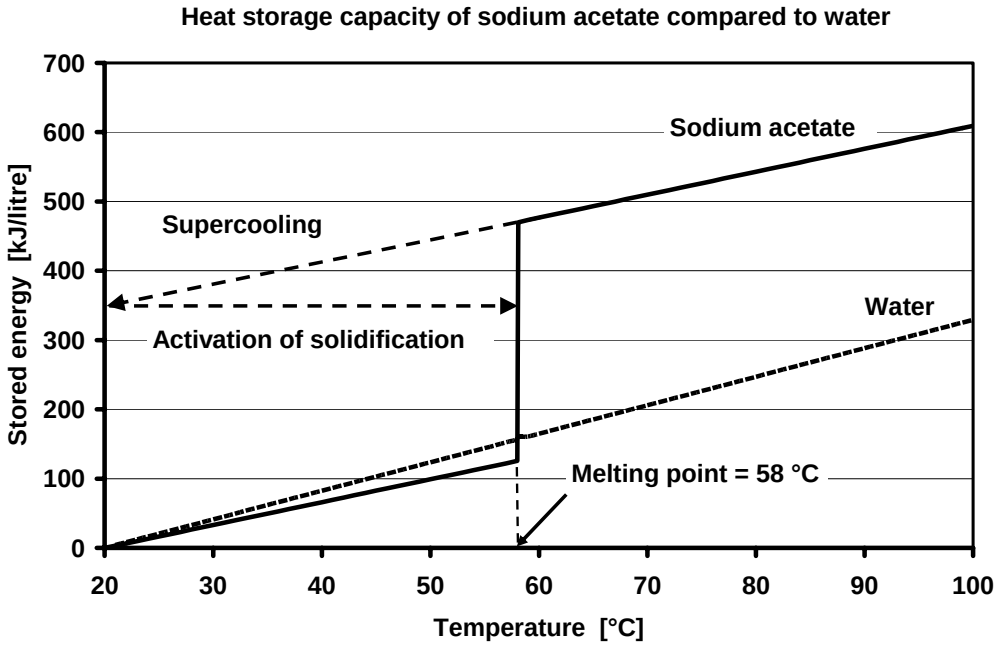

Figure 8.1.1 Illustration of energy density of sodium acetate compared to water as well as the super cooling process.

If the solidification is started the total volume will solidify, i.e. the total amount of latent heat in the supercooled PCM will be released and the supercooled state can only be reached after the total volume has been fully melted again. Therefore it is preferable to divide the total storage volume into several individual sub-volumes that can be controlled individually with respect to charging, discharging and activation of solidification, so the actual demand can be

met by activation of the required volume only. This has lead to definition of the following model.

Model description

Two different designs of the PCM storage can be modelled: 1) a cylindrical storage with the subsections stacked on top of each other (figure 8.1.2) or 2) a distributed storage, where the sub-volumes are placed side by side e.g. for the purpose of integrating the storage in a "slab on ground" floor construction.

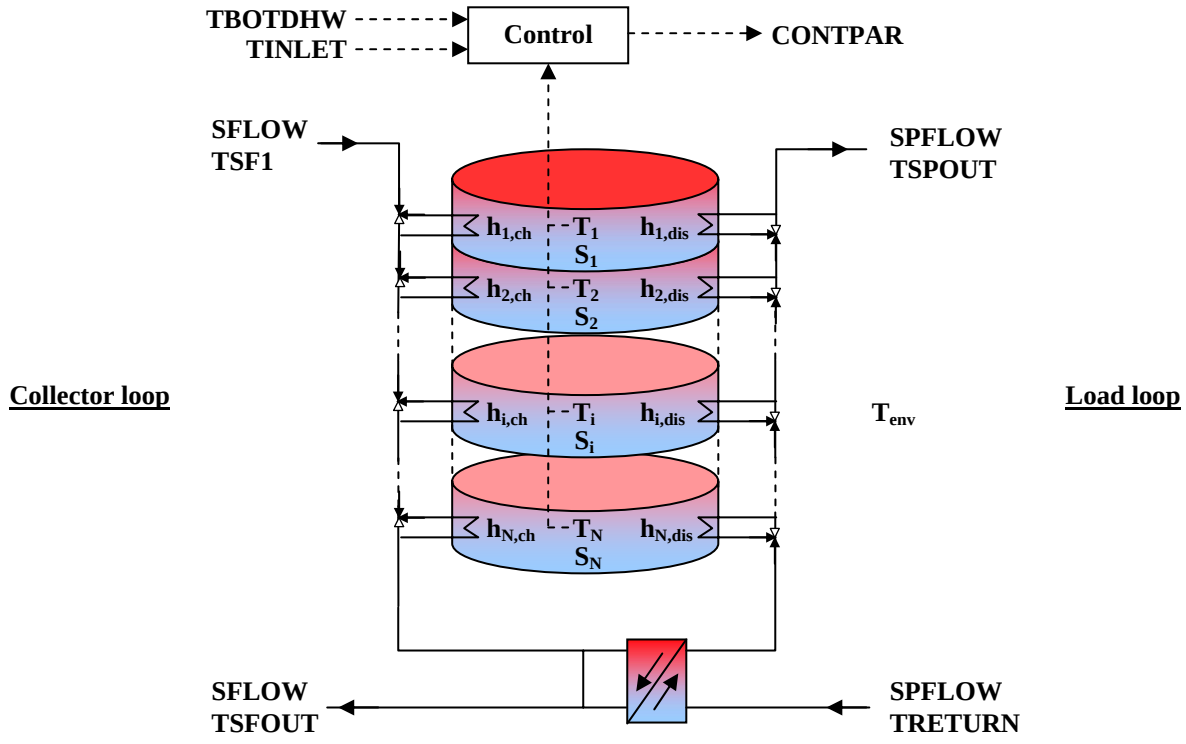

Figure 8.1.2 PCM storage divided into N subsections.

Each sub-volume includes a heat exchanger for the solar collector loop (figure 8.1.2, left) and for the load loop (figure 8.1.2, right). The heat transfer coefficient is assumed identical in all sub-volumes, but can be different between the solar collector loop and the load loop.

The energy content in each sub-volume is determined from the temperature, T_i, and the "degree of melting", S_i.

The storage is uniformly insulated and heat losses to the environment takes place through all free surfaces. For the cylindrical stacked storage solution this corresponds to the surface of the cylinder.

The storage model is "an ideal model", i.e. the boundaries between the sub-volumes are adiabatic. Furthermore, each sub-volume is treated as a lumped model with a uniform temperature and degree of melting.

The heat exchanger that connects the solar and load loop is modelled in the following way:

$$H = \frac{\text{Heat transfer area, A}}{\frac{1}{h_{primary}} + \frac{1}{h_{secondary}}} \quad W/K \quad , \quad h_{primary/secondary} = a \times (flow)^b$$

where, a and b are constants.

Two different charge strategies can be chosen for the model by setting the appropriate parameter:

0: the coldest sub volume is always charged first.
1: one (solidified) sub-volume is charged at the time until fully melted before charging the next

The model is developed for investigation of the benefit of supercooling, but the model can also be run without supercooling by setting the appropriate parameter:

0: no supercooling
1: with supercooling

Nomenclature

ASURF:	Surface area of PCM sub-volume [m^2]
CONTPAR:	Control parameter for controlling the collector loop pump [-]
CPCRYS:	Heat capacity of solidified PCM [J/(kg K)]
CPFLUE:	Heat capacity of liquid PCM [J/(kg K)]
CP_{fluid}:	Heat capacity of collector fluid / heat capacity of load loop fluid [J/(kg K)]
DIMENS1:	Diameter of cylindrical storage or smallest side length in rectangular storage [m]
DIMENS2:	Diameter of cylindrical storage or largest side length in rectangular storage [m]
LAYOUT:	0: Distributed sub-volumes. 1: Stacked sub-volumes
MODE1:	0: No supercooling. 1: With supercooling
MODE2:	0: Coldest sub-volume charged first. 1: One sub-volume charged at the time
NCONV1:	Number of iterations before averaging the output to the load loop
NCONV2:	Number of iterations before averaging the output to the collector loop
NFORM:	Storage cross section form: 0: Circular 1: Rectangular
NLAYER:	Number of sub-volumes
NSTEP:	Number of internal time steps **(Not used)**
QFUSION:	Heat of fusion [J/kg]
QHEAT:	Space heating demand [W]

QLOSS: Heat loss from PCM storage [kJ/hr]

QSTORE: Energy stored in the PCM storage [kJ/hr]

RHOCRYS: Density of solidified PCM [kg/m^3]

RHOFLUE: Density of liquid PCM [kg/m^3]

SFLOW: Mass flow in collector loop [kg/s], [kg/hr]

SPFLOW: Mass flow in load loop [kg/s], [kg/hr]

STATINIT: Initial average degree of melting in the storage [-]

STATUS: Degree of melting in PCM sub-volume [-]

STATUSMID: Average degree of melting in PCM storage [-]

TDELTA: Required difference between collector loop fluid temperature and TDHWBOT, TDHWSET and TDHWMAX to account for losses in the heat exchanger included in the model, when evaluating the charge options for the PCM storage [K]

TDHWBOT: Temperature in the bottom of the domestic hot water tank [°C]

TDHWMAX: Upper limit for domestic hot water tank temperature [°C]

TDHWSET: Set-point temperature for the domestic hot water tank [°C]

TDIFMIN: Minimum required temperature difference between collector fluid and PCM before charging if MODE2 = 1 [K]

TFUSION: PCM melting temperature [°C]

TGOAL: Required forward flow temperature in the load loop to meet the demands [°C]

TINLET: Required forward flow temperature in the space heating system [°C]

TIMESTP: Global time step in simulation [hr]

TINDOOR: Environmental temperature [°C]

TINIT: Initial average storage temperature [°C]

TOTVOL: Total storage volume [m^3]

TPCM: Temperature of PCM sub-volume [°C]

TPCMMID: Average temperature in PCM storage [°C]

TPCMOUT: Fluid temperature of solar fluid after charge of a PCM storage sub-volume [°C]

TREQ: Required forward flow fluid temperature in solar collector loop to heat exchanger if the energy demand in the load loop should be fulfilled [°C]

TRETURN Return flow temperature in space heating system [°C]

TSF: Output fluid temperature from collector [°C]

TSFOUT: Flow temperature to collector loop [°C]

TSPIN: Output temperature from secondary side of heat exchanger [°C]

TSPOUT:	Flow temperature to load loop [°C]
TSTEP:	Internal time step [s]
UVALUE:	Heat loss coefficient for the storage [W/(m^2 K)]
VEKAREA:	Heat transfer area in heat exchanger between the collector and the load loop [m^2]
VEKCOEF1:	Coefficient „a“ in the heat transfer calculation for the heat exchanger [-]
VEKCOEF2:	Exponent „b“ in the heat transfer calculation for the heat exchanger [-]
VOL:	Volume of PCM sub-volume [m^3]
XCH_CHAR:	Heat transfer coefficient between solar collector loop and PCM [W/K]
XCH_DISCH:	Heat transfer coefficient between load loop and PCM [W/K]
XLAMCRYS:	Thermal conductivity of solidified PCM **(Not used)** [W/(m K)]
XLAMFLUE:	Thermal conductivity of liquid PCM **(Not used)** [W/(m K)]

Mathematical description

Charging in case of a possible heat transfer directly from the solar collector loop to the demand loop

Based on the inputs TDHWBOT (temperature in the bottom of the DHW-tank), TINLET (required forward flow temperature in space heating loop) and QHEAT (space heating demand (>0)/(0)) and the parameter TDHWMAX (maximum allowable temperature in the DHW-tank) the required forward flow temperature (TREQ) in the solar collector loop to the heat exchanger connecting the solar and the load loop is estimated.

TSF > TREQ:

In this case there is a possibility for heat transfer to the PCM-storage and still fulfil the heating demand in the load loop.

The PCM sub-volume to be heated is determined depending on the setting of the parameter MODE2:

MODE2 = 0

The model uses TREQ to choose the PCM sub-volume that, if heated by the solar fluid, cools the solar fluid to a temperature (TPCMOUT) that match the required forward temperature to the heat exchanger in the best possible way

MODE2 = 1

TSF > TFUSION:

- First look for a partly melted PCM sub-volume that can be heated without cooling the solar fluid to a temperature below TREQ. The partly melted sub-volume closest to be fully melted is chosen.
- If no partly melted PCM sub-volume is found the model looks for a fully crystallized sub-volume that can be heated without cooling the solar fluid to a temperature below TREQ. The crystallized sub-volume with the highest temperature is chosen.
- If no partly melted or crystallized PCM sub-volume is found the model looks for a liquid sub-volume that can be heated without cooling the solar fluid to a temperature below TREQ. The liquid sub-volume that results in the best match between TREQ and TPCMOUT is chosen.

TSF ≤ TFUSION:

- First look for a crystallized PCM sub-volume that can be heated without cooling the solar fluid to a temperature below TREQ. The crystallized sub-volume with the highest temperature, but lower than (TSF – TDIFMIN), is chosen.
- If no crystallized PCM sub-volume is found the model looks for a sub-volume that can be heated without cooling the solar fluid to a temperature below TREQ independent of the sub-volume state.

*Charging in case of **no** possible heat transfer directly from the solar collector loop to the demand loop*

TSF ≤ TREQ:

In this case the required temperature in the demand loop is higher than the output temperature from the collector - or there is no energy demand in the load loop.

The PCM sub-volume to be heated is determined depending on the setting of the parameter MODE2:

MODE2 = 0

The model chooses the PCM sub-volume that result in the largest cooling of the fluid in the solar collector loop.

MODE2 = 1

TSF > TFUSION:

- First look for a partly melted PCM sub-volume that can be heated by the solar fluid. The partly melted sub-volume closest to be fully melted is chosen.
- If no partly melted PCM sub-volume is found the model looks for a fully crystallized sub-volume that can be heated. The crystallized sub-volume with the highest temperature, but lower than (TSF – TDIFMIN), is chosen.
- If no partly melted or crystallized PCM sub-volume is found the model looks for a liquid sub-volume that can be heated the most.

TSF ≤ TFUSION:

- First look for a crystallized PCM sub-volume that can be heated. The crystallized sub-volume with the highest temperature, but lower than (TSF – TDIFMIN), is chosen.
- If no crystallized PCM sub-volume is found the model looks for a sub-volume that can be heated the most independent of the sub-volume state.

Heat exchange between PCM sub-volume and the fluid in the solar collector loop

Charging of a PCM sub-volume will either increase the PCM temperature or increase the degree of melting or both depending on the initial "position" on the enthalpy curve:

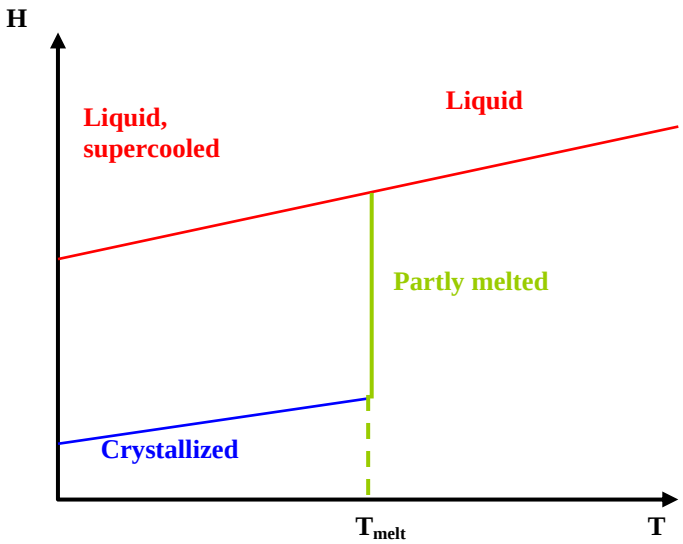

Initial state of PCM is liquid:

The PCM is liquid and energy added to the sub-volume will increase the PCM temperature described by the following equation:

$$TPCM_{new} = TSF - (TSF - TPCM_{old}) \cdot \exp\left(\frac{-TSTEP \cdot SFLOW \cdot CP_{fluid} \cdot \left(1 - \exp\left(\frac{-XCH\_CHAR}{SFLOW \cdot CP_{fluid}}\right)\right)}{VOL \cdot RHOFLUE \cdot CPFLUE} \right)$$

STATUS = 1, (degree of melting = 1)

The corresponding cooling of the solar collector loop fluid is described by:

$$TPCMOUT = TSF + \frac{VOL \cdot RHOFLUE \cdot CPFLUE \cdot (TPCM_{old} - TPCM_{new})}{SFLOW \cdot CP_{fluid} \cdot TSTEP}$$

Initial state of PCM is crystalline:

The PCM is in its crystalline form and energy added to the sub-volume will increase the PCM temperature described by the following equation:

$$TPCM_{new} = TSF - (TSF - TPCM_{old}) \cdot \exp\left(\frac{-TSTEP \cdot SFLOW \cdot CP_{fluid} \cdot \left(1 - \exp\left(\frac{-XCH\_CHAR}{SFLOW \cdot CP_{fluid}}\right)\right)}{VOL \cdot RHOCRYS \cdot CPCRYS} \right)$$

STATUS = 0

The corresponding cooling of the solar collector loop fluid is described by:

$$TPCMOUT = TSF + \frac{VOL \cdot RHOCRYS \cdot CPCRYS \cdot (TPCM_{old} - TPCM_{new})}{SFLOW \cdot CP_{fluid} \cdot TSTEP}$$

If the calculated temperature passes the melting point, TFUSION, the PCM temperature should stay at TFUSION and the “excess” energy is used to melt some (or all) of the PCM. This is described by the following equations:

Amount of “excess” energy: $DQ = VOL \cdot RHOCRYS \cdot CPCRYS \cdot (TPCM_{new,0} - TFUSION)$

New degree of melting: $STATUS_{new,1} = STATUS_{old} + \frac{DQ}{VOL \cdot RHOCRYS \cdot QFUSION}$

Temperature in PCM sub-volume: $TPCM_{new,1} = TFUSION$

If the "excess" energy is larger than the energy needed to melt the total PCM sub-volume, $STATUS_{new,1}$ becomes larger than 1. In this case the total sub-volume has become liquid and is further heated to a higher temperature than TFUSION. This is described by the following equations:

New temperature in PCM-sub-volume:
$$TPCM_{new,2} = TFUSION + \frac{(STATUS_{new,1} - 1) \cdot RHOCRYS \cdot QFUSION}{RHOFLUE \cdot CPFLUE}$$

New degree of melting:
$$STATUS_{new,2} = 1$$

Initial state of PCM is partly melted:

The PCM is partly melted and energy added to the sub-volume will increase the degree of melting and if the energy added exceeds the energy to fully melt the PCM-sub-volume the PCM becomes fully liquid and the temperature will increase to above TFUSION. This is described by the following equations:

Initial cooling of solar collector loop fluid:

$$TPCMOUT = TFUSION + (TSF - TFUSION) \cdot \exp\left(\frac{-XCH\_CHAR}{SFLOW \cdot CP_{fluid}}\right)$$

Temperature in PCM sub-volume:
$$TPCM_{new,1} = TFUSION$$

Degree of melting:
$$STATUS_{new,1} = STATUS_{old} + \frac{TSTEP \cdot SFLOW \cdot CP_{fluid} \cdot (TSF - TPCMOUT)}{VOL \cdot RHOCRYS \cdot QFUSION}$$

The cooling of the solar collector loop fluid has to be recalculated in case the degree of melting exceeds 1:

$$TPCMOUT = TSF + \frac{VOL \cdot RHOCRYS \cdot QFUSION \cdot (STATUS_{old} - STATUS_{new,1})}{SFLOW \cdot CP_{fluid} \cdot TSTEP}$$

If the calculated degree of melting exceeds 1 it is due to the fact that the energy added to the sub-volume exceeds the energy needed to fully melt the PCM sub-volume. The "excess" energy will lead to a temperature increase in the liquid PCM. This situation is described by:

New degree of melting:
$$STATUS_{new,2} = 1$$

New temperature in PCM-sub-volume:
$$TPCM_{new,2} = TFUSION + \frac{(STATUS_{new,1} - 1) \cdot RHOCRYS \cdot QFUSION}{RHOFLUE \cdot CPFLUE}$$

Discharge of PCM-storage

Based on the inputs TDHWBOT (temperature in the bottom of the DHW-tank) and TINLET (required forward flow temperature in space heating loop) and the parameter TDHWSET (set-

point temperature in the DHW-tank) the required forward flow temperature (TGOAL) in the load loop is estimated.

The PCM storage is discharged if the output temperature on the secondary side of the heat exchanger (TSPIN) is lower than TGOAL.

The PCM sub-volume to be discharged is determined in the following way:

1. First the model looks for a liquid PCM sub-volume that is able to heat the load loop fluid to the required temperature TGOAL. The sub-volume with the lowest temperature that meets the demand is chosen.
2. If no liquid sub-volume is found the model looks for a crystallized sub-volume that is able to heat the load loop fluid to the required temperature TGOAL. The sub-volume with the lowest temperature that meets the demand is chosen.
3. If neither a liquid nor a crystallized sub-volume is found the model looks for a partly melted sub-volume that is able to heat the load loop fluid to the required temperature TGOAL. The sub-volume closest to be fully crystallized that meets the demand is chosen.
4. If no liquid, crystallized or partly melted sub-volumes are found and MODE1 = 1 (supercooling possible) the model looks for a supercooled subsection, which by activation of the crystallization is able to meet the temperature demand.
5. If the temperature demand, TGOAL, cannot be met the model looks for a sub-volume that is warmer than the output temperature on the secondary side of the heat exchanger. The warmest sub-volume is chosen and the load loop fluid is preheated by the PCM storage sub-volume.

Initial state of PCM is liquid:

The PCM is liquid and discharge of the sub-volume will decrease the PCM temperature described by the following equations:

$$TPCM_{new,1} = TSPIN - (TSPIN - TPCM_{old}) \cdot \exp\left(\frac{-TSTEP \cdot SPFLOW \cdot CP_{fluid} \cdot \left(1 - \exp\left(\frac{-XCH\_DISCH}{SPFLOW \cdot CP_{fluid}}\right)\right)}{VOL \cdot RHOFLUE \cdot CPFLUE} \right)$$

$STATUS_{new,1} = 1$

The corresponding heating of the load loop fluid is described by:

$$TSPOUT = TSPIN + \frac{VOL \cdot RHOFLUE \cdot CPFLUE \cdot (TPCM_{old} - TPCM_{new,1})}{SPFLOW \cdot CP_{fluid} \cdot TSTEP}$$

In case of MODE1 = 0 (no supercooling) the temperature cannot decrease below the melting point without beginning of crystallization, so in this case the amount of discharged energy that exceeds the energy related to cooling down the PCM to the melting point comes from the heat of fusion related to the crystallization. This is described by the following equations:

New degree of melting:

$$STATUS_{new,1} = STATUS_{old} + \frac{RHOFLUE \cdot CPFLUE \cdot (TFUSION - TPCM_{new,1})}{RHOCRYS \cdot QFUSION}$$

Temperature in PCM sub-volume: $TPCM_{new,1} = TFUSION$

If $STATUS_{new,1}$ becomes negative it is due to the fact that the amount of discharged energy his larger than the heat of fusion energy + the sensible energy in the initial liquid phase of the PCM sub-volume. In this case the PCM sub-volume is fully crystallized and the PCM sub-volume temperature is further decreased:

$STATUS_{new,2} = 0$

Temperature in PCM sub-volume:

$$TPCM_{new,2} = TFUSION - \frac{RHOFLUE \cdot CPFLUE \cdot (TFUSION - TPCM_{new,1}) - RHOCRYS \cdot QFUSION}{RHOCRYS \cdot CPCRYS}$$

<u>Initial state of PCM is crystalline:</u>

The PCM is fully crystallized and discharge of the sub-volume will decrease the PCM temperature described by the following equations:

$$TPCM_{new,1} = TSPIN - (TSPIN - TPCM_{old}) \cdot \exp\left(\frac{-TSTEP \cdot SPFLOW \cdot CP_{fluid} \cdot \left(1 - \exp\left(\frac{-XCH\_DISCH}{SPFLOW \cdot CP_{fluid}}\right)\right)}{VOL \cdot RHOCRYS \cdot CPCRYS} \right)$$

$STATUS_{new,1} = 0$

The corresponding heating of the load loop fluid is described by:

$$TSPOUT = TSPIN + \frac{VOL \cdot RHOCRYS \cdot CPCRYS \cdot (TPCM_{old} - TPCM_{new,1})}{SPFLOW \cdot CP_{fluid} \cdot TSTEP}$$

<u>Initial state of PCM is partly melted:</u>

The PCM is partly melted and energy removed from the sub-volume will decrease the degree of melting and if the energy removed exceeds the energy released by fully crystallizing the PCM-sub-volume the PCM becomes fully crystallized and the temperature will decrease to below TFUSION. This is described by the following equations:

Initial heating of load loop fluid:

$$TSPOUT = TFUSION + (TSPIN - TFUSION) \cdot \exp\left(\frac{-XCH\_DISCH}{SPFLOW \cdot CP_{fluid}}\right)$$

Temperature in PCM sub-volume: $TPCM_{new,1} = TFUSION$

Degree of melting: $$STATUS_{new,1} = STATUS_{old} + \frac{TSTEP \cdot SPFLOW \cdot CP_{fluid} \cdot (TSPIN - TSPOUT)}{VOL \cdot RHOCRYS \cdot QFUSION}$$

In case the degree of melting ($STATUS_{new,1}$) becomes less than 0 it is due to the fact that the amount of discharged energy is larger than the available heat of fusion energy of the PCM sub-volume. In this case the PCM sub-volume is fully crystallized and the PCM sub-volume temperature is further decreased:

$STATUS_{new,2} = 0$

Temperature in PCM sub-volume: $$TPCM_{new,2} = TFUSION - \frac{QFUSION \cdot (0 - STATUS_{new,1})}{CPCRYS}$$

Initial state of PCM is supercooled:

The PCM is liquid and supercooled, which means that an activation of the crystallisation will make the PCM temperature increase to the melting temperature (TFUSION) and PCM will be in a partly melted state.

The degree of melting after activation of the crystallization but before discharge is lower than 1 because some of the heat of fusion energy is used to heat the PCM from its initial temperature ($TPCM_{old}$) to the melting temperature:

$$STATUS_{new,0} = 1 - \frac{RHOFLUE \cdot CPFLUE \cdot (TFUSION - TPCM_{old})}{RHOCRYS \cdot QFUSION}$$

The PCM sub-volume temperature etc. after discharge is calculated as described above in "Initial state of PCM is partly melted"

Method to enhance convergence

The concept of active use of supercooling introduces a discrete function - activation of a sub-volume or not, which has a large influence on the output temperatures both in the solar collector loop and the demand loop. This makes it almost impossible to make the model converge as the output temperatures may shift dramatically between iterations even if the inputs only differ slightly.

Therefore the model has a built-in convergence feature that becomes active after a user-specified number of iterations (NCONV1, NCONV2).

If the number of iterations exceeds NCONV1, the output solar collector loop fluid temperature from the model (TPCMOUT) is calculated as the successive average of the output temperature in the following iterations:

$$TPCMOUT_{average} = \frac{\sum_{i>NCONV1} TPCMOUT_i}{i - NCONV1}$$

Substitution of the actual calculated output temperature with the calculated average temperature would result in an error in the energy balance, which have to be taken into account. This is done by calculating the energy difference related to the change of the output temperature:

$$\Delta Q = SFLOW \cdot CP_{fluid} \cdot TSTEP \cdot (TPCMOUT_i - TPCMOUT_{average})$$

This energy difference is then distributed over all the sub-volumes relative to the energy content in each sub-volume. Only sub-volumes with a temperature higher than the temperature surrounding the storage (TINDOOR) are considered.

The same principle is used for the output load loop temperature from the model (TSPOUT) if the number of iterations exceeds NCONV2.

Calculation of heat loss

The heat loss and its influence on PCM storage temperature and degree of melting are calculated after the calculations of charging, discharging and convergence enhancement. The influence of the heat loss on PCM temperature and degree of melting is calculated for each sub-volume:

PCM liquid:

$$TPCM_{final} = TINDOOR + (TPCM_{new} - TINDOOR) \cdot \exp\left(\frac{-TSTEP \cdot ASURF \cdot UVALUE}{VOL \cdot RHOFLUE \cdot CPFLUE}\right)$$

$$STATUS_{final} = 1$$

PCM crystallized:

$$TPCM_{final} = TINDOOR + (TPCM_{new} - TINDOOR) \cdot \exp\left(\frac{-TSTEP \cdot ASURF \cdot UVALUE}{VOL \cdot RHOCRYS \cdot CPCRYS}\right)$$

$$STATUS_{final} = 0$$

PCM partly melted:

$$TPCM_{final} = TFUSION$$

$$STATUS_{final} = STATUS_{new} + \frac{TSTEP \cdot ASURF \cdot UVALUE \cdot (TFUSION - TINDOOR)}{VOL \cdot RHOCRYS \cdot QFUSION}$$

In case the heat loss leads to a change of the state, i.e. from partly to fully crystallized this is accounted for as described under "*Discharge of PCM-storage*".

TRNSYS component configuration

PARAM. NO.	LABEL	DESCRIPTION
01	TOTVOL	Total storage volume [m^3]
02	NLAYER	Number of sub-volumes
03	NFORM	Storage cross section form: 0: Circular 1: Rectangular
04	DIMENS1	Diameter of cylindrical storage or smallest side length in rectangular storage [m]
05	DIMENS2	Diameter of cylindrical storage or largest side length in rectangular storage [m]
06	LAYOUT	0: Distributed sub-volumes. 1: Stacked sub-volumes
07	UVALUE	Heat loss coefficient for the storage [W/(m^2 K)]
08	XCH_CHAR	Heat transfer coefficient between solar collector loop and PCM [W/K]
09	XCH_DISCH	Heat transfer coefficient between load loop and PCM [W/K]
10	VEKAREA	Heat transfer area in heat exchanger between the collector and the load loop [m^2]
11	VEKCOEF1	Coefficient „a“ in the heat transfer calculation for the heat exchanger [-]
12	VEKCOEF2	Exponent „b“ in the heat transfer calculation for the heat exchanger [-]
13	RHOCRYS	Density of solidified PCM [kg/m^3]
14	CPCRYS	Heat capacity of solidified PCM [J/(kg K)]
15	XLAMCRYS	Thermal conductivity of solidified PCM **(Not used)** [W/(m K)]
16	RHOFLUE	Density of liquid PCM [kg/m^3]
17	CPFLUE	Heat capacity of liquid PCM [J/(kg K)]
18	XLAMFLUE	Thermal conductivity of liquid PCM **(Not used)** [W/(m K)]
19	TFUSION	PCM melting temperature [°C]
20	QFUSION	Heat of fusion [J/kg]
21	MODE1	0: No supercooling. 1: With supercooling
22	MODE2	0: Coldest sub-volume charged first. 1: One sub-volume charged at the time
23	TDIFMIN	Minimum required temperature difference between collector fluid and PCM before charging if MODE2 = 1 [K]
24	TINIT	Initial average storage temperature [°C]
25	STATINIT	Initial average degree of melting in the storage [-]
26	TINDOOR	Environmental temperature [°C]
27	NCONV1	Number of iterations before averaging the output to the load loop
28	NCONV2	Number of iterations before averaging the output to the collector loop
29	NSTEP	Number of internal time steps **(Not used)**
30	TIMESTP	Global time step in simulation [hr]

INPUT NO.	LABEL	DESCRIPTION
01	SFLOW	Mass flow in collector loop [kg/hr]
02	TSF	Output fluid temperature from collector [°C]
03	TDHWMAX	Upper limit for domestic hot water tank temperature [°C]
04	TDHWSET	Set-point temperature for the domestic hot water tank [°C]
05	TDHWBOT	Temperature in the bottom of the domestic hot water tank [°C]
06	TINLET	Required forward flow temperature in the space heating system [°C]
07	TRETURN	Return flow temperature in space heating system [°C]
08	SPFLOW	Mass flow in load loop [kg/hr]
09	QHEAT	Required heating power in space heating loop [W]
10	TDELTA	Required difference between collector loop fluid temperature and TDHWBOT, TDHWSET and TDHWMAX to account for losses in the heat exchanger included in the model, when evaluating the charge options for the PCM storage [K]

OUTPUT NO.	LABEL	DESCRIPTION
1	TSFOUT	Flow temperature to collector loop [°C]
2	TSPOUT	Flow temperature to load loop [°C]
3	QLOSS	Heat loss from PCM storage [kJ/hr]
4	TPCMMID	Average temperature in PCM storage [°C]
5	STATUSMID	Average degree of melting in PCM storage [-]
6	QSTORE	Energy stored in the PCM storage [kJ/hr]
7	CONTPAR	Control parameter for controlling the collector loop pump [-]

Comments

The model includes a few minor theoretical errors related to the cases where the charged or discharged energy in one time step results in a shift in phase from partly melted to either fully liquid or fully crystallised. In these cases the fluid temperature is calculated from heat exchange with the PCM at its initial temperature, i.e. the melting temperature, but as illustrated below the fluid temperature should be somewhat higher or lower due to further heating or cooling of the PCM.

In case 1 in the figure below the end temperature of the PCM is higher than the melting temperature in which case the heat exchange between the fluid and the PCM at the end of the time step takes place at a lower temperature difference than at the beginning of the time step and the resulting fluid temperature in reality will be a little higher than calculated by the model. The same argument is valid for case 2 in the figure below except that the fluid in this case in reality will be a little lower than calculated.

The error is anticipated to be insignificant due to the normally small time steps used in combination with the high thermal capacity of both fluid and PCM.

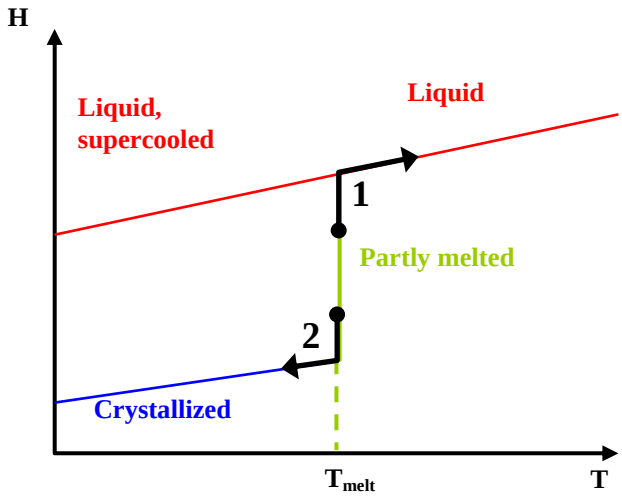

Bilag 3

Simulation and optimization report. System: PCM with supercooling.

IEA SH&C Task 32 Subtask C6. January 2008.

Jørgen M. Schultz

Simulation and optimization Report System: PCM with supercooling

A Report of IEA Solar Heating and Cooling programme - Task 32
Advanced storage concepts
for solar and low energy buildings
Report of Subtask C6

Date: January 14, 2008

Author:
Jørgen M. Schultz

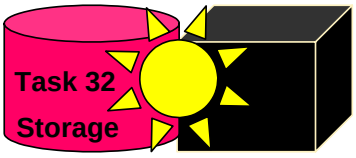

SOLAR HEATING & COOLING PROGRAMME
INTERNATIONAL ENERGY AGENCY

Content

1 General description of PCM system with supercooling

Main features

The system is designed for 100% coverage by solar of both domestic hot water (DHW) and space heating in a low energy single family house according to the passive house standard. This is achieved by means of a seasonal phase change material (PCM) storage combined with a small DHW tank. The phase change material is sodium acetate tri-hydrate with a melting point of 58°C and the ability of stable supercooling. The PCM storage is subdivided into several sub-volumes. The system benefits from the supercooling as the PCM when melted can cool down, e.g. due to heat loss, to surrounding temperature in its liquid phase preserving the energy related to the heat of fusion. When a storage sub-volume has reached the surrounding temperature this part of the storage is heat loss free. As soon as there is a need for heating that cannot be covered directly from the collector or from a liquid or solidified sub-volume the solidification in a supercooled sub-volume is activated in which case the heat of fusion energy is released and becomes usable for DHW and/or space heating. The DHW tank is required to meet the power demand during hot water draw offs. The heating system is a low temperature system, i.e. floor heating or radiators.

Heat management philosophy

Solar collector loop:

The pump in the solar collector loop is started if the temperature at the collector outlet is higher than either the minimum temperature of all sub-volumes in the PCM-storage or the minimum temperature in the DHW-tank or in case of space heating demand the return temperature from the space heating loop.

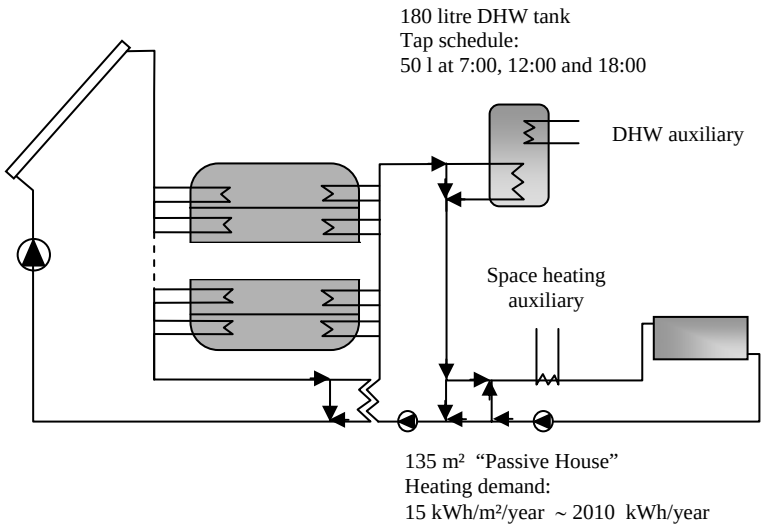

When the pump in the solar collector loop is running the highest priority is on covering the space heating demand. Second priority is to heat up the DHW-tank until the set-point of 55°C has been reached. Third priority is to charge the seasonal PCM-storage. The strategy for charging of the PCM storage sub-volumes is to charge one sub-volume at the time until fully melted. In case the outlet temperature of the solar collector is lower than the melting point one sub-volume at the time is heated to the maximum obtainable temperature under the actual conditions. When all sub-volumes has been melted the DHW-tank is further heated until 70°C, where after the PCM-storage is charged.

The pump stops either when the collector outlet temperature is lower than the minimum of the PCM storage sub-volume temperature, the minimum DHW-tank temperature and the space heating return temperature or when the DHW-tank has reached a temperature of 70°C and all sub-volumes in the PCM-storage has reached a temperature of 95°C.

Demand loop:

If possible the DHW-tank and/or the space heating loop are heated directly by the solar collector loop through the heat exchanger connecting the solar collector loop and the demand loop. In case the demand cannot be fulfilled by the collector loop the PCM-storage is

discharged. The discharge strategy is first to discharge a liquid sub-volume that has a temperature just high enough to cover the demand temperature. Next a solidified sub-section with a sufficient temperature is discharged. Finally, the solidification is activated in a supercooled sub-section and discharged. The DHW-tank is always heated to the set-point temperature of 55°C.

Auxiliary energy:

The solar heating system is designed for 100% coverage by solar of DHW and space heating so in principle auxiliary energy is not needed. However, if required auxiliary energy is supplied by electric heating elements in the DHW-tank and in the space heating loop.

Influence of auxiliary energy source on system design and dimensioning

Auxiliary energy will only be needed in rare cases, i.e. in case of extremely bad summers or extremely hard winters or in case of malfunctioning of the system.

Cost (range) and market distribution

The described design has not been tested yet.

2 Modelling of the system

The system has not been modelled using the reference template, but parametric studies have been carried out in TRNSYS 15 with the model described below. The simulations have been performed with the main goal to evaluate the potential of the concept. As a consequence no effort has been put into simulating details such as heat loss from pipes, and the PCM storage is also treated as a perfect working storage only considering heat losses to the surroundings.

2.1 TRNSYS model

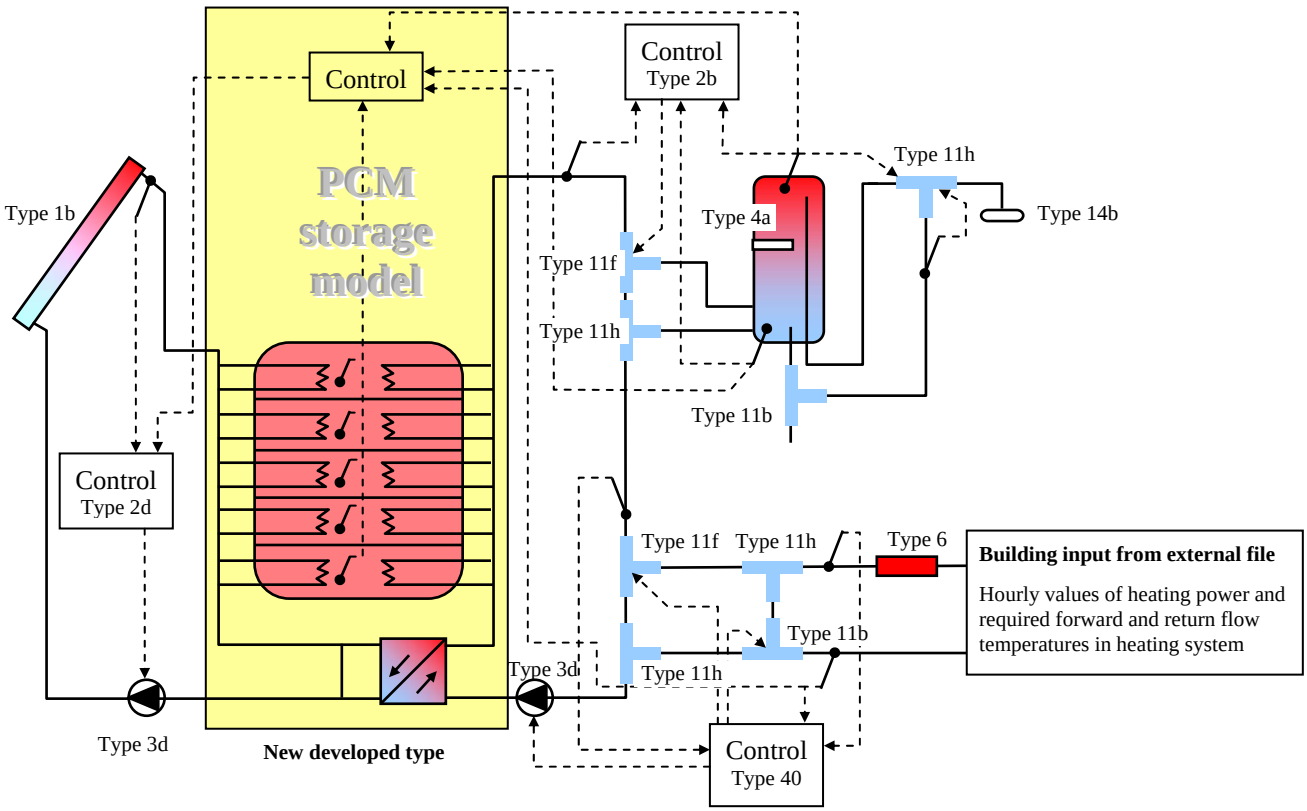

Figure 1. Modelling of the system "PCM with supercooling" in TRNSYS 15.

2.2 Definition of the components included in the system and standard inputs data

2.2.1 General Settings

General Settings:

Main	
simulation time step	0.01 h
tolerance integration / convergence	0.01 / 0.001
length of simulation	24 months
climate	Copenhagen
building	Passive house standard 15 kWh/m^2/year = 2015 kWh/year

Auxiliary (electrically) in DHW tank	
Nominal Power of Auxiliary	4320 kJ/h
Set temperature Auxiliary into store	55°C
Auxiliary temperature rise	4 K
Auxiliary (electrically) in space heating	
Nominal Power of Auxiliary	15000 kJ/h
Set temperature Auxiliary into store	Depends on heating load
Auxiliary temperature rise	-
Collector	
type	flat plate selective (ref)
aperture area	36 m^2
tilt angle	75°
azimuth (0° = south, 90° = west, 270° east)	0°
primary loop specific mass flow rate	50 kg/h/m^2
upper / lower dead band (switch on / off)	5 K / 1 K
cut-off temperature of collector	PCM-store > 95°C and DHW-tank > 70°C
DHW-store	
storage volume	0.18 m^3
effective heat loss coefficient	0.83 W/m^2K
PCM-store	
storage volume	10 m^3
effective heat loss coefficient	0.6 W/m^2K

2.2.2 Collector

Type: 1b Version Number:

Collector	η_0	0.82 -
	a_1	2.44 W/m²-K
	a_2	0.005 W/m²-K²
	1st order IAM	0.135
	2nd order IAM	-0.006
	Area	36 m²
	Specific mass flow	50 l/m²/h

2.2.3 Heat exchange in the collector loop

Heat exchange takes place either in the PCM storage, in the heat exchanger between the collector loop and the demand loop or both.

- The heat exchange in each PCM-storage sub-volume is simulated as a constant heat transfer coefficient of 500 W/K.
- The heat exchanger between the collector loop and the demand loop is simulated based on values from a specific plate heat exchanger as:

Heat exchanger area m² 0.6 m²

Heat transfer coefficient primary side: $10700 \times (\dot{q}_{primary})^{0.84}$ W/m^2K,
$\dot{q}_{primary}$ = primary flow (l/s)

Heat transfer coefficient secondary side: $10700 \times (\dot{q}_{secondary})^{0.84}$ W/m^2K,
$\dot{q}_{secondary}$ = secondary flow (l/s)

The approximate heat transfer coefficient in the heat exchanger with the flow rates appearing in the simulations is 800 W/K.

The heat exchange in the PCM storage as well as the heat exchanger between the collector loop and the demand loop is included in the developed PCM storage TRNSYS type.

2.2.4 Pipes between Collector and Storage:

Not modelled.

2.2.5 Control of the collector loop

The collector loop is controlled by a combined evaluation of the temperatures in the PCM storage, the DHW-storage and the required supply temperature in the space heating loop. The combined governing temperature is an output from the PCM storage TRNSYS type that goes to the controller (St-coll).

Type 2

Reason	***Sensor***	***Off-Criteria***	***Hyst.***
Upper dead beand (Udb)	Collector temperature (T-coll) and storage collector control (St-coll)	On: T-coll>st-coll + Udb	
Lower dead band (Ldb)	Collector temperature (T-coll) and storage collector control (St-coll)	Off: T-coll>st-coll + Ldb	
Storage tank protection	Combined storage collector control temperature (St-coll)	Cut off if: T-DHW > 70°C and T-PCM > 95°C and no space heating demand	5 K

2.2.6 PCM storage:

Type: New developed type Version Number:

Storage tank	Total volume	10 m³
	Height	2.50 m
	Diameter	2.50 m
	Store volume for auxiliary	None
	Number of nodes (sub-volumes)	40
	Media:	Sodium acetate tri-hydrate with active use of super cooling
	Effective heat loss coefficient	0.6 W/m^{2}K
	Heat exchange collector loop – storage sub-volume	500 W/K
	Heat exchange demand loop – storage sub-volume	500 W/K

The developed type is further described in Appendix 1.

2.2.7 Building

The building is a 135 m^2 detached single family low energy house with an annual energy consumption for space heating equal to 15 kWh/m^2/year according to passive house standard. The house has been simulated with the Danish building simulation tool tsbi3 and the output of the hourly space heating demand has been used as input for the TRNSYS simulations.

2.2.8 Heat distribution

The heat is distributed by a floor heating system or a low-temperature radiator heating system. The required supply temperature is calculated on hourly basis from the required power input the flow rate in the heating system (120 kg/hr) and a fixed return temperature in the heating system of 25°C.
The heating system is assumed to have an efficiency of 100%, i.e. no pipe losses.

2.2.9 Draw-Off loop

Hot water is tapped 3 times a day at a temperature of 50°C. The cold fresh water temperature is assumed constant at 10°C. A hot water consumption of 150 litres/day is assumed.

2.3 Validation of the system model

The investigated solar heating system has not been built and tested so no system model validation has been possible.

3 Simulations for testing the library and the accuracy

The accuracy of the simulations is checked by setting up the energy balance for the total system as well as for the PCM storage component and the DHW-tank. The energy balances have been used for determination of the best combination of time step (0.01 h) and integration and convergence tolerances: 0.01 and 0.001.

The main difficulties were related to the supercooling in the PCM-storage model or rather the activation of a supercooled sub-section, which is a discrete function: either the sub-section is at a low temperature of approximately 25 – 35°C or, if activated, at a temperature of 58°C. In several time steps such a sub-section will change between the two states from iteration to iteration leading to no convergence. The first attempt is in analogy to the on/off controllers to introduce a maximum number of oscillations where after the actual state of the sub-section is frozen, but the result were large energy imbalances. The final solution was still to operate with a maximum number of oscillations, but instead of freezing the state of the sub-section after the number of oscillations, the output temperatures from the storage model are averaged over the following iterations. After a few more iterations in the time step the simulation is converging. When the actual output temperature from the PCM-storage model is replaced with an average value of the previous iterations and the present an error in the energy balance is introduced. Therefore it became necessary to compensate for this in each iteration by changing the energy content in the storage accordingly. The result is a system energy balance below 10 kWh/year, which corresponds to approximately 0.05 % of the total annual energy flow.

4 Sensitivity Analysis and Optimization

4.1 Presentation of results

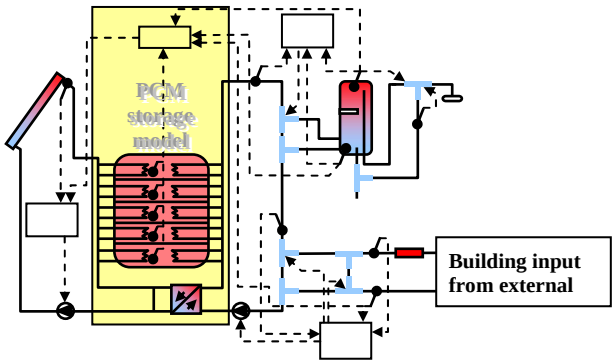

System: Seasonal PCM storage with active use of supercooling

Main parameters (optimised Base Case (BC)):			
Building:	*Passive house*	Storage Volume:	*PCM 10 m^3* *DHW 0.18 m^3*
Climate:	*Copenhagen*	Storage height	*2.5 m*
Collectors area:	*36 m^2*	Position of heat exchangers	*N/A*
Collector type:	*Flat Plate*	Position of in/outlets	*N/A*
Specific flow rate (Collector)	*50 kg/m^2-h*	Thermal insulation	*0.6 W/m^2K*
Collector azimuth/tilt angle	*0 / 75°*	Nominal auxiliary heating rate	*PCM: None* *DHW: 4320 kJ/h* *Sp.heat: 15000 kJ/h*
Collector upper dead band	*5 °K*	Heat Exchanger:	*PCM: 500 W/K* *Solar/demand 800 W/K*
Simulation parameter:		Storage nodes	*PCM: 40 (sub-sections)* *DHW: 8*
Time step	*1/100 h*	Tolerances Integration Convergence	*0.010/0.001*

The primary objective for the parametric studies has been to investigate the influence of different parameters on the required PCM-storage volume that will result in 100 % solar fraction. As the PCM-storage is expected to be the most costly part of the solar heating system focus has been on ways to reduce the necessary PCM-storage volume.

Summary of Sensitivity Parameters			
Parameter	Variation	[1]Variation in solar fraction	
Base Case (BC)	-	100%	
Collector size [m^2] and PCM storage volume [m^3] (fixed subsection volume = 100 litres)	18 – 36 m^2 1 – 23 m^3	70 – 100%	Figure 2
Sub-section and PCM storage volume [m^3] (fixed collector area: 36 m^2)	0.1 – 1.0 m^3 1 – 13 m^3	83 – 100%	Figure 3
Effective heat loss coefficient [W/m^2K] PCM storage heat loss usable/not usable (fixed collector area 36 m^2)	0.20 – 1.00	100%	Figure 4
PCM volume vs. water storage volume [m^3] (fixed collector area: 36 m^2)	1 – 20 m^3	78 - 100%	Figure 5

[1] The variation if fractional savings indicated in the table does not represent the values for the extremes of the range, rather the minimum and maximum values for the range indicated.

Sensitivity parameter:	Collector size [m^2] and PCM storage volume [m^3] (fixed subsection volume = 100 litres)	18 – 36 m2 1 – 23 m3

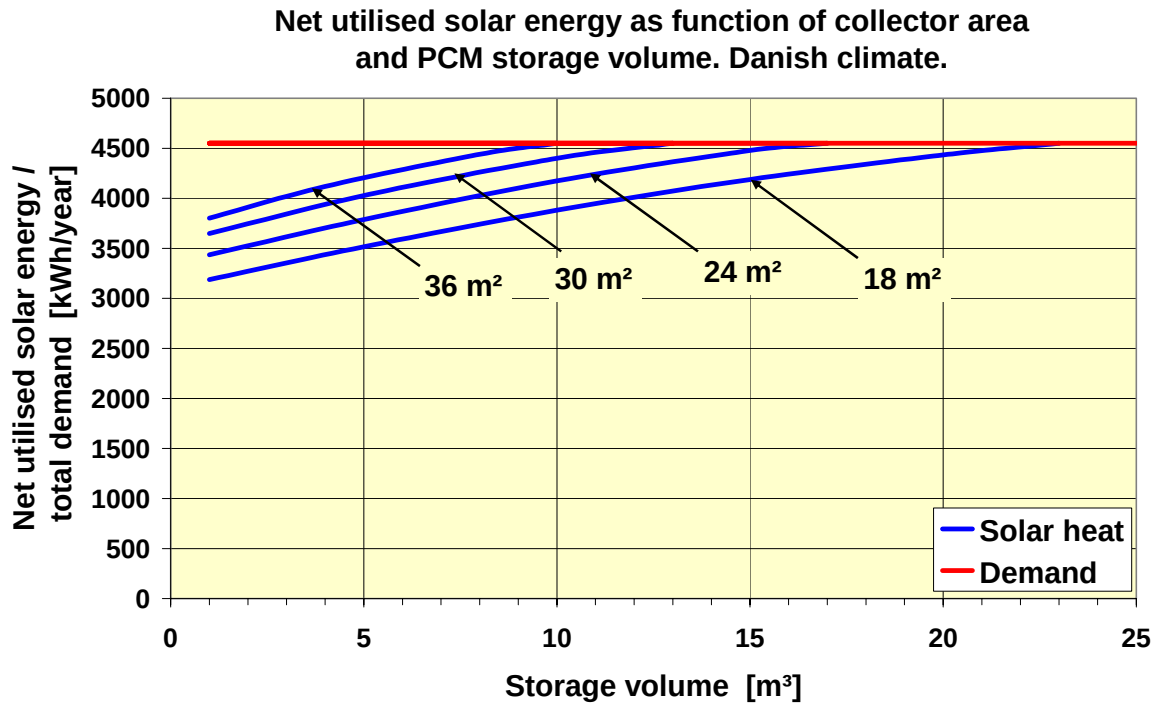

Figure 2. Net utilised solar energy as function of collector area and PCM storage volume. The red horizontal line indicates the total energy demand for both domestic hot water and space heating.

Differences from Base Case (BC)

The subsection volume has in this parametric study been set to 0.1 m^3 independent of the total PCM-storage volume, while the sub-section volume in the base case is 0.25 m^3.

Description of Results

The results show that an increase of the solar collector area from 18 – 36 m^2 results in a decrease in the required PCM-storage volume for 100 % solar fraction from 23 – 10 m^3. The optimum combination of solar collector area and PCM-storage volume will depend on an economical analysis.

Comments

None

Sensitivity parameter:	Sub-section and PCM storage volume [m^3] (fixed collector area: 36 m^2)	0.1 – 1.0 m^3 1 – 13 m^3

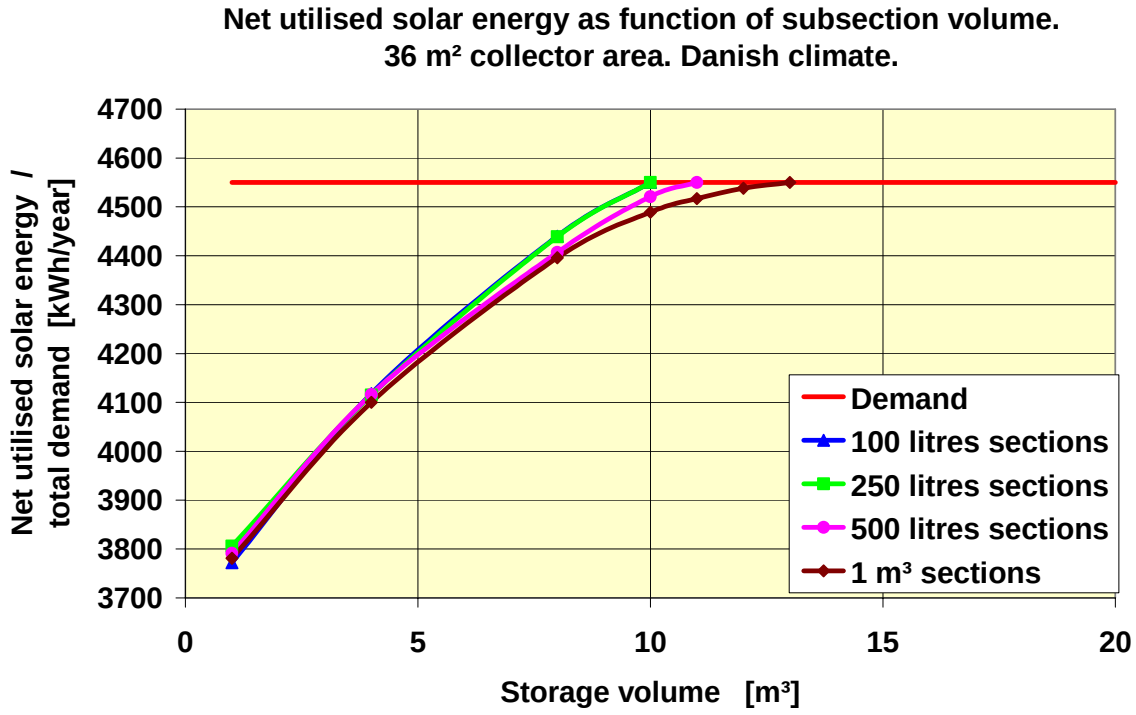

Figure 3. Net utilised solar energy as function of sub-sectionand total PCM storage volume. The red horizontal line indicates the total energy demand for both domestic hot water and space heating.

Differences from Base Case (BC)
Except for the parameters that are varied the model confirms with the base case.

Description of Results
The sub-section volume was expected to have an important influence on the PCM storage performance as many small volumes should make it easier to get a good match between the actual demand and the supercooled volume that have to be activated to cover the demand. However, the analysis shows that there is no difference in performance between sub-section volumes of 0.1 and 0.25 m^3. An increase of the sub-section volume to 0.5 m^3 influences the PCM-storage performance as the required total storage volume for 100% solar fraction increases from 10 m^3 to approximately 12 m^3 and further increase in sub-section volume to 1 m^3 increases the required total volume to approximately 14 m^3.

Comments
None

Sensitivity parameter:	Effective heat loss coefficient [W/m^{2}K] PCM storage heat loss usable/not usable (fixed collector area 36 m^2)	0.2 – 1.0 W/m^{2}K

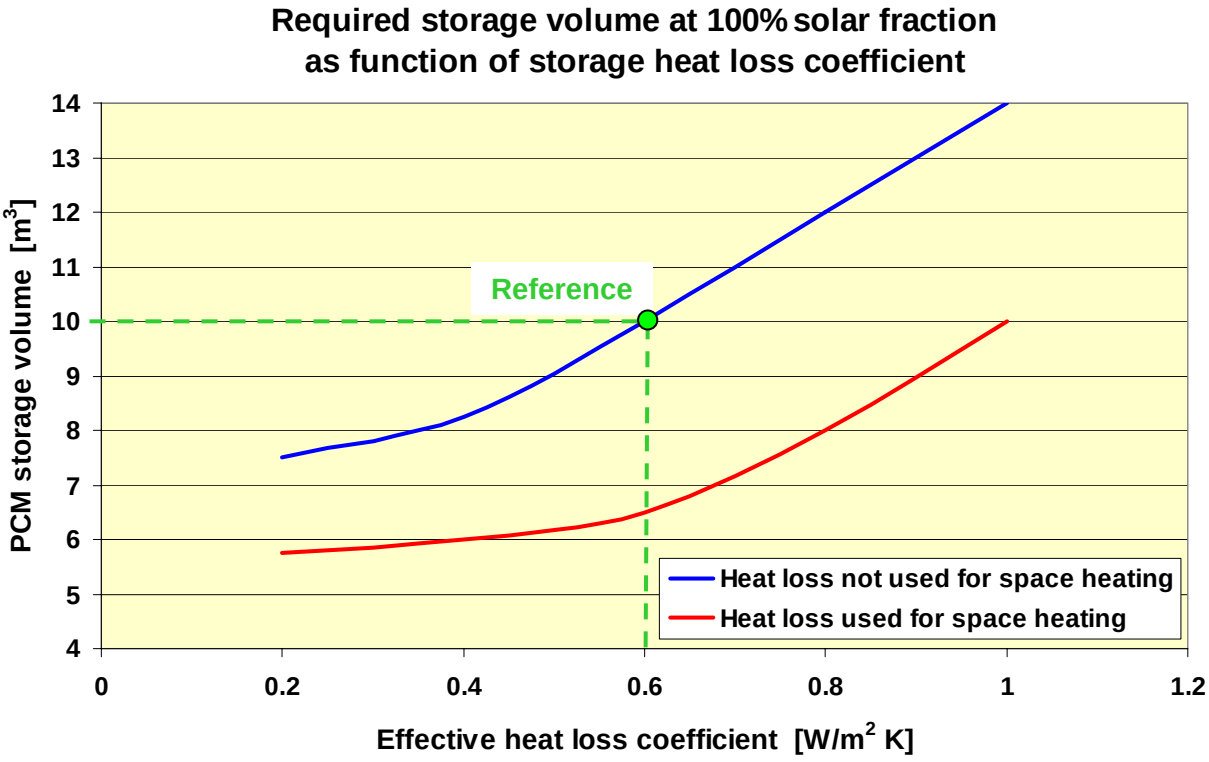

Figure 4. Required PCM storage volume for 100% solar fraction as function of effective storage heat loss coefficient. The blue curve shows the result if the storage heat loss is treated as pure waste. The red curve shows the result if the storage heat loss can be used for space heating in periods with space heating demand.

Differences from Base Case (BC)
Except for the parameters that are varied the model confirms with the base case.

Description of Results
Even though the benefit of the PCM storage with active use of supercooling is due to a considerably lower heat loss than for traditional water storage solutions the effective heat loss coefficient has a significant influence on the PCM storage performance. In case the storage heat loss cannot be used, a reduction of the effective heat loss coefficient from 0.6 W/m^{2}K to 0.4 W/m^{2}K leads to a reduction in the required total PCM storage volume from 10 m^3 to approximately 8 m^3.
In case the storage heat loss can be made usable for covering parts of the space heating demand when present the required PCM storage volume can be further reduced to approximately 6 m^3. In this case the influence of the effective heat loss coefficient becomes less important in the range 0.2 – 0.6 W/m^{2}K.

Comments
None

Sensitivity parameter:	PCM volume vs. water storage volume [m^3] (fixed collector area: 36 m^2)	1 - 20 m^3

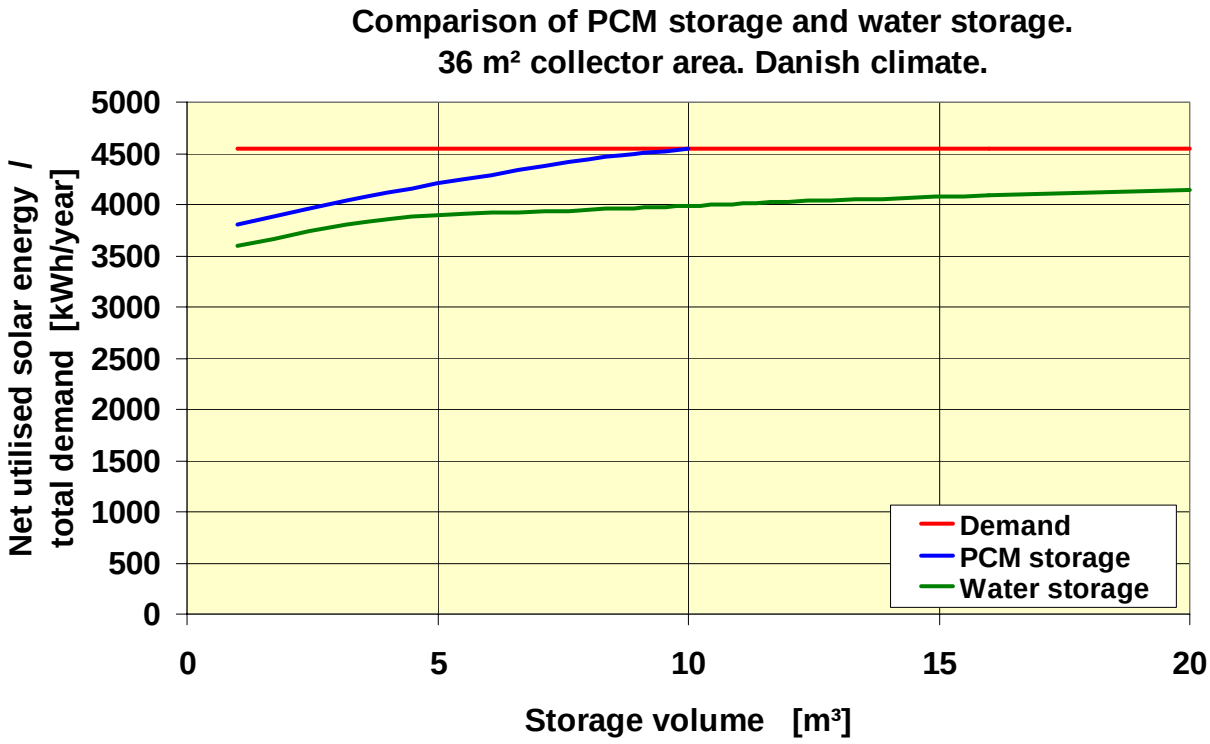

Figure 5. Net utilised solar energy as function of storage volume for a PCM-storage with active use of supercooling and a water storage. The red horizontal line indicates the total energy demand for both domestic hot water and space heating.

Differences from Base Case (BC)

The sub-section volume is 0.1 m^3 independent of the total storage volume.

Description of Results

The results show the benefit of the PCM-storage with active use of super cooling compared to a traditional water storage for which it only will be impossible to reach 100% solar fraction even with a very large volume. The difference between the PCM storage and the water storage is due to the difference in heat loss.

Comments

The PCM-storage and the water storage are simulated with the same model and the same insulation level. Using the same model eliminates differences due to model differences. The sub-sectioning in the model combined with the control strategy of charging one section at the time corresponds to an almost ideal stratification when simulating the water storage.

4.2 Definition of the optimized system

If there has been developed an optimized system, please describe or refer to another report

5 Analysis using FSC

The solar heating system has not been analysed using the FSC-method.

6 Lessons learned

Solar fractions of 100% are possible for low energy buildings in Denmark for solar heating systems with a PCM heat storage utilizing stable supercooling.

7 References

J.M. Schultz & S. Furbo. “Investigation of heat of fusion storage for solar low energy buildings”, Proceedings ISES Solar World Congress 2005.

J.M. Schultz & S. Furbo. “Heat of fusion storage with high solar fraction for solar low energy buildings”, Proceedings EUROSUN 2006.

J.M. Schultz & S. Furbo. “Solar heating systems with heat of fusion storage with 100% solar fraction for solar low energy buildings.” Proceedings ISES Solar World Congress 2007.

8 Appendix 1: Description of Components specific to this System

These are components that are

a) not part of the TRNSYS standard library AND
b) not part of the types used as "standard" by Task 26.

8.1 Type 185 : PCM storage with supercooling

Version 1.0

Parameters: 30
Inputs: 10
Outputs: 7

Please refer to description of TYPE 185 – Phase Change Material storage with super cooling by Jørgen M. Schultz, Department of Civil Engineering, Technical University of Denmark, Kgs. Lyngby, Denmark.

Availability: DTU

Bilag 4

Investigations of medium sized solar combisystems

Proceedings EuroSun 2006 Congress, Glasgow, Scotland.

Elsa Andersen & Simon Furbo

Investigations of medium sized solar combi systems

E. Andersen* **and S. Furbo**
Department of Civil Engineering. Technical University of Denmark
DK-2800 Kgs. Lyngby, Denmark
* Corresponding Author, email : ean@byg.dtu.dk

Abstract

A large variety of solar combi systems are on the market, but it is still too early to draw conclusions on optimum design of solar combi systems. Among others, the following questions need to be answered: Is an external domestic hot water preparation more desirable than an internal? What is the advantage by using inlet stratifiers? To answer the questions, theoretical investigations are carried out for differently designed solar combi systems. The work is carried out within the Solar Heating and Cooling Programme of the International Energy Agency (IEA SHC), Task 32 Advanced storage concepts for solar houses and low energy buildings.

Keywords: Solar combi system design; Inlet stratifier

1. Introduction

In the period 1998-2002, the IEA SHC, Task 26 Solar CombiSystems evaluated 21 solar combi systems which were on the European marked. The evaluation comprised both the system costs and the thermal performance. It was found that most of the systems for one family houses had solar collectors of 10 m^2- 30 m^2 with 0.3 m^3- 3 m^3 tank volumes, and that the best systems, regarding the performance/cost ratio, were the most advanced systems with inlet stratification pipes, an efficient integrated boiler and only one control system, which controls both the boiler and the solar collector loop [5].

A number of stratification inlet pipes, so-called stratifiers, were investigated [1]. It was found that thermal stratification in practice can be built up and maintained in a very good way with certain stratifiers, among others with multilayer fabric stratifiers and with rigid stratifiers with holes with flaps that work as non-return valves.

In this paper, three differently designed medium-sized solar combi systems are investigated theoretically by means of the simulation program Trnsys [3] and the multiport store model [2]. The systems have 1000 litre storage tanks and 20 m^2 solar collectors.

2. Investigations of differently designed solar combi systems

A number of solar combi system types are investigated theoretically. Fig. 1 shows schematic illustrations of the investigated solar combi system types. The investigation is based on three basically different system models, one model is based on a space heating storage with an external heat exchanger mounted in a side arm for domestic hot water preparation, one model is based on a domestic hot water tank with an internal heat exchanger spiral connected to the space heating system, and one model is based on a hot water tank in tank storage. The three system models are referred to as models 1, 2 and 3, respectively. Further, the models are improved by introducing stratifiers in the solar collector loop and in the space heating loop, and in both the solar collector loop and the space heating loop. The variations in each model are numbered successively, see Fig. 1. The advantage of using stratifiers is that incoming water of any temperature is led into the tank in a level where the temperature of the incoming water matches the temperature of the water in the tank. In this way, thermal stratification in the tank is enhanced without destroying the already existing thermal stratification in the tank. In the present investigation, the thermal stratification is assumed to be built up in a perfect way without any mixing by the inlet stratifier. In this way the investigations show the maximum potential of inlet stratifiers.

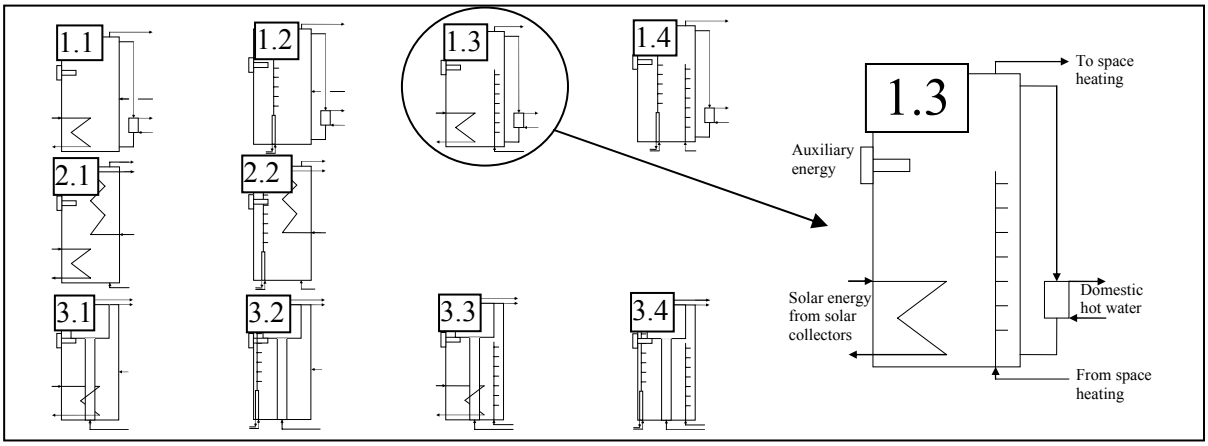

Fig. 1. Schematics of the three system models: Model 1 (top), model 2 (middle) and model 3 (bottom), and the successively numbered variations of the system models.

2.1 Assumptions for the calculations

The Danish Design Reference Year, DRY, is used as weather data [4]. The daily hot water consumption is 100 litres and 200 litres. Domestic water is heated from 10ºC to 50ºC. Hot water is tapped from the top of the tank at 7 am, noon and 7 pm in three equal portions with a volume flow rate of less than 2 l/min.

The temperature in the top of the heat storage is determined by the set point temperature of the auxiliary energy supply system and the temperature supplied from the solar collector during sunny hours. The set point temperature of the auxiliary volume is 57ºC.

The required heating power and the flow and return temperatures for the space heating system for three one family houses of 150 m^2 with different degrees of insulation are shown in Fig. 2. The heating demands of the three houses are about 30 kWh/(m^2 year), about 60 kWh/(m^2 year) and about 100 kWh/(m^2 year). The heating demands are referred to as LOA30, LOA60 and LOA100 corresponding to 4818 kWh/year, 9488 kWh/year and 15870 kWh/year, respectively.

All positions for inlet to the tank and outlet from the tank are given as relative heights defined as: inlet height / total height of the tank, where 0 equals the bottom of the tank and 1 equals the top of the tank.

The solar combi systems used in the calculations has a solar collector area of 20 m^2. The collector tilt is 65° and the collectors are oriented south. The solar collector fluid is a 40% (weight) propylene glycol/water mixture. The volume flow rate in the solar collector loop is 1.2 l/min/m^2 during high flow operation with an external heat exchanger and a heat exchanger spiral in the solar collector loop and 0.17 l/min/m^2 during low flow operation with a stratifier in the solar collector loop. A differential thermostat control with one sensor in the solar collector and one in the tank and with start/stop difference 10 K/0.5 K is used to control the pump in the solar collector loop. The relative heights of the temperature sensors in the tank during high and low flow operation are 0.14 and 0.01 respectively. The solar collector efficiency, η and the incidence angle modifier, k_θ are given by:

$$\eta = k_\theta \cdot \eta_0 - a_1 \cdot (T_m - T_a)/E - a_2 \cdot (T_m - T_a)^2/E \quad (1)$$

$$k_\theta = 1\text{-}\tan^{4.2}(\theta/2) \quad (2)$$

The start efficiency $\eta_0 = 0.756$, the heat loss coefficients $a_1 = 4.17$ W/(m^2·K) and $a_2 = 0.0095$ W/(m^2·K^2). T_m and T_a are the mean solar collector fluid and the ambient temperatures. E is the irradiance on the solar collector and θ is the incidence angle.

The efficiency of the auxiliary boiler is 100%. The storage volume is 1000 l (260 l DHW tank) and the auxiliary volume is 190 l. The tank height is 2 m and the diameter of the tank is 0.798 m. The heat loss coefficient of the tank, sidearm and DHW heat exchanger are 3.82 W/K, 0.39 W/K and 0.37 W/K respectively. The heat transfer coefficient of the external heat exchanger for the system with stratifier in solar collector loop, tank heat exchanger spiral in solar collector loop, heat exchanger spiral in space heating system and tank in tank heat transfer are 2000 W/K, 1500 W/K, 750 W/K and 278 W/K respectively. The relative outlet height for the space heating system is 0.98. Finally, the relative inlet and outlet height of spiral in solar collector loop are 0.305 and 0.06.

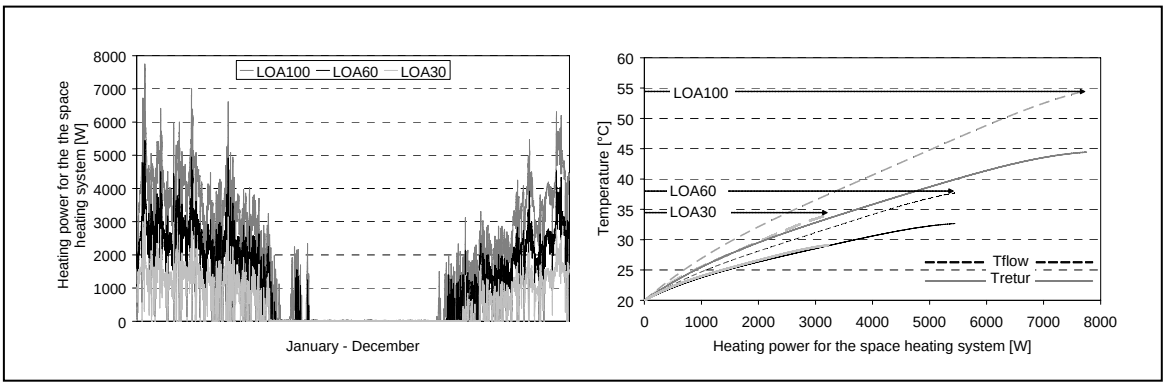

Fig. 2: Power for the space heating systems and flow and return temperatures in the space heating systems, used in the calculations.

The abbreviations spiralHX, fixSH, strsolar, strSH, 100 and 200 represent heat exchanger in the solar collector loop, fixed return inlet height from the space heating loop, stratifier in the solar collector loop, stratifier in the space heating loop, and daily domestic hot water consumption of 100 litres and 200 litres, respectively.

The net utilized solar energy is defined as: Energy for domestic hot water consumption + energy for space heating demand – auxiliary energy. Finally, the performance ratio is defined as: Net utilized energy for the system in question / net utilized solar energy for the system used as reference.

2.2 Results

The results are shown as the net utilized solar energy as a function of the parameter varied. Further, the results are shown as the performance ratio as a function of the parameter varied. The parameters varied are: The domestic hot water consumption, the space heating demand and the relative return inlet height from the space heating loop.

Fig. 3 shows the calculated yearly net utilized solar energy as a function of the relative return inlet height from the space heating loop for model 1.1 with a heat exchanger spiral in the solar collector loop and fixed return inlet height from the space heating loop. Further, the performance ratio relative to the optimal thermal performance of the system in question is shown. The space heating demand is varied in accordance with Fig. 2 and the daily domestic hot water consumption is 100 litres and 200 litres. Also the net utilized solar energy is shown for model 1.3 with a stratifier in the space heating loop.

The calculated yearly net utilized solar energy as a function of the relative return inlet height from the space heating loop for model 2 and model 3 are not shown. The results are similar to the results for model 1.

The figure shows that the optimal inlet position from the space heating loop varies with the daily domestic hot water consumption and the space heating demand. For low space heating demand,

and thereby low return inlet temperatures, the optimal inlet position is low. For increasing space heating demand, and thereby increasing return inlet temperature, the height of the optimal inlet position increases. Also the optimal return inlet position from the space heating loop increases for increasing domestic hot water consumption. This is due to a larger amount of cold water in the bottom of the tank, which leaves the warmer water that matches the temperature of the return water from the space heating loop at a higher level in the tank.

The yearly net utilized solar energy is reduced by less than 1% if the relative return inlet position from the space heating loop is 0.3 compared to the optimum return inlet position. This is also the case for the system model 2 and 3.

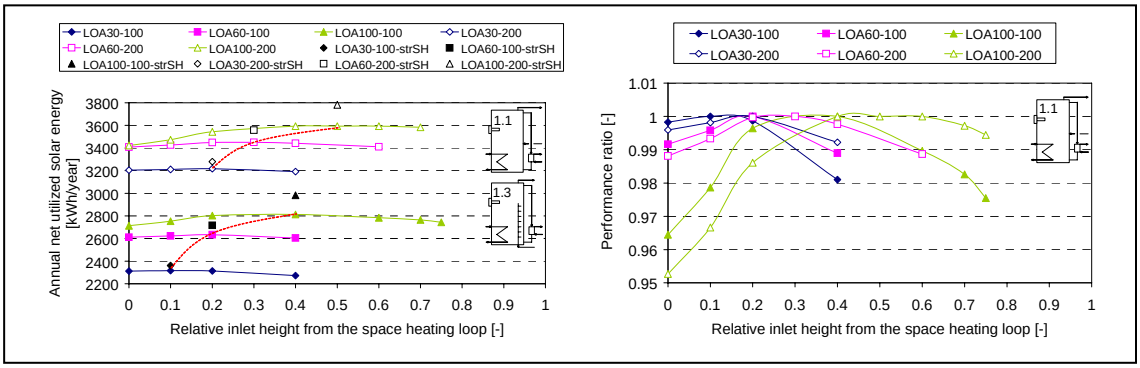

Fig. 3: Left: The annual net utilized solar energy as a function of the relative return inlet height from the space heating loop for model 1.1 and model 1.3. Right: The performance ratio relative to the optimal thermal performance of the system in question.

Fig. 4 shows the net utilized solar energy as a function of the space heating demand and the domestic hot water consumption for model 1 and a step by step improvement of the designs. Also the performance ratio relative to the least advanced model 1.1 is shown. In all the calculations with a fixed return inlet height from the space heating loop, the optimal return inlet height shown in Fig. 3 is used. The net utilized solar energy as a function of the space heating demand and the domestic hot water consumption for model 2 and model 3 are not shown. The results are similar to the results for model 1.

The figure shows that the thermal performance increases for increasing space heating demand and increasing domestic hot water consumption. Also, the figure shows that the thermal performance increases when the heat exchanger spiral is replaced with a stratifier in the solar collector loop and when an inlet stratifier is used for the returning water from the space heating system instead of a fixed return inlet position, and that the thermal performance advantage is larger with a stratifier in the solar collector loop than with a stratifier in the space heating loop. Finally, it can be seen that the best performing system has inlet stratifiers both in the solar collector loop and in the space heating loop.

The extra net utilized solar energy by using stratifiers increases for increasing space heating demand. This is due to the return temperature from the space heating system, which is higher for high space heating demands than for low space heating demands. Hence the variation in the return temperature from the space heating system is higher for high space heating demands than for low space heating demands, and this leads to a better utilization of a stratifier.

The increase in yearly net utilized solar energy by using a stratifier in the solar collector loop, in the space heating loop or in both the solar collector loop and in the space heating loop is in the range of 5 – 8%, 2 – 6% and 7 – 14%, respectively for the system model 1, model 2 and model 3.

It is obvious that the thermal performances of the systems are highly influenced by the consumption and the design of the systems.

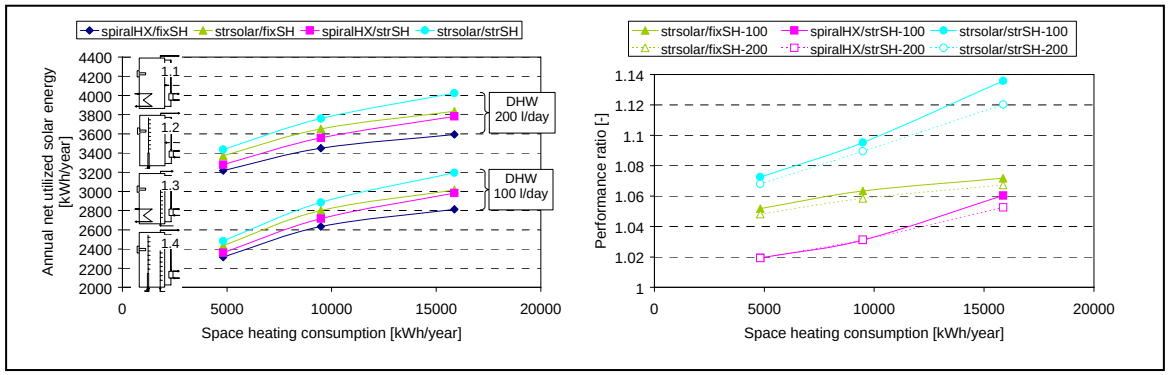

Fig. 4: Left: The annual net utilized solar energy as a function of the space heating demand and the domestic hot water consumption for model 1 and the step by step improvement of the models. Right: The performance ratio relative to the thermal performance of the least advanced models, model 1.1.

2.3 System comparison

Figure 5 shows the annual net utilized solar energy as a function of the space heating demand and a domestic hot water consumption of 100 l/day. The figure also shows the performance ratio where the reference system in all cases is the similar system model 1. In this way it can be seen how much better model 2.1 and model 3.1 perform than model 1.1, or how much better model 2.2 and model 3.2 perform than model 1.2 and so forth.

Figure 5 shows that model 1 has always the lowest thermal performance compared to the similar model 2 and model 3. Further, it can be seen that model 2 has a higher thermal performance than the similar model 3. The best performing system is the tank in tank system model 3.4 with inlet stratifiers in both the solar collector loop and in the space heating loop.

The reason why model 2 is performing better than the similar model 1 and model 3 is most likely because the tank is a domestic hot water tank where the incoming cold water is directly utilized to cool the lower part of the tank. In model 1 the water returning from the domestic hot water heat exchanger to the tank is somewhat warmer than the cold water temperature. In model 3 the incoming cold water reaches a higher level in the heat storage after a domestic hot water draw off caused by the shape of the inner tank. The reason why model 3 is performing better than model 1 is most likely due to the higher tank heat loss coefficient of model 1 since the heat loss coefficients of the sidearm and the external domestic hot water heat exchanger are added to the tank heat loss coefficient. A further disadvantage for model 1 is that the set point temperature of the auxiliary volume must be about 10 – 15 K higher than the required hot water temperature to meet the hot water demand. The set point temperature in model 2 and model 3 only needs to be slightly higher than the required hot water temperature to meet the same demand. This effect is not investigated by calculations in this paper.

The performance ratio is higher for low space heating demand than for high space heating demand. With domestic hot water consumption of 100 l/day, the performance increase by using model 2 instead of model 1 is in the range of 1.5 – 2.2% and 0.8 – 1.5% by using model 3 instead of model 1.

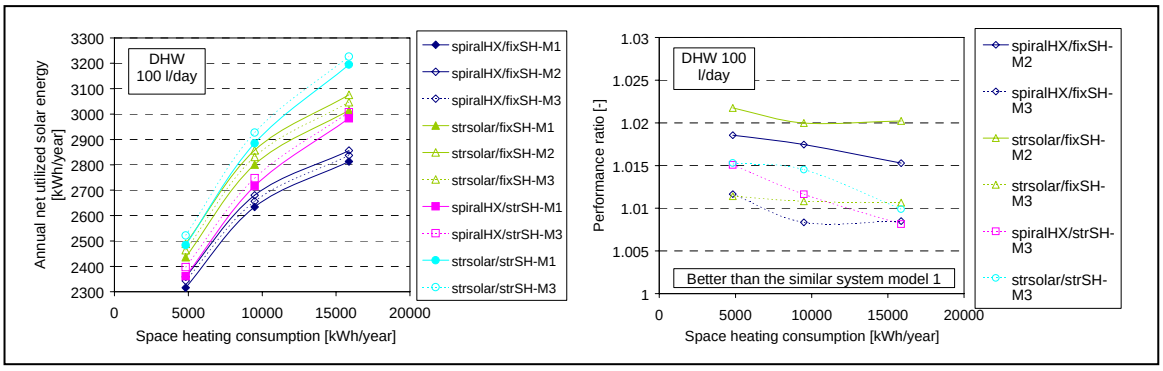

Fig. 5: Comparison of model 1, model 2 and model 3. Left: The annual net utilized solar energy as a function of the space heating demand and the domestic hot water consumption and the step by step improvement of the models. Right: The performance ratio relative to the thermal performance of the similar system model 1.

3. Conclusion

Three basically differently designed solar combi system models are investigated theoretically. The solar combi system systems have a storage volume of 1000 litres with 20 m^2 solar collector area.

Conclusions: **1)** The best performing solar combi system is based on a tank in tank storage with stratifiers both in the solar collector loop and the space heating loop. **2)** The thermal performance increases with 5 – 8% if stratifiers are used only in the solar collector loop. **3)** The thermal performance increases with 2 – 6% if stratifiers are used only in the space heating loop. **4)** The thermal performance increases with 7 – 14% if stratifiers are used both in the solar collector loop and in the space heating loop. **5)** The extra net utilized solar energy for a system with stratifiers in both the solar collector loop and the space heating loop equals the sum of the extra net utilized solar energy of the system only with stratifier in the solar collector loop and the system only with stratifier in the space heating loop. **6)** The thermal advantage by inlet stratifiers decreases for increasing solar fraction. **7)** If the system has a direct return inlet from the space heating loop to the storage, the optimal relative inlet position from the space heating loop is lower for low space heating demands and low domestic hot water consumptions than for high space heating demands and high domestic hot water consumptions. **8)** A suitable position for a direct inlet from the space heating loop, regardless of the space heating demand and the domestic hot water consumption is a relative return inlet height of 0.3

In practice there is an additional advantage by using stratifiers instead of internal heat exchanger spirals and direct inlets because the optimal design of solar combi systems vary with the consumption.

References

[1] Andersen E., Furbo S., Fan J., Investigations of fabric stratifiers for solar tanks, Proceedings of ISES Solar World Congress 2005, Orlando, Florida, USA, 2005.

[2] Drück H., MULTIPORT Store – Model, Type 140 for TrnSys. Institut für Thermodynamik und Wärmetechnik. Universität Stuttgart, 2000.

[3] Klein S.A et al., TRNSYS 15, User Manual. University of Wisconsin Solar Energy Laboratory, 1996.

[4] Skertveit, A., Lund, H., and Olseth, J. A., Design Reference Year, Report no. 1194 Klima, Det Norske Institutt, 1994.

[5] Weiss et al., Solar Heating Systems for Houses, a Design Handbook for Solar Combisystems. James & James Ltd, London. ISBN 1 902916 46 8, 2003.

Bilag 5

Fabric inlet stratifiers for solar tanks with different volume flow rates.

Proceedings EuroSun 2006 Congress, Glasgow, Scotland.

Elsa Andersen & Simon Furbo

Fabric inlet stratifiers for solar tanks with different volume flow rates

E. Andersen[1*] and S. Furbo[1]
[1] Department of Civil Engineering. Technical University of Denmark
DK-2800 Kgs. Lyngby, Denmark
[*] Corresponding Author, email : ean@byg.dtu.dk

Abstract

In this paper investigations of two different two layer fabric stratification pipes are presented and compared to a rigid stratification pipe with holes with "non-return" valves. The fabric stratification pipes are constructed of filament polyester and acrylic. The fabric pipes are mounted in the centre of a glass tank (400 x 400 x 900 mm). The forced volume flow rate is in the range of 6 – 10 l/min, and water enters the stratification pipe from the bottom of the tank. The thermal behaviour of the stratification pipes is investigated for different realistic operation conditions.

Keywords: Solar tanks, Thermal stratification, Inlet stratification pipes

1. Introduction

Thermal stratification in water storages can be achieved in different ways. For instance, water heated by the solar collectors or water returning from the heating system can enter the water storage through stratification inlet devices in such a way that the water enters the tank at a level, where the tank temperature is the same as the temperature of the entering water.

With a rigid stratification pipe with holes the water will flow through the holes depending on the pressure differences between inside and outside of the stratification pipe. With a well performing fabric stratification pipe, the cross section area is flexible. Hence, the fabric pipe can equalize the pressure difference between the inside of the pipe and the tank by contracting or expanding. During periods at tank levels where the temperature in the fabric pipe is higher than the temperature in the tank a contraction of the fabric pipe will reduce the cross section area of the fabric pipe. This leads to a higher velocity inside the fabric stratification pipe and thereby a higher pressure. The fabric pipe contracts until the pressure difference between the inside of the pipe and the tank is eliminated. Consequently, no water from the tank will enter the fabric pipe. The water in the fabric stratification pipe enters the tank when it either reaches the top of the pipe where it is forced to leave the pipe because new water is constantly feed into the pipe or when the temperature in the pipe equals the temperature in the tank leading to a slightly higher pressure in the fabric pipe than in the tank. The fabric pipe will at the right tank level expand in an attempt to equalize the pressure difference, but the expansion is limited by the expansion properties of the fabric and this leads to a flow of liquid from the pipe into the tank in the right temperature level.

Previously a number of fabric stratification inlet pipes have been investigated. Different operation conditions were applied and water with a volume flow rate of 2 l/min entered the fabric stratification pipes through the bottom of the tank. The results were compared to similar results with a good marketed rigid stratification pipe with holes with "non-return" valves. The fabric stratification inlet pipes were constructed of one and two fabric layers. The investigation showed that the largest disadvantage of the fabric stratification inlet pipe was the high horizontal heat transfer through the very thin fabric. The horizontal heat transfer was dramatically reduced when the fabric pipe was constructed of two fabric layers instead of one fabric layer. Further, the investigation showed that a two layer fabric stratification pipe performed as well as the rigid stratification pipe with holes with "non-return" valves [1].

2. Experimental investigations

2.1 Experimental setup

Two fabric stratification pipes made of two fabric layers as well as a marketed rigid stratification pipe with three holes with “non-return” valves are investigated experimentally. The aim of the investigations is to determine how well thermal stratification is build up during different realistic operation conditions. Figure 1 shows to the left: a schematic of the experimental setup, consisting of a glass tank (400 x 400 x 900 mm), a heating and a cooling unit. To the right, the figure shows a schematic of the rigid stratification pipe with a hole with “non-return” valve.

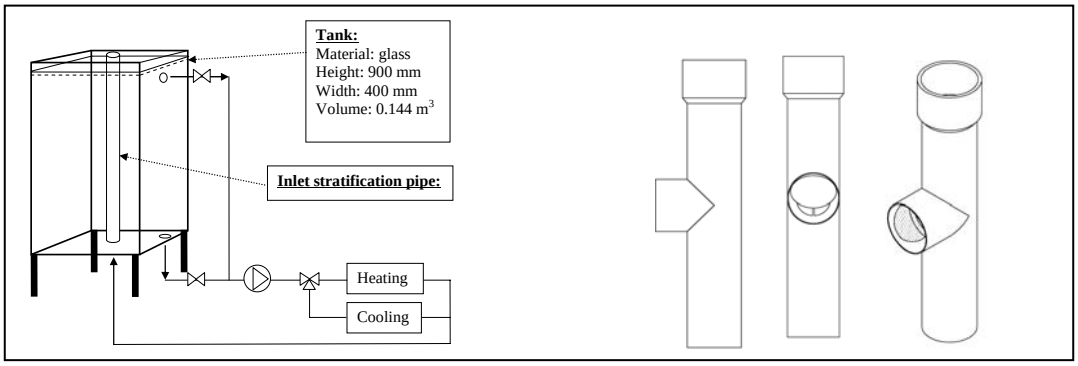

Fig. 1. Left, a schematic of the experimental setup with a stratification pipe mounted in the centre of the tank. Right, schematic illustrations of a rigid stratification pipe with a hole with “non-return” valve.

The inlet stratification pipe is mounted in the centre of the glass tank with the possibility to have a forced flow to enter the stratification pipe from bottom of the tank. The outlet can take place in the top and the bottom of the tank. The thickness of the tank wall is 12 mm and the tank is not insulated. The tank temperatures are measured in 13 different uniformly distributed levels in the tank. The temperatures are measured with copper-constantan thermocouples type TT with an accuracy of 0.5 K. The volume flow rate is measured with an electro magnetic inductive flow meter, type HGQ1 from Brunata HG a/s. The flow meter has an accuracy of about ± 1 %.

2.2 Stratification pipes

The fabric stratification pipes are constructed of an inner pipe with diameter of 40 mm and an outer pipe with diameter of 70 mm. The fabrics are from the US Company Test Fabric Inc. [4]

The rigid stratification inlet pipe has a height of 328 mm and an inner/outer diameter of 52/60 mm. When the inlet stratification pipes are compound the distance between the centres of each inlet is about 292 mm. The stratification pipe is from the German company Solvis GmbH & Co KG [2,3]

2.3 Experiments

The thermal performance of the inlet stratification pipes are investigated for three sets of operation conditions:

- heating tests where the tank is heated from 20°C through the inlet stratification pipe with an inlet temperature of about 32- 40°C. The inlet to the fabric stratification pipe is through the bottom of the tank. The outlet is in the bottom of the tank.
- stratified heating test with an initially stratified tank of 50°C/20°C and an inlet temperature higher than 20°C and lower than 50°C through inlet stratification pipe. The inlet to the fabric stratification pipe is through the bottom of the tank. The outlet is in the bottom of the tank.
- cooling test with an initially heated tank of 50°C and an inlet temperature of about 25-30°C is lead into the tank through the stratification pipe. The inlet to the fabric stratification pipe is through the bottom of the tank. The outlet is in the top of the tank.

The heating tests simulate the thermal behaviour of a stratification pipe in a solar collector loop while the cooling tests simulate the behaviour of a stratification pipe in a space heating loop.

The forced volume flow rates are 6 l/min, 8 l/min and 10 l/min. In each experiment about 90 litres of water are circulated through the tank.

The upper hole of the rigid stratification pipe is situated about 60 mm below the water level in the tank.

The fabric stratification pipes are closed in the top. This is important in order to make the fabric pipes behave as intended. The water in the fabric pipes flows from the pipes into the tank when the total pressure in the pipes exceeds the total pressure in the tank in the corresponding level and where the resistance against passing the fabric pipe walls is lowest. If the fabric stratification pipes are left open in the top, the lowest resistance might be through the top of the pipes regardless of the temperature conditions in the pipes and the tank. The experiments are carried out with two fabric styles:

- Style 864, Spun Orlon Type 75 Acrylic Plain Weave (non-stretchable)
- Style 700-12, Filament polyester, Poly-Lycra (stretchable)

2.4 Results – heating and cooling experiments

The temperature profiles during the heating and the cooling tests with forced volume flow rates of 6 l/min, 8 l/min and 10 l/min are shown in Fig. 2, Fig. 3 and Fig. 4, respectively. The figures show the normalized temperatures in different levels in the tank. The curves show the temperature profile after 30 litres, 60 litres and 90 litres of water have been circulated through the tank.

During the heating tests with a volume flow rate of 6 l/min, the rigid stratification pipe with holes and “non-return” valves perform better than the fabric stratification pipes, but only slightly better than the fabric stratification pipe style 700-12. The fabric stratification pipes perform better for volume flow rates of 8 l/min and 10 l/min than for a volume flow rate of 6 l/min and much better than the rigid stratification pipe. The reason why the thermal performance of the fabric stratification pipe improves for increasing volume flow rates is most likely that the horizontal heat transfer through the thin fabric pipe to the tank decreases for increasing volume flow rates.

During the cooling tests, the fabric stratification pipes perform better than the rigid stratification pipe for all volume flow rates used in the tests.

Especially the fabric stratification pipe style 700-12 performs very well in all the experiments.

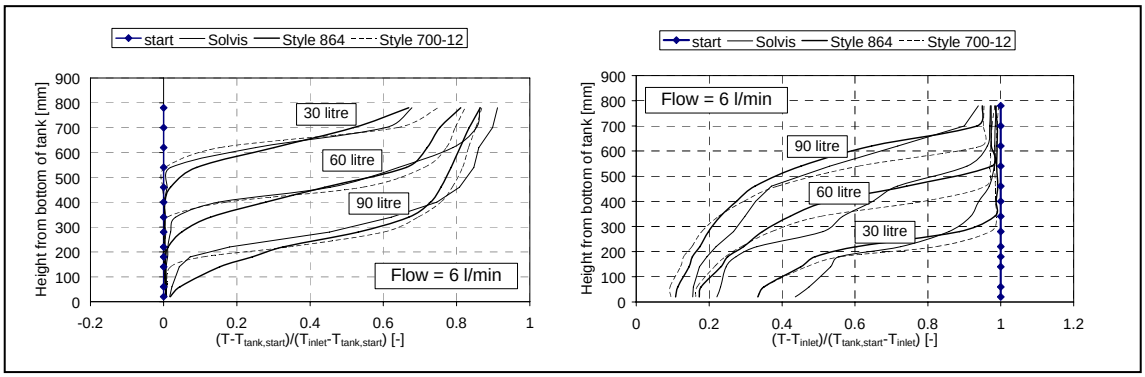

Fig. 2. Temperature profiles from heating (left) and cooling tests (right) with the rigid inlet stratification pipe with holes with “non-return” valves and fabric inlet stratification pipes style 864 and style 700-12. The forced volume flow rate is 6 l/min.

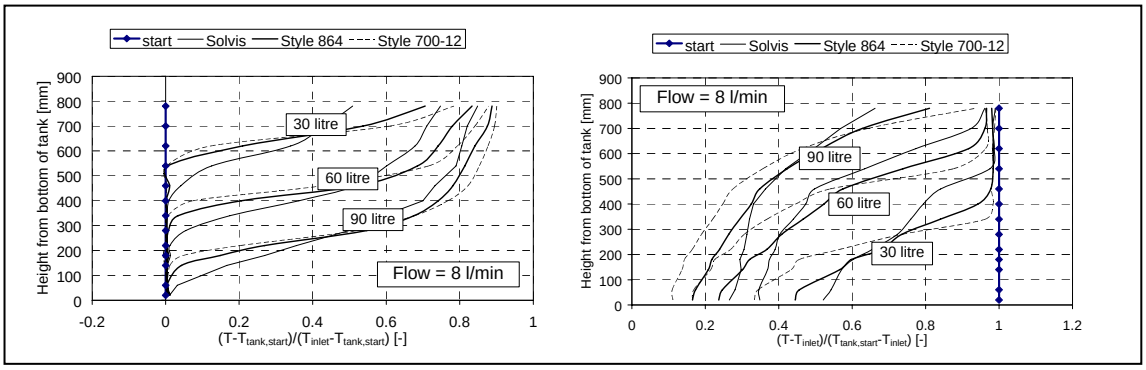

Fig. 3. Temperature profiles from heating (left) and cooling tests (right) with the rigid inlet stratification pipe with holes with "non-return" valves and fabric inlet stratification pipes style 864 and style 700-12. The forced volume flow rate is 8 l/min.

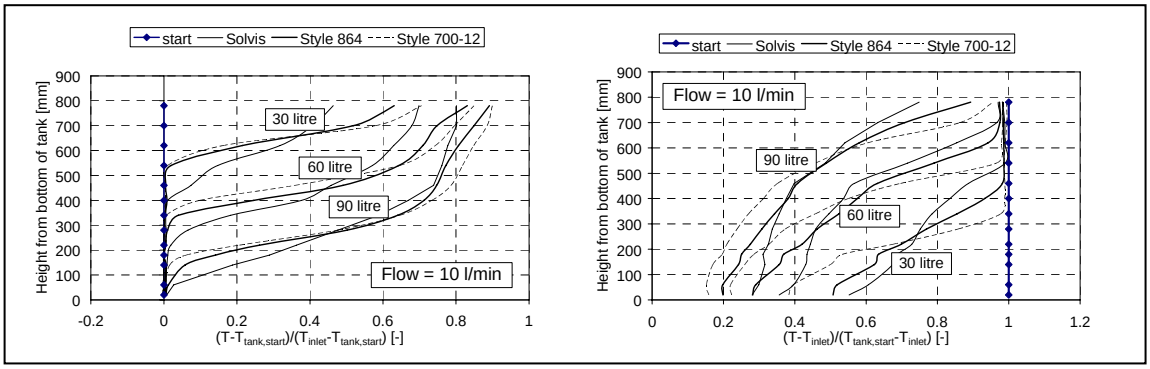

Fig. 4. Temperature profiles from heating (left) and cooling tests (right) with the rigid inlet stratification pipe with holes with "non-return" valves and fabric inlet stratification pipes style 864 and style 700-12. The forced volume flow rate is 10 l/min.

2.4 Results – stratified heating experiments

The temperature profiles during the stratified heating tests with forced volume flow rates of 6 l/min, 8 l/min and 10 l/min are shown in Fig. 5. The figures show the temperatures in different levels in the tank. The curves show the temperature profile after 30 litres, 60 litres and 90 litres of water have been circulated through the tank. The inlet temperatures used in the tests with volume flow rates of 6 l/min, 8 l/min and 10 l/min are about 41°C, 37°C and 33°C respectively. The start temperature at the top of the tank is about 50°C and the aim of the tests is to investigate if the stratification pipes can build up thermal stratification without destroying the already existing thermal stratification.

The figure shows that the fabric stratification pipes succeed to heat up the middle part of the tank without destroying the already existing thermal stratification in all the tests with different volume flow rates while the rigid stratification pipe is not able to maintain the already existing thermal stratification. The reason the rigid stratification pipe is not able to maintain the existing thermal stratification in the same good way as the fabric stratification pipe, is that water can only leave the rigid stratification pipe through one of the three holes and when the right temperature level lies between two holes, the water leaves through both the hole above and the hole below the right temperature level.

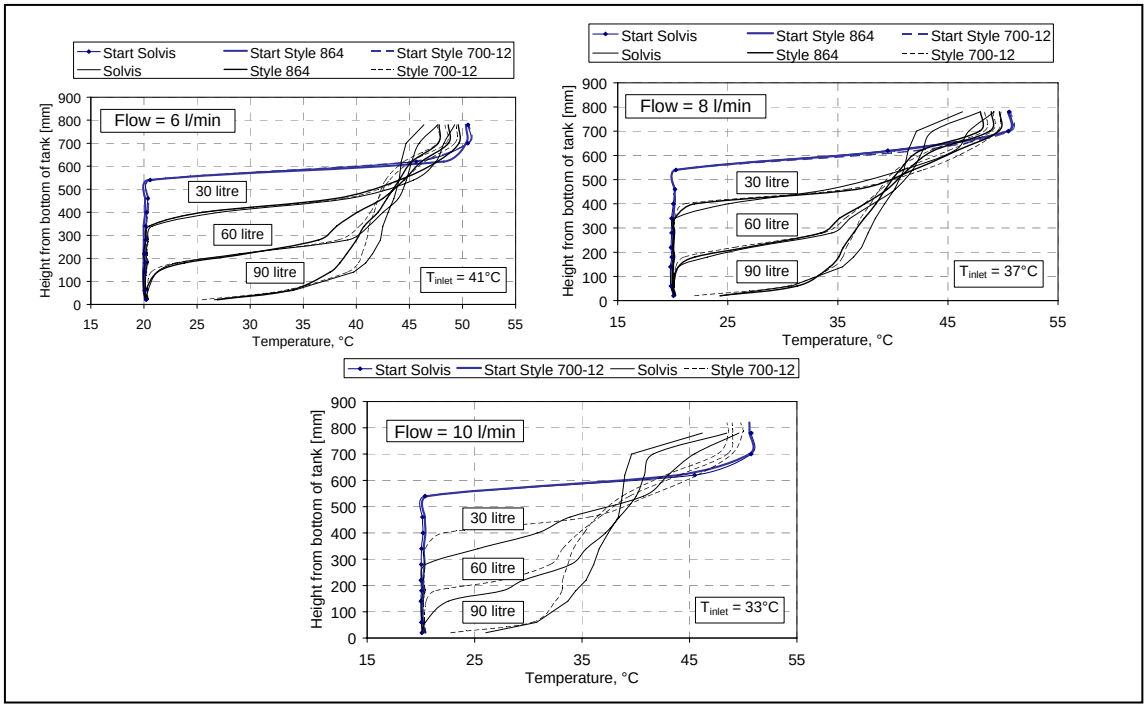

Fig. 5. Temperature profiles from stratified heating tests with the rigid inlet stratification pipe with holes with “non-return” valves and fabric inlet stratification pipes style 864 and style 700-12. The forced volume flow rate is 6 l/min, 8 l/min and 10 l/min.

3. Summary and outlook

Figure 6 shows the temperature profiles during the heating tests with forced volume flow rates of 6 l/min, 8 l/min and 10 l/min. The figures show the normalized temperatures in different levels in the tank. The curves show the temperature profile after 30 litres, 60 litres and 90 litres of water have been circulated through the tank. The results are shown for the rigid stratification pipe with holes with “non-return” valves and the two layer fabric stratification pipes style 864 and style 700-12.

The figure shows that, for the rigid stratification pipe, the thermal stratification is build up in a very good way with a volume flow rate of 6 l/min and worse for increasing volume flow rates. For the fabric stratification pipes the picture is the opposite. The thermal stratification is build up in a better way for high volume flow rates than for low volume flow rates. With low volume flow rates, the heat loss from the surface of the fabric stratification pipes to the tank destroys the thermal stratification. One way of reducing the heat loss for low volume flow rates is to use fabric stratification pipes with a smaller diameter and thereby a smaller surface area and higher velocity in the pipes. Consequently, it is expected that fabric stratification pipes can work well for all volume flow rates, provided that the pipe diameter is adjusted to the flow rate.

From the investigation, it is obvious, that the fabric stratification pipes work very well under the applied realistic operation conditions. The disadvantage at this point, is that knowledge of the long term durability of fabric stratification pipes has not yet been obtained. Long term durability tests will be carried out at the Technical University of Denmark from the end of year 2006.

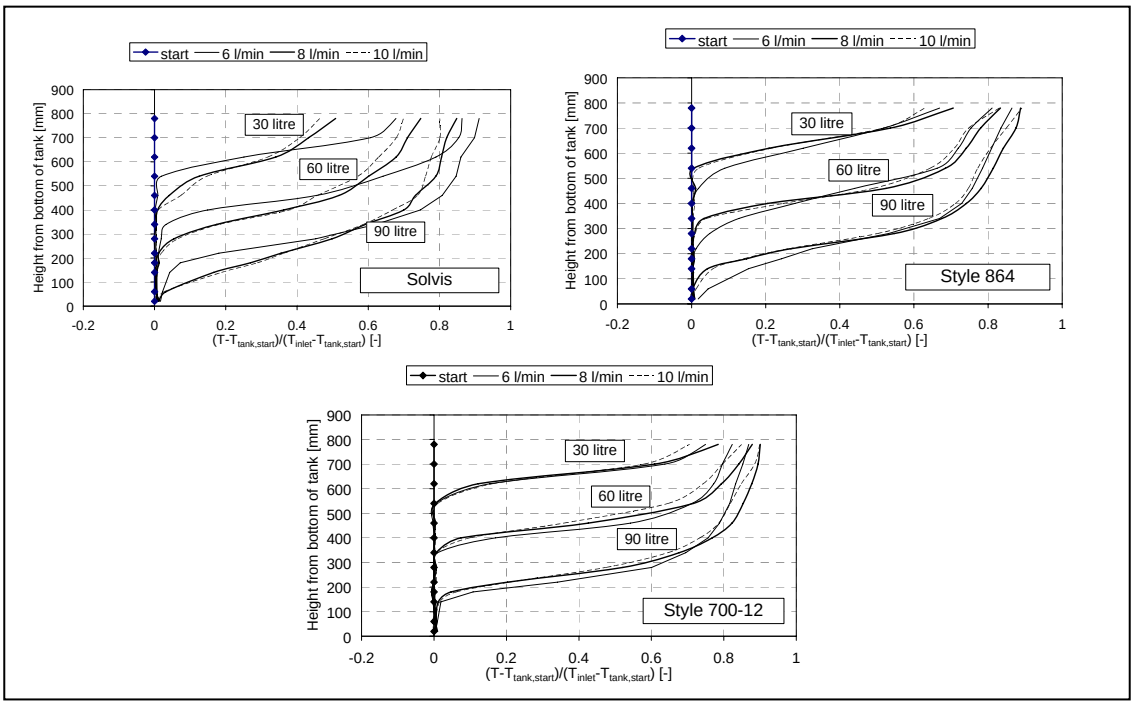

Fig. 6. Temperature profiles from heating tests with the rigid stratification pipe and fabric pipes style 864 and style 700-12. The forced volume flow rates are 6 l/min, 8 l/min and 10 l/min.

4. Conclusion

Two inlet stratification pipes made of two fabric layers are investigated at different operation conditions. The results are compared to identical tests with a marketed rigid stratification pipe with three holes with “non-return” valves. The thermal performance of the stratification pipes is investigated during heating, stratified heating and cooling tests with volume flow rates of 6 l/min, 8 l/min and 10 l/min.

The investigation shows that the thermal stratification is build up in a very good way with the investigated fabric stratification pipes during all the experiments, especially with the stretchable fabric style 700-12. Further, the investigation shows that the thermal stratification is build up in a better way with volume flow rates of 8 and 10 l/min than with a volume flow rate of 6 l/min. It is expected that fabric stratification pipes can work well for all volume flow rates, provided that the pipe diameter is adjusted to the flow rate.

The investigation also shows that the rigid stratification pipe works very well during the heating test with a volume flow rate 6 l/min and that the thermal performance decreases with increasing volume flow rates. Finally, the investigation shows that, during the stratified heating test and the cooling test, the thermal stratification is not maintained in the same good way as with the fabric stratification pipes.

References

[1] Andersen E., Furbo S., Fan J., Investigations of fabric stratifiers for solar tanks, Proceedings of ISES Solar World Congress 2005, Orlando, Florida, USA, 2005.

[2] Krause Th., Kühl L. Solares Heizen: Konzepte, Auslegung und Praxiserfahrungen, 2001.

[3] Shah L.J. Stratifikationsindløbsrør. Department of Civil Engineering, Technical University of Denmark, DTU, 2002.

[4] www.testfabrics.com

Bilag 6

Heat of fusion storage with high solar fraction for solar low energy buildings.

Proceedings EuroSun 2006 Congress, Glasgow, Scotland.

Jørgen M. Schultz & Simon Furbo

Heat of Fusion Storage with High Solar Fraction for Solar Low Energy Buildings

J.M. Schultz[1*] and S. Furbo[1]
[1] Department of Civil Engineering, Technical University of Denmark,
Build. 118, Brovej, DK-2800 Kgs. Lyngby, DENMARK
[*] Corresponding Author, email : js@byg.dtu.dk

Abstract

This paper presents the theoretical investigation on a concept for a seasonal thermal storage based on the phase change material sodium acetate trihydrate with active use of supercooling as a measure to achieve a partly heat loss free thermal storage. The effect of supercooling allows a melted part of the storage to cool down below the melting point without solidification preserving the heat of fusion energy. If the supercooled storage reaches the surrounding temperature no heat loss will take place until the supercooled salt is activated. The investigation shows that this concept makes it possible to achieve 100% coverage of space heating and domestic hot water in a low energy house in a Danish climate with a solar heating system with 36 m² flat plate solar collector and approximately 10 m³ storage with sodium acetate. A traditional water storage solution aiming at 100% coverage will require a storage volume several times larger.

Keywords: Solar heating systems, heat of fusion storage, seasonal storage, sodium acetate

1. Introduction

A key parameter for increasing the yield of solar heating systems is efficient thermal storages that can store large amounts of energy in a reasonable storage volume with limited thermal losses. Water storages are the most common used storage technology and large improvements with respect to reaching almost ideal stratification as well as efficient control strategies have been achieved.

Combined solar heating systems, i.e. systems for both domestic hot water (DHW) and space heating, require larger storage capacities than DHW-systems leading to larger storage volumes in order to store the energy for longer periods. Storage of heat for longer periods often means that the average storage temperature in periods with surplus of solar energy will be very high leading to higher heat losses reducing the useful energy for space heating. Therefore phase change materials (PCM's) with a melting point at a useful temperature level are interesting in order to increase the thermal storage capacity at moderate temperatures. One of these phase change materials is sodium acetate trihydrate, $NaCH_3COO\ 3H_2O$, which melts at 58 °C with a heat of fusion energy of approximately 265 kJ/kg [1]. Sodium acetate is capable of supercooling, i.e. it is able to cool down to temperatures below its melting/freezing point without solidification. This is normally seen as a drawback as the heat of fusion energy is not released.

However, as part of the IEA Solar, Heating and Cooling programme, Task 32: "Advanced Storage Concepts for Solar and Low Energy Buildings", the idea of active use of stable super cooling as a measure to obtain a partly heat loss free seasonal storage is investigated. When first melted the storage will cool down to the surrounding temperature without phase change preserving the latent heat related to the phase change. In this state the storage will have no heat loss until the phase change is activated. The principle of super cooling is shown in Fig. 1.

Theoretical comparison between sodium acetate storages with active use of supercooling and water storages shows that the benefit of using a PCM storage compared to a traditional water storage is limited with respect to absolute annual energy savings for storage sizes up to 1 m^3, but if the same amount of net utilised solar energy should be reached it would require a water storage that is 2 – 3 times larger [2]. But for larger storage volumes - at fixed solar collector areas - PCM

storages will result in an increased solar fraction, which will not be the case for water storages due to larger heat losses compared to the PCM-storages.

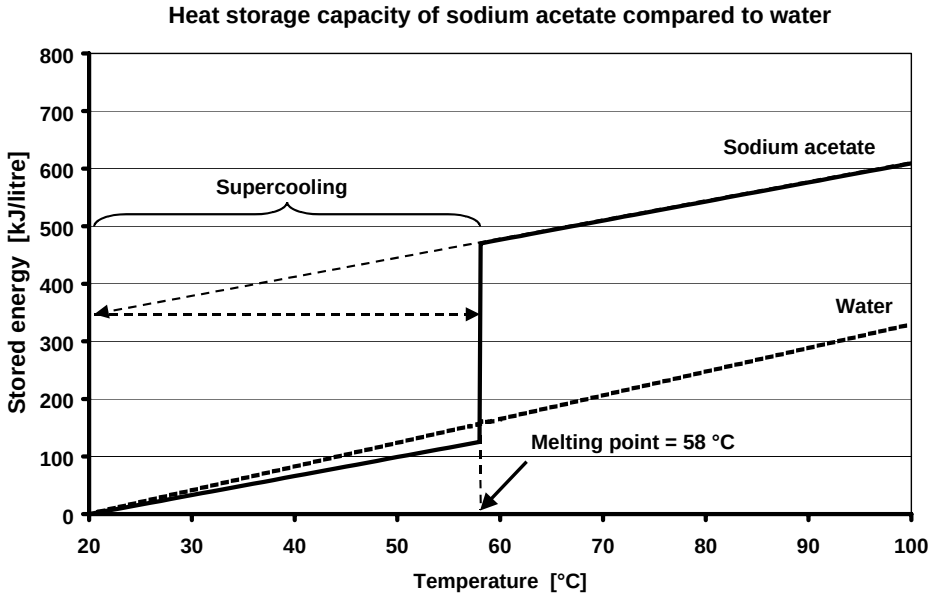

Fig.1. Illustration of energy content of sodium acetate compared to water as well as the super cooling process.

The theoretical investigations [2] also showed that the effect of the supercooling is limited for PCM storage volumes up to approximately 3 m^3 as the heat loss free state is seldom reached. However for larger PCM storage volumes the heat loss free state may become reality, and it might be possible to achieve very large solar fractions by active use of the supercooling process.

This paper presents the theoretical study of the potential of a seasonal phase change material storage with active use of supercooling for achievement of 100% solar coverage of both domestic hot water and space heating in a low energy single family house in a Danish climate (56° north, approx. 3000 degree days).

2. System description

2.1 System design

The solar heating system design is shown in Fig. 2. The system is made up of a solar collector loop and a load loop interconnected by the heat of fusion storage and a heat exchanger. The collectors are high efficient flat plate south facing collectors with a start efficiency of 0.82, 1st order heat loss coefficient = 2.44 /m²K, 2nd order heat loss coefficient = 0.005 W/m²K² and incident angle modifier (tangens equation) = 3.6. The collector tilt is 75°. The flow in the solar loop is set to 50 kg/hr per m² collector (0.833 l/min/m²). The flow in the load loop is in all cases constant at 120 kg/hr (2 l/min).

The system has two individual heat storages – a heat of fusion storage and a 180 litres domestic hot water storage with water as storage medium. The PCM storage and the DHW storage are both insulated reaching an effective U-value of approximately 0.6 W/m²K.

The DHW water storage makes it possible to fulfil the power requirement related to DHW draw offs, which will be difficult to achieve by direct discharging of the PCM storage. The solar collector loop can transfer energy to the PCM storage and/or the load loop through the heat exchanger. Depending on the demand the load loop fluid can be heated by discharge of the PCM-storage.

The heat exchangers (charging and discharging) in the PCM storage have a heat transfer coefficient of 500 W/K and the heat transfer coefficient in the DHW tank is assumed indefinite in the TRNSYS type used. The external heat exchanger connecting the solar collector loop and the load loop is a counter flow plate heat exchanger with a heat transfer coefficient of approximately 800 W/K.

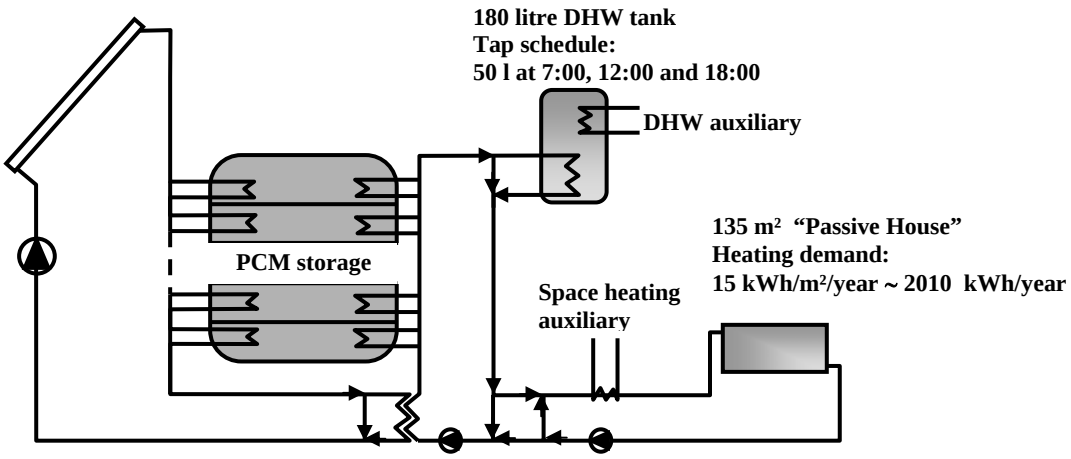

Fig. 2. Outline of the system design.

The PCM storage is a sodium acetate tri-hydrate storage made up of a number of individual sections, which can be fully controlled with respect to charging, discharging and activation of solidification if in a supercooled state. Each section is considered thermally independent of each other but heat loss to the surroundings is accounted for. The purpose of the subsections is to avoid activating the total volume of supercooled PCM at one time, i.e. the subsections make it possible to match the demand in a more efficient way. In the simulations the storage is anticipated to have a cylindrical form with the most favourable relation between diameter and height with respect to minimising the surface area.

Electrical heaters supply auxiliary energy for DHW and space heating. The top volume of the hot water tank heated by electric heating elements is 72 litres. The space heating system is a low-temperature system e.g. floor heating with a constant return temperature of 25°C. The low energy house conforms with the so-called "Passive house" standard, i.e. an annual energy consumption for space heating of 15 kWh/m² corresponding to approximately 2010 kWh/year for a 135 m² floor area. The space heating demand is simulated by the building simulation tool tsbi3 [3] and entered into the model, as hourly values of space heating demand and corresponding required supply temperatures in the heating system. A daily hot water consumption of 150 l heated from 10 °C to 50 °C corresponding to approximately 2500 kWh/year is assumed.

2.2 Control strategy

When solar energy is available the control strategy is:

- If possible the DHW storage is heated until a temperature of 55°C is reached in the bottom of the storage by-passing the PCM storage.
- Next the space heating demand is covered directly - if possible. In case the solar collector fluid temperature is at a level where it allows for both heating of a section in the PCM storage and covering the space heating demand this will be done.
- If the hot water tank temperature is high enough and no space heating demand is present the PCM storage will be charged one section at the time until fully melted (if possible). After all sections are melted the DHW storage is charged until a maximum temperature of 70 °C has been reached. The charging of the PCM storage will continue until a maximum storage temperature of 100°C is reached.

Discharging of the PCM storage:

- If the DHW storage requires energy, if possible a liquid PCM storage section with a temperature higher than 55°C is discharged. If no liquid storage section fulfilling the requirements is present the control looks for a solidified section with a temperature higher than 55°C. If this also fails, the control looks for a supercooled section that can be activated in which case the storage section temperature immediately increases to the melting temperature (58°C) and can be discharged. The supercooled section with the highest temperature is used.
- If only energy for the space heating is required the same strategy is used, but the governing temperature is the required supply temperature in the space-heating loop.

3. Parametric studies

The ideal PCM storage has been modelled as a TRNSYS [4] type and the solar heating system shown in figure 2 has been simulated for a range of different parameters with respect to collector area, PCM storage volume and influence of section volume size on the overall performance.

The overall goal for the investigations is to theoretically design a solar heating system with 100% solar fraction in low energy house in a Danish climate. Therefore the parametric studies are focused on reaching this goal.

3.1 Collector area versus storage volume

Fig. 3 shows calculated results of a parametric study on collector area versus storage volume. The subsection volume is fixed to 100 litres in all cases. The net utilised solar energy is defined as the sum of space heating and domestic hot water demand minus the sum of supplied auxiliary energy.

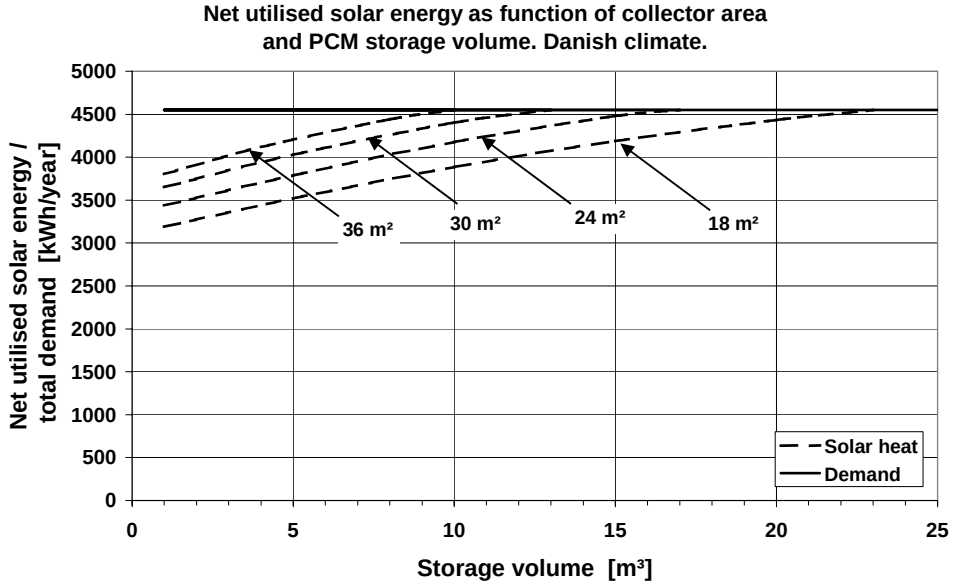

Fig. 3. Net utilised solar energy as function of collector area and PCM storage volume. The dotted curves are the net utilised solar energy for 18, 24, 30, 36 m² collector area respectively. The solid line represents the total space heating and DHW demand.

Fig. 3 shows that increasing the solar collector area can reduce the required storage volume significantly, i.e. doubling the collector area from 18 m² to 36 m² reduces the required PCM storage volume from 23 m³ to 10 m³. This does not only save space and PCM material but it also reduces the total number of subsections and by that the required amount of control hardware (valves, sensors, etc.) to be able to control the subsections individually.

3.2 Influence of subsection volume

The simulations described above were carried out with a fixed subsection volume of 100 litres independent of the total storage volume. The subsections make it possible only to activate one small part of a supercooled storage and not the total storage volume in which case all the latent heat in the supercooled state would be released and most of it lost as heat loss. In theory the thermal performance of the solar heating system will increase by increasing the number of subsections so only the PCM volume exactly matching the demand will be activated. However, increasing the number of subsections also increases the amount of control hardware, which makes fewer subsections desirable. Therefore a parametric study is carried out for the system with 36 m² collector area varying the subsection volume between 100 litres and 1 m³. The result is shown in Fig. 4.

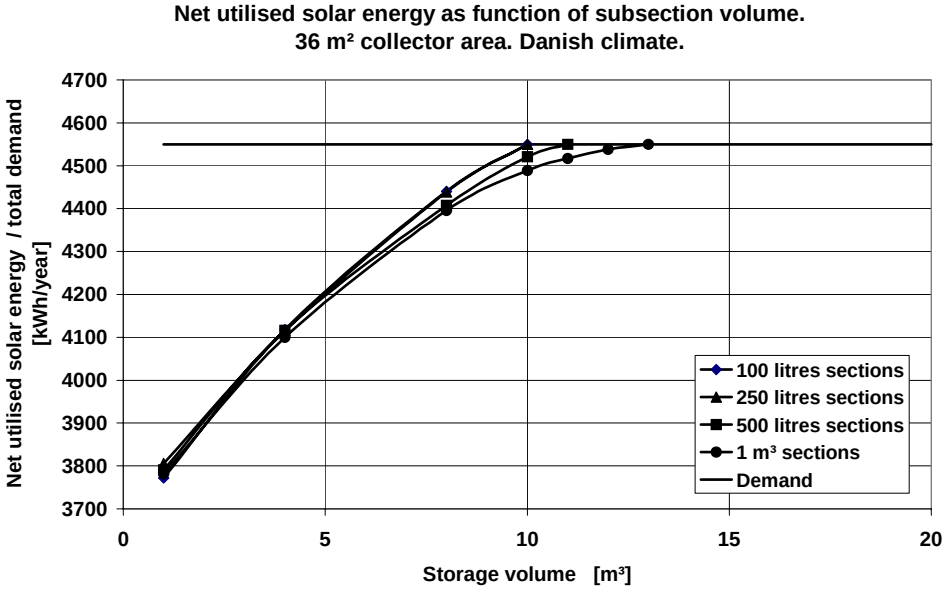

Fig.4. Net utilised solar energy as function of subsection volume. Collector area = 36 m².

The parametric study shows almost no effect of increasing the subsection volume from 100 litres to 250 litres. Increasing the subsection volume to 500 litres has only minor effect for storage sizes up to approximately 5 m³. If full solar coverage of the total heating demand should be met the total storage volume need to be increased with approximately 1 m³ if the subsection volume is 500 litres. Increasing the subsection volume to 1 m³ would further increase the necessary total storage volume to approximately 13 m³.

The effect of increasing the subsection volume is surprisingly small, but may be due to the large solar collector area that is able to recharge a rather large storage volume in a short time either the DHW storage directly or a PCM section.

3.3 Comparison of PCM- and water seasonal storage solutions

The basic idea for the investigations described in this paper is the active use of supercooling to achieve a partly heat loss free seasonal storage. This can be achieved by use of a phase change material as sodium acetate, which furthermore results in a higher energy density in the storage compared to water for temperatures above the melting point.

In order to quantify the effect simulations have been carried out for the 36 m² collector area case substituting the PCM material in the model with water. The model is operated in exactly the same way as for the PCM storage, i.e. one section at the time is charged until a temperature of 58 °C is reached (if possible), before the next section is charged. When all sections are at 58 °C the charging continues until the upper limit of 100 °C is reached. The heat of fusion energy is set to 0 kJ/kg for the simulation with water. This operation mode will be close to the way a stratified

storage will work and using the same model for both the PCM storage simulations and the water storage simulations exclude any differences in the calculations due to different models.

Fig. 5 shows the system performance as function of storage volume for the PCM storage and the water storage respectively. In both simulations the subsection volume is constant at 100 litres.

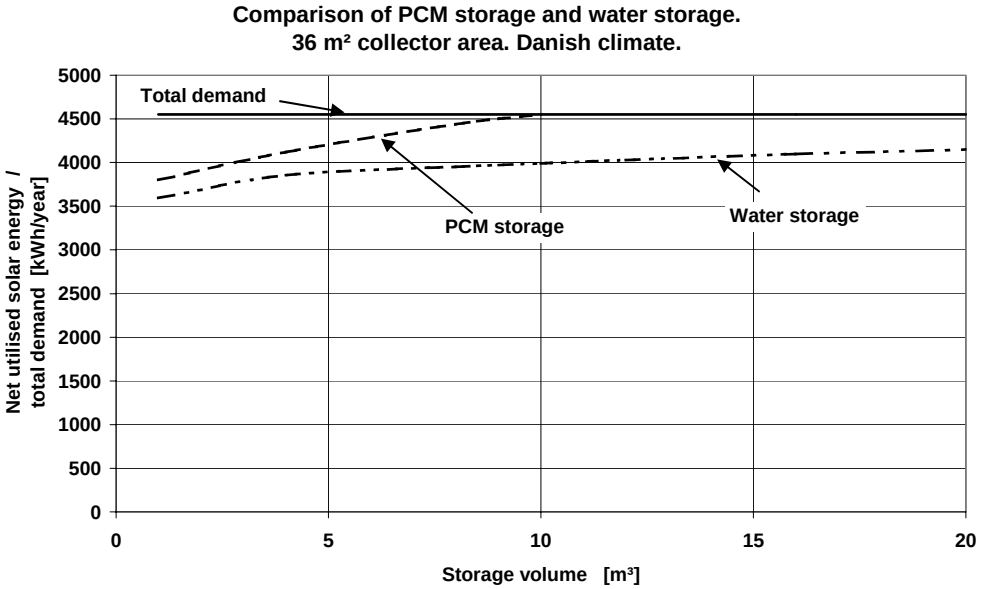

Fig. 5. Comparison of net utilised solar energy as function of storage volume for a PCM storage with sodium acetate and a water storage respectively.

The results in Fig. 5 show that very large storage volumes will be needed if a water storage should cover 100% of the space heating and domestic hot water demand if at all possible without increasing the collector area. This result clearly shows the benefit of the partly heat loss free PCM storage solution, where a storage volume of approximately 10 m³ is sufficient.

4. Conclusion

The theoretical investigations have illustrated the large potential of the use of phase change materials that can supercool in a stable way for seasonal thermal storages in solar heating systems. A 36 m² collector area and a 10 m³ sodium acetate trihydrate seasonal storage results in a solar fraction of 100% in a low energy house in a Danish climate. The PCM storage is subdivided into individual controllable sections of 250 litres, i.e. 40 sections in a 10 m³ storage.

A water storage that should achieve a solar fraction of 100% need to be several times larger and probably also need a larger collector area.

Future work is to build and test a PCM heat storage prototype solving the different design and control requirements, e.g. how to activate the storage on demand and how to monitor the status (melted, supercooled, partly melted, etc.) of the individual subsections.

References

[1] S. Furbo & S. Svendsen. Report on heat storage in a solar heating system using salt hydrates. Report no. 70, Thermal Insulation Laboratory, Technical University of Denmark. (1977)

[2] J.M. Schultz & S. Furbo. Investigation of heat of fusion storage for solar low energy buildings. Proceedings ISES Solar World Congress 2005. (2005)

[3] tsbi3. Danish Building Research Institute. (1993)

[3] TRNSYS 15, ver. 3.0.0.20

Bilag 7

Solar heating systems with heat of fusion storage with 100% solar fraction for low energy buildings.

ISES Solar World Congress 2007 Proceedings, Beijing, China.

Jørgen M. Schultz & Simon Furbo

SOLAR HEATING SYSTEMS WITH HEAT OF FUSION STORAGE WITH 100% SOLAR FRACTION FOR SOLAR LOW ENERGY BUILIDNGS

Jørgen M. Schultz & Simon Furbo
Department of Civil Engineering, Technical University of Denmark
Building 118, Brovej
DK-2800 Kgs. Lyngby. Denmark
js@byg.dtu.dk

ABSTRACT

A storage concept based on the phase change material (PCM) sodium acetate trihydrate and active use of supercooling is theoretically investigated by means of TRNSYS simulations. The supercooling makes it possible to obtain a partly heat loss free storage when the melted salt due to heat loss supercools to the surrounding temperature and no further heat loss occur. The heat of fusion energy is preserved and can be released by activation of the solidification on demand. The investigations show that 100% solar fraction can be reached in a low energy house in a Danish climate with a solar collector area of 36 m^2 and a PCM storage volume of 6 m^3 combined with a 180 litres DHW tank. Experiments have proved that it is possible to melt large volumes of sodium acetate and an automatic controllable activation mechanism has been developed and tested.

1. INTRODUCTION

Solar heating systems can play an important role in connection with reduction of the use of fossil fuels and the related emission of greenhouse gasses. Solar heating systems for domestic hot water (DHW) are widely used but a large part of the heat demand of buildings is related to space heating. In order to achieve a larger solar fraction combined solar heating systems (combi-systems), i.e. systems for both DHW and space heating, are making progress. Typical combi-systems with a tank volume in the range of 300 – 1500 litres and a collector area of 10 – 20 m^2, reaches solar fractions in the range of 15 – 30% [1].

The ultimate goal is to achieve 100% solar fraction which requires a large collector area combined with a water tank volume of 40 – 50 m^3, which makes it inconvenient for application in single family houses. Therefore phase change materials (PCM's) have been investigated for many years as a measure to increase the heat storage energy density by exploitation of the heat of fusion energy. Many PCM's supercool, i.e. the melted PCM remains liquid even if the temperature becomes lower than the freezing point of the PCM. Supercooling can be more or less stable and is in the general application undesirable as it blocks for the use of the heat of fusion energy.

However, as part of the IEA Solar Heating and Cooling programme Task 32, "Advanced storage concepts for solar and low energy buildings" a new concept for a thermal storage with PCM is investigated. This storage concept is based on the advantage of stable supercooling to achieve a partly heat loss free storage, i.e. if the PCM has been fully melted it can cool down in its liquid phase to surrounding temperature and still preserve the latent heat related to the heat of fusion energy. The storage can be left in this state with no heat loss until a demand occurs in which case the solidification is activated, the heat of fusion energy is released and the storage temperature increases almost immediately to the melting temperature of the PCM.

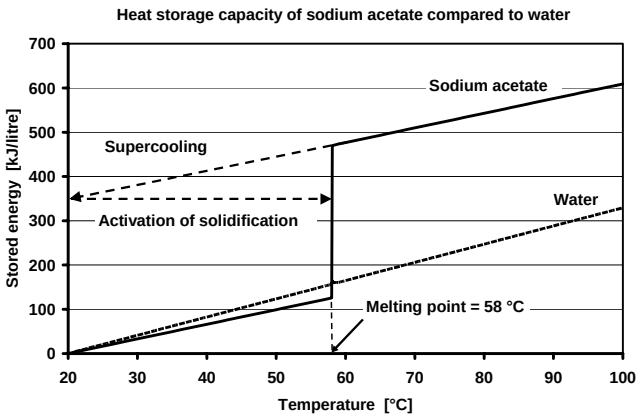

Fig. 1: Illustration of energy density of sodium acetate compared to water as well as the super cooling process.

Fig. 1 illustrates this effect for sodium acetate trihydrate ($NaCH3COO{\cdot}3H_2O$), which melts at approximately 58°C with a heat of fusion energy of approximately 265 kJ/kg (~345 kJ/litre). As shown in Fig. 1 not all the heat of fusion energy is regained as some of the energy is used for heating up the PCM to its melting point. The energy density of the PCM storage is approximately two times higher than for a water storage if the PCM is fully melted.

This paper presents the results from parametric studies with respect to storage and system design and the first experimental results forming the basis for storage prototype development.

2. SYSTEM DESIGN

The solar heating system design is shown in Fig. 2. The system includes two tanks: The PCM storage and a 180 litres DHW tank. The DHW tank is required to fulfil the power demand related to hot water draw offs, which will be difficult to fulfil with direct discharge of the PCM storage.

Energy from the solar collectors can either be used for direct charge of the PCM storage or transferred to the demand loop through the heat exchanger connecting the solar collector loop and the demand loop. Here the energy can either be used for heating of the DHW tank or for space heating.

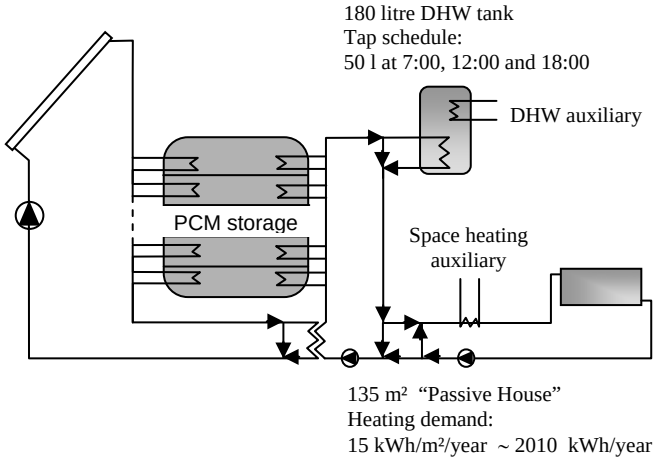

Fig. 2: System design and main boundary conditions.

The PCM storage is made up of a number of subsections that can be individually controlled with respect to charging, discharging and activation of solidification. The sub-sectioning of the PCM storage makes it possible only to activate a small part of the total storage volume to match the demand, but saving the rest of the supercooled sections for later activation.

Previous analyses [2], [3] have shown that the optimum control strategy for charging is first to heat up the DHW tank if the forward temperature from the collector is sufficient. When the DHW tank has reached a temperature of 70°C the PCM storage is thereafter charged one section at the time until fully melted if the forward temperature from the collector is high enough. Otherwise the section with the highest temperature that can be further heated is chosen. In case of space heating demand the necessary forward temperature to the space heating loop is secured by controlling the flow rate through the DHW heat exchanger if relevant or by charging a section in the PCM storage that results in the necessary forward flow temperature to the heat exchanger.

When discharging the PCM storage the section that just has the sufficient temperature for covering the actual demand is chosen. A supercooled section is activated if no liquid or solidified section has the required temperature level.

3. PARAMETRIC STUDIES

The PCM storage with sodium acetate trihydrate including the control has been modelled in a new TRNSYS [4] type and a series of parametric studies have been carried out in TRNSYS with the system design shown in Fig. 2. The solar collectors are high efficient flat plate collectors with a start efficiency of 0.82, 1st and 2nd order heat loss coefficients of 2.44 $W/(m^2{\cdot}K)$ and 0.005 $W/(m^2{\cdot}K^2)$ respectively and incident angle modifier (tangens equation) = 3.6. The collectors are facing south with a collector tilt of 75°. The PCM storage and the DHW tank are in the reference case insulated corresponding to an effective heat loss coefficient of 0.6 $W/(m^2{\cdot}K)$. The flow rate in the collector loop is set to 50 kg/hr per m^2 collector area. The heat transfer rate for charge and discharge of the PCM storage is 500 W/K. The daily DHW consumption is set to 150 litres/day (50 litres draw off at 7.00, 12:00 and 18:00 respectively). The DHW temperature is 50°C and the cold water temperature is 10°C resulting in an annual DHW energy consumption of approximately 2540 kWh/year. The space heating demand is calculated on hourly basis with the building energy simulation tool, tsbi3 [5] for a low energy house built according to the passive house standard [6] located in a Danish climate (~ 3000 degree days; horizontal solar radiation: ~ 1020 kWh/m^2/year). The space heating system is a low temperature system, e.g. floor heating.

Investigations [2], [3] with PCM storage volumes in the range of 0.5 – 3.0 m^3 have shown a limited effect of the supercooling on the yearly system performance as the heat loss free state only was realised for short periods during the year. However, increasing the PCM storage volume increases the benefit of the supercooling and it was found that the total heating demand (DHW + space heating)

probably could be covered 100% by solar with a seasonal PCM storage volume of 10 m^3 and a collector area of 36 m^2. This is less than 25% of the required volume for a water storage if 100% solar fraction should reached. Fig. 3 shows the net utilised solar energy as function of storage volume for the PCM storage and a water storage as well.

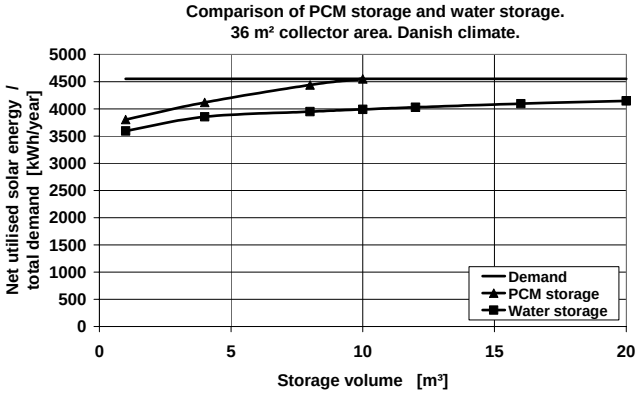

Fig. 3: Comparison of net utilised solar energy as function of storage volume for a PCM storage with sodium acetate and a water storage respectively.

Based on the previous findings the parametric studies carried out and presented in this paper are based on achievement of 100% solar coverage of both DHW and space heating in a low energy house in a Danish climate.

3.1 Influence of section volume

The total PCM storage volume has to be divided into several subsections in order not to activate the solidification of the total supercooled volume but only a volume that matches the actual demand. As a consequence each of these subsections needs their own set of heat exchangers and activation control so from a practical and economical point of view the number of subsection should be as low as possible. Fig. 4 shows the result of a parametric study of the influence of subsection volume on the solar fraction.

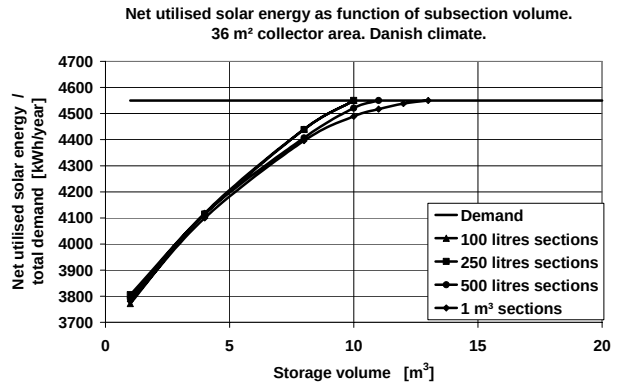

Fig. 4: Net utilised solar energy as function of subsection volume. Collector area = 36 m^2.

The required total PCM storage volume in order to achieve 100% solar fraction is 10 m^3 for subsection volumes up to 250 litres.

Further increase of subsection volume e.g. 500 litres leads to an increase in required total storage volume from 10 m^3 to 11 m^3 to achieve 100% solar fraction. However, the number of subsection is in this case reduced from 40 to 22. The optimum combination must be based on an economical evaluation taking into account the costs for heat exchangers, control equipment, PCM material and required space in the house.

3.2 Influence of storage heat loss

The storage heat loss has been treated as a complete loss but if the storage is placed inside the building the heat loss may be useful for space heating leading to a reduction of the actual space heating demand and consequently the required PCM storage volume. The storage heat loss depends on the insulation level of the storage and the storage surface area.

Fig. 5 shows the required storage volume to achieve 100% solar fraction as function of the storage heat loss coefficient with and without taking into account the usable part of the heat loss for reduction of the space heating demand.

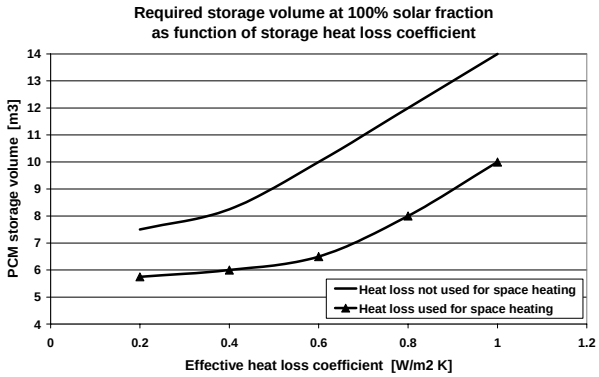

Fig. 5: Required storage volume for 100% solar fraction as function of storage heat loss coefficient and the possible use of the storage heat loss for space heating reduction.

Increasing the insulation level has a significant effect on the required PCM storage volume even though the storage concept is partly heat loss free. The main reason should be found in the autumn where the storage is fully charged and at a high temperature while the heating demand is limited. In this case the more the storage is insulated the more sensible heat is saved for later use.

Taking into account the storage heat loss as a source for space heating would also reduce the necessary PCM storage volume significantly and combining this effect with a highly

insulated storage leads to a reduction in storage volume from 10 m^3 to approx. 6 m^3.

4. EXPERIMENTS

The simulation studies are performed on an ideal model of the PCM storage where the subsections are treated as an ideal material having the same temperature and phase in the total volume (lumped model). The promising simulation results have initiated experiments to clarify and try out different solutions to overcome the foreseen practical problems, e.g. melting and supercooling of large volumes of sodium acetate; how to activate the solidification automatically; etc.

4.1 Melting

Experiences with melting of larger volumes of sodium acetate have been obtained with a 135 litres stainless mantle steel tank. Hot water (80°C) was circulated in the mantle to melt the salt hydrate. A tube pump connected to the tank by flexible tubes going to the bottom and the top respectively makes it possible to pump the melted salt in order to stir the solution during the melting process. The melting process was registered by continuous measurements of the temperatures at several heights in the salt hydrate. It was experienced that even when the temperature in the melted salt was well above the melting point of 58°C some salt crystals still remained deposited at the bottom the tank. Stirring the solution by circulating the salt with the tube pump did not fully solve the problem. Therefore additional water was added to increase the water content above the 40% originally in the salt hydrate to increase the solubility. It was found that increasing the water content just a little had a very positive effect on the problem

4.2 Activation of solidification

Solidification can be activated by dropping a salt crystal into the supercooled salt hydrate and the solidification will start immediately. In commercially available hand warmers a small flexible metal disk with a very thin slit is used. Clicking the metal disk activates the solidification. These two activation mechanisms have formed the basis for development of a mechanical device that could be used. A piston controlled by an electromagnet is pushed into the melted salt and when withdrawn some crystals will be present at the end of the piston. Next time the piston is pushed into a supercooled storage section the crystals will activate the solidification. Initial small scale experiments have been carried out with success. Alternatively the piston could mechanically perform the “clicking” of a metal disk.

5. CONCLUSIONS

Theoretical investigations on an ideal seasonal PCM storage with sodium acetate trihydrate and active use of supercooling show a high potential for achievement of 100% solar fraction in a low energy house located in a Danish climate. The solar heating system has a collector area of 36 m^2 and a PCM storage volume of 6 m^3 subdivided into 24 subsections that can be individually controlled.

Experiments have proved that it is possible to melt larger volumes of sodium acetate if the water content is increased to just a little above 40%. Activation of the solidification can be automated by an electromagnetic controlled piston injecting a salt crystal or clicking a metal disk.

6. FUTURE WORK

Future theoretical work will focus on the effect of using tubular evacuated collectors that has the possibility of higher solar gains in the winter period.

An economically evaluation and optimisation will be carried out for the total solar heating system.

Future experimental work will focus on the building of a laboratory prototype storage with a few sections to demonstrate and test the control system and to evaluate the heat transfer to and from the salt hydrate in its different states.

7. ACKNOWLEDGMENTS

The project is financed by the Danish Energy Authority.

8. REFERENCES

1. A. Thür, “Compact Solar Combisystem”, Ph.D. thesis, report R-160, Department of Civil Engineering, Technical University of Denmark, 2007. ISBN 97-88778-772-343.
2. J.M. Schultz & S. Furbo. “Investigation of heat of fusion storage for solar low energy buildings”, Proceedings ISES Solar World Congress 2005.
3. J.M. Schultz & S. Furbo. “Heat of fusion storage with high solar fraction for solar low energy buildings”, Proceedings EUROSUN 2006.
4. TRNSYS 15, ver. 3.0.0.20
5. “tsbi3”. Danish Building Research Institute, 1993.
6. http://www.passivehouse.com/

Bilag 8

Theoretical comparison of solar combi systems and stratification design options.

Journal of Solar Energy Engineering, Volume 129, pp. 438-448, 2007.

Elsa Andersen & Simon Furbo

Theoretical comparison of solar combi systems and stratification design options

E. Andersen and S. Furbo

Department of Civil Engineering. Technical University of Denmark

Building 118, DK-2800 Kgs. Lyngby, Denmark

e-mail : ean@byg.dtu.dk

Abstract

A theoretical analysis of differently designed solar combi systems is performed with weather data from the Danish Design Reference Year (55ºN). Three solar combi system designs found on the market are investigated. The investigation focuses on the influence of stratification on the thermal performance under different operation conditions with different domestic hot water and space heating demands. The solar combi systems are initially equipped with heat exchanger spirals and direct inlets to the tank. A step-by-step investigation is performed demonstrating the influence on the thermal performance of using inlet stratification pipes at the different inlets. Also, it is investigated how the design of the space heating system, the control system of the solar collectors, and the system size influence the thermal performance of solar combi systems.

The work is carried out within the Solar Heating and Cooling Programme of the International Energy Agency (IEA SHC), Task 32.

Keywords Solar combi system design; Solar combi system size; Space heating system; Inlet stratifier; Net utilized solar energy; Solar fraction.

1 Introduction

In the period 1998-2002, the IEA SHC, Task 26 Solar CombiSystems evaluated 21 solar combi systems on the European market. The evaluation comprised both the system costs and the thermal performance. It was found that most of the systems for one family houses had solar collectors of 10 m^2- 30 m^2 with 0.3 m^3- 3 m^3 tank volumes. The best systems, regarding the performance/cost ratio, were the most advanced systems with inlet stratification pipes, an efficient integrated boiler, and only one control system for both the boiler and the solar collector loop [1].

Further, a sensitivity analysis of 9 of the investigated Task 26 systems was performed [2]. The influence of climate and heat load and of the solar collector, the storage tank, the boiler and the space heating system were investigated. It was found that the optimal

collector tilt depends on the latitude and the solar fraction. The optimal collector tilt increases with increasing solar fraction in order to better utilize the solar irradiation during the heating season. The thermal performance decreases for increasing volume flow rate in the solar collector loop. The heat exchange capacity rate in the solar collector loop should be about 40 W/K per m^2 solar collector. For heat storages with an internal heat exchanger in the solar collector loop, the temperature sensor of the control system should be placed on a level with the lower 1/3 – 1/2 of the heat exchanger. The optimal storage volume is about 100 l/m^2 solar collector area. Storage insulation thicknesses above 15 cm do not increase the thermal performances. Top insulation is less significant than side insulation because the top area is smaller. The auxiliary volume should be kept small and the set point temperature for the auxiliary energy supply system low. The sensor for the auxiliary heater should be placed below the space heating outlet. No big influence on the position of the return inlet pipe from the space heating loop in the heat storage was found. The thermal performance decreases slightly with increasing position of the outlet height for the space heating loop. Most important for the achieved energy savings is the boiler efficiency.

Finally, 3 of the 9 investigated systems were improved significantly by design changes determined by the sensitivity analysis [3]. The strategies used for the improvement were: Keep the boiler efficiency as high as possible, keep the collector inlet as cold as possible, avoid temperature losses through mixing, keep heat losses as low as possible, and use efficient pumps to decrease the electricity demand. This work showed that optimization can improve the system performance significantly and that, for different system designs, the performance is nearly the same if all aspects of the system are optimized.

In [4] it was shown how the thermal performance of a typical Swedish solar combi system with 20 m^2 solar collectors and a 0.75 m^3 storage tank with three internal heat exchanger spirals could be improved by 10% by small design changes without additional system costs. Further, it was shown that the thermal performance can be improved by 25% – 35% by introducing a highly stratified tank.

The advantage of a stratification inlet pipe instead of a fixed inlet height for transferring solar energy to the storage tank by means of a thermosyphon loop was investigated [5]. It was found that for a solar combi system with a solar fraction of about 25%, the thermal performance increased by only 1 – 2% by using a stratification manifold instead of a fixed inlet.

Similar low performance improvements of about 3% by using low flow and inlet stratifiers were measured for solar combi systems with a solar fraction of about 20% [6].

Simulations of solar combi systems were carried out, and it was found that the solar fraction could be roughly estimated by three parameters: The solar collector area, the storage volume and the heat load of the system. The investigations included Austrian, German, Danish and Swedish climates [7].

The thermal performances of four highly advanced and differently designed solar combi systems were compared [8]. The authors found that the most important parameters for a well performing solar combi system are low heat losses and a small auxiliary volume in the heat storage with a low set point temperature. All pipe connections for the auxiliary

and space heating loop should be at appropriate positions. Only then additional thermal performance is achieved with stratification devices.

A number of stratification inlet pipes, so-called stratifiers, were investigated [9]. It was found that in practice thermal stratification can be built up in a nearly perfect way with certain stratifiers, among others with multilayer fabric stratifiers and with rigid stratifiers with holes with flaps that work as non-return valves.

Some of the investigations mentioned above show large thermal advantages by using inlet stratifiers, some show small advantages. The thermal advantage of inlet stratifiers depends strongly on the solar fraction of the solar combi system, the system design, the heating system and the performance of the inlet stratifiers. Further the advantage depends on the reference system used for the comparison. Some of the reference systems in the above mentioned investigations have partially stratified storage tanks. This study focuses on the thermal advantage by using storage tanks with ideally working inlet stratifiers instead of storage tanks without inlet stratifiers for different sizes and designs of solar heating and space heating systems with the same reference conditions. Also, it is investigated how the control system in the solar collector loop influences the thermal performance of solar combi systems. The investigation is carried out by means of the simulation program Trnsys [10] and the multiport store model [11]. The differently designed systems have 1000 litre storage tanks and 20 m^2 solar collectors. The differently sized solar combi systems are based on one system design with storage tanks of 500 litres, 1000 litres and 1500 litres, and solar collector areas from 5 m^2 to 60 m^2.

2 Investigations of differently designed solar combi systems

Figure 1 shows schematic illustrations of the investigated solar combi system types. The first system model is based on a space heating storage with an external heat exchanger mounted in a side arm for domestic hot water preparation. The second system model is based on a domestic hot water tank with an internal heat exchanger spiral connected to the space heating system. The third system model is based on a hot water tank-in-tank storage.

The three system models are referred to as models 1, 2 and 3, respectively. Further, the models are improved by introducing stratifiers in the solar collector loop and in the space heating loop, and in both the solar collector loop and the space heating loop. The variations in each model are numbered successively (Figure 1). The advantage of using stratifiers is that incoming water of any temperature is led into the tank in a level where the temperature of the incoming water matches the temperature of the water in the tank. In this way, thermal stratification in the tank is enhanced without destroying the already existing thermal stratification in the tank. In the present investigation, the thermal stratification is assumed to be built up in a perfect way without any mixing by the inlet stratifier. In this way the investigations show the maximum potential of inlet stratifiers.

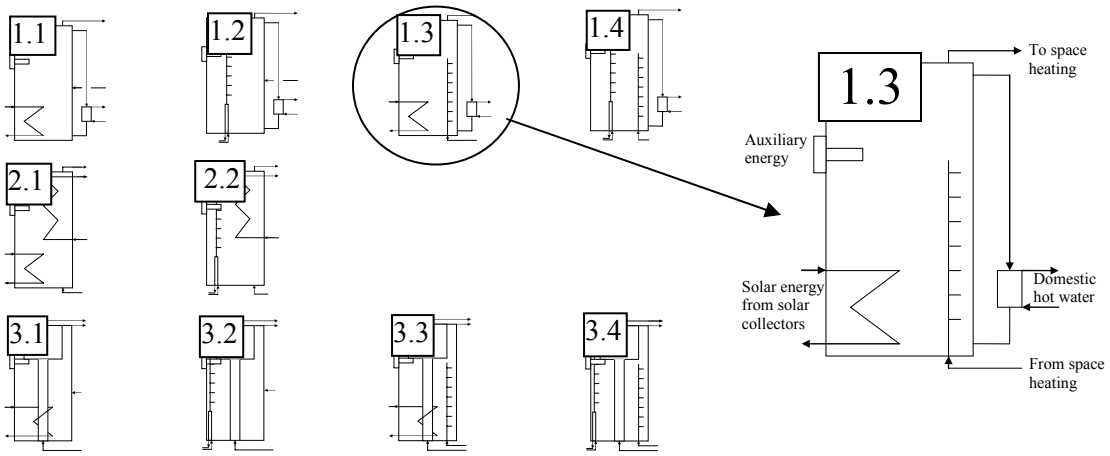

Figure 1: Schematics of the three system models: Model 1 (top), model 2 (middle) and model 3 (bottom), and the successively numbered variations of the system models.

2.1 Assumptions for the calculations

The Danish Design Reference Year, DRY data file, is used as weather data [12]. The daily hot water consumption is either 100 litres (DHW100) or 200 litres (DHW200). Domestic water is heated from 10ºC to 50ºC. Hot water is tapped from the top of the tank at 7 am, noon and 7 pm in three equal portions with a volume flow rate of less than 2 l/min. Neither the size of the external heat exchanger for domestic hot water preparation nor the power of the auxiliary energy supply system is part of the investigation and hence the volume flow rate during domestic hot water draw-off is unimportant. The influence of the draw-off profile was investigated for a solar combi system [13] and it was found that a realistic draw-off profile (statistical derived) decreases the yearly thermal performance 2% mainly because a realistic draw-off profile includes vacation during the summer period. A similar investigation for solar domestic hot water systems [14] showed a yearly thermal performance decrease of 11% – 14% when a realistic draw-off profile was applied. The draw-off profile influences the thermal performance of solar heating systems but the influence is much lower for solar combi systems than for solar domestic hot water systems. Therefore investigations of the hot water consumption pattern are not included in this study.

The temperature in the top of the heat storage is determined by the set point temperature of the auxiliary energy supply system and the temperature supplied from the solar collector during sunny hours. The set point temperature of the auxiliary volume is 57ºC. The efficiency of the boiler is assumed to be 100%.

The required heating power and the flow and return temperatures for the space heating system for three one family houses of 150 m^2 with different degrees of insulation are shown in Figure 2 and Figure 3. The heating demand of the three houses is about 108 MJ/(m^2 year), about 216 MJ/(m^2 year) and about 360 MJ/(m^2 year). The heating demand is referred to as SH108, SH216 and SH360, respectively, corresponding to 17345 MJ/year, 34157 MJ/year and 57132 MJ/year, respectively.

All positions for inlet to the tank and outlet from the tank are given as relative heights defined as: inlet height / total height of the tank, where 0 equals the bottom of the tank and 1 equals the top of the tank.

Table 1 shows data of the solar combi systems used in the calculations. The heat loss coefficient of the sidearm and the external heat exchanger for domestic hot water preparation are measured on a well insulated solar combi system. The heat loss coefficient of the tank is calculated. Investigations of the tank-in-tank heat transfer coefficient based on experiments and Computational Fluid Dynamics calculations showed that the heat transfer coefficient varies with the operation conditions, the design of the inner tank and the temperature level [15]. For simplification, a constant is used.

Table 1: Data used in the calculations.

Solar collector area	20 m^2
Optical efficiency of incident radiation, η_0	0.756
Heat loss coefficients, a_1 / a_2	4.17 W/m^2/K / 0.0095 W/m^2/K^2
Efficiency for all incidence angles, η	$\eta_0 \cdot k_\theta - a_1 \cdot (T_m - T_a)/E - a_2 \cdot (T_m - T_a)^2/E$
Incidence angle modifier for beam radiation, k_θ	$1\text{-}\tan^{4.2}(\theta/2)$
Collector tilt / Orientation	65° / South
Solar collector fluid	40% (weight) propylene glycol/water mixture
Volume flow rate in solar collector loop, high / low	1.2 l/min/m^2 / 0.17 l/min/m^2
Storage volume / auxiliary volume	1000 l (260 l DHW tank) / 190 l
Height/diameter	2 / 0.798 m
Heat loss coefficient, tank / sidearm / domestic hot water heat exchanger	3.82 W/K / 0.39 W/K / 0.37 W/K
Heat transfer coefficient of external heat exchanger when stratifier in solar collector loop is used	100 W/K per m^2 collector
Heat transfer coefficient of: spiral in solar collector loop / spiral in space heating system / tank in tank heat transfer	75 W/K per m^2 collector / 750 W/K / 278 W/K
Volume between temperature sensor that controls the supply of auxiliary energy and the lowest part of the auxiliary volume	50 l
Relative inlet/outlet height of domestic hot water loop	0 / 1

Relative outlet height of space heating system	0.98
Relative inlet/outlet height of heat exchanger spiral in solar collector loop	0.305 / 0.06
Control system – Differential thermostat control with one sensor in the solar collector and one in the tank	
Relative height of temperature sensor: spiral in solar collector loop / stratifier in solar collector loop (Figure 10)	0.14 / 0.01
Maximum/Minimum temperature differential	10 K/0.5 K

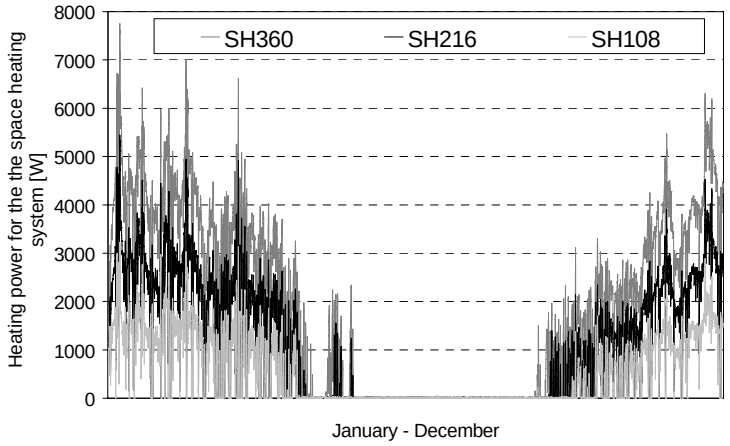

Figure 2: Power for the space heating systems, used in the calculations.

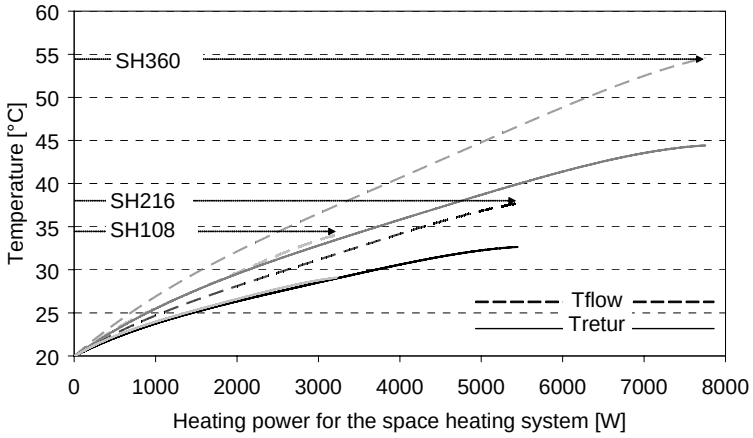

Figure 3: Flow and return temperatures in the space heating systems, used in the calculations.

The net utilized solar energy, the solar fraction and the performance ratio are defined as:

$$Q_{NET} = Q_{DHW} + Q_{SH} - Q_{AUX} \quad (1)$$

$$SF = \frac{Q_{NET}}{Q_{DHW} + Q_{SH}} \cdot 100\% \quad (2)$$

$$PR = \frac{Q_{NET}}{Q_{NET,REF}} \quad (3)$$

2.2 Results

The results are shown as the net utilized solar energy as a function of the parameter varied. Further, the results are shown as the performance ratio as a function of the parameter varied. The parameters varied are: The domestic hot water consumption, the space heating demand and the relative return inlet height from the space heating loop.

Figure 4 shows the calculated yearly net utilized solar energy as a function of the relative return inlet height from the space heating loop for model 1.1 with a heat exchanger spiral in the solar collector loop and fixed return inlet height from the space heating loop. Further, the performance ratio relative to the optimal thermal performance of the system in question is shown. The space heating demand is varied in accordance with Figure 2, and the daily domestic hot water consumption is 100 litres and 200 litres. Also the net utilized solar energy is shown for model 1.3 with a stratifier in the space heating loop.

The calculated yearly net utilized solar energy as a function of the relative return inlet height from the space heating loop for models 2 and 3 are not shown. The results are similar to the results for model 1.

The figure shows that the optimal inlet position from the space heating loop varies with the daily domestic hot water consumption and the space heating demand. For low space heating demand, and thereby low return inlet temperatures, the optimal inlet position is low. For increasing space heating demand, and thereby increasing return inlet temperature, the height of the optimal inlet position increases (indicated by the dotted curve connecting the optimum of the curves). Also the optimal return inlet position from the space heating loop increases for increasing domestic hot water consumption. This is due to a larger amount of cold water in the bottom of the tank, which leaves the warmer water that matches the temperature of the return water from the space heating loop at a higher level in the tank.

The yearly net utilized solar energy is reduced by less than 1% if the relative return inlet position from the space heating loop is 0.3 compared to the optimum return inlet position. This is also the case for the system models 2 and 3.

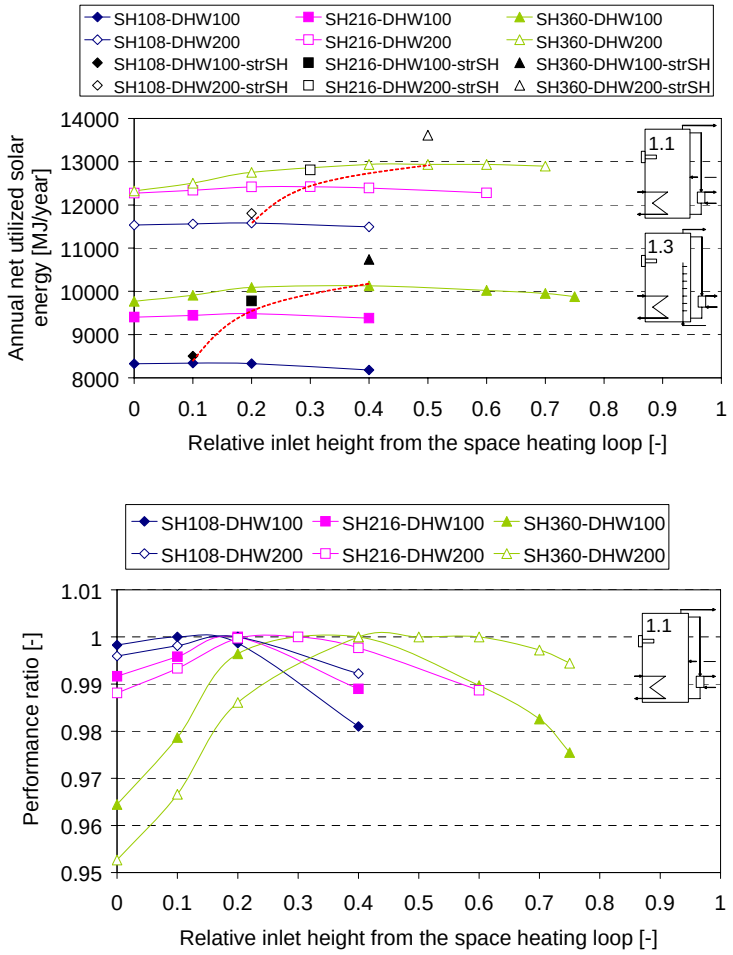

Figure 4: Top: The annual net utilized solar energy as a function of the relative return inlet height from the space heating loop for model 1.1 and model 1.3. Bottom: The performance ratio relative to the optimal thermal performance of the system in question.

Figure 5 shows the net utilized solar energy as a function of the space heating demand and the domestic hot water consumption for model 1 and a step by step improvement of the design. Also the performance ratio relative to the least advanced model 1.1 is shown. In all the calculations with a fixed return inlet height from the space heating loop, the optimal return inlet height shown in Figure 4 is used. The results for system models 2 and 3 are not shown but are similar to the results for system model 1.

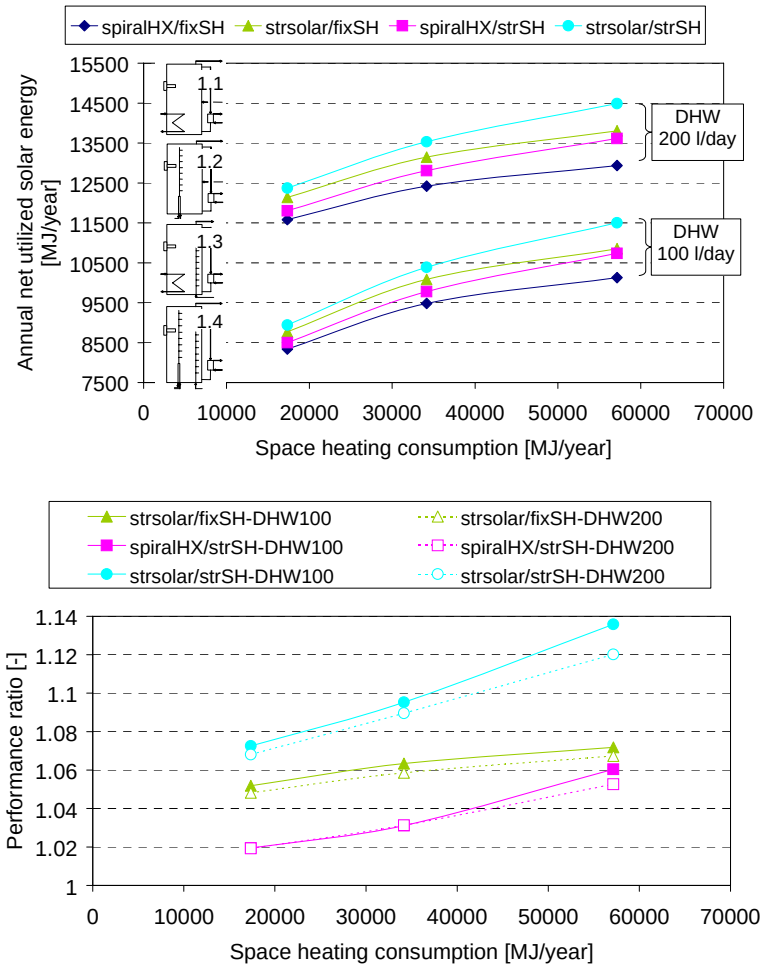

Figure 5: Top: The annual net utilized solar energy as a function of the space heating demand and the domestic hot water consumption for model 1 and the step by step improvement of the models. Bottom: The performance ratio relative to the thermal performance of the least advanced model, model 1.1.

The figure shows that the thermal performance increases for increasing space heating demand and increasing domestic hot water consumption. Also the thermal performance increases when inlet stratifiers are used, and most when an inlet stratifier is used in the solar collector loop. The best performing system has inlet stratifiers both in the solar collector loop and in the space heating loop.

The extra net utilized solar energy by using stratifiers increases for increasing space heating demand. This is because the return temperature from the space heating system is higher for high space heating demand than for low space heating demand. Hence the variation in the return temperature from the space heating system is higher for houses with high space heating demand than for houses with low space heating demand and this leads to a better utilization of a stratifier.

The increase in yearly net utilized solar energy by using a stratifier in the solar collector loop, in the space heating loop, or in both the solar collector loop and the space heating

loop is in the range of 5 – 8%, 2 – 6% and 7 – 14%, respectively, for the system models 1, 2 and 3.

It is obvious that the thermal performances of the systems are highly influenced by the total energy consumption and the design of the systems.

2.3 System comparison

Figure 6 shows the annual net utilized solar energy as a function of the space heating demand and a domestic hot water consumption of 100 l/day for system model 1, 2 and 3. The figure also shows the performance ratio where, in all cases, the reference system is the similar system model 1.

Figure 6 shows that model 1 always has the lowest thermal performance compared to the similar models 2 and model 3. Further, it can be seen that model 2 has a higher thermal performance than the similar model 3. The best performing system is the tank-in-tank system model 3.4 with inlet stratifiers in both the solar collector loop and in the space heating loop.

The reason why model 2 is performing better than the similar models 1 and 3 is most likely because the tank is a domestic hot water tank where the incoming cold water is directly utilized to cool the lower part of the tank. In model 1 the water returning from the domestic hot water heat exchanger to the tank is somewhat warmer than the cold water. In model 3 the incoming cold water reaches a higher level in the heat storage after a domestic hot water draw off caused by the shape of the inner tank. The reason why model 3 is performing better than model 1 is most likely due to the higher tank heat loss coefficient of model 1 since the heat loss coefficients of the sidearm and the external domestic hot water heat exchanger are added to the tank heat loss coefficient. A further disadvantage for model 1 is that the set point temperature of the auxiliary volume must be about 10 – 15 K higher than the required hot water temperature to meet the hot water demand. The set point temperature in models 2 and 3 only needs to be slightly higher than the required hot water temperature to meet the same demand. This effect is not investigated by calculations in this paper.

The performance ratio is higher for low space heating demand than for high space heating demand. With domestic hot water consumption of 100 l/day, the performance increase by using model 2 instead of model 1 is in the range of 1.5 – 2.2%, and in the range of 0.8 – 1.5% by using model 3 instead of model 1. The same investigations with domestic hot water consumption of 200 l/day show that the performance increase by using models 2 and 3 instead of model 1 is in the range of 3.4 – 3.9% and 0.4 – 1.9%, respectively.

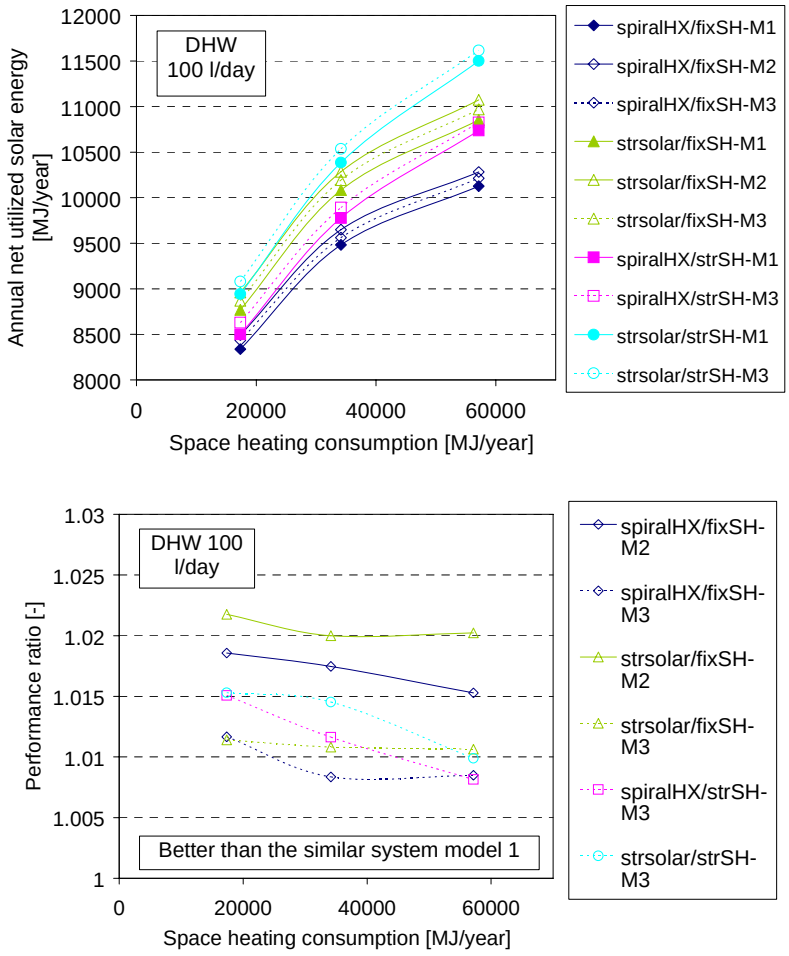

Figure 6: Comparison of model 1, model 2 and model 3. Top: The annual net utilized solar energy as a function of the space heating demand and the domestic hot water consumption and the step by step improvement of the models. Bottom: The performance ratio relative to the thermal performance of the similar system model 1.

3 Further investigations of solar combi systems

It is investigated how the size of the space heating system influences the thermal performance of solar combi systems. Also the influence on the thermal performance of different operation conditions of the control system for the solar collector loop is investigated. The investigation is only carried out for system model 1.

3.1 Space heating system

The size of the space heating system is varied for the house with a heating load of about 216 MJ/(m^2·year). The flow and return temperatures for a small, a standard and a large space heating system as a function of the heating power demand are shown in Figure 7.

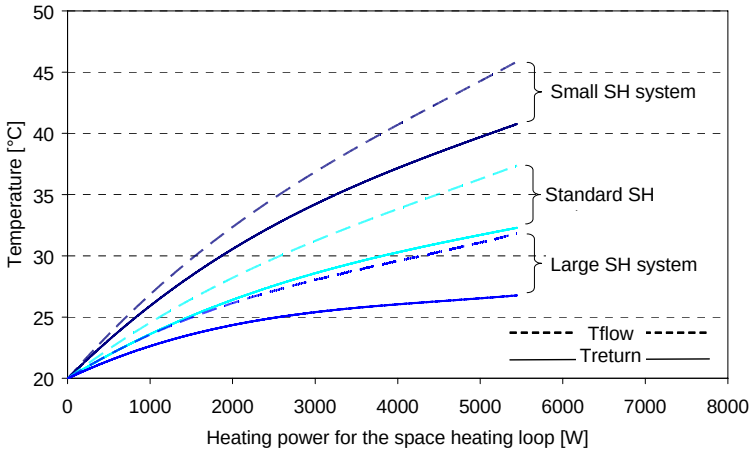

Figure 7: The flow and return temperatures for the space heating systems as a function of the heating power demand.

Figure 8 shows the annual net utilized solar energy as a function of the relative return inlet height from the space heating loop and the performance ratio, relative to the optimal thermal performance, of the system in question. Figure 9 shows the performance ratio, relative to the optimal thermal performance, of the system with the standard space heating system.

Figure 8 shows that the annual net utilized solar energy is strongly influenced by the size of the space heating system. The larger the space heating system, the larger is the thermal performance of the solar heating system. Also the optimal relative return inlet height from the space heating loop is influenced by the size of the space heating system. For small space heating systems, the optimal relative return inlet height increases, while the optimal return inlet height decreases for large space heating systems. Further, the figure shows the benefit of replacing the fixed inlet from the space heating loop with a stratifier, and it can be seen that the largest improvement of the thermal performance is achieved for small space heating systems. This is caused by the fact that the return inlet temperature varies more for houses with small space heating systems than for houses with larger space heating systems.

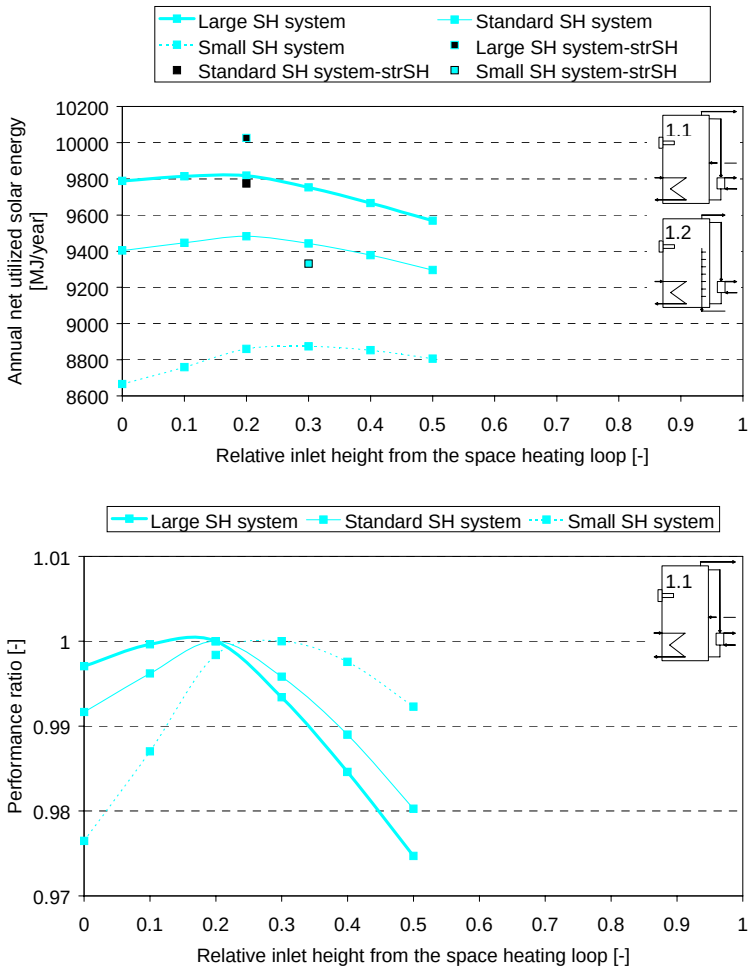

Figure 8: Top: The annual net utilized solar energy as a function of the relative return inlet height from the space heating loop. Bottom: The performance ratio, relative to the optimal thermal performance, of the system in question.

Figure 9 shows that the thermal performance of model 1.1 with the standard space heating system increases about 3% when a stratifier is used in the space heating loop instead of a fixed return inlet height. The thermal performance of models 1.1 and 1.2 with the large space heating system is about 4% and 6% higher than the thermal performance of model 1.1 with the standard space heating system. The thermal performance of models 1.1 and 1.2 with the small space heating system is about 6% and 2% lower than the thermal performance of model 1.1 with the standard space heating system.

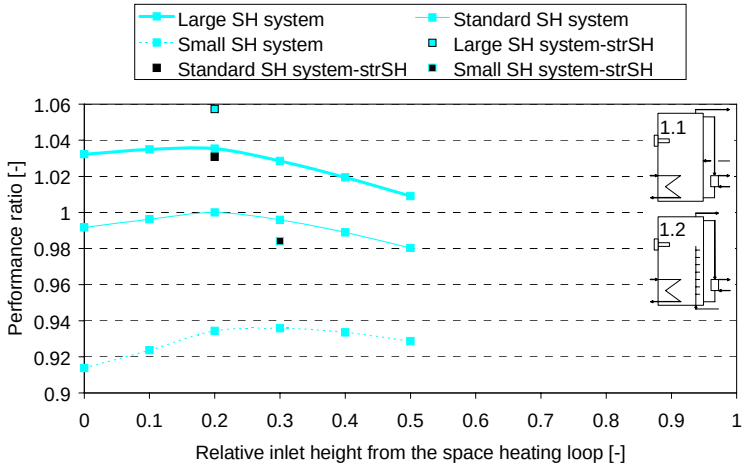

Figure 9: The performance ratio as a function of the relative return inlet height from the space heating loop. The performance is relative to the optimal thermal performance of the system with the standard space heating system.

It is clearly an advantage to use a stratifier instead of a fixed return inlet position from the space heating loop, especially because the size of the space heating system is normally not known in advance when the storage tanks are designed. Therefore the optimum fixed position of the return inlet from the space heating loop is not known.

3.2 Control system in the solar collector loop

The position of the temperature sensor mounted in the tank and the minimum temperature differential that controls the operation of the pump in the solar collector loop are investigated for different operation conditions:

- Space heating demand: 108 MJ/(m^2·year), 216 MJ/(m^2·year) and 360 MJ/(m^2·year).
- Domestic hot water consumption: 100 l/day and 200 l/day.
- Daily domestic hot water consumption patterns: 7 am, noon, 7 pm and 6 am, 7 am, 8 am and 7 pm, 8 pm, 9 pm.
- Fixed inlet heights (optimal position) and stratified inlet from the space heating loop.
- Volume flow rates in the solar collector loop: 1.2 l/(min·m^2), 0.5 l/(min·m^2) and 0.2 l/(min·m^2).
- Lengths of the pipe from/to the solar collector to/from the tank: 5, 10 and 15 m
- Stratifier in solar collector loop.
- Including the energy consumption of one and two pumps in the solar collector loop.

In Figure 10 the different positions of the temperature sensor used in the calculations are shown. The numbers next to the temperature sensors, seen to the right in the figure, correspond to the relative position in the tank. The relative positions 0.3 and 0.065 correspond to the top and the bottom of the heat exchanger, while the relative positions of 0.18, 0.14, 0.085 and 0.075 correspond to 1/2, 1/3, 1/10 and 1/20 of the heat exchanger height calculated from the bottom of the heat exchanger.

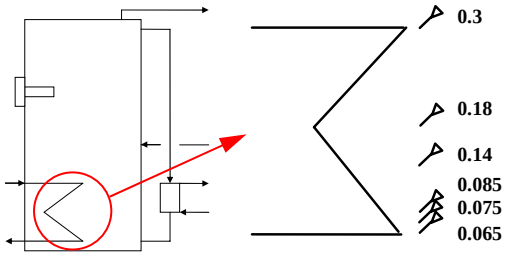

Figure 10: Different positions of the temperature sensor in the tank.

The investigations are carried out with sensor positions according to Figure 10 with minimum temperature differential varied between -1 K and 3 K.

In Figure 11 an example of such an investigation for one set of operation conditions is shown. The figure shows the net utilized solar energy for model 1.3 as a function of the position of the temperature sensor in the tank and the minimum temperature differential for the pump in the solar collector loop and the performance ratio relative to the thermal performance of the system with the highest thermal performance. The space heating demand is 216 MJ/(m^2·year), the domestic hot water consumption is 100 l/day, and domestic hot water is tapped at 7 am, noon and 7 pm. The volume flow rate in the solar collector loop is 1.2 l/(min·m^2).

From Figure 11 it can be seen that the optimal position of the temperature sensor is 1/10 of the heat exchanger height calculated from the bottom of the heat exchanger with a minimum temperature differential of about 0 K. Also it can be seen that for lower stop temperature differences, the optimal position of the temperature sensor is higher than 1/10 of the heat exchanger height, while for higher minimum temperature differentials the optimal position of the temperature sensor is lower than 1/10 of the heat exchanger height.

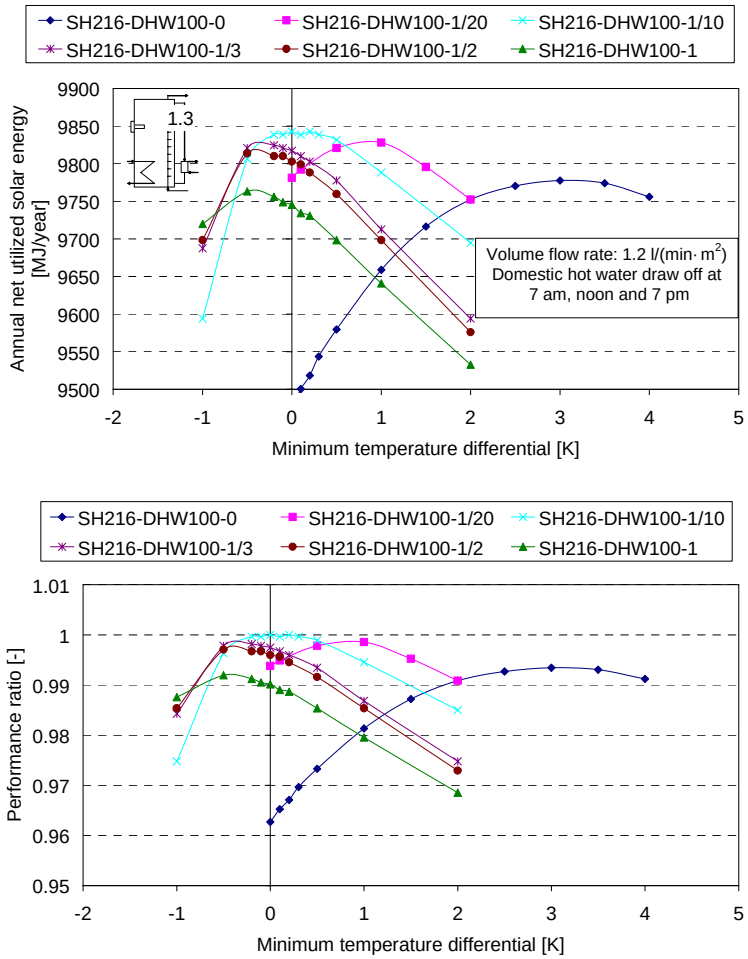

Figure 11: Top: The annual net utilized solar energy as a function of the position of the temperature sensor in the tank and the minimum temperature differential of the pump in the solar collector loop. Bottom: The performance ratio relative to the thermal performance of the system with the highest thermal performance.

The investigation including all the different operation conditions shows that, regardless of the applied operation conditions, the optimal position of the temperature sensor in a tank with a heat exchanger spiral in the solar collector loop is between 1/10 and 1/20 of the heat exchanger height with a minimum temperature differential between 0 K and 1 K. The optimum position of the temperature sensor and the optimum stop temperature difference will not be changed even when the pump energy is included in the calculations. Further, the investigation shows that the optimal position of the temperature sensor in a tank with a stratifier in the solar collector loop is at the very bottom of the tank and that the optimal minimum temperature differential lies in a quite wide range from -1 to 2 K. Consequently, a stratifier makes a system less sensitive regarding correct installations of temperature sensors and settings of the control parameters in the solar collector loop.

4 Investigations of different sized solar combi systems

It is investigated how the size of the solar combi system influences the thermal performance. Table 1 shows the data of one system size and Table 2 shows data of further system sizes used in the calculations. Only data that differ from data given in Table 1 are listed in Table 2.

Table 2: Data of the systems.

Solar collector area	10 m^2 / 30 m^2
Storage volume	500 l / 1500 l
Height of tank	1.5 m / 2.5 m
Diameter of tank	0.652 m / 0.874 m
Heat loss coefficient, tank	2.42 W/K / 5.09 W/K

4.1 Differently sized solar combi systems with varying space heating demand and daily hot water consumption

The investigation is carried out for different sizes of system model 1 and a step by step improvement of the model. The results with the system model with 1000 litre storage tank and 20 m^2 solar collector areas are shown in section 2.2.

Figure 12 shows the annual net utilized solar energy as a function of the relative return inlet height from the space heating loop for different sizes of model 1. Further, the performance ratio relative to the optimal thermal performance of the system in question is shown.

Figure 13 shows the yearly net utilized solar energy as a function of the space heating demand and the domestic hot water consumption for the two different sizes of model 1, and a step by step improvement of the model. Also the performance ratio relative to the performance of the least advanced model 1.1 is shown. In all the calculations with a fixed return inlet height from the space heating loop, the optimal return inlet height shown in Figure 12 is used.

Figure 14 shows the monthly net utilized solar energy for the three differently sized models 1 and the step by step improvement of the models. Also the monthly solar radiation per m^2 solar collector is shown. Finally, Figure 14 shows the extra net utilized solar energy gained by replacing the heat exchanger spiral in the solar collector loop and the fixed return inlet height from the space heating loop with stratifiers. The calculations are made for a space heating demand of about 216 MJ/(m^2 year) and with a domestic hot water consumption of 100 l/day.

Table 3 shows the thermal performance increase by using stratifiers.

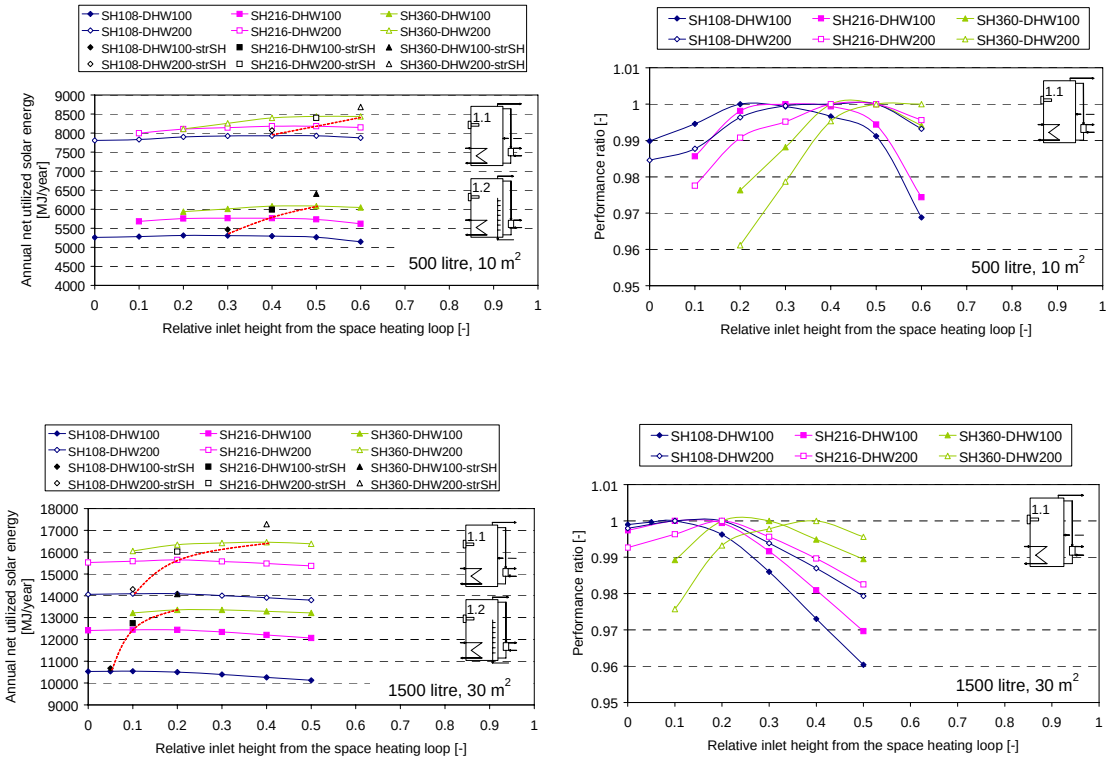

Figure 12: Left: The annual net utilized solar energy as a function of the relative return inlet height from the space heating loop for different sizes of model 1.1 and model 1.2. Right: The performance ratio relative to the optimal thermal performance of the system in question. Top: 10 m^2 collector, Bottom: 30 m^2 collector.

Figure 12 shows that the optimal inlet position from the space heating loop varies with the daily domestic hot water consumption and the space heating demand. For low space heating demand and thereby low return inlet temperatures from the space heating loop, the optimal inlet position is low. For increasing space heating demand and thereby increasing return inlet temperature from the space heating loop, the height of the optimal inlet position increases (indicated by the dotted line connecting the optimum of the curves). Also the optimal return inlet position from the space heating loop increases for increasing domestic hot water consumption. This is due to a larger amount of cold water in the bottom of the tank which leaves the warmer water that matches the temperature of the return water form the space heating loop at a higher level in the tank. The most suitable relative position of the inlet from the space heating loop in the systems with 500 litre tank, 1000 litre tank and 1500 litre tank are 0.4, 0.3 and 0.2, respectively. Regardless of the space heating demand and the hot water consumption, these positions will be close to the optimum positions.

The tendency is that the relative inlet position from the space heating loop is lower for larger systems than for smaller systems. However, the volume below the inlet from the space heating loop is in the same range between 200 litres and 300 litres for all three system sizes.

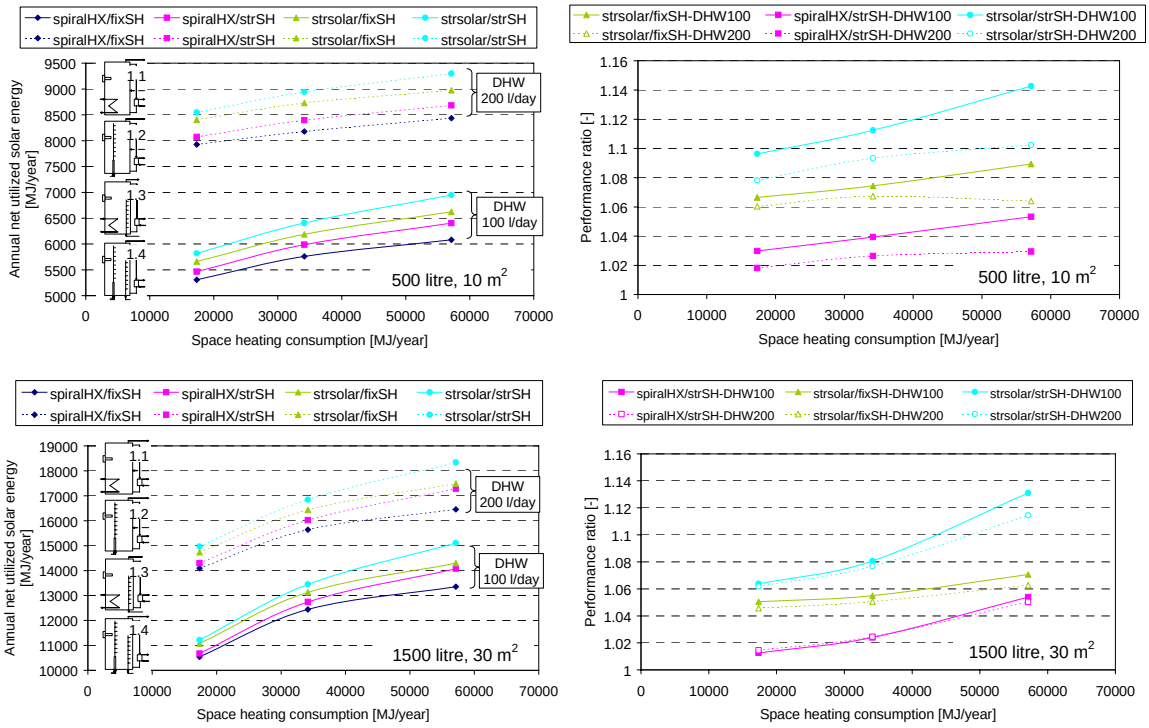

Figure 13: Left: The annual net utilized solar energy as a function of the space heating demand and the domestic hot water consumption for different sizes of model 1, and the step by step improvement of the model. Right: The performance ratio relative to the thermal performance of the least advanced model 1.1. Top: 10 m^2 collector, Bottom: 30 m^2 collector.

Figure 13 shows that the thermal performance increases for increasing space heating demand and increasing domestic hot water consumption. Also, the figure shows that the thermal performance increases when the heat exchanger spiral in the solar collector loop and the fixed return inlet from the space heating loop are replaced with stratifiers and this especially applies to the heat exchanger spiral in the solar collector loop. The performance ratio of the system by using inlet stratifiers is almost the same, regardless of the size of the solar combi system.

The increase in net utilized solar energy by using a stratifier in the solar collector loop, in the space heating loop, and in both the solar collector loop and the space heating loop is in the range of 5 – 9%, 1 – 6% and 6 – 14%, respectively. The additional gained net utilized solar energy by using stratifiers is increasing for increasing space heating demand due to higher temperature variations in the space heating loop and thereby better utilization of a stratifier.

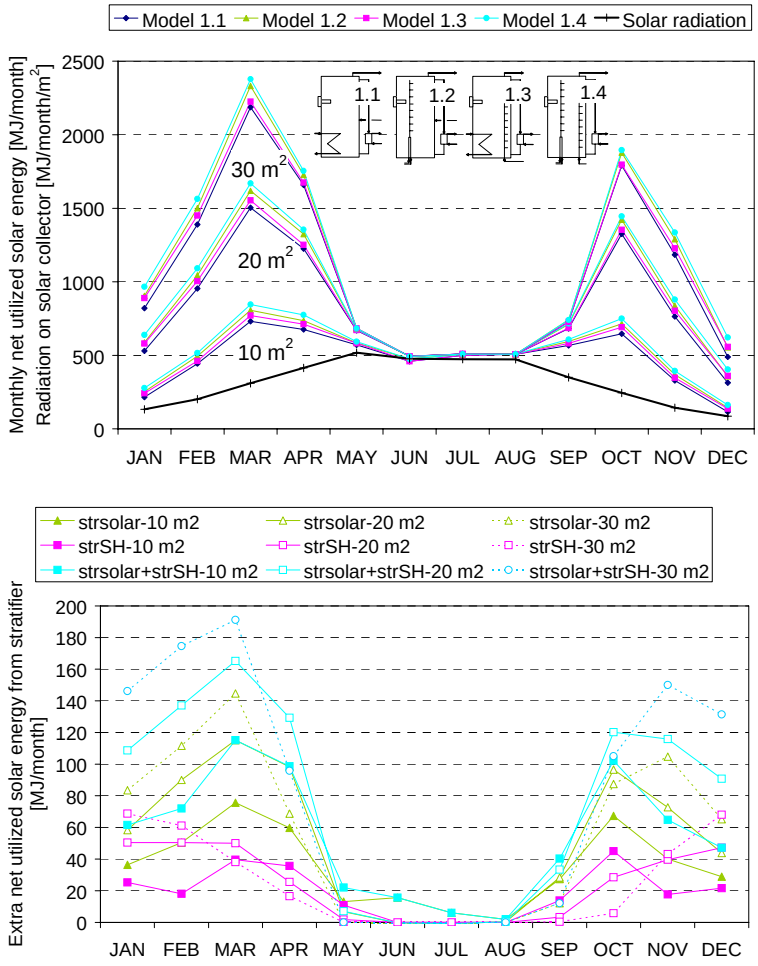

Figure 14: Top: Monthly net utilized solar energy for the three different size models 1.1, 1.2, 1.3 and 1.4 with solar collector areas of 10 m^2, 20 m^2 and 30 m^2. Bottom: Extra net utilized solar energy by using stratifiers.

From Figure 14 it is obvious that the solar fraction is 100% during the summer months. Further, it is obvious that the increased performance of larger solar combi systems is especially due to higher thermal performance during spring and autumn. Also the figure shows that small solar combi systems benefit from stratifiers in the space heating loop during a longer period than larger systems due to the lower solar fraction for small systems. For high solar fractions close to 100%, there is little or no benefit by using stratifiers.

From Table 3 it can be seen that large and medium sized solar combi systems benefit more from stratifiers than a small solar combi system. Finally, it is seen that the extra net utilized solar energy for a system with stratifiers in both the solar collector loop and the space heating loop equals the sum of the extra net utilized solar energy of the system with only one stratifier in the solar collector loop and the system with only one stratifier in the space heating loop.

Table 3: The net utilized solar energy and the extra net utilized solar energy with stratifiers in solar collector loop and in space heating loop and in both the solar collector loop and the space heating loop.

Solar collector area	10 m^2	20 m^2	30 m^2
Net utilized solar energy and solar fraction for model 1.1	5760 MJ/year	9482 MJ/year	12442 MJ/year
	14.3%	23.6%	31.0%
Extra net utilized solar energy and	421 MJ/year	608 MJ/year	677 MJ/year
solar fraction for model 1.2	15.4%	25.1%	32.6%
Extra net utilized solar energy and	227 MJ/year	295 MJ/year	302 MJ/year
solar fraction for model 1.3	14.9%	24.3%	31.7%
Extra net utilized solar energy and	648 MJ/year	907 MJ/year	1004 MJ/year
solar fraction for model 1.4	15.9%	25.8%	33.5%

4.2 Differently sized solar combi systems with constant space heating demand and constant daily hot water consumption

The investigation is carried out for different sizes of system model 1 and a step by step improvement of the model. The storage tanks are described in Tables 1 and 2. The solar collector areas vary from 5 m^2 to 60 m^2. The space heating demand is 216 MJ/(m^2·year) and the daily domestic hot water consumption is 100 litres.

Figure 15 shows the annual net utilized solar energy and the extra annual net utilized solar energy from stratifiers as a function of the solar collector area.

Figure 16 shows, on the left side, the performance ratio as a function of the solar collector area for the solar combi systems with the operation conditions used in the calculations. On the right side, the figure shows the performance ratio as a function of the solar fraction. The reference system in the performance ratio is the corresponding system model 1.1 with heat exchanger spiral in the solar collector loop and optimum fixed return inlet position from the space heating loop.

Figure 15 shows that the annual net utilized solar energy increases for increasing solar collector area. Further, the figure shows that, with the applied operation conditions, there is an optimum ratio between storage volume and solar collector area regarding extra thermal performance from a stratifier in the solar collector loop. For the storage tanks of 500 litres and 1000 litres, the ratio is 50 l/m^2 solar collector area, and for the storage tank of 1500 litres the ratio is 30 l/m^2 solar collector area (indicated by the circles in the figure). Consequently, the stratifiers are most advantageous for typical storage volume/collector area ratios. There is no optimum ratio between storage volume and solar collector area regarding extra thermal performance from a stratifier in the space heating loop within the investigated system sizes and operation conditions.

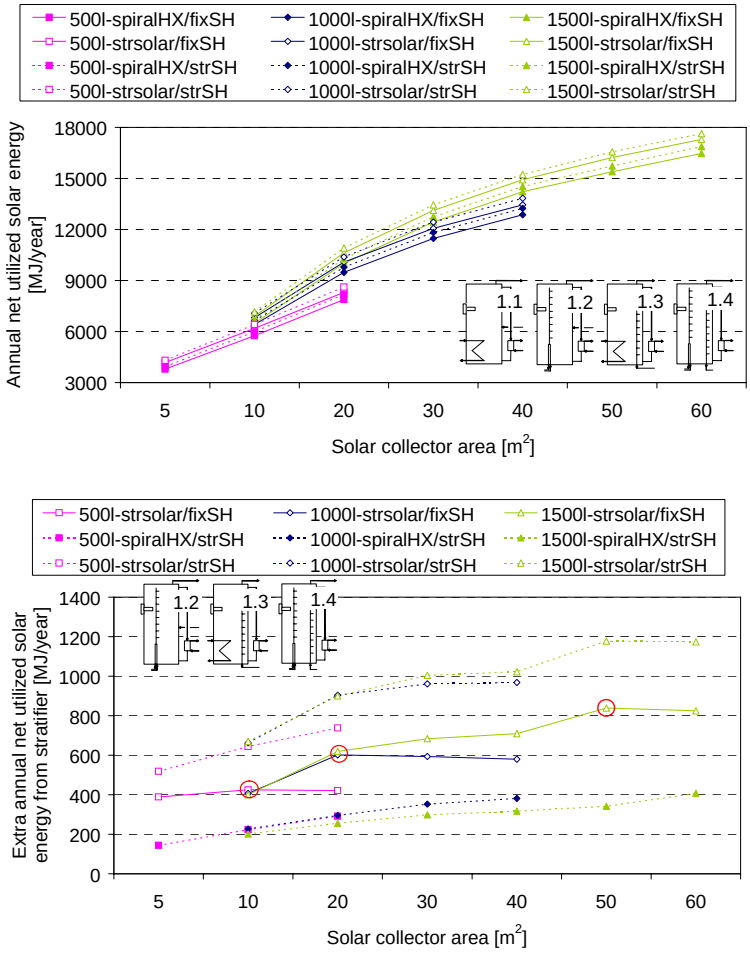

Figure 15: Top: The annual net utilized solar energy as a function of the solar collector area and heat storage volume. Bottom: The extra annual net utilized solar energy from stratifiers as a function of the solar collector area and heat storage volume. The annual thermal performances are shown for system model 1 and a step by step improvement of the system model.

Figure 16 shows that the performance ratio decreases for increasing solar collector area and solar fraction. Further, it can be seen that the curves for the step by step improvements of the solar combi systems lie in continuation of each other for different solar collector areas and different solar fractions. Consequently, the extra percentage thermal performance of the stratifiers is strongly depending on the solar fraction. The higher the solar fraction, the smaller the extra percentage thermal performance of stratifiers.

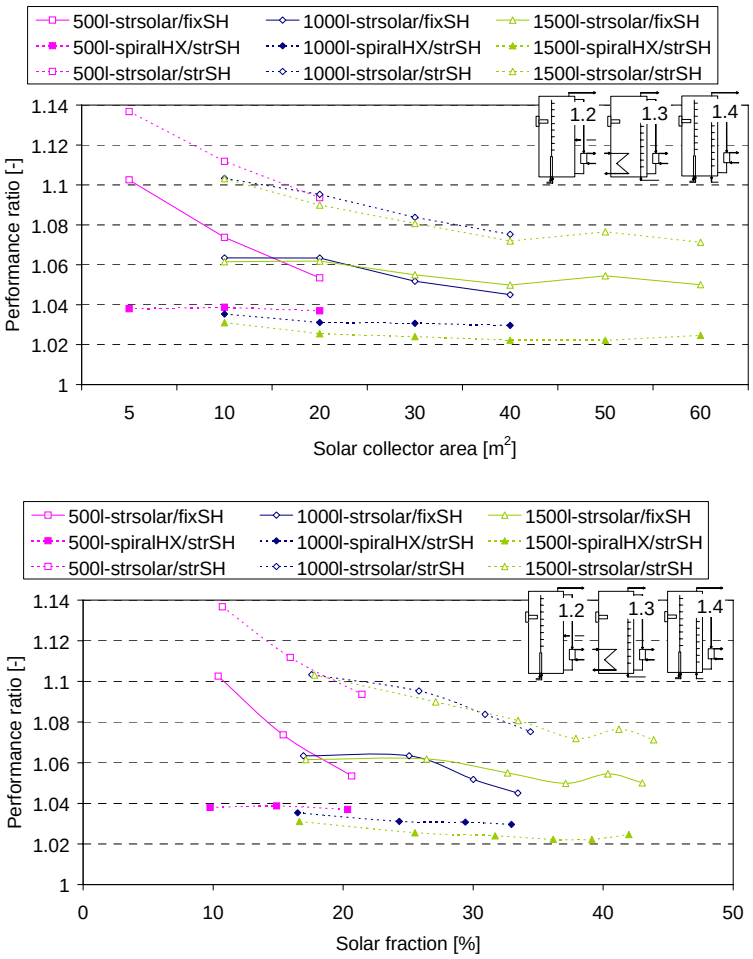

Figure 16: Top: The performance ratio as a function of the solar collector area. Bottom: The performance ratio as a function of the solar fraction. The reference system is the corresponding system model 1.1 with heat exchanger spiral in the solar collector loop and optimum fixed return inlet position from the space heating loop.

5 Conclusion

Three basically differently designed solar combi system models are investigated theoretically. The solar combi systems have a storage volume of 1000 litres with 20 m^2 solar collector area. The investigation includes the influence of thermal stratification, the size of the space heating system, space heating demand, domestic hot water consumption, and the control system in the solar collector loop. Also differently sized solar combi systems with storage tank volumes of 500 litres, 1000 litres and 1500 litres and solar collector areas between 5 m^2 and 60 m^2 are investigated.

Conclusions: **1)** The best performing solar combi system is based on a tank-in-tank storage with stratifiers both in the solar collector loop and the space heating loop. **2)** The thermal performance increases 5 – 10% if stratifiers are used only in the solar collector

loop. **3)** The thermal performance increases 2 – 6% if stratifiers are used only in the space heating loop. **4)** The thermal performance increases 7 – 14% if stratifiers are used both in the solar collector loop and the space heating loop. **5)** The extra net utilized solar energy for a system with stratifiers in both the solar collector loop and the space heating loop equals the sum of the extra net utilized solar energy of the system with stratifier in the solar collector loop and the system with stratifier in the space heating loop. **6)** The thermal performance is strongly increased for increasing size of the space heating system. **7)** The thermal performance increase by using stratifiers is highest for small space heating systems. **8)** The percentage thermal advantage by inlet stratifiers decreases for increasing solar fraction. **9)** Small solar combi systems benefit from stratifiers in the space heating loop during a longer period than larger systems due to a lower solar fraction. **10)** If the system has a direct return inlet from the space heating loop to the storage, the optimal relative inlet position from the space heating loop is lower for larger systems than for smaller systems, while the absolute inlet position as well as the optimum volume below the inlet from the space heating loop is in the same range. The optimal volume below the inlet is between 200 litres and 300 litres. **11)** In a tank with heat exchanger in the solar collector loop (high flow system), the best position of the temperature sensor in the tank for controlling the pump in the solar collector loop is between 1/10 and 1/20 of the heat exchanger height, calculated from the bottom of the heat exchanger with a minimum temperature differential between 0 K and 1 K regardless of the operation conditions. **12)** In a tank with stratifier in the solar collector loop (low flow system), the best position of the temperature sensor in the tank for controlling the pump in the solar collector loop is in the very bottom of the tank with a minimum temperature differential between -1 K and 2 K regardless of the operation conditions.

In practice there is a great advantage by using ideal working stratifiers instead of internal heat exchanger spirals and direct inlets because the optimal design of solar combi systems varies with the consumption and because solar combi systems with stratifiers are less sensitive towards non-optimal operation conditions.

Nomenclature

η_0	Optical efficiency of incident radiation	[-]
η	Solar collector efficiency	[-]
θ	Incidence angle	[-]
k_θ	Incidence angle modifier for beam radiation	[-]
a_1	Heat loss coefficient	[W/m^2/K]
a_2	Heat loss coefficient	[W/m^2/K^2]
T_m	Mean collector fluid temperature	[ºC]
T_a	Ambient temperature	[ºC]
E	Total solar irradiance on collector	[W/m^2]

Q_{AUX}	Auxiliary energy consumption	[J]
Q_{DHW}	Domestic hot water load	[J]
Q_{NET}	Net utilized solar energy	[J]
$Q_{NET,REF}$	Net utilized solar energy of reference system	[J]
Q_{SH}	Space heating load	[J]
SF	Solar fraction	[%]
PR	Performance ratio	[-]

Abbreviations

DHW	Domestic hot water
SH	Space Heating
spiralHX	Heat exchanger spiral in the solar collector loop
fixSH	Fixed return inlet height from the space heating loop
strsolar	Stratifier in the solar collector loop
strSH	Stratified return inlet from space heating loop

References

[1] Weiss et al., Solar Heating Systems for Houses, a Design Handbook for Solar Combisystems. James & James Ltd, London. ISBN 1 902916 46 8, 2003.

[2] Streicher W., Heimrath R., Analysis of System Reports of Task 26 for Sensitivity of Parameters, Technical Report for Subtask C, IEA SHC-Task 26, 2004.

[3] Streicher W., Elements and Examples of "Dream Systems" of Solar Combisystems. A Report of IEA SHC – Task 26, 2004.

[4] Lorenz K., Kombisolvärmesystem – Utvärdering av möjliga systemförbättringar. Ph.D Thesis, Institutionen för Installationsteknik, Chalmers Tekniska Högskola, Göteborg, 2001.

[5] Jordan U., Untersuchungen eines Solarspeichers zur kombinierten Trinkwassererwärmung und Heizungsunterstützung. Dissertation, Universität Marburg, 2001.

[6] Pauschinger, T., Drück, H., Hahne, E., Comparison test of solar heating systems for domestic hot water preparation and space heating, Proceedings of Second International ISES Solar Congress, 1998.

[7] Streicher W., Simple estimation of the solar fraction of combisystems and centralized big solar plants, Proceedings of Second International ISES Solar Congress, 1998.

[8] Drück H., Hahne E., Test and comparison of hot water stores for solar combisystems, Proceedings of Second International ISES Solar Congress, 1998.

[9] Andersen E., Furbo S., Fan J., Investigations of fabric stratifiers for solar tanks, Accepted for publication in Journal of Solar Energy, November 2006.

[10] Klein S.A et al., TRNSYS 15, User Manual. University of Wisconsin Solar Energy Laboratory, 1996.

[11] Drück H., MULTIPORT Store – Model, Type 140 for TrnSys. Institut für Thermodynamik und Wärmetechnik. Universität Stuttgart, 2000.

[12] Skertveit, A., Lund, H., and Olseth, J. A., Design Reference Year, Report no. 1194 Klima, Det Norske Institutt, 1994.

[13] Jordan, U., Vajen, K., Influence of the DHW-load profile on the fractional energy savings: a case study of a solar combi-system with TRNSYS simulations, Proceedings of EuroSun 2000 Congress, Copenhagen, Denmark, 2000.

[14] Knudsen, S., Consumers' influence on the thermal performance of small SDHW systems – theoretical investigations, Solar Energy Vol. 73, No. 1, pp. 33-42, 2002.

[15] Knudsen S., Heat transfer in a „tank-in-tank" combi store. Department of Civil Engineering, Technical University of Denmark, report R-025, ISBN 87-7877-083-1, 2002.

Bilag 9

Multilayer stratification pipes for solar tanks.

Journal of Solar Energy, Volume 81, no. 10, pp. 1219-1226, 2007.

Elsa Andersen & Simon Furbo

Multilayer Fabric Stratification Pipes for Solar Tanks

Elsa Andersen, Simon Furbo and Jianhua Fan

Department of Civil Engineering Technical University of Denmark

DK-2800 Kgs. Lyngby, Denmark, e-mail: ean@byg.dtu.dk

Abstract

The thermal performance of solar heating systems is strongly influenced by the thermal stratification in the heat storage. The higher the degree of thermal stratification is, the higher the thermal performance of the solar heating systems. Thermal stratification in water storages can for instance be achieved by use of inlet stratifiers combined with low flow operation in the solar collector loop.

In this paper, investigations of a number of different fabric stratification pipes are presented and compared to a non flexible inlet stratifier.

Additional, detailed investigations of the flow structure close to two fabric stratification pipes are presented for one set of operating conditions by means of the optical PIV (Particle Image Velocimetry) method.

1 Introduction

The thermal performance of solar heating systems is strongly influenced by the thermal stratification in the heat storage tank. Investigations by (van Koppen et al., 1979, Hollands and Lightstone, 1989) showed that the thermal performance is increasing for increasing thermal stratification in the heat storage.

Thermal stratification in solar storage tanks is normally established in two ways:

- During charge periods, where heat from the auxiliary energy supply system or from the solar collectors is transferred to the "right" level of the tank. That is, the heat from the auxiliary energy supply system is normally transferred to the top of the tank and the solar heat is transferred to the level in the storage tank, where the tank temperature is close to the temperature of the incoming fluid transferring the solar heat to the tank. Shah and Furbo (1998) and Knudsen and Furbo (2004) showed that for small SDHW systems this is with advantage done by means of a vertical mantle heat exchanger. For large SDHW systems and for solar combisystems this is with advantage done by means of inlet stratifiers as shown by (Weiss, 2003, Furbo et al., 2005).

- During discharge periods where heat is discharged from a fixed level of the tank, for instance domestic hot water from the top of the tank for SDHW systems or hot water for space heating from a level just above the lower level of the auxiliary volume in a

storage tank for solar combisystems. Thermal stratification is best established during discharge if cold water enters the bottom of the tank in SDHW systems during draw-offs, and if the returning water from the space heating system enters the tank through inlet stratifiers in solar combisystems as described by (Weiss, 2003).

Consequently, inlet stratifiers can be used to build up thermal stratification in solar heat storages both during charge and discharge periods.

A wide variety of inlet stratifiers such as rigid tubes with either open holes and perforated vertical plates inside the pipes (Loehrke, 1979, Gari and Loehrke, 1992, Davidson, 1992,) or openings in form of balls (e.g. Leibfried, 2000) or flaps (e.g. described by Essert, 1995, Krause, 2001, Shah, 2002, Andersen et al., 2004) have been investigated in the past. Some of these have entered the market during the recent years. Also flexible stratification pipes (fabric manifolds) have been investigated for example by (Davidson and Adams, 1992, Loehrke, 1979, Gari and Loehrke, 1992, Yee and Lai, 2001). These investigations are carried out with flexible stratification manifolds made of one fabric layer and inlet through the top or the middle of the tank. (Davidson et al., 1994) found that fabrics with limited ability to stretch (i.e. woven fabrics) were unsuitable as stratification inlet pipes when the water enters the stratification inlet pipe through the top of the tank.

No guidelines for choosing the diameter of a fabric pipe in this type of application were found in previous studies. (Davidson et. al, 1994) investigated fabric pipes with diameters of 73 and 89 mm with a volume flow rate of 4.2 l/min. (Loehrke et al., 1979) investigated a fabric pipe with a diameter of 100 mm and a volume flow rate of 23 l/min.

In spite of promising results, fabric stratification pipes have not yet entered the market.

In this paper, stratification manifolds made of one or two fabric layers with diameters between 40 mm and 70 mm and with inlet through the bottom of the tank are investigated. The fabric stratifiers are made of Nylon, filament polyester, spun polyester and acrylic.

By leading water into the tank through a stratification pipe, good thermal stratification can be achieved in the tank. By placing the inlet at the bottom of the tank where the coldest water is situated, thermal bridges with high heat losses can be avoided, (Furbo, 1983). Good thermal stratification increases the thermal performance of solar heating systems.

The advantage of using a flexible fabric pipe as a stratification inlet pipe is that the fabric pipe can expand or contract leading to an equalization of the pressure in the pipe and in the tank in all levels of the tank. In this way the water in the tank will not be driven into the pipe by a higher pressure in the tank than in the pipe. The water in the pipe will first enter the tank when it either reaches the top of the pipe where it is forced to leave the pipe because new water is constantly feed into the pipe or when the temperature in the pipe equals the temperature in the tank leading to a slightly higher pressure in the pipe than in the tank. The pipe will expand in an attempt to equalize the pressure difference, but the expansion is limited by the expansion properties of the fabric and this leads to a flow of liquid from the pipe into the tank in the right temperature level.

Because one layer of fabric is very thin, heat is constantly transferred horizontally between the fabric pipe and the tank. By designing the stratification inlet pipe of more

than one fabric layer with a distance between the fabric layers the unwanted horizontal heat transfer is reduced. Figure 1 shows a picture of a two fabric layers pipe during an experiment where hot water enters a cold tank through the fabric pipe. Also the cross section area of the collapsed (lower right corner) and the expanded (upper right corner) fabric pipe is shown.

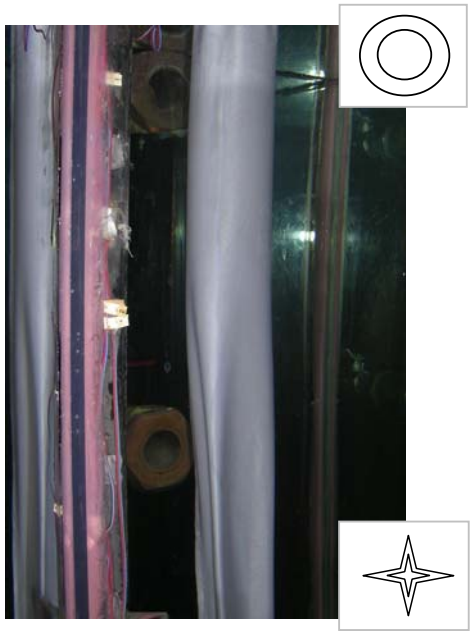

Figure 1: Picture of the two fabric layers pipe during a heating experiment. Upper right corner: cross section of the expanded fabric pipe where hot water leaves the pipe. Lower right corner: cross section of the collapsed pipe.

The heat transferred through each fabric layer leads to an up going flow around each fabric layer. It is assumed that when the distance between the fabric layers is large enough a laminar flow can develop between the two fabric layers and a small amount of heat is transferred from the inlet stratification pipe to the tank. When the distance between the fabric layers is too narrow the flow is disturbed and becomes turbulent and a larger amount of heat is transferred from the inlet stratification pipe to the tank. On the other hand, a larger fabric pipe diameter results in a larger surface area of the pipe increasing the heat transfer between the inlet stratification pipe and the tank. Therefore detailed investigations are needed in order to determine the optimum diameters of the fabric pipes.

2 Experimental investigations

2.1 Experimental set up

The experimental setup shown in Figure 2 consists of a glass tank (400 x 400 x 900 mm), a heating and a cooling unit and standard PIV equipment from Dantec Dynamics. Table 1 shows data for the PIV equipment.

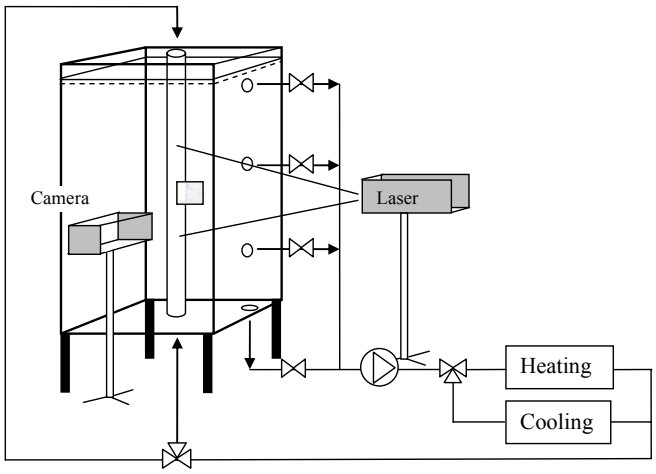

Figure 2: Experimental setup with the glass tank, the laser and the camera.

laser	type	Nd:YAG, NewWave Solo (Neodym-Yttrium-Aluminium-Granat)
	energy/pulses	100 mJ/pulse
	wavelength	532 nm (frequency doubled)
CCD camera	type	HiSense 12 bit
	resolution	1280 x 1024 pixel (64 x 64 pixel interrogation area)
particles		Polyamid, 5µm (PSP-5)
software		Flowmanager, Dantec Dynamics

Table 1: PIV equipment.

The PIV method has previous been used to investigate flow structures in water tanks by for example (Knudsen et al., 2005).

The camera is placed perpendicular to the laser that illuminates a thin slide in the flow. The fabric stratification pipe is mounted in the centre of the glass tank with the possibility to have a forced flow to enter the stratification pipe either from the top or the bottom of the tank. The outlet can take place in four different levels between the top and the bottom of the tank. The thickness of the tank wall is 12 mm and the tank is not insulated. !4 temperature sensors are mounted on a plate of Perspex in one corner of the tank (Figure 2) The temperatures are measured with copper-constantan thermocouples type TT with an accuracy of 0.5 K. The volume flow rate is measured with an electro magnetic inductive flow meter, type HGQ1 from Brunata HG a/s. The flow meter has an accuracy of about ± 1 %.

2.2 Experiments

The thermal performance of the fabric stratifiers are investigated for three sets of operation conditions:

- heating tests where the tank is heated from 20°C to 40°C through one layer fabric stratification pipes with diameters of 60 mm and two layers fabric stratification pipes with diameters of 40 mm and 70 mm. The inlet to the fabric stratification pipe is through the bottom of the tank. The outlet is in the bottom of the tank.
- heating test with an initially stratified tank 50°C/20°C and an inlet temperature of 30°C through two fabric layers stratification pipe with diameters of 40 mm and 70 mm. The inlet to the fabric stratification pipe is through the bottom of the tank. The outlet is in the bottom of the tank.
- cooling test where cold water of 20°C is lead into the tank with a temperature of 50°C through two fabric layers stratification pipe with diameters of 40 mm and 70 mm. The inlet to the fabric stratification pipe is through the bottom of the tank. The outlet is in the top of the tank.

The fabric stratifiers are closed in the top.

The duration of the heating and the cooling tests is 50 minutes. The duration of the stratified test is 35 minutes. The volume flow rate is 2 l/min.

The investigated fabrics are listed in Table 2. The fabrics are obtained from the US company Test Fabric Inc. The fabrics are a mixture of knit and woven fabrics and the ability to stretch that was found important by (Davidson et al., 1994) seems not important at all in the application investigated here where the water is entering the stratification inlet pipe through the bottom of the tank. The important properties are the ability to reduce the cross section area by more or less collapse. Hence, the permeability and the density of the fabrics are found to be more important than the stretch abilities.

Fabric Style
Style 314, Texturized Nylon 6.6 Stretch Fabric, Double Knit
Style 361, Spun Nylon 6.6 DuPont Type 200 Woven Fabric (ISO 105/F03)
Style 703, Texturized Polyester, Woven
Style 769, 100% Spun Dacron Type 54 Knit (Disperse Dyeable)
Style 864, Spun Orlon Type 75 Acrylic Plain Weave
Style 867, Spun Acrilan 16 Acrylic Knit
Style 981, Creslan Acrylic Type 61

Table 2: Investigated fabrics.

Further , the test results obtained with two fabric layers stratification pipes are compared to results of identical tests with a marketed rigid stratification pipe with three holes with “non-return” valves from Solvis GmbH & Co KG (Krause, 2001, Shah, 2002, Andersen et al., 2004). Figure 3 shows a schematic of the rigid stratification pipe.

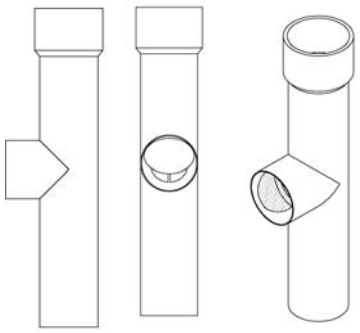

Figure 3: Schematic illustrations of the SOLVIS stratification inlet pipe.

Finally, the flow structure close to the fabric stratification pipes with one and two fabric layers, S361 are investigated during a heating test by means of the PIV method. The method is described in (Andersen et al., 2004).

Recordings of the velocity field are taken in a frame of 65.5 x 80 mm^2 about 450 mm from the bottom of the tan as shown in Figure 2.The duration between two succeeding illuminations of the particle field is 100 ms. Time delay between succeeding velocity vector recordings is about 250 ms.

2.3 Analysis method

There are different ways to evaluate thermal stratification of thermal energy storages. (Rosen, 2001) describes how to perform an exergy analysis of a thermal energy storage. (Adams, 1993; Davidson et al., 1994) describe how to analyse a thermal energy storage with a quantitative "momentum of energy" analysis. Both methods are suitable for comparing differently designed heat storages. The latter is used to analyse the results in this paper.

The tank is divided into N equal sized horizontal layers with the volume V. The temperature is not measured in each volume. Therefore the temperatures of the volumes are determined by linear interpolation between the measured temperatures.

In the analysis of the "momentum of energy", M, the energy of each layer of the tank, $E_i = \rho_i \cdot c_i \cdot V \cdot T_i$ is weighted by the vertical distance from the bottom of the tank to the centre of each layer, y_i. The "momentum of energy" is:

$$M = \sum_{i=1}^{N} y_i \cdot E_i , \tag{1}$$

A mixing number is derived based on the measured temperature profile and the corresponding ideal stratified and fully mixed temperature profiles.

The mix number is:

$$MIX = \frac{M_{str} - M_{\exp}}{M_{str} - M_{mix}} , \tag{2}$$

M_{str}, $M_{\exp}$ and M_{mix} are the "momentum of energy" of a perfectly stratified tank, the experiment and a fully mixed tank respectively. The value of the mix number is

between 0 and 1 where 0 corresponds to a perfectly stratified tank and 1 corresponds to a fully mixed tank.

For the experiment where the tank is heated from the surrounding temperature to a higher temperature level the temperature profiles for the perfectly stratified tank and the fully mixed tank are calculated by means of the measured temperatures.

The temperature of the fully mixed tank is calculated as the measured weighted average temperature. The temperature in the perfectly stratified tank consists of a high temperature in the upper part of the tank and a low temperature in the lower part of the tank. In the charging case, the low temperature equals the start temperature of the tank. The lower part of the tank has a volume equal to the total water volume in the tank minus the water volume which has entered the tank during the test. Based on the measured temperatures the temperature in the upper part of the tank with a volume equal to the water volume which has entered the tank during the test is determined in such a way that the energy of the perfectly stratified tank is equal to the measured energy in the tank.

For the experiment where the tank is cooled from a high temperature to a lower temperature the temperature profiles for the perfectly stratified and fully mixed tank are calculated in a similar way. In this way heat losses and the heat capacity of the tank material are accounted for. No mix number is calculated for the stratified experiment. In this case only $M_{\exp}$ is calculated with the ambient temperature as the reference temperature.

3 Results

3.1 Heating tests

Figure 4 and Figure 5 shows the temperature stratification in the tank in different heights every 5 minutes during the heating test with stratification manifolds of one and two fabric layers, style 361. For comparison, the temperature stratification profile with the marketed rigid stratification pipe (ref. Figure 3) with three holes with “non-return” valves is shown in Figure 6. In each of the figures the perfectly stratified temperature profile after 20 minutes and after 50 minutes are shown.

From the figures it is clear that the temperature stratification profile is much more desirable when a stratification manifold of two fabric layers instead of one fabric layer is used. With two layers of fabric the temperature curves are more horizontal and the temperature at the top of the tank is increased and the temperature at the bottom of the tank is decreased compared to the test with the one layer fabric stratification pipe. Also it can be seen that the stratification profile with the marketed rigid stratification pipe with three holes with “non-return” valves is very close to the perfectly stratified profile.

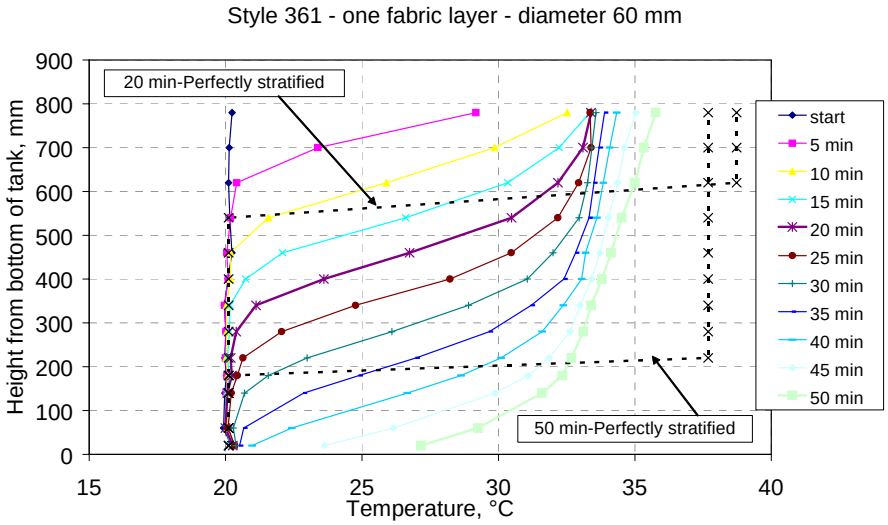

Figure 4: Temperature profile during a heating test with fabric stratification pipes, Style 361 with one fabric layer.

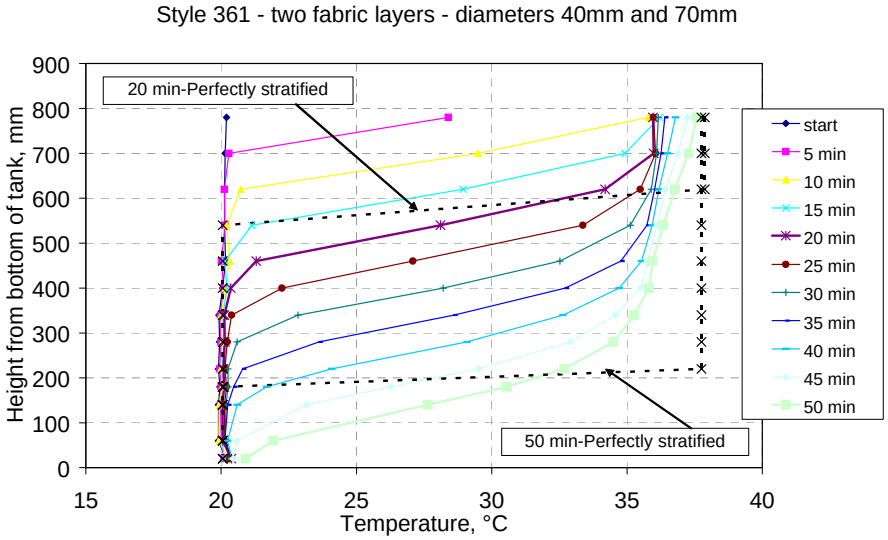

Figure 5: Temperature profile during a heating test with fabric stratification pipes, Style 361 with two fabric layers.

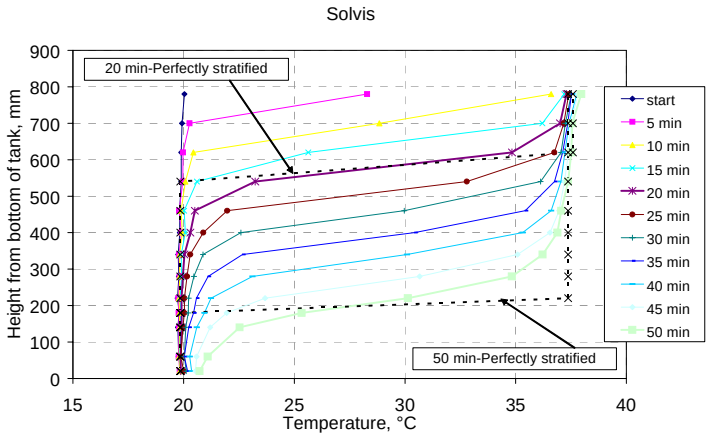

Figure 6: Temperature profile during a heating test with the rigid stratification pipe.

The rigid stratifier performs slightly better than the two fabric layer stratification pipe because the horizontal heat transfer between the hot water in the pipe and the cold water in the tank is lower.

Figure 7 and Figure 8 show the mix numbers during the heating test with one and two fabric layer stratification pipes. In Figure 8 the mix number of the rigid pipe with three holes with “non-return” valves is also shown.

From Figure 7 and Figure 8 it is seen that the mix numbers are dramatically reduced by using two fabric layers with a distance between the layers instead of only one fabric layer. The mix number increases during the experiment because the hot water enters the bottom of the tank and heat is transferred from the fabric pipe to the tank water in the lower part of the tank during the whole heating test. The mix number obtained with the rigid stratification pipe is very low and somewhat lower than the mix numbers obtained with the fabric stratification pipes. This is because the horizontal heat transfer through the wall of the rigid pipe is much lower than the horizontal heat transfer through the fabric wall.

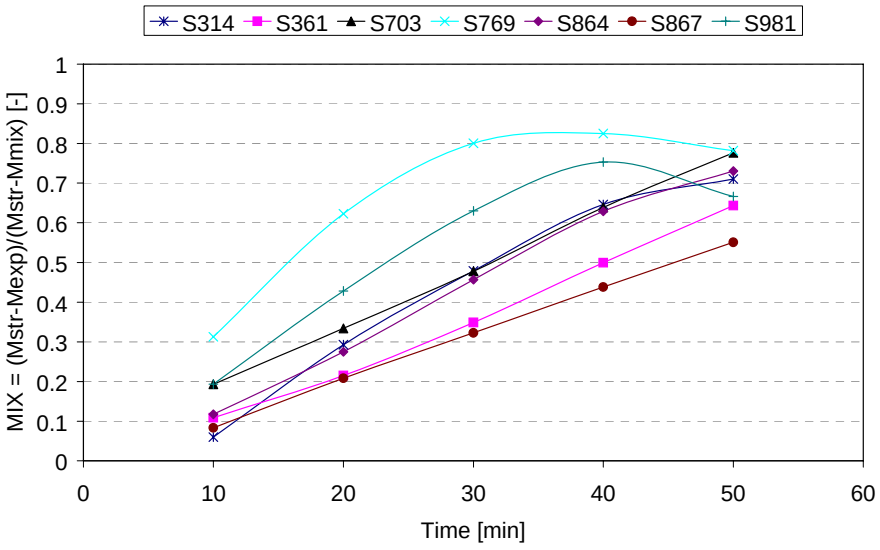

Figure 7: Mix numbers for fabric stratification pipes of one fabric layer.

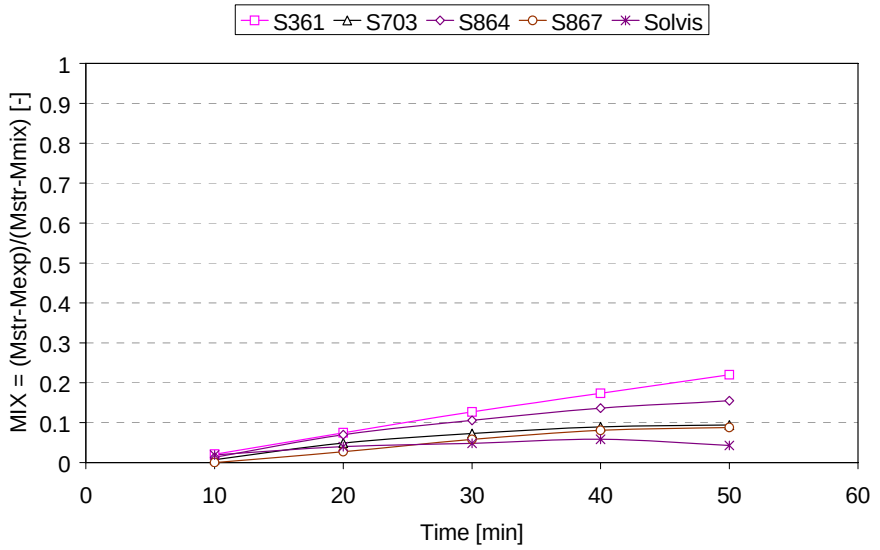

Figure 8: Mix numbers for fabric stratification pipes of two fabric layers and the rigid pipe.

3.2 Stratified heating tests

Figure 9 shows the experimental "momentum of energy" during the stratified heating test with two fabric layer stratification pipes, S361 and the rigid pipe with holes with "non-return" valves.

From the figure it obvious that the fabric stratification pipe with two fabric layers and the rigid pipe with holes with "non-return" valves perform almost equally under the applied test conditions. After about 10 minutes the curve for the rigid pipe switches place with the curve for the fabric pipe. In the start of the test the incoming water has entered the tank through the upper hole in the rigid pipe. After 10 minutes the inlet

temperature is too low to enter the upper hole and too high to enter the middle hole. Hence, the incoming water enters both the upper and the middle hole and the temperature difference between the upper and the middle hole decreases.

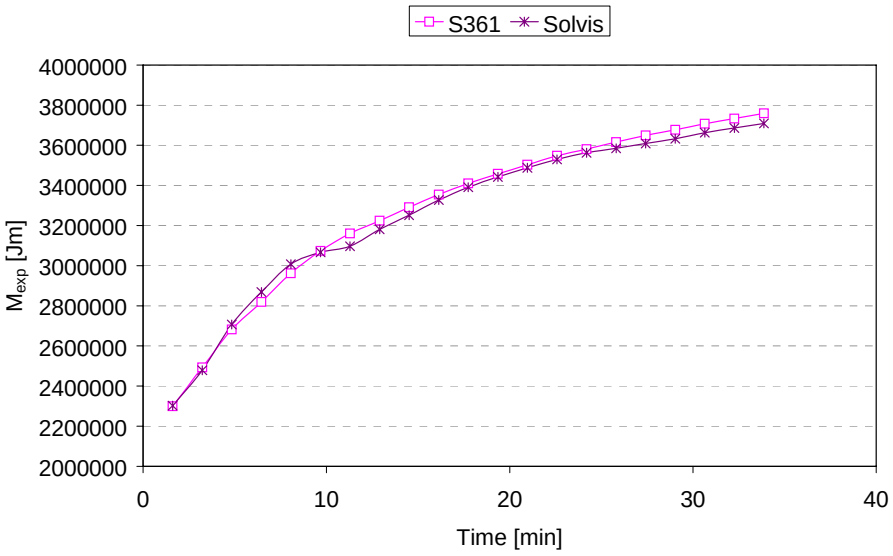

Figure 9: Moment of energy M_{exp} of the experimental data.

3.3 Cooling tests

Figure 10 shows the mix numbers during the cooling test with a two fabric layer stratification pipe, S361 and the rigid pipe with three holes with “non-return” valves.

From the figure it can be seen that the mix number is lower for the fabric stratification pipe than for the rigid pipe with holes with “non-return” valves. This is due to the fact that the incoming cold water only can leave the rigid pipe through the lowest hole whereas the incoming cold water can leave the fabric stratification pipe in any desired level.

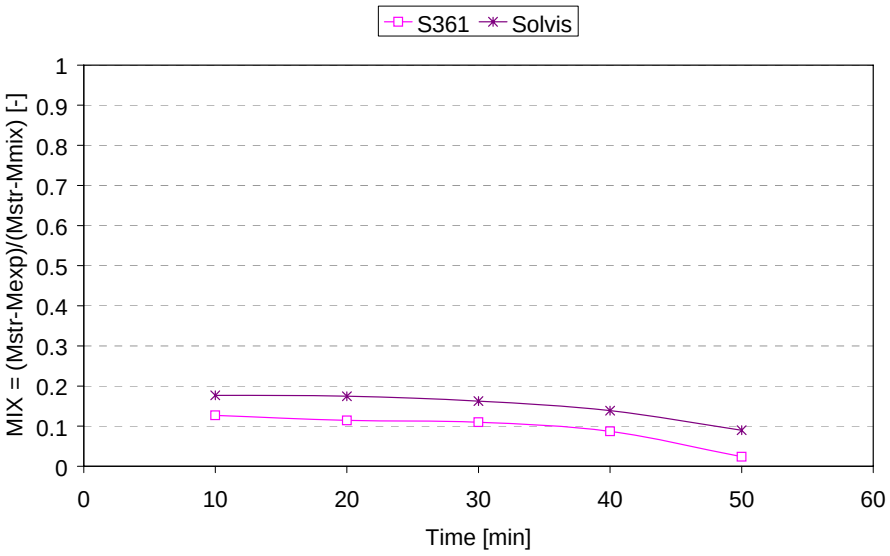

Figure 10: Mix number for fabric stratification pipes with two fabric layers and the rigid pipe with holes with “non-return” valves.

3.4 PIV measurements

Figure 11 and Figure 12 show the velocity vector maps and the corresponding streamlines to the vector maps 10, 20, 26 and 36 minutes after the heating is started. The velocity vector maps are calculated as mean values from 10 instantaneous velocity recordings by adaptive cross correlations and finally range validation procedure is applied. The corresponding temperature profiles are shown in Figure 4 and Figure 5.

From the figures it can be seen that the primary movement of the tank water after 10 minutes is downward towards the outlet in the bottom of the tank. Close to the fabric stratification pipe the direction of the water is upwards due to horizontal heat transfer through the fabric stratification pipe, especially for the one layer pipe. After 20 minutes the upward flow has stopped close to the one layer fabric pipe because thermal stratification has been built up in the level where the pictures are taken. The thermal stratification stops the upward flow. Water is leaving the pipe just above the level of the picture. This is not the case close to the two layer fabric pipe where the picture is the same as after 10 minutes. After 26 minutes water leaves the one layer fabric pipe in the level where the picture is taken. There apparently is a mismatch temperature difference between water entering the tank and the tank water creating eddies. After 36 minutes water starts to leave the two layer fabric pipe. At this time the temperature thermocline has reached the level of the picture. The pictures illustrate very well the advantages of using stratification fabric pipes with two fabric layers instead of one fabric layer.

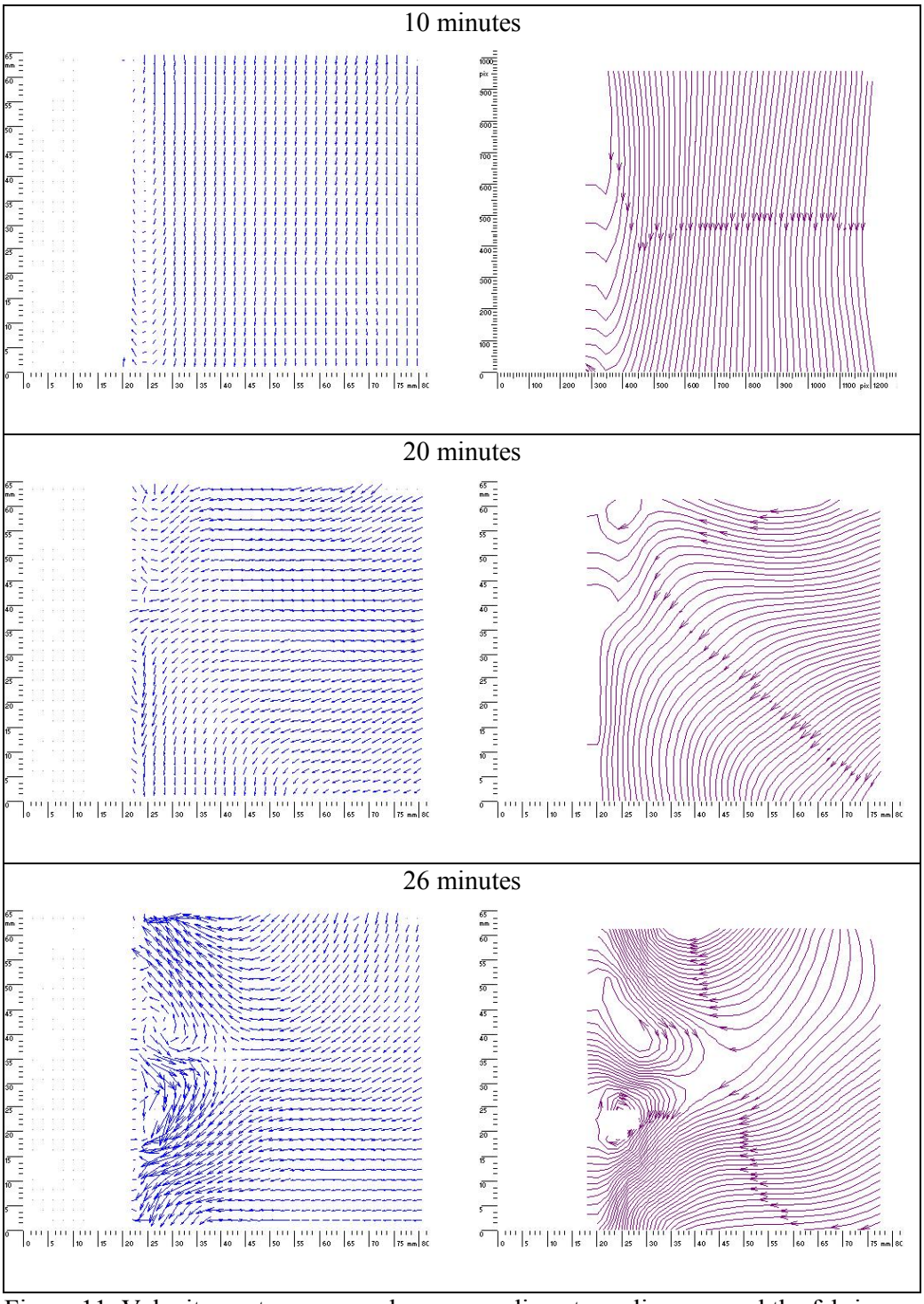

Figure 11: Velocity vector maps and corresponding streamlines around the fabric stratification pipes with one fabric layer.

Style 361 – two fabric layers – 40 mm/ 70 mm

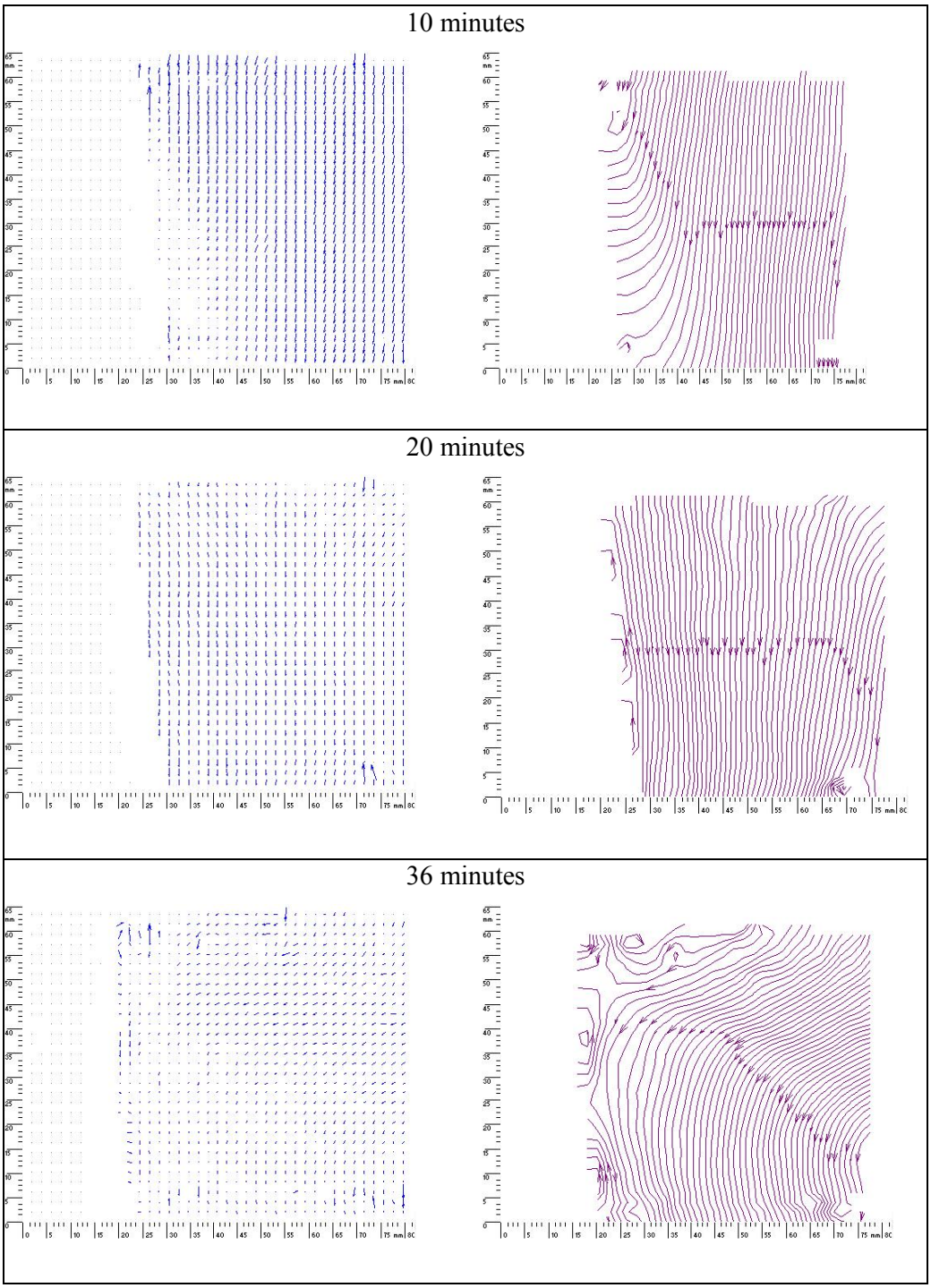

Figure 12: Velocity vector maps and corresponding streamlines around the fabric stratification pipes with two fabric layers.

4 Conclusions

A number of stratifications pipes for hot water tanks made of different fabrics are investigated. The investigation comprises stratification pipes of one and two fabric layers. The performance of the fabric stratification pipes is investigated during

heating, cooling and stratified heating tests. In all the tests, water enters the stratification pipe through the bottom of the tank. Further the performances of the fabric stratification pipes are compared to the performance of a marketed rigid stratification pipe with three holes with “non-return” valves.

The investigation shows that the performance of fabric stratification pipes can be improved significant by using two fabric layers with a distance of about 10 mm between each fabric layer instead of using one fabric layer.

The investigation also shows that the largest disadvantage of the fabric stratification pipes is the high horizontal heat transfer through the very thin fabric. This disadvantage is most significant when hot water enters a cold tank and flows from the bottom to the top of the fabric stratification pipe. In this particular case the rigid stratifier has an advantage because of the low horizontal heat transfer through the pipe wall.

For the cooling test the two fabric layer stratification pipe performs somewhat better than the rigid stratifier, while the two fabric layer stratification pipe and the rigid stratifier perform identical during stratified heating tests.

Nomenclature

M	=	“Momentum of energy” (J·m)
E	=	Energy (J)
y	=	Vertical distance (m)
V	=	Volume (m^3)
c	=	Specific heat capacity (kJ/kg/K)
ρ	=	Density (kg/m^3)
T	=	Temperature (K)
N	=	Number of tank layers

Subscripts

i	=	Tank layer
str	=	Stratified
exp	=	Experimental
mix	=	Mixed

References

Adams D. E. Design of a Flexible Stratification Manifold for Solar Water Heating Systems. Master Thesis, Colorado State University, Fort Collins, CO. 1993.

Andersen E., Jordan U., Shah L.J., Furbo S. Investigation of the Solvis Stratification Inlet Pipe for Solar Tanks. Proceedings of ISES Solar World Congress 2004, Freiburg, Germany, pp. 659-668, 2004.

Davidson J.H., Adams D.A., Miller J.A. A Coefficient to Characterize Mixing in Solar Water Storage Tanks. Journal of Solar Energy Engineering, Vol. 116, pp. 94-99, 1994.

Davidson J.H., Adams D.A. Fabric Stratification Manifolds for Solar Water Heating. Journal of Solar Energy Engineering, Vol. 116, pp. 130-136, 1994.

Essert H. Aufbau und Inbetriebnahme eines Speicherversuchsstandes. Diploma Thesis, Graz University, Austria, 1995.

Furbo S. Test Procedure for Heat Storages for Solar Heating Systems. Int. J. Solar Energy, Vol. 1, 1983.

Furbo, S., Vejen, N.K., Shah, L.J., 2005. Thermal performance of a large low flow solar heating system with a highly thermally stratified tank. Journal of Solar Energy Engineering, Vol. 127, no.1, 15-20.

Gari H.N., Loehrke R.I. A controlled buoyant jet for enhancing stratification in a liquid storage tank. Journal of Fluids Engineering, Vol. 104, pp. 475-481, 1982.

Hollands K.G.T., Lightstone, M.F., 1989. A review of low-flow, stratified-tank solar water heating systems. Solar Energy 43, 97-105.

Knudsen, S., Furbo, S., 2004. Thermal stratification in vertical mantle heat exchangers with application to solar domestic hot water systems. Applied Energy, Vol 78/3, 257-272.

Knudsen, S. Morrison, G.L., Behnia, M., Furbo, S., 2005. Analysis of the flow structure and heat transfer in vertical mantle heat exchanger. Solar Energy 78, 281-289.

Krause Th., Kühl L. Solares Heizen: Konzepte, Auslegung und Praxiserfahrungen, 2001.

Liebfried U. Combitanks with internal thermosyphonically driven heat exchangers for hot water – comparison of existing systems, 2000. Proceedings Terrastock Conference, pp. 315-320.

Loehrke R.I., Holzer J.C., Gari H.N., SharpM.K. Stratification enhancement in liquid thermal storage tanks. Journal of Energy, Vol. 3, No. 3, pp. 129-130, 1979.

Rosen M. A. The Exergy of Stratified Thermal Energy Storages. Solar Energy, Vol. 71, pp. 173-185, 2001.

Shah, L.J., Furbo, S., 1998. Correlation of Experimental and Theoretical Heat Transfer in Mantle Tanks used in Low Flow SDHW Systems". Solar Energy, Vol. 64 (4-6), 245-256.

Shah L.J. Stratifikationsindløbsrør. Department of Civil Engineering, Technical University of Denmark, DTU, 2002.

van Koppen, C.W.J., Thomas, J.P.X., Veltkamp, W.B., 1979. The Actual Benefits of Thermally Stratified Storage in a Small and Medium Size Solar System. In Proceedings of ISES Solar Wor.ld Congress, Atlanta, USA, 579-80.

Weiss, W. (Ed.), 2003. Solar Heating Systems for Houses. A design Handbook for Solar Combisystems. James & James Ltd. Solar Heating and Cooling Executive Committee of International Energy Agency (IEA).

Test Fabric Inc., www.testfabrics.com.

Yee C. K., Lai F. C. Effects of a Porous Manifold on Thermal Stratification in a liquid Storage Tank. Solar Energy, Vol. 71, pp. 241-254, 2001.

Bilag 10

Investigations on stratification devices for hot water stores.

International Journal of Energy Research, 2007.

Elsa Andersen, Simon Furbo, Mathias Hampel, Wolfgang Heidemann & Hans Müller-Steinhagen

INVESTIGATIONS ON STRATIFICATION DEVICES FOR HOT WATER HEAT STORES

E. Andersen & S. Furbo
Department of Civil Engineering. Technical University of Denmark
DK-2800 Kgs. Lyngby, Denmark
Corresponding Author, email : ean@byg.dtu.dk

M. Hampel, W. Heidemann & H. Müller-Steinhagen
Institut für Thermodynamik und Wärmetechnik (ITW), Universität Stuttgart
Pfaffenwaldring 6, D-70550 Stuttgart, Germany

Keywords: Solar tanks, thermal stratification, inlet stratification pipes, CFD, PIV, LIF

Abstract

The significance of the thermal stratification for the energy efficiency of small solar-thermal hot water heat stores is pointed out. Exemplary the thermal stratification build-up with devices already marketed as well as with devices still in development has been investigated experimentally and theoretically, taking into account different realistic operation conditions. The methods (selective temperature measurement, non-invasive field measuring methods PIV and LIF, Computational Fluid Dynamics (CFD)) suitable for the experimental and theoretical analysis of thermal stratification devices are introduced.

1. Introduction

Since the 1960s the influence of thermal stratification in hot water stores on the thermal performance of solar heating systems has been studied intensively in order to improve the overall performance of solar thermal systems. Experimental and theoretical investigations showed that the overall system performance of a solar heating system for domestic hot water preparation can be increased with an optimal thermal stratification in the solar storage compared to systems without stratified conditions in the storage.

An overview of direct charging and discharging systems which are nowadays available is given by Göppert et al. (2006). Simple systems suitable for small- and large-sized solar storages use slotted pipe diffusers or radial diffusers with baffles to suppress mixing effects due to high inflow velocities (Bahnfleth et al. (2003), (2005)). The diffusers are mounted in fixed heights of the storage. More sophisticated stratification systems enable an inflow at variable heights of the storage. The choice of the admission height of the charged fluid can take place through mechanical procedures (Neal (1981)) or through gravitationally induced flow whereas vertically installed tubes with free or lockable openings are used. The last-mentioned charging method represents the state-of the-art and is subject of numerous research and development activities: A large number of differently designed rigid and flexible inlet stratification pipes have been studied in the past by van Koppen et al. (1979), Loehrke et al. (1979), Davidson and Adams (1994), Abu-Hamdan

(1992), Essert (1995) and Andersen et al. (2004). Among these, the most promising devices are rigid inlet stratifiers equipped with openings and so-called “non-return” valves as well as flexible inlet stratification pipes mounted vertically in the storage tanks.

By means of experimental and theoretical investigations, Shah et al. (2005) showed that a long tube with a number of openings in different levels works more as a mixing device than a stratifying device, because cold water was sucked into the stratifier especially through the lowest opening. Further tests with “non-return” valves mounted in the openings revealed that the unwanted flow at the lowest openings was reduced.

Several fabric stratification inlet pipes were experimentally investigated by Andersen et al. (2005). The authors found that the largest disadvantage of the fabric stratification inlet pipe - namely the high horizontal heat transfer through the very thin fabric - can be dramatically reduced when using fabric pipes consisting of two fabric layers instead of one fabric layer. Further, the investigation showed that a two layer fabric stratification pipe performs as well as a good performing rigid stratification pipe.

In the following sections the thermal behaviour of three different modern stratification devices with fabric and rigid pipes are presented in detail. Next to the well known measurements with thermocouples, which allow measurements at selected points only, non-invasive field measuring methods like Particle Image Velocimetry (PIV) and Laser Induced Fluorescence (LIF) are used for the assessment of the stratification devices considered. The application of numerical calculations (CFD – Computational Fluid Dynamics) allows a theoretical prognosis of the thermo-hydraulic behaviour of the devices.

2. Inlet stratification pipes and testing equipment

Typical inlet stratifiers used for the investigations presented in this paper are shown in Figures 1-3.

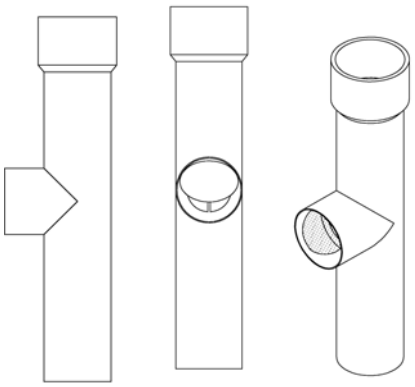

Figure 1: Section of a rigid stratification pipe with lockable openings

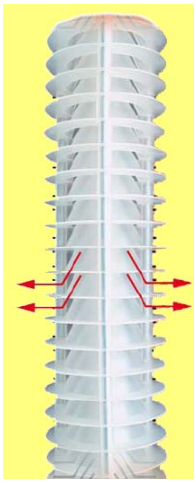

Figure 2: Sketch of a rigid stratification pipe with circular openings

Figure 3: Fabric stratifier

In Figure 1 a section of a rigid inlet stratification pipe with lockable openings is shown. The pipe is made of polypropylene (PP) with a height of 328 mm, an outer diameter of 60 mm and a thickness of 3 mm (Krause (2001), Shah (2002)). The complete stratification inlet pipe is composed of several pipe sections according to Fig. 1 and has a distance between the centres of each opening of about 292 mm. The pipe is patented and marketed by the German company Solvis GmbH & Co KG and was tested at the Technical University of Denmark, DTU.

In Figure 2 a rigid inlet stratification pipe with circular openings is depicted. The device is made of 2 mm thick synthetic material resistant to temperature and deformation and is built up by a variable number of "hats" connected by 3 thread rods forming an inner flow channel of 24 mm with an outer diameter of 100 mm. Free convection induced fluid flow can leave the stratification pipe through all circular openings which have a height of 18 mm. The device is patented and marketed by the German company Sailer GmbH & Co KG and was tested at ITW of the University of Stuttgart.

A two-layer fabric inlet stratification pipe is shown in Figure 3. The investigated samples consist of pipes with an inner/outer diameter of 40 mm/70 mm and 25 mm/45mm, the pipes are closed at the top. The following two different fabric styles are used: Style 864, Spun Orlon Type 75 Acrylic Plain Weave (non-stretchable fabric) and Style 700-12, Filament polyester, Poly-Lycra (stretchable fabric). The fabric pipe is patented and was mainly tested at DTU.

Due to different experimental equipment available at the Technical University of Denmark, DTU, and the ITW, University of Stuttgart, for the testing of the stratification devices, the following modes of operation are possible:

At DTU experiments are carried out in a glass tank (not insulated) with a volume of 144 litres (400 x 400 x 900 mm) with a wall thickness of the tank of 12 mm. Temperatures within the tank are measured at 13 different uniformly distributed tank levels using copper-constantan thermocouples type T with an accuracy of 0.5 K. The volumetric flow rate is measured using an electro-magnetic inductive flow meter (accuracy 1% of the measured value). Figure 4 shows the setup for experiments with forced volume flow and thermosyphonical flow at DTU.

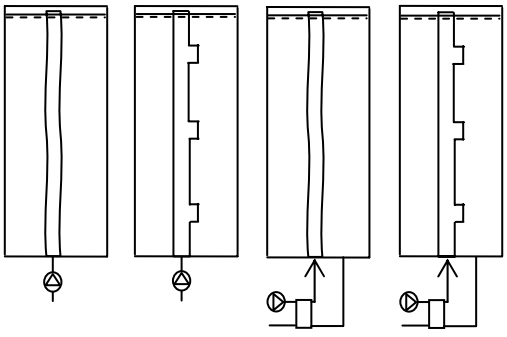

Figure 4: Investigations with forced volume flow and natural buoyancy flow (performed at DTU)

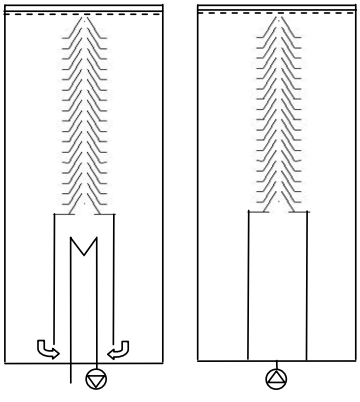

Figure 5: Investigations with natural buoyancy flow and forced volume flow (performed at ITW)

At ITW experiments are carried out in a cylindrical steel tank (volume 550 litres, height 1530 mm, diameter 700 mm). The tank temperatures are measured at up to 10 uniformly distributed levels in the tank with thermocouples (type T, accuracy 0.5 K). Inside the tank mantle view-windows of glass are placed which enable the use of laser-light based PIV/LIF measurement technique for the determination of flow and temperature fields. In Figure 5 and 8 an outline of the experiments at ITW is shown.

3. Experimental investigations

3.1 Test conditions

In order to investigate the thermal performance of the inlet stratification pipes (cf. Fig. 1-3) experiments with forced volume flow rates of 2, 6, 8 and 10 l/min are carried out for two sets of operation conditions: (I) heating tests, where the tank water is heated up from 20°C through the inlet stratification pipe with inlet fluid temperatures of (32- 40)°C, (II) stratified heating tests with an initially stratified tank (50°C-20°C) through the inlet stratification pipe with an inlet fluid temperature higher than 20°C and lower than 50°C. In both cases (I, II) the outlet is at the bottom of the tank located as depicted in Figure 4.

Furthermore, experiments with free convection driven flow, generated via an external heat exchanger, are carried out with the test equipment available at DTU (cf. Figure 4). Starting from an initial temperature of 20°C the working fluid water is heated up with a heat flux of 3 kW transferred from the external heat exchanger into the tank.

The heating tests simulate the thermal behaviour of a stratification pipe in a solar collector loop.

3.2 Test results

3.2.1 Forced flow with constant flow rate

In Figure 6 normalized temperatures as a function of the relative height in the tank obtained during heating tests with forced volume flow rates of 6, 8 and 10 l/min are shown. The volume ratio, defined as the ratio between the volume circulated through the tank and the tank volume, is used as a parameter. Curves for 20, 40 and 60% are shown, that is temperatures are shown when 26.9 litres, 53.8 litres and 80.6 litres of water has been circulated through the tank which had a water volume of 134.4 litres.

It can be seen that during the heating tests with a low volume flow rate (6 l/min), the rigid stratification pipe with lockable openings (Solvis) performs better than the fabric stratification pipes (style 864 and style 700-12). The thermal performance of the fabric stratification pipes increases for higher volume flow rates (8 l/min, 10 l/min) and is then better than the performance of the rigid stratification pipe. The reason for that is most likely that the horizontal heat transfer through the thin fabric pipe to the tank decreases for increasing volume flow rates.

In order to examine whether the stratification pipes are able to build up thermal stratification without destroying the already existing thermal stratification so-called stratified heating tests are performed. The resulting temperature profiles for different volume flow rates (2, 6, 8 and 10 l/min) are shown in Figure 7.

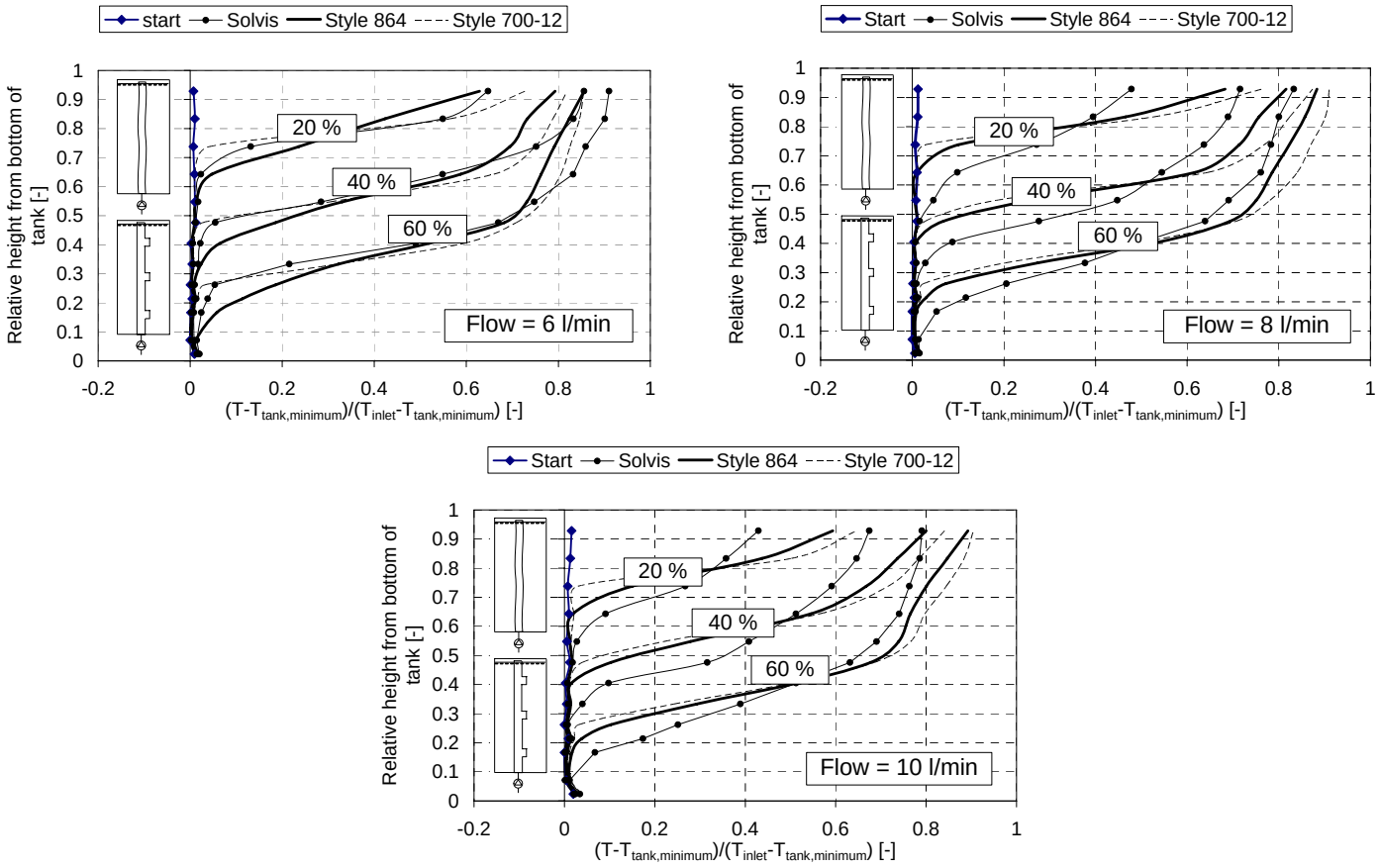

Figure 6: Temperature profiles for rigid inlet stratification pipe with lockable openings (Solvis) and fabric inlet stratification pipes (style 864 and style 700-12) with the diameters 40 mm/70 mm, heating mode

The initial temperature at the top of the tank is always 50°C except for the volume rate 2 l/min where it is 57°C. In the start of the tests, the inlet temperature is as high as the temperature in the top of the tank. After about 18 % of the water has been circulated through the tank the inlet temperature stabilizes and only the middle part of the tank is heated. However in the test with the stratifier with circular openings, the inlet temperature is constant during the whole experiment.

The fabric stratification pipes succeed to heat up the middle part of the tank without decreasing the already existing high temperature at the top of the tank in all the tests. The rigid stratification pipe with lockable openings is not able to maintain the already existing high temperature at the top of the tank. This is due to the fact that the rigid stratification pipe has only a limited number of openings. When the correct temperature level lies between two openings, the water leaves through both the opening above and below the right temperature level which results in mixing in the tank between the two opening levels.

The rigid stratification pipe with circular openings (Sailer) which was tested only with a volume flow rate of 2 l/min, also succeeds to heat up the middle part of the tank without

destroying the already existing thermal stratification. The temperature decrease in the top of the tank is due to heat loss from the not insulated tank.

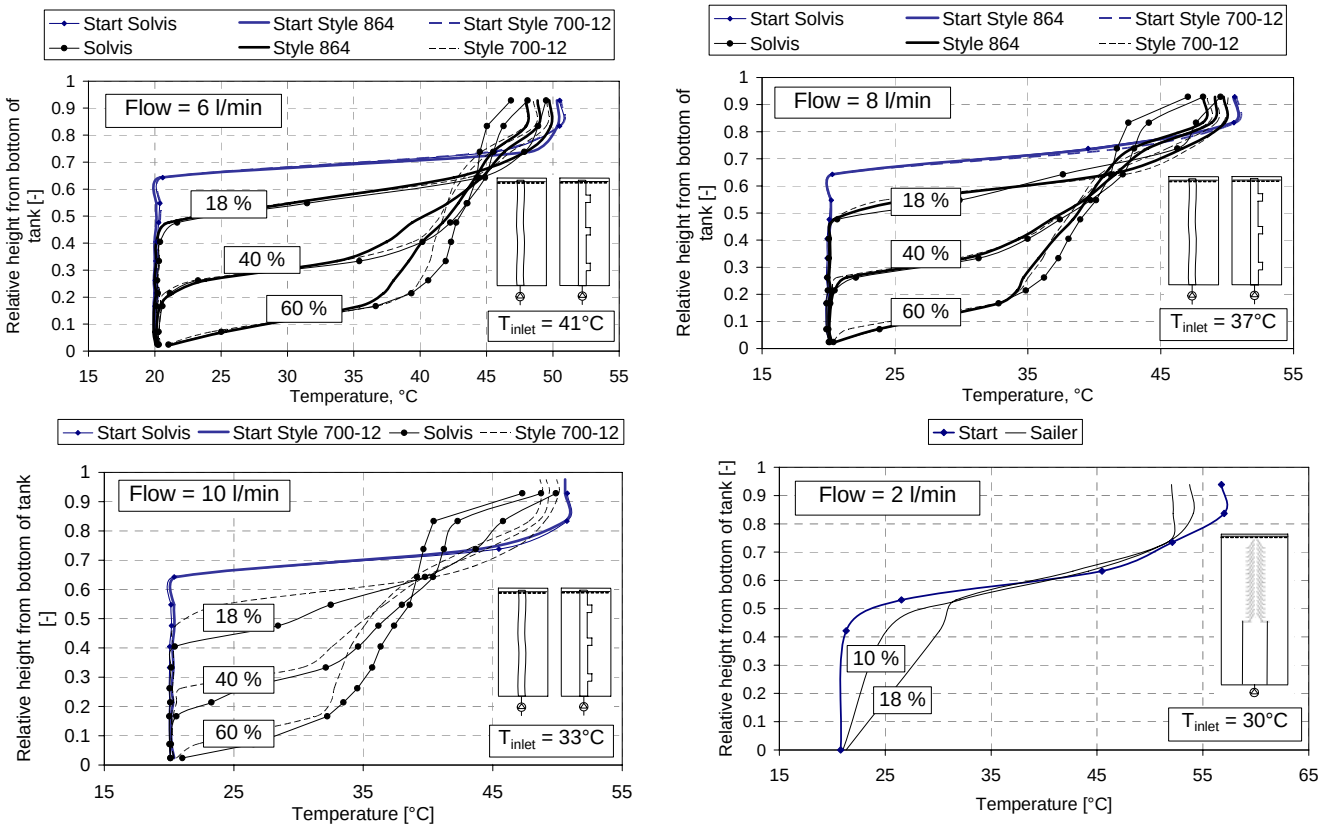

Figure 7: Temperature profiles for the rigid inlet stratification pipe with lockable openings, the fabric inlet stratification pipes with diameters of 40 mm/70 mm and the rigid inlet stratification pipe with circular openings (stratified heating mode)

3.2.2 Experimental validation of numerical calculations

Theoretical investigations for inlet stratifiers can be carried out with CFD models which allow the prediction of the thermal and hydrodynamic behaviour in detail just by knowing the geometry of the system and the boundary conditions. Reliable numerical models still need to be adapted to physical phenomena like tubulence and should be validated afterwards by comparing calculated and measured values.

With so-called field-measuring-methods like Particle Image Velocimetry (PIV) and Laser Induced Fluorescence (LIF) velocity and temperature measurements for a complete flow and temperature field can be done. The convincing advantage is that data can be gathered without having to insert any testing probes. Tracer particles with the same density as the fluid are added and move with the flow. They reflect the light flashes of a laser and these reflections are recorded by a CCD-camera. The pulsing laser beam is expanded to a very thin light-sheet of approximately 1 mm thickness (see Fig. 8). Perpendicular to this, the

CCD-camera takes pictures of the reflections of the tracer particles. Some milliseconds later, a second particle picture is taken. A superposition of both pictures gives a double-frame picture which shows the displaced particles. From the distance between the particles and the time between both frames, the velocity and flow direction can be calculated. Adding a fluorescent dye (e.g. Rhodamine B) to the fluid additionally gives the possibility to measure the temperature in the field of observation (LIF-method). After excitation with laser-light this dye emits fluorescence light, and its intensity is proportional to the temperature. The fluorescence signal is recorded by a camera and processed electronically.

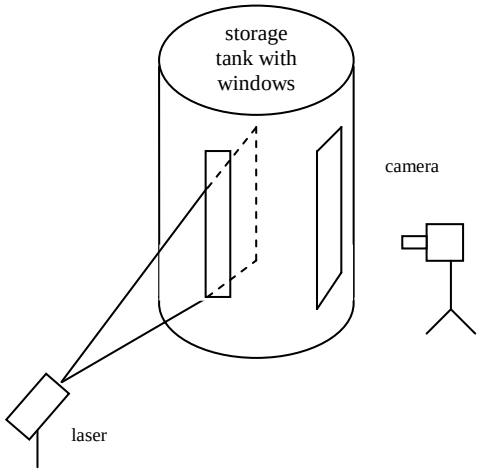

Figure 8: Experimental setup for PIV and LIF measurements

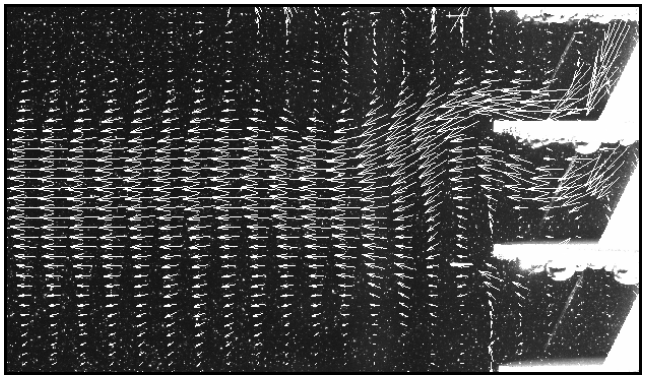

Figure 9: Example of a PIV-measurement: outflow from a stratifier as pictured in Fig. 2

Figure 9 shows, as an example, a cutting from a typical PIV-measurement on a rigid stratifier system with circular openings as depicted in Figure 2. Storage water is heated up by a heat exchanger below a convection chimney. Buoyancy forces transport the water into the chimney. At the same time cold water from the lower part of the storage flows into the heat exchanger area. The warm water leaves the chimney at a height where it has approximately the same temperature (respectively density) as the storage water. PIV-measurements allow the determination of the velocity of the leaving water. For the investigated stratifier system values between 10 to 20 mm/s at the openings and below 10 mm/s further away from the openings occur. When looking at a wider field of view, it is obvious that the flow is not always as straightforward as it appears in this picture, instead a lot of eddies and other flows are made visible.

For the stratification device with circular openings CFD data were compared with thermocouple- and LIF-measurements. The CFD calculations were simulated with a two-dimensional model with axial-symmetry. For the transient simulation of turbulence the realizable k-ε-model was chosen, as laminar simulations produced non-physical results.

Fig. 10 shows the direct comparison between LIF measurement and CFD calculations. The measurement was done 32 minutes after the start of the loading process. The start temperature at all levels of the tank is 20°C, the storage is loaded thermosyphonically

with a power of 12 kW. It is clearly visible that the biggest temperature change from 22°C to 44°C is within 20 cm in the storage.

In Fig. 11 the quantitative comparison between the thermocouples temperature, the LIF measurement and the CFD simulation is shown for the vertical line where the thermocouples are placed, both at t=22 min and t=32 min after starting of the loading process. It is obvious that the LIF temperatures at higher temperatures are a little bit lower than the more reliable thermocouple measurements. There can be several reasons for this: mistakes in calibration and dye concentration as well as fluctuations in laser intensity are possible. Apart from this the CFD calculations reflect the temperature gradient very well. Especially the height of the transition zone from hot to cold water is predicted accurately.

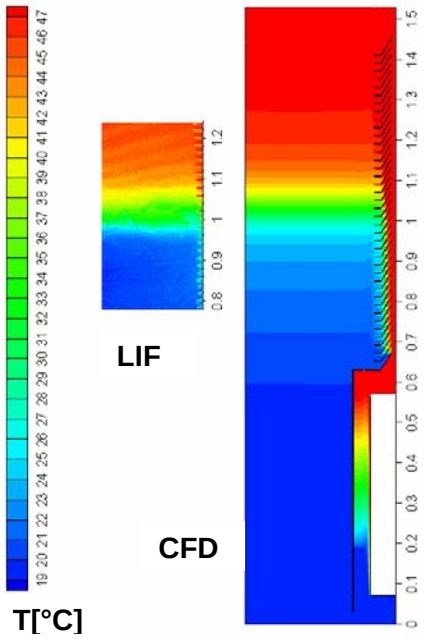

Figure 10: Comparison of CFD and LIF results

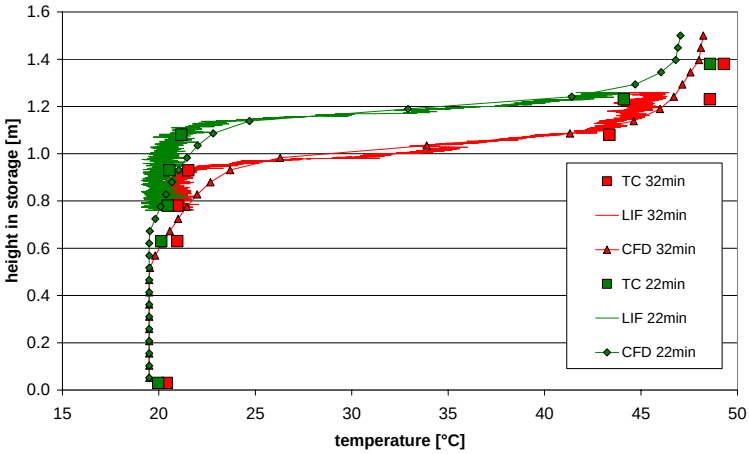

Figure 11: Comparison between measured (thermocouples (TC) and LIF) and calculated (CFD) results

CFD-calculations allow an insight into flows in areas which are difficult to measure (cf. Fig. 12). For the stratifier with the circular openings it is difficult to determine, how much water is sucked in at the bottom of the chimney due to the pressure differences between the water in the tank and the fast flowing water in the chimney.

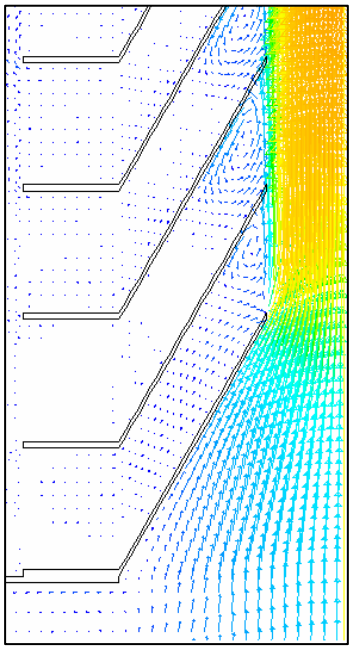

Figure 12: Velocity vectors at the entrance and the first circular openings (bottom-up) of the stratifier system according to Fig. 2.

Thermocouple measurements do not provide a satisfying answer to this as well. The inflow through the circular openings will reduce the temperature of the hot upward moving fluid in the centre of the stratifier. The design of the stratifier with circular openings can not fully eliminate the inflow as it is the case for the fabric stratifier and the stratifier with lockable openings (Andersen et al. (2004)). However, a CFD analysis shows that the inflow into the stratifier is about 5.25 l/min, whereas the inflow through the first 4 circular openings from the tank into the chimney is only 0.31 l/min (6%). The simulation also shows that in the upper openings of Fig. 12 eddies are created between the warm water in the chimney and the cold tank water.

3.2.3 Buoyancy forced flow

Temperature profiles occurring during heating tests with buoyancy-driven forced flow for different stratifier systems are shown in Fig. 13. Depicted are normalized temperatures as a function of the relative heights in the tank for the rigid pipe with lockable openings (Solvis), fabric pipes style 864 and style 700-12 with inner/outer diameters of 40/70 mm as well as fabric pipes style 864 and style 700-12 with inner/outer diameters of 25/45 mm. The volume ratio of the water which has been circulated through the tank is used as parameter.

During the heating tests with a volume flow rate in the thermosyphon loop of about 1 l/min, the rigid stratification pipe with lockable openings perform better than the fabric stratification pipes with the large diameters. A reason for this is most likely the higher pressure drop in the fabric pipes. It was observed that the calculated thermosyphonical flow rate is slightly lower during the tests with the fabric pipes. Also, the horizontal heat transfer through the thin fabric pipe to the tank is larger than the heat transfer through the rigid pipe.

By reducing the inner and outer diameter of the fabric pipes, the horizontal heat transfer in reduced. From the right diagram of Fig. 13 it can be seen, that a smaller inner/outer diameter of the fabric pipe leads to better thermal stratification in the tank. The stretchable fabric stratification pipe style 700-12 that performed very well with high forced volume flow rates (cf. chapter 3.2.1) performs worse than the rigid pipe with lockable openings and the non-stretchable fabric pipe style 864 with low volume flow rates.

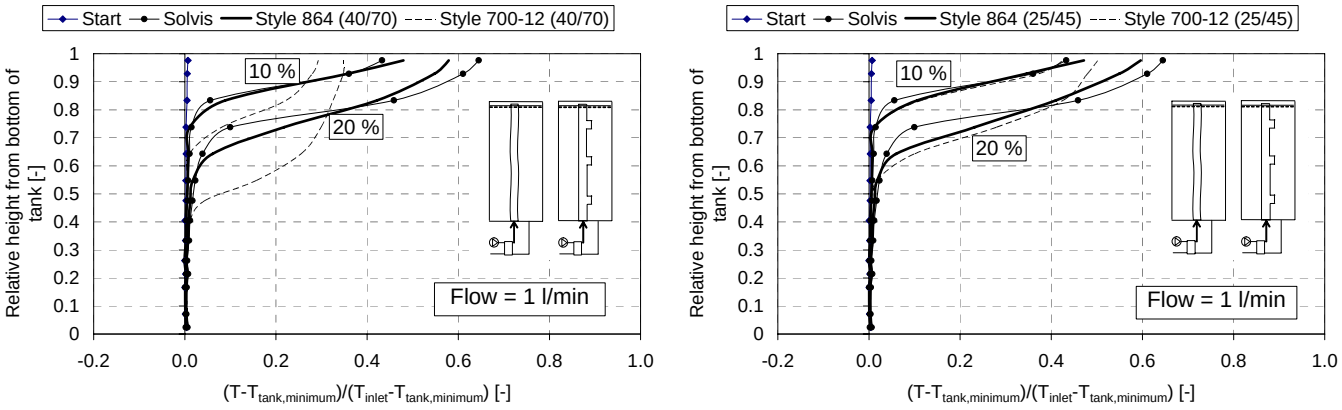

Fig. 13: Temperature as a function of the tank height for different stratifier systems, heating mode, thermosyphonical flow

4. Summary and Conclusion

Two commercially available rigid inlet stratification pipes and two not yet available two-layer fabric inlet stratification pipes are investigated. The stratification pipes are tested with both forced volume flow rates and thermosyphonical flow rates. The investigation shows advantages and disadvantages of the stratification pipes under the applied operation conditions.

Furthermore, the advantages of numerical simulations (CFD) methods are discussed, which can help to achieve new developments for solar storage tanks. In order to create confidence in CFD methods, they still need to be validated. An example of validation with the use of thermocouples and by new measuring methods called PIV and LIF is shown.

The investigation only deals with inlet stratification pipes in laboratory tests with a limited number of operating conditions appearing in solar collector loops. Further investigations should include inlet stratification pipes with operation conditions similar to those in a space heating loop. Also tests in practice should be carried out in order to evaluate inlet stratification pipes under real fluctuating operation conditions. Validated numerical models describing the thermal behaviour of inlet stratification pipes seem to be the most promising tool for future cost- and time-effective R&D activities.

References

C.W.J. van Koppen, J.P.S. Thomas, W.B. Veltkamp. 1979. The actual benefits of thermally stratified storage in small and medium size solar systems. In Proceedings ISES Biennial Meeting, Vol. 2, Atlanta, pp. 576-580.

R.I. Loehrke, J.C. Holtzer, H.N. Gari, M.K. Sharp. 1979. Stratification enhancement in liquid thermal storage tanks. Journal of Energy 3 (3), pp. 129-130.

W.E.J. Neal. 1981. Thermal energy storage. Phys. Technol. 12 (1981), 5, pp. 213-226

J.H. Davidson, D.A. Adams. 1994. Fabric stratification manifolds for solar water heating. Journal of Solar Energy Engineering130, pp. 130-136.

M.G. Abu-Hamdan, Y.H. Zurigat, A.J. Ghajar. 1992. An experimental study of a stratified thermal storage under variable inlet temperature of different inlet designs. International Journal of Heat and Mass Transfer 35 (8), pp. 1927-1934.

W.P. Bahnfleth, J. Song, J.M. Cimbala. 2003. Measured and modelled charging of a stratified chilled water thermal storage tank with slotted pipe diffusors. HVAC&R Res. 9, 4, pp 467-491.

W.P. Bahnfleth, J. Song. 2005. Constant flow rate charging characteristics of a full-scale stratified chilled water storage tank with double-ring slotted pipe diffusers. Appl. Therm. Eng. 25, 17-18, pp. 3067 – 3082.

H. Essert. 1995. Aufbau und Inbetriebnahme eines Speicherversuchsstandes. Diploma Thesis, Graz University, Austria.

E. Andersen, U. Jordan, L.J. Shah, S. Furbo. 2004. Investigations of the Solvis stratification inlet pipe for solar tanks. Proceedings Eurosun 2004, vol. 1, Freiburg, Germany, pp. 76-85. ISBN. 3-9809656-1-9.

E. Andersen, S. Furbo, J. Fan. 2005. Investigations of fabric inlet stratifiers for solar tanks. Proceedings of ISES Solar World Congress, Orlando, Florida, USA.

T. Krause, L. Kühl. 2001. Solares Heizen Konzepte, Auslegung und Praxiserfahrungen.

L.J. Shah. 2002. Stratifikationsindløbsrør. Department of Civil Engineering, Technical University of Denmark, DTU.

L.J. Shah, E. Andersen, S. Furbo. 2005. Theoretical and experimental investigations of inlet stratifiers for solar storage tanks. Applied Thermal Engineering 25, pp. 2086-2099.

M. Hampel, W. Heidemann, H. Drück, H. Müller-Steinhagen 2006. Nicht invasive Messung von Temperaturfeldern in Flüssigkeiten mit LIF. Proceedings for the 16th symposium on solar thermal energy, OTTI, Regensburg, 2006

S. Göppert, T. Urbaneck, U. Schirmer, R. Lohse, B. Platzer 2006. Be- und Entlade-systeme zur thermischen Schichtung. Proceedings for the 16th symposium on solar thermal energy, OTTI, Regensburg.